STATISTICAL EVALUATION OF COMPUTATIONAL INTELLIGENCE TECHNIQUES FOR THE PREDICTION OF HYDRODYNAMIC PERFORMANCE OF QUARTER CIRCLE BREAKWATER

Thesis

Submitted in partial fulfilment of the requirements for the degree of

DOCTOR OF PHILOSOPHY

by

RAMESH N

(155227AM15P02)

DEPARTMENT OF WATER RESOURCES AND OCEAN ENGINEERING

NATIONAL INSTITUTE OF TECHNOLOGY KARNATAKA, SURATHKAL, MANGALORE - 575 025, INDIA

APRIL, 2024

STATISTICAL EVALUATION OF COMPUTATIONAL INTELLIGENCE TECHNIQUES FOR THE PREDICTION OF HYDRODYNAMIC PERFORMANCE OF QUARTER CIRCLE BREAKWATER

Thesis

submitted in partial fulfilment of the requirements for the degree of

DOCTOR OF PHILOSOPHY

by

RAMESH N

(155227AM15P02)

Under the guidance of

Prof. (Retd.) SUBBA RAO

Prof. (Retd.) ARKAL VITTAL HEGDE

DEPARTMENT OF WATER RESOURCES AND OCEAN ENGINEERING

NATIONAL INSTITUTE OF TECHNOLOGY KARNATAKA, SURATHKAL, MANGALORE - 575 025, INDIA

APRIL, 2024

DECLARATION

I hereby declare that the Ph.D. Thesis entitled **"STATISTICAL EVALUATION OF COMPUTATIONAL INTELLIGENCE TECHNIQUES FOR THE PREDICTION OF HYDRODYNAMIC PERFORMANCE OF QUARTER CIRCLE BREAKWATER"** which is being submitted to **National Institute of Technology Karnataka, Surathkal,** for the partial fulfillment of the requirement for the award of degree of **Doctor of Philosophy** in the **Department of Water Resources and Ocean Engineering** is a bonafide report of the work carried out by me. The material contained in this Ph.D. Thesis has not been submitted to any university or Institution for the award of any degree.

6/4/2024

.....

(155227AM15P02)

RAMESH N

Department of Water Resources and Ocean Engineering

National Institute of Technology Karnataka, Surathkal

Place: NITK-Surathkal

Date:

CERTIFICATE

This is to certify that the Ph.D. Thesis entitled **"STATISTICAL EVALUATION OF COMPUTATIONAL INTELLIGENCE TECHNIQUES FOR THE PREDICTION OF HYDRODYNAMIC PERFORMANCE OF QUARTER CIRCLE BREAKWATER"** submitted by **RAMESH N (155227AM15P02)**, as the record of the work carried out by him, is accepted as the Ph.D. Thesis submission in partial fulfillment of the requirements for the award of the degree of **Doctor of Philosophy** in the **Department of Water Resources and Ocean Engineering, National Institute of Technology Karnataka, Surathkal**, is a bonafide work carried out by him under our supervision and guidance.

06/04/24

Prof. (Retd) SUBBA RAO
(Research Guide)

Prof. (Retd) ARKAL VITTAL HEGDE
(Research Guide)

Vanja K
6.4.24

.....

Chairman - DRPC
Department of Water Resources and Ocean Engineering
National Institute of Technology Karnataka, Surathkal

ACKNOWLEDGEMENT

I express my deep sense of gratitude to my research supervisors **Prof. Subba Rao** and **Prof. (Retd.) Arkal Vittal Hegde,** Professors Department Water Resources and Ocean Engineering, NITK for their encouraging, logical and critical suggestions during this work. The interaction and the time spent in discussions are imprinted in my memory permanently. Only with their moral support and guidance, this research work could be completed and I could publish my work in journals and conferences.

I express my deep sense of gratitude to the **Directo**r, **National Institute of Technology Karnataka, Surathkal,** for permitting me to carry out my research work and to make use of institutional infrastructure facilities.

I express my deep sense of gratitude to the **Director**, **Central Water and Power Research Station, Pune,** for permitting me to carry out my research work and to make use of institutional infrastructure facilities.

I am greatly indebted to Research Progress Appraisal Committee members, **Prof. Shrihari** of the Department of Civil Engineering and **Prof. G.S.Dwarkish**, of the Department of Water Resources and Ocean Engineering for their useful suggestions during the progress of the work.

I sincerely acknowledge the help and support of **Prof. K Varija,** present Head of the department and **Prof. B.M. Dodamani, Prof. Amba Shetty**, **Prof. Amai Mahesha, Prof. G. S. Dwarakish**, former Head of the Department, for permitting me to use the departmental computing and laboratory facilities and his continuous support in completing the work.

I express my deep sense of gratitude to the Research Scholar **Mr. Kumaran Vishwanathan, Mr. Shankara Krishna, Mr. Harikrishnan, Mr. Hithyshi A S** and **Mr. Arun Kumar** who helped me in editing of my thesis and to successfully complete my research work.

I sincerely acknowledge the help and support of all the Professors, Associate Professors, Assistant Professors and Teaching and non-teaching staff of Department of Water Resources and Ocean Engineering NITK, Surathkal, in completing the work.

I sincerely acknowledge **Mr. B. Jagadish, Mr. Sitaram, former Foreman,** Department of Water Resources and Ocean Engineering, and **Mr. Balakrishna, Literary Assistant, Mr. Anil, Mr. Ananda Devadiga, Mr. Gopal Krishna, Mr. Padmanabha Achar, Mr. Harish, Ms. Ashwini and Ms. Sweekritha** and all the non-teaching staff for their support and help during the research work.

I express my heartfelt gratitude to the authors of all those research publications which have been referred to in preparing this thesis.

Finally, I wish to express love and affection to my beloved Brothers and Sisters and my wife Shreya Ramesh, son Ujjwal Ramesh and daughter Nayana Ramesh for their continuous support and all the sacrifices they had to make.

Thanks for all your encouragement!

Ramesh N Rao

ABSTRACT

The development of a country generally depends on its per capita power consumption and hence its trade. Coastal areas are vital for developing Ports and harbours, which are to be planned and prepared properly for safely handling ships and boats for efficient trade by constructing proper protective structures. Breakwater is one such structure constructed in ocean water to attenuate the wave energy to create a tranquil region on its lee side. With the increasing demand for coastal development and the increase in the cost of construction of the conventional type of breakwater, innovative breakwaters have been developed in the last two decades. The various coastal developmental proposal, such as the size and length of the breakwater, its orientation, and sediment studies, were used to be studied in a laboratory before their implementation in arriving at an optimal solution. These laboratory studies are not only involved huge costs but also time-consuming. The advancement both in computing methods and enhancement of knowledge in using artificial intelligence technology is being applied in various fields of application and has encouraged even to tackle complex non-linear problems in coastal engineering.

The thesis aims to evaluate various computational intelligence techniques to predict the hydrodynamic performance of quarter circle breakwater subjected to wave–structure interaction with perforation on its seaside.

Computational methods such as ANN, ANFIS, SVM, and Deep learning are trained and tested for non-dimensional input parameters obtained from earlier Physical model studies for four different perforation conditions viz., S/D=2. 3, 4, and 5. The data is segregated into 70% and 30% for training and testing the network. In the case of the ANN model Levenberg Marquardt and Conjugate gradient algorithms were considered. For ANFIS, Gambel's and triangular memberships were considered. For the SVM model, Gaussian and Sigmoidal kernels were considered, and in deep learning, Decision tree and Deep forests were studied. Model performance Index from the statistical study is adopted for evaluating the performance of each model and suggesting the best model for the prediction.

The experimental study is very robust and efficient in handling issues involving structures having arbitrary configurations in finite water depths. The physical problems are analyzed in the context of linear water wave theory. The role of several physical and numerical parameters associated with wave scattering and trapping are investigated by non-perforated and perforated

caisson structures. In addition, an attempt is made to study the effect of slotted barriers on the hydrodynamic performance of the caisson breakwater by introducing the horizontal and vertical slotted barriers in front of the caisson breakwater. Both the cases of horizontal and vertical structures are considered in different cases for handling problems of varied configurations. The numerical convergence of the solution is also analyzed using finite volume code Fluent. The numerical results are validated against the existing literature and experimental results for most of the physical problems considered in this thesis.

Keywords: Caisson Breakwater, Slotted Barrier, Perforated Caisson, Finite Volume Analysis.

TABLE OF CONTENTS

LIST OF FIGURES

LIST OF TABLES

NOMENCLATURE

d	Depth below SWL
h	Height of the structure above bed level
H_i	Incident Wave Height
H_r	Reflected Wave Height
ξ_0	Surf Similarity Parameter
T	Wave Period
L	Wave Length
B	Width of structure
H_i / gT^2	Wave Steepness
H_i / d	Relative Wave Height
d / gT^2	Relative Water Depth
R/gT^2	Relative wave Runup
S	Center to Center spacing of perforations
D	Diameter of perforation
R	Radius if quarter circle caisson
K_r	Reflection coefficient
K_l	Loss coefficient

CHAPTER 1

INTRODUCTION

1.1 GENERAL

The coast, also known as the coastline or seashore, is the area where land meets the ocean. Coasts are significant and dynamic zones in natural ecosystems, often home to a wide range of transport of passengers and goods and biodiversity. According to a United Nations atlas, 44% of the people live within 150 km from the coast . Because of their social significance and high population density, the coast is vital to many aspects of the world's agrarian and economic systems, offering humanity a variety of environmental services. However, due to climate change, which brings about more extreme weather, rising sea levels, and related issues like coastal erosion, saltwater intrusion, and coastal flooding, many communities are at risk.A coastline's perimeter cannot be delineated since the coastlines constantly keep shifting. The coastal dilemma is a measurement conundrum. As a result, it becomes necessary to build various types of protection to safeguard the coast and the communities that live there. Structures like breakwaters, groins, and spurs are frequently built to reduce the damage that ocean forces do to the land, people, and coastline. The location and function for which breakwaters are built determine their orientation. Although some structures fulfilling their roles effectively, others have not. Failure might be due to either poor structural choice, location, or design. The main purposes of a breakwater are to disperse wave energy and lessen wave action on its lee side area. It is crucial to provide a tranquil space in any port or harbour to conduct numerous transactions, including the handling of passengers and cargo, among other things. Artificial structures are to be built in several locations to shield them from wave activity and create a tranquil environment.

1.2 INTRODUCTION TO BREAKWATERS

The development of coastal engineering dates back to the neolithic era in the regions around the Mediterranean Sea, Red Sea, and Persian Gulf. When it comes to harbours, coastal engineering dates back to the emergence of maritime transportation, possibly before 3500B.C. The expansion of navigation and communication enhanced the knowledge of coastal engineering. Due to the abundance of workforce during this

time, docks, breakwaters, and other harbour works were meticulously constructed on a vast scale, much like their monuments. Some of these works are still in operation even today. Archaeologists have obtained a few of these historic harbours using contemporary survey methods. A quay for loading ships and seawalls or breakwaters was often placed in most ancient ports, just like in modern ports today Quinn et al., (1972). The ancient Egyptians built boatbasins with breakwaters on the Nile River at Zoser's step pyramid Inman et al., (1974).

1.3 FUNCTIONS OF A BREAKWATER

- Protect from wave action and create a calm water area for harbour operations by dissipating wave energy.
- To control erosion in the littoral zone.
- It can also function as a protective work from physical ocean hazards that directly impact the coastal zone.

1.3.1 Types of breakwaters

Breakwaters are broadly classified as (i) Rubble mound breakwaters, (ii) Vertical wall breakwaters, (iii) Composite breakwaters, and (iv) Special type breakwaters.

1.3.2 Rubble mound Breakwater:

Conventional breakwater is generally constructed using huge quarry stones in layers. The innermost layer, known as the core, consists of finer material to minimize the transmission of wave effect on the other side. No skilled construction workers are needed for the purpose.

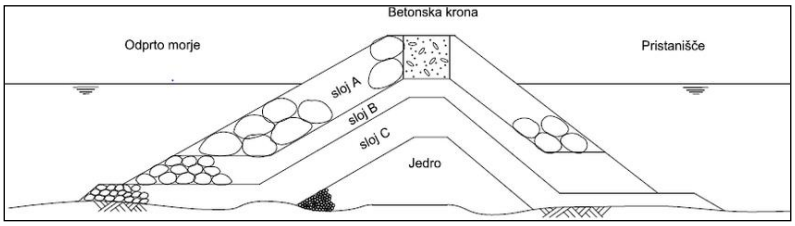

Figure 1.1 Cross section of Rubble Mound Breakwater
(Source: Cehovin and Zagar, 2019).

1.3.3 Vertical breakwaters

These breakwaters are huge concrete blocks, gravity walls, concrete caissons, rock-filled timber cribs, and concrete or steel sheet pile walls. Vertical wall structures are used as breakwaters, seawalls, and bulkheads in harbours. The vertical breakwaters are designed to prevent the incident wave and act as a mooring platform. The Source of wave energy may damage the foundation of the structure and cause failure.

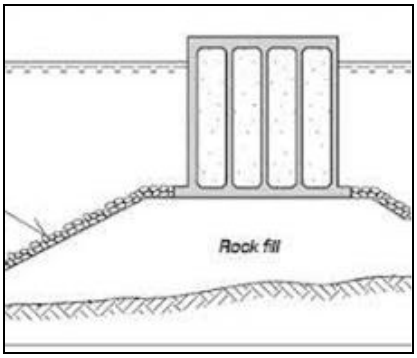

Figure 1.2 Vertical composite caisson Breakwater
(Source: Alexandre Maia and Rodrigues 2017).

1.3.4 Composite breakwaters

A composite breakwater is a vertical monolithic structure on a rubble mound base. The rubble base strengthens the foundation of the composite structure, and the upright portion offers to moor. Generally, composite breakwaters are constructed in deep water, where quarry stones are readily available.

Figure 1.3 Composite Breakwater
(Source: Prashanth et al., 2014)

1.3.5 Distinctive kind of breakwaters

Distinctive kind of breakwaters are mainly classified into two categories. i.e) conventional breakwaters & floating types of breakwaters. All conventional breakwaters are gravity type of breakwaters, and floating types of breakwaters are such as curtain wall, sheet pile, horizontal plate, and pneumatic type breakwaters are considered non-gravity types. Based on the mobility of the structure, breakwater can be further classified intoPermanent breakwater and Temporary breakwater. A Quarter-circle breakwater (QBW) can be utilized at shallow depths and relocated if necessary. Because of their lesser weight, these structures can also be constructed on a weaker foundation.

1.3.6 Floating breakwaters

Floating breakwaters are an alternative solution to protect an area from wave attack compared to the conventional breakwater in coastal areas with mild wave conditions. They have been increasingly used at small craft harbours, marinas, or, less frequently, the shoreline, aiming at erosion control. Some of the conditions that favour floating breakwaters are:

- Floating breakwaters might be a proper solution where weak undulations prevail.
- Conventional breakwaters are often more expensive in water depths of more than 6 m.
- Interference is minimum with Floating breakwaters for watercirculation and fish migration.
- Floating breakwaters can be removed and towed to protected areas if ice formation is a problem. They may be suitable for areas where summer anchorage or moorage is required.
- Floating breakwaters can usually be rearranged into a new layout withminimum effort.

Types of floating breakwaters:

Floating breakwaters are commonly divided into four general categories, viz., Box, Pontoon, Mat, and Tethered float.

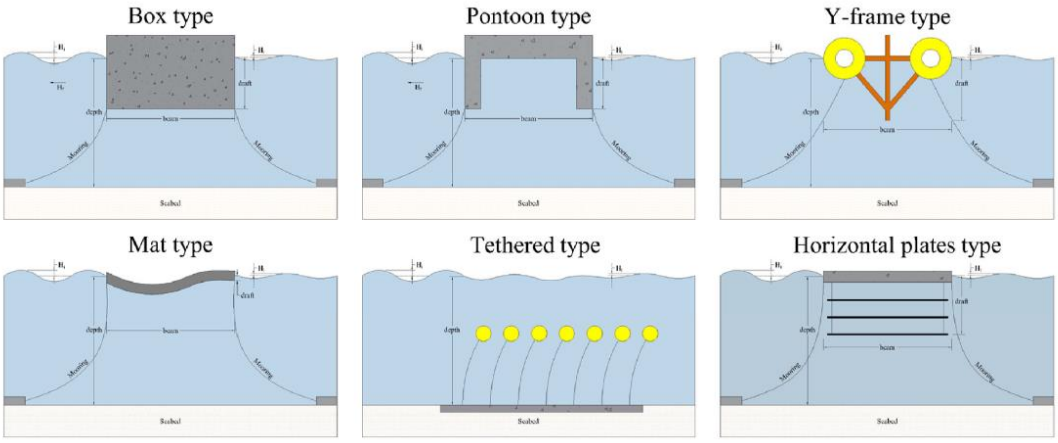

Figure 1.4 Floating Breakwater

(Source: Mario Lopez, 2022)

1.4 CLASSIFICATION OF CONCRETE CAISSON BREAKWATER

Concrete caisson breakwaters are classified depending on their shape:

i. Semi-circular breakwater and

ii. Quarter circle breakwater

These caisson breakwaters are composite breakwaters resting on a rubble mound base. The objective of Caisson breakwaters is to dissipate the incident wave energy and creates tranquility on its lee side. These structures can be fabricated and placed where the foundation is weak, and construction of a conventional breakwateris uneconomical.

The Semi-Circular Breakwater (SBW) (Fig. 1.5) has a semi-circular-shaped low caisson founded on a rubble mound. These are cast as pre-stressed concrete elements and can be transported easily. Since the caisson is hollow, the required material is considerably less, hence its weight. Due to better stability against wave action and a curved feature, it can serve well as a coastal protection structure.

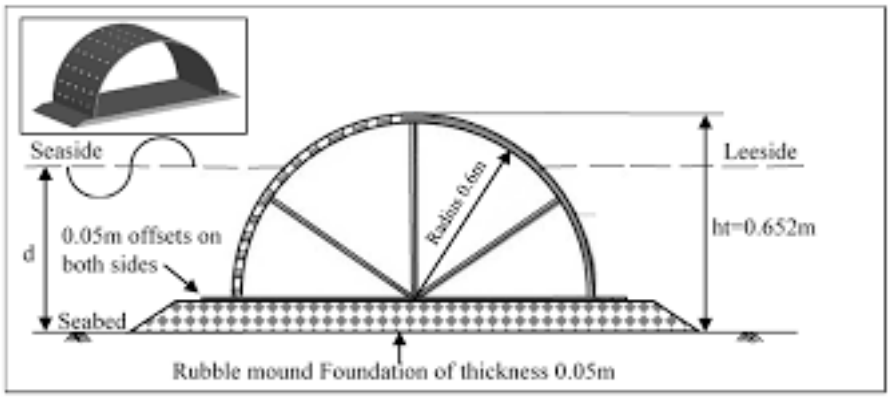

Figure 1.5 Cross section of a Semi-circular Breakwater (Source: Gomes et al., 2020)

1.4.1 Advantages of the semi-circular breakwater

- Wave force acting on a semi-circular breakwater is considerably less because of its shape.
- The resultant due to overturning movement passing through its Centre.
- Force acting on the structure is uniform and hence more stable.
- Suitable at locations where the soil is week.

A QBW is an improvement over a semi-circle breakwater first proposed by Xie et al. (2006). QBW consists of a rear vertical wall, a horizontal bottom, and a quarter-circular surface facing incident waves that make up the superstructure placed on a base of rubble stones and also offers the same benefits as SBW. The most important benefit of QBW is the reduction in the material required for construction and hence the cost. Among the several available breakwaters, QBW is advantageous in the case of minor port and fishing harbours and shore protection works. In the case of QBW, wave energy is reduced because of wave Reflection from the structure and its porosity.

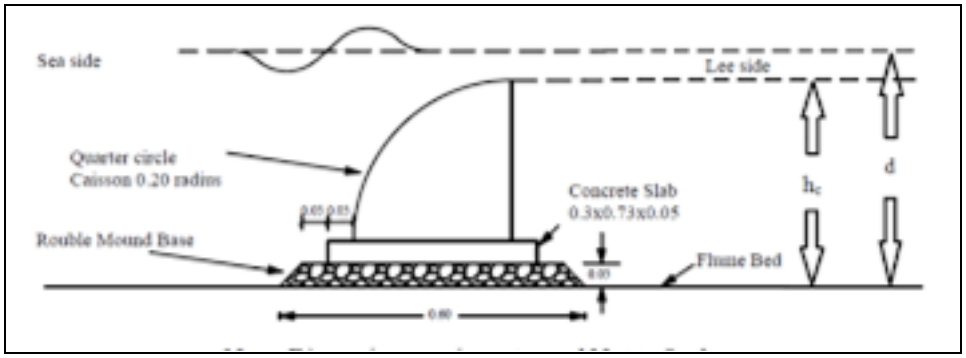

Figure 1.6 Cross section of a QBW (Source: Binumol et al., 2017)

1.4.2 Advantages of quarter circle breakwater

- Quarter circle breakwaters are economical compared to other types of breakwater structures.
- It can be constructed in poor soil conditions and easily re-oriented, removed, and replaced.
- These are more aesthetically pleasing than fixed structures.

1.5 HYDRAULIC PERFORMANCE OF QUARTER CIRCLE BREAKWATER

Due to wave structure interaction, the hydraulic behavior of a perforated QBW is significant. Many times, clapotis are formed because of the interaction between the incident and the source of the wave and hence the instability of small boats in the region. Also, the energy released during Reflection and the turbulence created in and around the pores results in local sediment movement. It is essential to understand the processes because of Reflection and porosity. Different soft computing techniques such as Artificial Neural Networks (ANN), Artificial Neuro-Fuzzy Inference Systems (ANFIS), Support Vector Machine (SVM), and Deep Learning are adopted in the present study to forecast the Reflection coefficient and loss coefficient due to the porosity of a QBW. The data required for the present study was collected from Binumol et al. (2017), who conducted physical model studies at the Marine Structures laboratory, NITK, Surathkal.

1.6 SOFT COMPUTING TECHNIQUES

In recent years, much of the field of computational Intelligence (CI) methods has evolved to address various problems effectively. Soft computing is one such method involving machine learning, fuzzy logic, and Bayesian statistics. Soft computing methods can be applied independently or combined to solve complex non-linear problems. Since most coastal engineering problems are complex and non-linear, these can be addressed effectively and efficiently by soft computing.

Forecasting of the Reflection coefficient and loss coefficient associated with QBW using various soft computing techniques is discussed in the succeeding chapters. There have been quite a several researchers who have applied soft computing to predict various aspects like wave-runup, transmission, stability, and damage of breakwater

(Dwarakish et al. 2016). In recent years, many researchers have studied the behavior of various types of breakwaters by applying soft computing methods. The literature survey indicated that very few studies had been taken up related to QBW and sparsely applied the soft computing method to forecast the hydraulic parameters. The present study attempts to apply ANN, ANFIS, SVM, and Deep learning to predict the Reflection and loss coefficient and compare the result from the model performance index from statistical analysis.

1.7 SCOPE OF THE PRESENT INVESTIGATIONS

Breakwaters are constructed and are bring used over centuries. These structures are continuously studied to improve their performance and economize their cost by changing their shape and design to meet the requirement of the situation. At the beginning of the 21st century, due to the increase in demand for coastal development and hence the construction of protective structures like breakwaters increased considerably. The material required in constructing a conventional breakwater is very huge. To optimize material requirements and economize the cost of breakwaters, where conventional breakwaters can be avoided, researchers conducted studies on caisson breakwaters. Quarter circle breakwater (QBW) is a new type of caisson breakwater that has evolved in recent times. These breakwaters are of low weight, have perforation on their curved surface, require less material, can be fabricated/cast on the surface, and can easily be transported and placed at the desired location. Most of the studies so far are conducted in a laboratory on QBW to understand the wave effect on these structures.

For designing a QBW requires details such as a change in water levels, Wave step ness, wave Reflection characteristics, wave run-up and run-down, etc. There are no mathematical models or empirical relations readily available to calculate these parameters. To meet the design requirement each time, laboratory studies are to be taken up, which are tedious, time-consuming, and uneconomical. To overcome this limitation, in the present work, an attempt has been made to predict the hydrodynamic performance of a sea-side perforated QBW using various CL techniques and evaluate its performance statistically, and to suggest the most suitable algorithm.

1.8 BRIEF OVERVIEW OF THE THESIS

This thesis consists of seven chapters, and each chapter's content is given below.

In Chapter 1, a basic introduction and motivation behind the current work are presented. And introduces the history of breakwaters and types of breakwaters with special emphasis on artificial Intelligence (AI) / Computational Intelligence models (CIM) of breakwaters. Further, it also includes the need and scope of the present research work.

Chapter 2, the relevant literature survey to the present work, is performed thoroughly, followed by a brief introduction to applications of computational intelligence in coastal/ocean engineering, which in turn leads to the motivation and objectives of the present research work.

Chapter 3, Details of the present experimental investigation, including the details of laboratory conditions carried out by earlier investigators and experimental data utilized for developing AI models for the present work, are explained.

Chapter 4 deals with the materials and methods: Theoretical background about AI models, such asANN, ANFIS, SVM, and Deep learning methods to forecast the wave reflectioncoefficient and loss coefficient of QBW, are discussed in detail.

Chapter 5 elaborates on the prediction of the reflection coefficient and the results obtained from various CI models in the prediction of the wave reflection coefficient.

Chapter 6 discusses the prediction of the loss coefficient (K_l) based on the energy balance equation and the predicted values from various CI models.

Chapter 7 presents the summary and conclusions of the work done in the thesis. The contribution from the present study, limitations, and future scope are also presented in this chapter.

The literature work contributed to the present study is presented in the reference section. A list of publications based on the present research work and a brief resume is given at the end of the report

CHAPTER 2

LITERATURE REVIEW

2.1 GENERAL

Breakwaters are structures constructed to withstand and dissipate dynamic wave energy to create a tranquil region. Due to increased demand to improve and develop the coast across the globe and improvements in technology, innovations are being madeto evolve different types of breakwaters. Quarter-circular Break Water (QBW) is a new type of breakwater developed in the People's Republic of China (2006) based on the semi-circular breakwater concept. QBW is hollow, requires fewer materials, and hence they are quite light in weight, suit where soil conditions are poor,can easily be cast on land and placed at the desired location, and are cost-effective andaesthetically pleasing. This chapter details a critical review of the current state of knowledge of the application of soft computing techniques in coastal engineering, particularly the QBW. A rubble mound breakwater acts as a barrier for the movement of fish, bottom-dwellingmicro-organisms. Apart from this, the breakwater restricts water circulation, affecting water quality and sediment movement in the nearby region.

Jarlan (1961) introduced a front perforated wall breakwater with a wave energy dissipating chamber and a solid back wall. A considerable amount of attenuation of incoming waves was achieved by the generation of eddies and turbulence near the perforations. Isaacson (1991) made an effort to quantify wave reflection caused by a breakwater subjected to regular waves. He explained three techniques utilizing two and three fixed probes to offer precise answers for the incident wave height, the reflection coefficient, and the phase of the wave train. They also compared the range of applications and validated the accuracy of methods used in the study. Also, they made recommendations for relative probe spacing while using three-probe procedures to prevent situations where the methods might fail.

Tanimoto and Goda (1992) explained the global history of breakwater construction and its testing. Also, introduced recent developments in breakwater construction in Japan. From the first natural stone breakwaters to the more modern ones with higher stability against waves. They also stated in Japan, there has been interest in both the construction

of complex caisson breakwaters and the rebirth of the archaic berm breakwater in the recent past.

Jang (1993) implemented the architecture and learning procedure underlying the Adaptive Network-based Fuzzy Inference System (ANFIS), which is a fuzzy inference system in the framework of adaptive networks. He proposed ANFIS to construct an input-output mapping based on both human knowledge (in the form of fuzzy if-then rules) and stipulated input-output data pairs. He employed ANFIS architecture to simulate nonlinear functions, identify nonlinear components online in a control system, and predict a chaotic time series. Compared the results with artificial neural networks and earlier work on fuzzy modeling.

Tanimoto and Takahashi (1994) studied the development of breakwaters in Japan throughout the years, and current vertical breakwater design techniques were explored in terms of wave forces and breakwater stability. They considered Goda's formula for the construction of breakwaters since it reliably forecasts the design wave forces under the majority of vertical breakwater circumstances. Under some circumstances, the upright part is subjected to high impulsive forces brought on by the action of breaking waves. They discussed the stability of armour units under such situations and the bearing capability of rubble mound foundations.

Mase et al. (1995) investigated the use of a neural network to interpret test data from a model testing for the stability of rubble-mound breakwaters. They used the stability number, the damage level, the number of attacking waves, the surf-similarity parameter, the permeability parameter, the dimensionless water depth in front of the structure, and the spectral shape parameter to determine the stability of rock slopes. They observed the damage levels of another part of the data source by Van der Meer (1988) and Smith et al. (1992).

Shinsuke et al. (1996) extensively tested the world's first semicircular caisson breakwater, which was constructed in Miyazaki Port in Japan. Evaluated several types of data, including wave pressures placed on the caissons and stresses produced in the structural elements collected since 1993. By carrying out the field study, they also confirmed the stability and structural member safety of semi-circular caisson breakwaters in a harsh sea environment.

Sundar and Raghu (1997) performed laboratory tests on a semi-circular breakwater having no perforations exposed to monochromatic waves. They reported that the wave Reflection coefficient (Kr) varied with relative water depth (hw/L).

Deo and Sridhar Naidu (1999) offered a straightforward strategy for creating a point forecast of waves in real-time based on the current observation of waves at a spot using the neural networks technique. They compared the results of neural output and autoregression models.

Deo et al. (2001) investigated the use of neural networks for wave prediction by constructing a three-layered feed-forward network to acquire significant wave heights and average wave periods in open, wide locations and deep water, using wind speeds as input.

Mandal et al. (2001) developed a back propagation neural network model using quick learning to predict the time series of hourly tides. They concluded that the correlation coefficient between predicted tides and measured tides was close to one.

Sundar and Subbarao (2002) conducted experiments to study the hydrodynamic pressure forces on a quadrant, front-face pile-supported breakwater for three different water depths and plotted dimensionless force with a reflection coefficient.

Ultsch and Roske (2002) adopted self-organizing feature maps to study sea level prediction using a neural network model and compared the results obtained from six different models, including statistical, nearest neighbor, hydrodynamic, persistence model, and verbal forecasts.

Deo and Jagdale (2003) developed a neural network model and trained it with a deterministic and random component for predicting breaking waves, which was validated with laboratory observations.

Londhe and Deo (2003) constructed a neural network model to calculate wave heights along a dredging approach channel that leads to the harbor's entrance. They used the data from two port areas in India for the study. They tested the network capacity to carry out wave tranquility investigations using various error criteria and adopted a number of learning schemes and search procedures to choose the optimal training for the network.

Sunder and Subbarao (2003) performed the physical model tests for different S/D (pile spacing/pile diameter) and relative water depth on quadrant front face pile supported

breakwater. They concluded that the K_r and K_l are proportional to the depth of water (d) and scattering parameter (Ka=2Πa/L).

Yuan and Tao (2003) used a computational model based on a combination of the boundary element method (BEM) and the finite difference method (FDM) to study the wave forces acting on submerged, alternately submerged and emerged semicircular breakwaters. They used a dissipative tool to model the energy loss that occurs when a wave breaks close to the breakwater and reported that the results of the calibration and verification were in agreement with the experimental data.

Jeng et al. (2004) examined different strategies for predicting the maximum liquefaction depth using neural networks (NN). Suggested NN model is based on data learning knowledge rather than mechanism knowledge. They indicated that the NN model forecasts the depth of wave-induced liquefaction Using numerical examples.

Lee (2004) used a back-propagation neural network in predicting tidal levels by employing short-term measured data. To evaluate the model's performance, they used tidal-level data from Taichung Harbor in Taiwan. They concluded that the back-propagation neural network effectively predicted the long-term tidal levels, according to comparisons with conventional harmonic approaches.

Makarynskyy (2004) made an effort to enhance wave short-term projections by applying artificial neural networks. They trained and evaluated these networks in two different ways using hourly measurements of major wave heights and zero-up-crossing wave times from two sites offshore the Irish Sea and Atlantic coastlines.

Mohandas et al**.** (2004) predicted the mean daily wind speed Support Vector Machine (SVM) and Multi-Layer Perceptron (MLP) models of Madinah City, Saudi Arabia. They compared the performance of both models by computing various statistical parameters and reported that SVM performed better.

Kazeminezhad. et al. (2005) compared the effectiveness of the Coastal Engineering Manual (CEM), and ANFIS approaches for forecasting wave characteristics. For this purpose, they used a 2003 data set of over-water wind data and fetch-limited wave data collected from deep-water locations in Lake Ontario. They indicated that ANFIS results were better since the wave height and peak spectral period were overestimated by CEM.

Karla et al. (2005) studied the mapping of remotely sensed deep-water waves with coastal waves by the radial basis function (RBF) type of artificial neural network. They

estimated the major wave heights at a nearshore site using significant wave heights at many places along a track parallel to the coast. They observed that the satellite data require 'local tuning' similar to that carried out in the RBF before being used in network calculations and emphasized the value of creative methods for calibrating networks using a particular amount of data.

Mandal et al. (2005) adopted backpropagation neural networks (BNN) in estimating ocean wave characteristics using theoretical Pierson-Moskowitz spectra as well as observed ocean wave spectra. They compared the results obtained between the Scott and NN spectra.

Naithani and Deo (2005) estimated the wave surface density from a wide range of frequencies using H_s, T_z, Spectral width, and peakedness parameters. They also compared the ANN predicted values with values obtained from JONSWAP and Scott's spectra.

Subba Rao & Mandal (2005) estimated the wave parameters from cyclone-generated wind fields using a neural network technique. For their study, they used three algorithms: R-prop, Quick-prop, and super-SAB. At the same time, estimating wave heights and periods used (i) the difference between central and peripheral pressure, the maximum wind speed, and the speed of the cyclone's forward motion as parameters. (ii) Wave heights and durations act as output nodes, while wind speed and fetch act as input nodes. They used eleven cyclones' data between 1962 and 1979 passed over India's southern east coast and were considered for the study.

Yagci et al. (2005) evaluated the damage ratio of a breakwater using three different artificial neural network techniques and a fuzzy model using mean wave period, wave steepness, significant wave height, and breakwater slope. They recorded that the experimental values were quite well estimated by all artificial neural network techniques and fuzzy logic models. Also mentioned that the findings of the testing stage were noticeably better than those of the traditional multi-linear regression approach.

Lee (2006) carried out a study on storm surge forecasting of Taiwan's Jiangjyun stations by applying NN. He evaluated the model results by using the input variables viz., wind velocity, wind direction, pressure, and tidal level and found that NN can efficiently anticipate storm surges.

Mandal and Prabaharan (2006) used a recurrent neural network (RNN) with the rprop method, a type of artificial neural network, to anticipate waves. They used measured ocean wave data at Marmugao, west coast of India for their study. They concluded that RNN with rprop produces better outcomes during wave forecasting.

Rajasekaran et al. (2006) utilized relatively brief observations for training functional and sequential learning neural networks for tide prediction, which usually does not require harmonic parameters. They anticipated three days' tide and one month's tide using oneday of observation and compared the result with the results given by Tsai and Lee.

Bateni and Jeng (2007) made an effort to create an ANFIS model that can anticipate the depth and width of scour for a cluster of piles supporting a pier. They considered dimensional parameters like wave height, wave period, and water depth and nondimensional numbers like the Reynolds number, the Keulegan-Carpenter number, the Shields parameter, and the sediment number as two different sets of data. They reported that the results obtained from ANFIS outperformed the results obtained from using dimensional data were current empirical equations.

Han et al. (2007) discussed SVM application across the bird creek watershed and touched on several key challenges in the creation and use of SVM in flood forecasting. Also demonstrated how to choose the best choice out of a vast number of different input combinations while using SVMs. They compared several benchmarking, including the Transfer Function, Trend, and Naive models, and stated that SVM outperformed all of them in the test data set while requiring a significant amount of time and effort.

Karla and Deo (2007) adopted an artificial neural network (ANN) to estimate equivalent values of three parameters, i.e., significant wave heights, average wave period, and wind speed at various points along a satellite track parallel to a coastline, and used data from the TOPEX satellite's deeper locations on wind and wave information to a chosen coastal spot. They concluded that statistical homogeneity of the data sets affects the reported accuracy of the results and also noted that the difficulty of modeling wind speeds that are usually connected with extremely significant variability in their magnitudes was resolved.

Matthew Browne et al. (2007) provided a thorough assessment of two data-driven techniques for predicting waves near-shore, i.e., linear and ANN model, and contrasted

them with a more conventional spectral wave simulation model (SWAN). They evaluated their performance using information acquired over a 7-month period from a total of 17 near-shore sites with diverse geology and bathymetry all over the Australian continent.

Tseng et al. (2007) applied Back-Propagation Neural Network (BPNN) for the typhoon surge forecasting model to choose a more accurate forecasting model using typhoon surges and local meteorological conditions. They considered twelve of the sixteen typhoon occurrences that occurred between 1993 and 2000 at Ken-fang Tidal Station near the coast of northeastern Taiwan, together with the related typhoon surges and local meteorological conditions for their study. They reported that typhoon surge forecasting data at the Ken-fang tidal station was analyzed, and the findings revealed that Model D, which comprises 18 input parameters, performs better and is a good BPN-based model for typhoon surge forecasting.

Gian Mario Beltrami (2008) compared the algorithm created as part of the Deep-ocean Assessment and Reporting of Tsunamis (DART) program run by the U.S. National Oceanic and Atmospheric Administration to the structure they adopted an algorithm based on the use of ANN to be implemented in the software of bottom pressure recorders (BPRs) for the automatic, real-time detection of a tsunami within recorded signals. They examined the effectiveness and performance of both the algorithms using both simulated and real-world time series and reported that the ANN algorithm's results had improved the performance of detection.

Jiang et al. (2008) conducted both numerical and laboratory studies on SBW and QBW to understand hydrodynamic performances. They reported that relative values were close under the same conditions on comparing Reflection coefficients. Also mentioned that the relative free board is proportional to the Reflection coefficient.

Kemal Günaydın (2008) considered both ANN and regression techniques in forecast monthly mean significant wave heights using meteorological data. He developed seven distinct ANN models and used varied ratios of monthly mean wind speeds, sea level pressures, and air temperature as input to predict wave height. He reported that ANN results were superior as compared to another model.

Liang et al. (2008) applied BPNN) and suggested an iterative multi-step prediction method and periodic analysis. They mentioned that the BPNN model can forecast

across stations accurately the tidal level independent of the type of tide at different locations. They constructed three BPNN (1) Weather-Data-based Neural Networks model for set up and set down. (2) Difference Neural Network model for augmenting tidal record. (3) Minus-Mean-Value Neural Network model for matching prediction between tidal gauge stations, based on the non-stationary nature of hourly tidal level, to improve the accuracy of prediction.

Londhe (2008). demonstrated a soft computing method for a real-time estimate of missing wave heights at a certain site using wave heights at other places. He created a network of sic buoys in the Eastern Gulf of Mexico, sing soft computing methods tools such as ANN and Genetic Programming (GP). The estimated the wave height at the sixth station by considering the wave heights at the remaining five locations. The accuracy of prediction was evaluated using various statical parameters. During severe conditions, the GP model outperformed the ANN model. He compared the results of these models with WAVEWATCH III, a large-scale continuous wave forecasting system results.

Surabhi Gaur and Deo (2008) adopted the genetic programming for wave forecasting by considering wave rider buoy observations from two different parts of the Gulf of Mexico. They considered a sample span of 15 years. From the results, they concluded that GP can be made used for forecasting various ocean parameters.

Zamani et al. (2008) constructed the Instance-Based Learning (IBL) and ANN models to estimate significant wave heights using buoy measurements. Their study indicated that the ANN results are better than the IBL results and closely in agreement with the measured data.

Dinakaran et al. (2009) conducted physical model studies on the semi-circular breakwater and reported 11% as optimum perforations for perforated SCB. They also mentioned that increased perforation results in decreased wave Reflection, and the wave loss is proportional to the height rubble mound Base.

Mahjoobi and Mosabbeb (2009) used the wave and wind data collected from deep Lake Michigan sites to predict significant wave height (Hs). They compared the obtained results from the result of other models, such as ANN, MLP, and RBF, and reported that SVM results were more precise and accurate.

Zanaganeh et al. (2009). used the clustering and rule base parameters of a hybrid genetic algorithm-adaptive network-based FIS (GA-ANFIS) model to forecast wave characteristics such as significant wave height and peak spectral period in Lake Michigan using data from the years 2001 and 2004. They compared the results with adoptive neuro fuzzy inference system (ANFIS) and coastal engineering manual (CEM) results and concluded that gentitic algorithm (GA) GA-ANFIS results were superior.

Hegde et al. (2010) studied the wave run-up and run-down for different incident wave heights H, wave times T, water depths d, and spacing (S) to diameter (D) ratios of perforations (S/D) of a semicircular breakwater. They reported that relative wave run-up increases and relative wave run-down decreases with increasing wave steepness (H_i/gT^2), and the depth parameter (d/gT^2) increases as the relative wave run-up and wave run-down increases.

Jiao et al. (2011) conducted laboratory studies on both emerged and submerged QBW and concluded that wave energy loss is higher in the emerged condition than in the submerged condition. Also, they stated that the Reflection coefficient increases with reflected wave height to incident wave height (K_r/Hi).

Jabbari et al. (2011) applied MLP with a back propagation network (BPN) to sketch the input-output system in an attempt to predict the scour at the head of the vertical wall breakwater. They used two sets of data such as dimensional (breakwater head diameter, wave height, wave period, angle of attack, and velocity) and non-dimensional (Reynolds number, Sheilds parameter, and Keulegan- carpenter). They reported that model results were more accurate than the results obtained from using empirical relation in predicting the scour depth at the head of the vertical breakwater.

Patil et al. (2011) used a neuro-fuzzy-based approach for predicting wave transmission (Kt) of Horizontally Interlaced Multilayer Moored Floating Pipe Breakwater (HIMMFPB). They carried out the principal component analysis to check the influence of each input parameter before feeding it to the network. They compared the results of the ANFIS model with the ANN model and concluded that the ANFIS model results were superior.

Shi et al. (2011) carried out the physical model study to examine the resolution Reflection and circular surface Reflection and transmitting performance due to QBW-subjected regular and random waves. They compared the results obtained from

laboratory studies and numerical studies and concluded that the effect from irregular waves was stronger than from regular waves.

Harish et al. (2014) developed an ANFIS model using experimental data set to predict the damage level of berm breakwater. They computed various statistical parameters like root mean square error (RMSE), coefficient of correlation CC and ScatterIndex (SI) and, based on this result, concluded that ANFIS could be used as an effective tool in predicting the damage level of a breakwater.

Koç and Balas (2012) created a fuzzy neural network (FNN) model to predict the stability number of rubble mound breakwaters. The adopted hybrid genetic algorithm-based fuzzy neural network (or "HGA-FNN") and the genetic algorithm-based fuzzy neural network (or "GA-FNN"). As reported by them, HGA-FNN has a higher predictive performance than GA-FNN and has a lot of promise for determining the stability of coastal structures.

Mandal et al. (2012) studied ANN, SVM, and ANFIS models to predict the damage levels for non-reshaped berm breakwater. They concluded that the results of the study indicated that the ANFIS model's predictive capability is better when compared with ANN and SVM in predicting damage levels.

Patil et al. (2012). a hybrid Genetic Algorithm tuned Support Vector Machine Regression (GA-SVMR) model was developed to estimate wave transmission of a horizontally interlaced multilayer moored floating pipe breakwater (HIMMFPB). They expressed results in terms of statistical parameters and compared them with ANN and ANFIS results and concluded as GA-SVMR consistently performed better with the b-spline kernel function as compared to other kernel functions.

Zanuttigh et al. (2013) developed an ANN model to forecast the wave Reflection coefficient from a variety of coastal and port structures. They used over 6000 data sets which include smooth, rock, and armour unit slopes, berm breakwaters, vertical walls, low crested structures, and oblique wave assaults. They selected 13 parameters to represent the physics of the Reflection process based on sensitivity analysis, the algorithms, and accordingly. Selected the input elements. They concluded as the average root mean square error was very small.

Hegde and Naseeb (2014) studied the transmission properties of scaled-down semicircular breakwater (SBW) physical models of various radii (R) for different

submergence ratios (d/h_c). They mentioned that for various submergence ratios, the transmission coefficient increases as the incident wave steepness increase.

Harish et al. (2014) adopted Support Vector Machines (SVM) and Genetic Algorithm (GA) to forecast the degree of damage to non-reshaped berm breakwaters. They arrived at the ideal kernel parameter for the support vectoe machine (SVM) model from genetic algorithm (GA), computed various statistical parameters, and compared the results of the SVM and GA-SVM models. From the comparison of results, they concluded that GA-SVM performs better than SVM models.

Rushi Goyal et al. (2015) proposed a stepwise regression strategy based on MATLAB to construct prediction models for the quarter circle breakwater (QBW) transmission coefficient. They arrived at a relation between the transmission coefficient (K_t) and independent variables such as wave height (H), wave period (T), and sea depth(d) using the stepwise approach of multi-linear regression.

Hegde et al. (2015) examined stability against sliding of a seashore perforated non-overtopping QBW model in order to determine how the dimensionless depth parameter varies with different values of incident wave steepness. They created a nomogram to calculate the sliding stability of the breakwater.

Binumol et al. (2015) conducted physical model studies of impermeable and sea-side perforated QBW with three different radii and S/D (spacing to the diameter of perforations) ratio. They reported that as the wave height increases, an increase in wave energy results in more wave run-up and less run-down. Also reported that as the water depth decreases, the effect of curvature is more pronounced, resulting in lower run-up and hence more run-down.

Harish et al. (2015) used the GA-SVM model by taking various non-dimensional parameters such as wave steepness (H/Lo), surf similarity, relative berm position by water depth (h_B/d), armour stone weight (W_{50}/W_{50max}), relative berm width (B/Lo), and relative berm location (h_B/L_o) as input to the network to assess the extent of damage of a non-reshaped berm breakwater.

Harish et al. (2015) applied SVM and PSO-SVM hybrid models to forecast the degree of damage to berm breakwaters that have not been altered. They compared the results with various statistical petameters and concluded that the PSO-SVM model with polynomial kernel function performed well.

Hodaei et al. (2016) conducted a series of tests in a towing tank to examine how the curvature of perforated plates affects the wave reflection coefficient (K_r). The parabolic equation $y= - x^2$ was used by them in modifying the curvature of a perforated plate by rotating a perforated plate about its origin and computing the Reflection coefficients using a method developed by Goda and Suzuki. They concluded that the results were better compared to the results obtained with either vertical or sloping wave absorbers. And also mentioned that the perforated plate with a curved profile was extremely effective in reducing the wave Reflection coefficient.

Koç et al. (2016) examined the potential application of genetic programming to evaluate the stability of rubble-mound breakwaters using a variety of explicit models. They made use of the experimental data from Van Der Meer's study. As per their finding genetic programming model outperformed Van Der Meer's stability equation in predicting accuracy.

Binumol et al. (2017) conducted laboratory experiments on a perforated QBW model with a perforation ratio (S/D) equal to 4. They selected the dimensions such that at any given condition, the structure will be emerged conditions. They concluded the Reflection coefficient increases with an increase in wave steepness and decreases with an increase in water depth.

Jiang and Zhang (2017) analyzed the features of wave loading on submerged circular-front breakwaters caused by irregular waves in a laboratory. They used the RANS-VOF model in investigating local hydrodynamic disturbance due to submerged structure and its effect on the structure. They concluded that as compared to submerged quarter circle breakwater, the effect was more on semicircular breakwater by wave-induced vortices at the structure.

Pourzangbar et al. (2017b) attempted to study maximum scour depth at breakwaters caused by non-breaking waves using GP and ANNs. They used 95 data sets collected from published literature for the purpose. They mentioned that the GP model results outperformed the results obtained both from the ANN model and the existing empirical relations.

Geetha et al. (2017) constructed the ANFIS model to predict the effect of structure and wave characteristics on the hydraulic performance of the reef structure of a tandem breakwater. They used experimental data to train ANFIS models, expressed their results

in terms of statistical parameters, and reported that ANFIS could be an efficient tool in predicting the performance of reef structures.

Hegde et al. (2018) studied a two-dimensional monochromatic wave flume to ascertain the crucial (minimum) weight needed to prevent the sliding of an emerging seashore perforated semicircular breakwater model. They used non-dimensional parameters acquired from a dimensional analysis using Buckingham's theorem to graphically record fluctuations.

Kuntoji et al. (2018) studied the wave transmission coefficient through a submerged reef tandem breakwater by soft computing techniques like Particle Swarm Optimization (PSO-ANN) and PSO-SVM models. They compared the results from both models and expressed them in terms of statistical parameters, and concluded that PSO-SVM outperformed the PSO-ANN model.

Suman et al. (2019) developed a novel methodology to predict the Reflection coefficient (K_r) of seaside perforated semicircular breakwaters under low wave heights, using ANFIS and ANN techniques to predict below the data range. They also reported that the predictions made by the ANFIS model outperformed the ANN model. According to a literature review on computational intelligence applications in coastal engineering, many researchers have used ANNs to forecast ocean wave parameters and studied seabed liquefaction, storm surges, damage to coastal structures, and wave transmission. For the calibration and validation of neural network models, several researchers employed field data, experimental data, and data produced by numerical models.

2.2 PROBLEM FORMULATION

Due to the complexity and ambiguity of numerous variables and their effects are exceedingly complicated on the breakwaters. As a result, choosing a specific type of breakwater is challenging since it depends on several variables, including environmental considerations, cost and utilization, etc. In recent years, quarter-circle breakwaters are becoming popular since they require less construction material, are cost-effective, are simple to handle, can be constructed on weak soil foundations, and they aesthetically better. It is clear from the literature review that few studies have been done on QBW and are in the primitive stage. The energy dissipation process in the case

of a quarter-circle breakwater depends mainly on structural parameters and porosity. There are no mathematical models or empirical relations readily available to quantify the effect on reflection and loss due to the wave-structure interaction phenomenon. Since the studies related to QBW are in the primitive stage and also due to the nonlinearity involved, no simple mathematical model is available for predicting wave reflection and loss parameters. Doing physical model studies every time to assess the hydrodynamic parameters is uneconomical and time-consuming. The literature review also shows that complex non-linear problems can also be solved successfully using computational intelligence models (CIM). By considering the above facts, efforts have been made to predict the reflection and loss coefficients of QBW by applying various CIM. The data used in the study is retrieved from earlier studies conducted in the Marine Structures laboratory at NITK, Surathkal (Binumol, 2017).

2.3 RESEARCH OBJECTIVES

The present study aims to develop computational intelligence models to predict the hydrodynamic parameters of Quarter Circle Breakwaters:

1. To predict the wave reflection coefficient K_r of an emerged quarter circle breakwater using ANN, ANFIS, SVM, and Deep Learning.
2. To predict the loss coefficient K_l of an emerged quarter circle breakwater using ANN, ANFIS, SVM, and Deep Learning.
3. To select the best soft computing model for predicting hydrodynamic parameters based on a statistical approach.

2.4 SUMMARY

In this chapter, a detailed literature review on QBW has been discussed. The literature review indicated that in the recent past, researchers have carried out laboratory investigations on semi-circular breakwater and quarter-circle breakwater. Since the studies related to QBW are in the primitive stage, no simple mathematical model is available to forecast its hydrodynamic parameters because of the complexity and non-linearity associated with wave-structure interaction. CIM is successfully used in

overcoming many coastal engineering problems involved with complexity and non-linearity. Hence, it is decided to explore and develop a CIM for predicting the hydrodynamic performance of QBW that helps practicing engineers in the field of coastal engineering when similar site conditions are encountered.

CHAPTER 3

MATERIALS AND METHODS

3.1 GENERAL

The data used in the present research work was retrieved from the wave flume studies carried out on the Quarter circle breakwater (QBW) scale model with a scale of 1:30 by Binumol et al. (2017) in the Marine Structures Laboratory, Department of Water Resources and Ocean Engineering, National Institute of Technology Karnataka, Surathkal, India. The prevailing field conditions of the Mangalore coast of Karnataka were considered while conducting laboratory studies. The single largest wave recorded off the Mangalore coast, as reported by Dattatri and the KREC study team (1994), is about 5.4 m. During the monsoon season, the wave period varied between 9 to 10 sec. However, it was a bit longer during fair weather, which may be due to less wave height (October to May). Though the tides at Mangalore are semi-diurnal, the range is about 1.6 to 1.7 m. Therefore, while conducting flume studies, wave heights in the range of 1.0 to 5.4 m with a wave period ranging from 1.4 to 2.5 s were considered. These parameters were scaled down by Binumol during her experimental study and are mentioned in Table 3.1. The results of K_r and K_l obtained from the earlier physical model study were utilized, and computational intelligence models (CIM) were developed to predict the wave Reflection coefficient (K_r) and loss coefficient (K_l) due to QBW. The experimental database was gathered, sorted, compiled, and divided into two sets to train and test the CIM.

3.2 DESCRIPTION OF WAVE FLUME

A wave flume of 50 m x 0.71 m x 1.1 m was available. One side of the flume was fitted with a glass panel for about 15.0 m to facilitate the observations and photography. It has a wave-generating chamber of 6.3 m x 1.5 m x 1.4 m at one end. The wave flaps were hinged at the bottom and are controlled by an induction motor of 11 kW having a torque of 1450 rpm. The induction motor was regulated by an inverter drive of frequency 0-50 Hz and speed ranging from 0-155 rpm. A wave of 0.08 to 0.24 m in height having a wave period of 0.8 to 4.0 s could be operated in the flume. The bed

level in the generating chamber was matched with a gradual slope with the flume bed level. A series of vertical filters dampen the disturbances caused by the generation end due to successive waves.

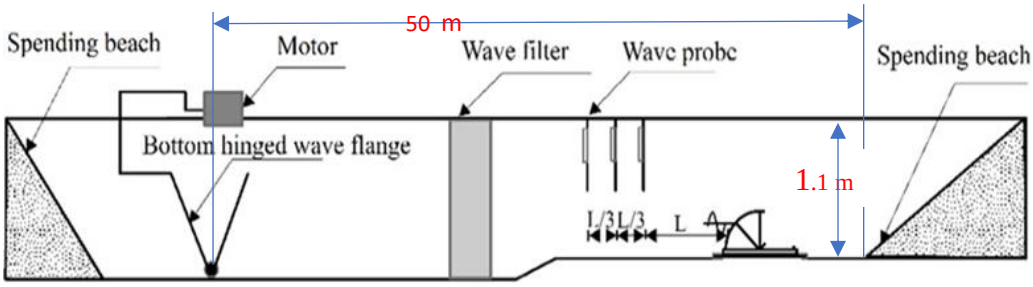

Figure 3.1 Cross-sectional View of Experimental Setup of wave flume (Not to scale)

Table 3.1 Experimental parameters with data range used in the prediction of K_r and K_l

Input parameters	Data range
Incident wave height (H_i) (m)	0.06-0.18
Wave period (T_s) (sec)	1.2s, 1.4s, 1.6s, 1.8s, 2.0s and 2.2s
Radius (R) of quarter circle caisson (m)	0.45,0.50,0.55 and 0.60
Depth (d) of water- d (m)	0.40,0.45, 0.50,0.55 and 0.60
Perforation diameter (D) (m)	0.016 m
Spacing (S) of perforations(m)	2D, 3D, 4D and 5D
The base height of the structure (h_s) (m)	0.15

Table 3.1 presents the parameters and their range considered in the experimental study for the prediction of the Reflection coefficient and loss coefficient.

3.3 TEST MODEL OF QBW

For the hydraulic performance of QBW, models were fabricated. Froud's criteria were considered for simulating the conditions in the physical model because of gravity's effect on free surface wave motion. All physical parameters were scaled to the 1:30 scale. The wave height was selected so the model won't get submerged. During the investigation, wave probes of the capacitance type were utilized. The readings are accurate to within 0.001 m. The probes recorded the incident wave properties. The

three-probe approach proposed by Issacson (1991) was used to decompose the incident and reflected waves from superposed waves recorded by wave probes.

3.4 DESIGN CONDITIONS

As reported by the KREC (Karnataka Regional Engineering College) study team in 1994, the wave conditions of the Mangalore coast were considered when the investigations were undertaken by Binumol et al. (2017). Maximum wave heights off the coast of Mangalore during the monsoon range from 4.5 to 5.4 m. Wave height during the normal weather condition barely ever rises above 1 m. During the monsoon season, the typical wave period varied from 8 to 11 s. The good weather occasionally witnesses wave periods up to 15s. The tidal variation relative to the mean sea level is roughly 1.68 m along the Mangalore coast. Consequently, a prototype design wave equivalent of 4.5 m height was considered to study the QBW.

The following procedure was followed while conducting the experimental study:

i. The models required to be tested were positioned 30 m away from the wave flap on a foundation made of stone metal.
ii. Tap water was used to fill the wave flume, and the complete experimental set-up, including the wave probes, was calibrated for every water depth.
iii. Three probe method was used to measure the incident, reflected, and superposed waves. For a given depth, the wavelength determines the probe spacing maintained at a distance of L/3. The first probe was positioned L (wavelengths) away from the structure, with L (wavelengths) between each probe.

3.5 DATA NORMALIZATION

Data normalization is the systematic process of grouping similar values into one common value, bringing greater context and accuracy to the database. Data normalization formats the data to look and read the same across all records in a database which reduces the possibility of duplication of data as illustrated in Figure 3.2 Normalizing the data formatting helps the network to get trained quickly and properly. The various parameters obtained from the experimental study were normalized between 0 and 1 by using the following equation:

$$Z_i = \frac{(x_i - x_{min})}{(x_{max} - x_{min})} \quad (3.1)$$

Where Z_i is the normalized data for the i^{th} variable, max(xi) is the maximum value of the i^{th} data point,and min(x_i) is the minimum value of the i^{th} data point.

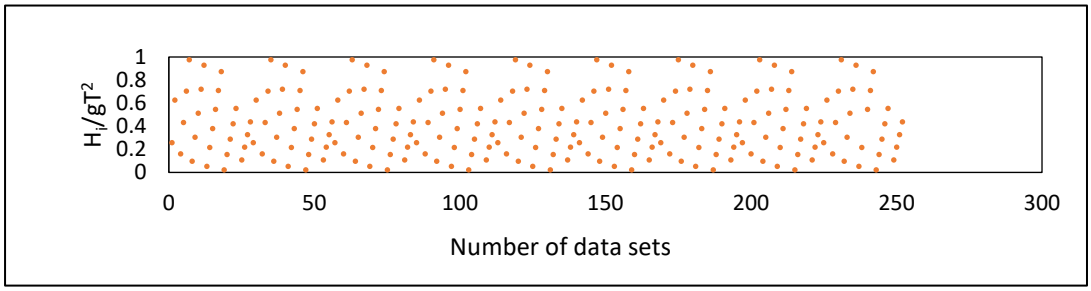

Figure 3.2 Normalized plot of wave steepness (H_i/ gT^2)

3.6 PRINCIPAL COMPONENT ANALYSIS

In Principal Component Analysis (PCA), the dimensionality of the extensive data set is reduced by changing a large number of variables into a smaller one, such that even a smaller set of data still contains most of the original information as in the large set. Sufficient precautions are to be taken while reducing the number of variables, which may sometimes miss out on original information. These smaller sets of data are easy to explore, visualize, handle, and analyze. This helps machine learning methods understand and do computations easily and faster. The following steps are involved:

i. The range of continuous variables from the data set is standardized. Sometimes, variables are highly correlated, indicating redundancy among them.
ii. Eigenvalues and Eigenvectors of the covariance matrix are considered for computing the predominant variables.

Generally, the first principal components are constructed such that the component accounts for the largest possible variance. The second component is also calculated similarly; however, it is uncorrelated with the first component, which accounts for the second-highest variance. The process continues till all the components are calculated equal to the initial number of variables.

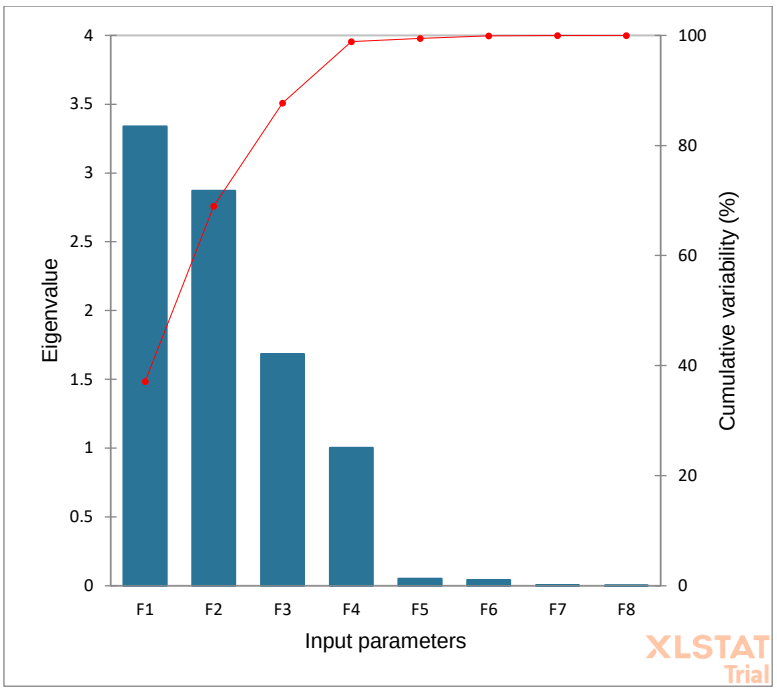

Figure 3.3 Predominant Variables

In the present study, parameters such as Radius of Quarter circle (R), depth of water (d) in front of QBW, wave height (Hi), wave period (T), Wave steepness (Hi/gT^2), Reflection coefficient (Kr) and loss coefficient (K_l) were subjected to principal component analysis using Statistical package for social sciences (IBMSPSS – www.ibm.com/spss) software. The details of eigen values and eigen vectors obtained are tabulated in Table 3.2 and Table 3.3, respectively. Also, predominating variables are shown in Figure 3.1.

Table 3.2 Eigenvalues

	F1	F2	F3	F4	F5	F6	F7	F8
Eigenvalue	3.339	2.870	1.685	1.004	0.052	0.041	0.005	0.003
Variability (%)	37.104	31.890	18.718	11.155	0.575	0.459	0.060	0.038
Cumulative %	37.104	68.994	87.712	98.867	99.443	99.902	99.962	100.000

Table 3.3 Eigenvectors

	F1	F2	F3	F4	F5	F6	F7	F8
R	0.015	-0.017	-0.014	0.997	-0.037	-0.003	-0.062	-0.007
d	0.344	0.459	0.018	0.005	-0.037	-0.004	0.007	0.412
Hi	-0.053	0.029	0.759	0.022	0.312	-0.568	0.013	0.001
T	-0.417	0.363	0.069	0.042	0.653	0.510	0.039	0.002
Hi/gt2	0.230	-0.216	0.630	-0.008	-0.301	0.643	-0.012	-0.001
d/gT2	0.490	-0.241	-0.100	-0.039	0.465	0.046	-0.682	-0.082
R/gT2	0.420	-0.363	-0.108	0.046	0.405	0.038	0.711	0.083
hs/d	-0.343	-0.458	-0.018	-0.005	0.041	0.004	-0.151	0.804
d/hs	0.344	0.459	0.018	0.005	-0.037	-0.004	0.007	0.412

From the analysis, it is found that the eigenvalues of dimensional parameters (i.e., R, d, Hi, and T) are greater than one as compared to the non-dimensional parameters (Hi/gT^2, D/gT^2, R/gT^2 and Hs/d) indicate the predominance in predicting the Reflection and loss coefficients of QBW.

3.7 METHODOLOGY FLOWCHART

A flow chart indicating Step by step procedure adopted in the study is shown in Figure 3.4:

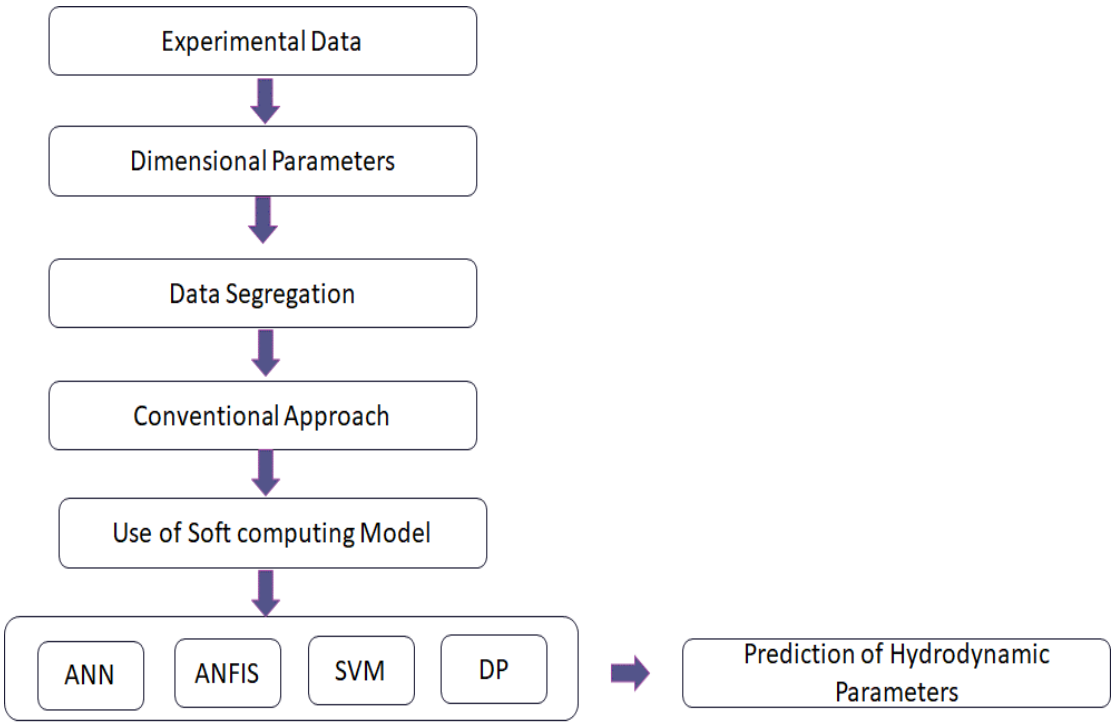

Figure 3.4 Flowchart of Methodology

3.8 EFFECT OF REFLECTION AND LOSS DUE TO HYDRAULIC STRUCTURE

Reflected wave intensifies sediment movement, which can destabilize the nearby structure. Hence this aspect should also be considered while designing a coastal structure. The reflection coefficient indicates an index to design the seaward side of a protective structure. When the wave hits a non-over topping barrier, some energy is reflected back in the incoming direction. The reflection coefficient (Kr) depends upon various factors such as incident wave height, still water level in front of the structure/barrier, roughness on the surface of the barrier, porosity, and location of the structure, etc.

3.9 SUMMARY

This chapter presented a physical model study on QBW carried out by Binumol et al. (2017). The experimental setup and QBW parameters were specific to waves and structures, and several input parameters that affect QBW's wave Reflection coefficient and loss coefficient were also presented in this chapter. In addition, various factors, viz., gathering, grouping, compilation, and structuring of the data, which were considered in the creation of CIM techniques, were also described.

CHAPTER 4

RESEARCH METHODOLOGY AND MODEL DEVELOPMENT

4.1 GENERAL

The ocean waves are mostly non-linearity and complex, and it is very challenging to solve real-world problems like wave-structure interaction and its hydrodynamic performance by considering all boundary conditions and extracting knowledge from huge amounts of experimental or in-situ data. To solve such problems, precise models are non-existent. Even if the information is provided, it typically takes the form of input-output data that illustrates the system's behaviour and prior empirical knowledge. Therefore, there is a need for an approximate reasoning system capable of handling such non-linear and complex information. Such methods are described by James C Bezdek (1996) within a framework known as computational intelligence techniques (CIT).

This study is to develop CIT for predicting the wave reflection coefficient (Kr) and loss coefficient (Kl) of QBW. In this chapter, the fundamentals of several CIT paradigms, including Artificial Neural Networks (ANN), Adaptive Neuro-Fuzzy Inference Systems (ANFIS), Support Vector Machines (SVM), and Deep Learning methods are covered.

4.2 ARTIFICIAL NEURAL NETWORKS (ANN)

The term "ANN" is derived from biological neural networks (BNN) that develop the structure of a human brain. Similar to the human brain, which has neurons interconnected to one another, artificial neural networks also have neurons interconnected to one another in various layers of the networks. These neurons are known as nodes.

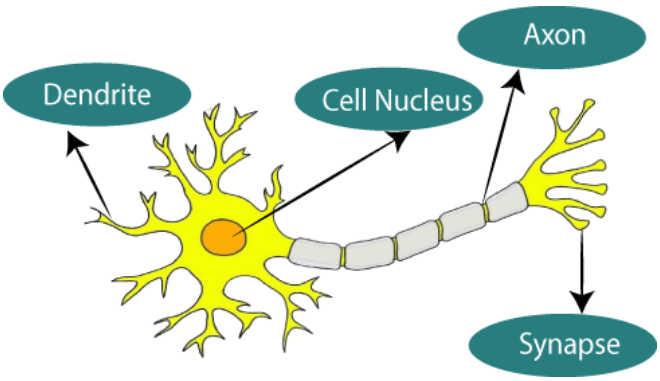

Figure 4.1 Typical diagram of Biological Neural Network

(Source: https://www.javatpoint.com/artificial-neural-network)

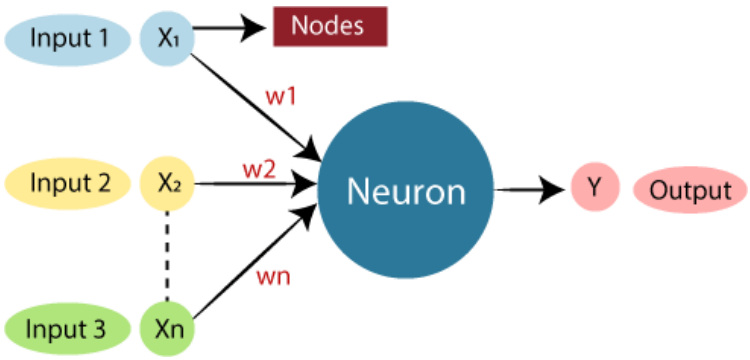

Figure 4.2 Typical diagram of ANN

(Source: https://www.javatpoint.com/artificial-neural-network)

An artificial neuron mimics the biological neuron and its characteristics, as shown in Figure 4.2. ANN consists of many artificial neurons, termed units, arranged in a sequence of layers.

4.2.1 Architecture of ANN

Generally, an ANN has three layers that include an input layer, a hidden layer, and an output layer.

Input Layer: The input layer accepts inputs in various programming-provided formats.

Hidden Layer: Between the input and output layers is the hidden layer. It makes all the computations necessary to uncover patterns and hidden features.

Output Layer: The hidden layer transforms the input into various outputs, which are then communicated through this layer.

When given input, the artificial neural network computes the weighted total of the inputs and incorporates a bias. A transfer function is used to visualize this computation.

$$\sum_{i=1}^{n} w_i \ . x_i + b \qquad (4.1)$$

where W_i –is the weight, X_i – the input variable, and b = bias.

It passes the weighted total as an input to an activation function to produce the output. A node's activation functions determine whether or not it should fire. The output layer is only accessible to individuals who are fired. Many activation functions can be used depending on the task we are completing. The network architecture must be chosen as a preliminary step before selecting a network. Recurrent networks or feed-forward networks are typically taken into consideration.

4.2.2 Feed-forward Back Propagation Network (FBPN)

An FBPN is used in the current research project. This network is capable of handling non-linear fixes for poorly characterized issues. An input layer, an output layer, and at least one hidden layer are features of a conventional BPN. The network may have hidden layers, but generally, one or two layers are considered. Each layer is fully connected to the next layer, as shown in Figure 4.3.

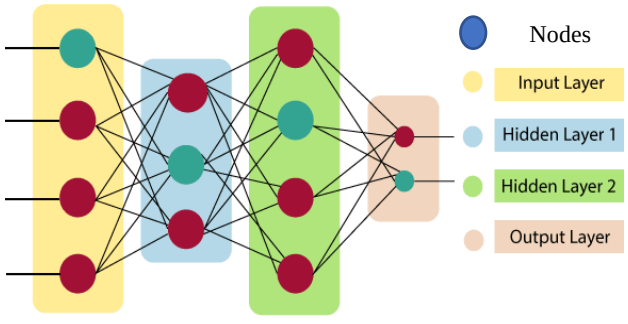

Figure 4.3 Typical diagram of FBPN

(Source: https://www.javatpoint.com/artificial-neural-network)

A variation of the Delta Rule serves as the foundation for learning FBPN (Kosko, 2003). Determining the gap between the actual and desired outputs is the first step. The

challenging aspect of this method is for the system to identify which input significantly influenced an incorrect output and how to adjust that input to fix the mistake. A node that is not active won't cause an error and won't need to adjust its weights. The network's input layer is used to apply training inputs to this issue, and the output layer compares desired results. The network is swept forward during the learning process, and each element's output is calculated layer by layer. The derivative of the transfer function is often used to modify the difference between the output of the final layer and the intended output, and the Delta Rule is typically used to modify the connection weights. This process continues for the preceding layer(s) until the input layer is reached. The learning guidelines for BPN come in a wide variety. It is possible to utilize a variety of transfer functions, error functions, and even the modifying technique of the derivative of the transfer function.

Multiple-layer neural networks are frequently adopted to enable the network to learn non-linear and linear correlations between input and output nodes. In the present study, feed-forward backpropagation neural network is used, where the input nodes are represented as the first layer, the hidden nodes as the second layer, and the output nodes as the third layer. Mathematically, the feed-forward artificial neural network is expressed as:

$$Z_x = \sum_{i=1}^{m} W_{kj} \, . T_x(y) + \, b_{ko} \tag{4.2}$$

$$y = \, W_i \, . X_i + \, b_i \tag{4.3}$$

Where, x_i – is the input value from 1 to n, Wi - are weights in between the input layer and hidden layer nodes, and W_{kj} - are weights in between hidden layer and output layer nodes, ii and b_{ko} are bias values of hidden and output layers, respectively, m- no. of hidden layer nodes and $T_x(y)$- tan-sigmoidal transfer function.

The total of the inputs is converted into output using a transfer function. Tansig is employed as the transfer function in the current research study and is written as:

$$T_x \, (y) = \left(\frac{2}{1 + \, e^{-2xy}} - 1 \right) \tag{4.4}$$

Where y is the total of input values adjusted for weights and biases. The bias values for the hidden layer (b_{ji}) and the output layer (b_{ko}) are modified at each iteration. The modified Levenberg-Marquardt method calculates the weights between the hidden and output layers.

The linear transfer function, purelin, is also applied between the hidden layer and output layer while using the CG algorithm in the current study and is expressed as follows:

$$Purelin\ (n) = n \tag{4.5}$$

The overall objective of the training method is to reduce the global error, E, defined as:

$$E = \frac{1}{y}\sum_{1}^{p}\left[\sum_{k=1}^{k}\left(d_{kp} - \sigma_{kp}\right)^2\right] \tag{4.6}$$

Where p -is the total number of training patterns, d_{kp} is the desired value of the k^{th} output and the pth pattern, o_{kp} is the actual value of the k^{th} output and p^{th} pattern.

The correlation coefficient is determined to determine how well the network projected values match the measured values. A straight line is created between the two axes at a 45^o angle to fit the data. A strong correlation is attained when every point is precisely on this straight line.

4.2.3 Levenberg-Marquardt Method

The FBPN is trained in the current study using the Levenberg-Marquardt (LM) method. The Gaussian-Newton method and the steepest descent are combined to form the LM. LM method converges faster than other methods and obtains the lowest mean square error in many cases. Many researchers have mentioned that most studies using ANN models have been studied using only one hidden layer. In the current study, wave Reflection and loss due to QBW are predicted using a 3- layered feedforward, backpropagation method with a Levenberg-Marquardt method.

4.2.4 Conjugate gradient method

The conjugate gradient (CG) method is motivated to accelerate the typically slow convergence associated with gradient descent. This method avoids the information requirements associated with the Hessian matrix's storage, evaluation, and inversion. In the CG method, the search is performed along with conjugate directions. They

generally produce faster convergence than gradient descent directions. These training directions are conjugated concerning the Hessian matrix. This method has proved to be more effective in training neural networks.

4.2.5 Training of Network Data

Due to the non-linearity and complexities involved in various coastal engineering problems, researchers, in recent years, have shown interest in exploring ANN to address various coastal/ ocean engineering applications such as predicting ocean wave height, wave period, impact wave force, etc.(Deo et.al 2001; Deo and Jagdale, 2003; Gunaydin, 2008; Londhe and Deo, 2003). Because of their learning capacity and ability to approximate non-linear functions, neural networks are incredibly versatile. Through the input layer, the data enters the network. The input layer nodes are not computational; instead, they only broadcast the data to the hidden nodes across weighted connections (Patil et al., 2012). The training set consists of known input and output pairings and is used to train the ANN. The weights are tuned during network training to obtain a particular response from ANN. The network weights are initialized using either a set of random values or some prior knowledge. Following that, a training (learning) procedure rectifies these initial weight values. Equations 4.7 and 4.8 are used to calculate the weights in the hidden and output layer neurons, respectively.

$$W(N+1)\,W(N) - \eta\,\delta\varphi \tag{4.7}$$

$$W(N+1) = W)N) + \eta x \sum_{q=1}^{r} \delta_q \tag{4.8}$$

Where w is the training weight, N is the number of iterations, x is the input parameter, η is the learning weight, and ϕ is the output. δ is defined as 2εq ∂ϕ/ ∂I, where I is the weighted sum of inputs, q is the neuron index of the output layer, and εq is the error signal. Figure 4.3 also depicts the architecture of the typical FBPN used in this investigation. During training, results from the network are allied to the target, and any errors are subsequently back-propagated to change the weights required to minimize the errors. The neural network model stops iterating for training when the error is less than the target error. Weights are adjusted repeatedly until the necessary degree of precision between target values and computed outputs is attained. Then a testing data

set is presented to validate the network performance. Once it is satisfactory, the ANN could be used for its profound purpose.

4.3 ADAPTIVE NEURO-FUZZY INFERENCE SYSTEM

In soft computing, fuzzy inference systems are the most often used component. The first to mention this (1993). Fuzzy logic can express knowledge very precisely while providing clear justification and reasoning. However, ANN is capable of learning on its own and is fault tolerant. However, the representation of the knowledge that is being stored takes the form of connections between neurons, which is challenging to comprehend. Consequently, self-learning and understanding knowledge representation are greatly enhanced if both strategies are used. Additionally, accurate data preparation for ANN is laborious and time-consuming. This can be avoided by employing fuzzy logic to create an interface that accepts ambient fuzzy data directly. This combination is the neuro-fuzzy method, developed as the Adaptive Neuro-Fuzzy Inference System (ANFIS), introduces the typical architecture of fuzzy inference systems (FIS), Takagi and Sugeno (1985) and Jang et al. (1997). A fuzzy system having a generalized bell membership function, product inference rule, and weighted average de-fuzzifier has become the standard method in most applications. Takagi and Sugeno (1985) changed the defuzzification procedure, where dynamic systems are introduced as defuzzification subsystems.

4.3.1 Architecture of ANFIS

When training a Takagi-Sugeno-type fuzzy inference system, ANFIS combines least-squares and backpropagation gradient descent methods. It is used to find the best parameters for producing a single output by feeding numerous inputs. It can serve as a springboard for creating a collection of fuzzily worded "if-then" rules that use the proper membership functions to produce fixed input-output pairings. ANFIS is a straightforward structure with a quick and efficient learning method (Vairappan et al.,

2009). Alternative methods can be used in ANFIS training to lower training errors. Since the hybrid approach shrinks, it converges much faster than the backpropagation method used in neural networks, which have larger search space dimensions. ANFIS models are created utilizing various membership functions on the experimental data. The resulting results will be validated by comparison to experimental data.

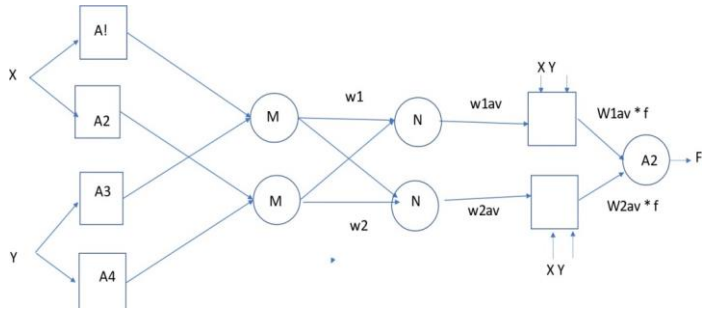

Figure 4.4 Typical diagram of ANFIS architecture

A general and simple architecture of ANFIS with the five input variables, namely:

I_1= R, I_2=d, I_3=Hi, I_4=T, I_5=Hi/gT2 and the output variable is O =K_r (Reflection coefficient)

and K_l (loss coefficient). A conventional ANFIS model consists of five layers is explained below in brief by Jang et al. (1997).

Layer 1

Every node in this layer is an adaptive node with a node function.

$$O_{i,j} = \mu A_i(x) \qquad \text{for i} = 1,3 \tag{4.9}$$

x or y is the input node, and Ai or Bi-2 is the linguistic variable associated with membership functions of a fuzzy set A1, A2, B1, B2. A Typical membership function:

$$O_{i,j} = \mu B_i(y) \qquad for\ i = 3,4 \tag{4.10}$$

Where a_i, b_i, and c_i is a parameter set. These parameters are called premise parameters.

Layer 2

Each node in this layer is a fixed node, indicated by π Norm. The output is the product ofall the incoming signals.

$$O_{i,j} = \mu A_i(\text{x}).\ \mu B_i(y) \quad for\ i = 1,2 \tag{4.11}$$

Output signalw_i represents the fire strength of a rule.

Layer 3

Each node in this layer is a fixed node, N Norm. The i[th] node calculates the ratio of the firing strength to the sum of the firing strength.

$$O_{3,j} = w_{(avg)i} = \frac{w_i}{w_1 + w_2} \quad for\ i = 1,2 \qquad (4.12)$$

Output signal $\bar{w}_i$ is called normalized firing strengths.

Layer 4

Each node in this layer is an adaptive node, indicated by the square node with a nodefunction:

$$O_{4,i} = w_i f_i = w_i (p_i x + q_i y + r_i) \qquad (4.13)$$

Where w_i is the normalized firing strength from layer 3. $\{p_i, q_i, r_i\}$is the parameter set,which is called consequent parameters.

Layer 5

Each node in this layer is a fixed node, indicated by a circle which computes the overall output as the summation of all incoming signals:

$$overall\ out\ put = S = O_i = \sum W_{(avg)i}\ , f_i = \frac{\sum W_i . f_i}{W_i} \qquad (4.14)$$

The different membership functions assigned for input parameters are Gaussian membership functions:

$$f(x, \sigma, c) = e^{\frac{-(x-c)^2}{2\sigma^2}} \qquad (4.15)$$

Where x is input parameters, c, and σ are mean and variance, respectively. Linear membership function

$$f(x, a, b, c) = \left(\min(\frac{x-a}{b-a}; \frac{c-x}{c-b}\right) . O \qquad (4.16)$$

Where x is an input parameter, $a\ and\ b$ represents the feet of the triangle a and b indicates the peak. The equation for the generalized bell-shaped membership function is:

$$f(x, a, b, c) = \left(\frac{1}{1 + \left(\frac{x-c}{a}\right)^{2b}}\right) \qquad (4.17)$$

Where c locates the center of the curve.

Therefore, a fuzzy inference system of the Sugeno type and an adaptive network is functionally similar. In this study, a hybrid strategy combining backpropagation and least square error methodology is employed to construct all the ANFIS models with linear, and Gumbel's membership functions (MF) are evaluated to identify the most effective model.

4.4 SUPPORT VECTOR MACHINE

Support Vector Machine (SVM) analysis is a popular machine-learning tool for classification and regression. SVM regression is considered a non-parametric technique because it relies on kernel functions. Support Vector Regression (SVR) is a supervised learning method used to predict discrete values. SVR uses the same principle as the SVMs. The basic idea behind SVR is to find the best-fit line. In SVR, the best-fit line is the hyperplane with the maximum number of points. The data points on either side of the hyperplane closest to the hyperplane are called support vectors. These influence the position and orientation of the hyperplane and thus help build the SVM.

Hyperplane: Hyperplanes are decision boundaries used to predict the continuous output. The data points on either side of the hyperplane closest to the hyperplane are called.

Support Vectors. These are used to plot the required line that shows the predicted output of the method.

Kernel: A kernel is a set of mathematical functions that take data as input and transforms it into the required form. These are generally used for finding a hyperplane in the higher dimensional space.

The methodology used in the present study is to develop the best kernel-configured SVM model to predict the wave Reflection and loss coefficient.

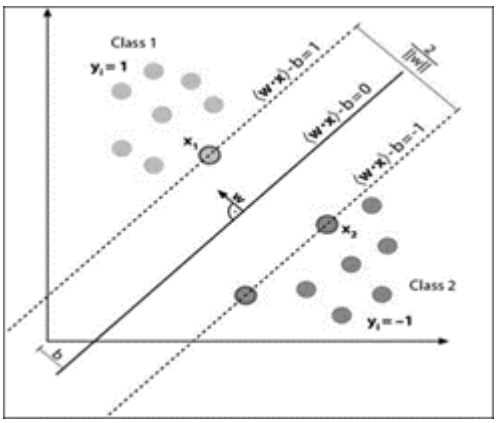

Figure 4.5 Margin setting to one-dimensional linear SVM (Source: www.techguruspeaks.com)

A simple description of the SVM method is elaborated. Let a training set be $\{(x_i , y_i)$, i =1, … …, n$\}$, where x_i and y_i are ith input training pattern & ith target output and has 'n' datasets for training. For nonlinear cases, SVM has the form as shown below;

$$f(x, \alpha) = (w \cdot \varphi(x)) + b \qquad (4.18)$$

Where w − weight vector, b − bias, and □(x) - mapping function to a higher dimensional feature space from input features.

The regression problem is the same as minimizing the regularized risk function (Lee et al., 2007) is shown below.

$$R(f) = \frac{1}{n} \sum_{i=1}^{n} L\,(y_i\ , f(x_i, w)) \qquad (4.19)$$

$$L\left(y_i\ , f(x_i, w)\right) = \begin{Bmatrix} \varepsilon_0\ if\ [y_i - f(x_i, w)]\ \leq\ \varepsilon \\ \left[[y_i - f(x_i, w)]\right] -\ \varepsilon\ otherwise \end{Bmatrix} \qquad (4.20)$$

The smoothness of the target function increases as the weight parameter decreases, improving its generalizability. In the SV regression issue, the target function (y i ", f" (x i," w)") is identified with the least amount of error (Smola et al., 2004). Vapnik invented the insensitive loss function to achieve this. This idea states that |y i ", f" (x i, "w") should not be more than. Fig. 4.5 can be used to help explain this. A linear SVM model's soft margin loss is depicted in the previous graphic. In the illustration, the dashed lines are measured, or goal values inside the insensitive tube, and the round points are the solid lines representing the anticipated values. The deviation between the actual target function (y i ", f" (x i, "w)") or forecasted values is less than ε at these

circular locations. The box points, however, are outside of the insensitive tube. Three box points are provided as examples. One point deviates from the upper bound by ξ,_i, whereas another point deviates from the lower bound by ξ i*. Therefore, the prediction model's convex optimization should penalize these spots for retaining the precision. Where ε is an insensitive loss function, on substitution in Equation (4.19), the optimization equation is minimized,

$$\frac{1}{2}\, w \,.w + C\left(\sum_{i=1}^{n} \xi_i^* + \sum_{i=1}^{n} \xi_i\right) \qquad (4.21)$$

where,

$$\text{Subject to } \begin{Bmatrix} \sum_{i=1}^{n} (a_i^* - a_i) = 0 \\ 0 \le a_i^*,\ a_i \le C \end{Bmatrix} \qquad (4.22)$$

Where α_i* and α_i are Lagrange multipliers and ($\varphi(x_i).\varphi(x_j)$ = K (x_i, x_j)) is the kernel function

The important concept is to use the dual set of variables to create the Lagrange function from the primary goal function and accompanying restrictions. The nonlinear regression function is obtained as follows using the maximization mentioned in the earlier function:

xr and xs are support vectors (SVs), number of support vectors, $0 \le \alpha i *, \alpha i \le$ C.

There are various kernels like linear, polynomial, sigmoid, radial basis function, Gaussian kernel, etc.

Gaussian Kernel: It is used to perform transformation when there is no prior knowledge about data.

$$K(x, y) = e^{-\left(\frac{\|x-y\|^2}{2\sigma^2}\right)} \qquad (4.23)$$

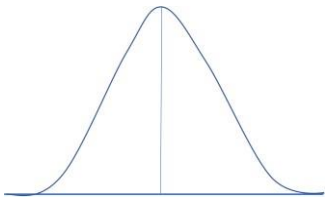

Figure 4.6 Gaussian Kernel Graph

(Source: https://www.geeksforgeeks.org/major-kernel-functions-in-support-vector-machine-SVM)

Sigmoid Kernel: This function serves as an activation function for artificial neurons andis analogous to a two-layer perceptron neural network architecture.

$$K(x, y) = \tan(\gamma\, x^{r} y + c) \qquad (4.24)$$

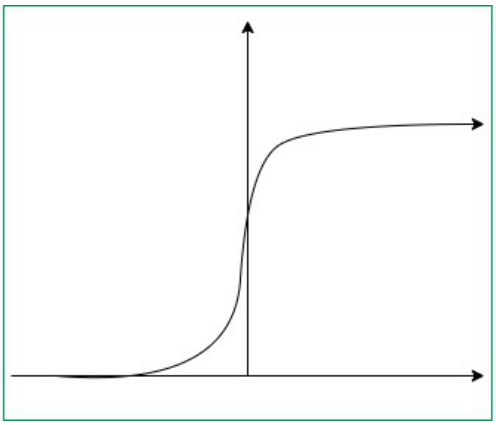

Figure 4.7 Sigmoidal Kernel Graph

(Source: https://www.geeksforgeeks.org/major-kernel-functions-in-support-vector-machine-SVM)

Two kernel functions, such as the Gaussian radial basis function and the Sigmoidal kernel, are used in the present study.

Table 4.1 Different Kernel Functions

Kernel	Function
Gaussian	$f(x) = a \;\; e^{\left(\frac{(x-b)^2}{2\sigma^2}\right)}$ Where a and b are constant, σ^2 - variance
Sigmoidal	$K(x, y) = \tanh(\gamma\, x^{r}\, y + C)$ Where x and y = input column vectors, γ= slope and C=constant

A proper setting of the kernel parameters γ and, as well as C and, affects SVM performance. The trade-off between flatness (model complexity) and deviations more significant than tube is determined by parameter C. (Smola, 1996; Gunn, 1998). The goal is to minimize the empirical risk alone without taking into account the complexity of the model if C is too great (infinity) (Cherkassky and Ma, 2004). The loss function used is to disregard errors present within a predetermined range of the true value. The

data compression is achieved by reducing the number of support vectors NSV used to build a regression function as the size of the regression function increases (Kecman, 2001). The best values are established using the two-stage grid search method because there are no universal guidelines for choosing the free parameters. To find the near-optimal values, a coarse search is first carried out, followed by a fine search by the trial-and-error method by choosing different values of C. The study uses the K-fold technique based on leave-one-out cross-validation to derive the regularization gamma parameter (γ) and kernel function-based tuning parameter.

4.5 DEEP LEARNING

Deep learning is a particular kind of machine learning that achieves great power and flexibility by learning to represent the world as a nested hierarchy of concepts, with each concept defined concerning simpler concepts and more abstract representations computed in terms of less abstract ones. In deep learning, we don't need to program everything explicitly. These methods are on hype due to their better processing power and data handling capacity. In the present study, two types of deep methods are adopted: decision tree and random forest.

4.5.1 Decision Trees

For both regression and classification, Decision Trees methods can be used. These decision tree flowcharts or methods are supervised methods. The decision trees visualize or mimic the thinking process of human beings, and decision trees are easily understood and interpreted in the same manner as one thinks. The decision tree is a diagram showing how decisions are made from a set of solutions. The diagram starts with a root and then branches to possible solutions. It consists of a root node, leaf nodes, and branches. It resembles a tree-like structure and is called a decision tree. Branches are the lines that connect the nodes. These lines also represent a flow from question to answer. Each of the nodes would branch to more than one node. Finally, a leaf node or terminal node would lead to a decision or desired solution. A decision tree can extend as much as needed to get a suitable solution.

4.5.2 Random Forest in Machine Learning

Random forest is a Supervised Machine Learning Method that is used widely in Classification and Regression problems. It builds decision trees on different samples (Figure 4.6) and takes their majority vote for classification and average in case of regression. One of the most important features of the Random Forest Method is that it can handle the data set containing continuous variables, as in the case of regression, and categorical variables, as in the case of classification. It performs better for classification problems.

Steps involved in the random forest method:

Step 1: In Random Forest, n number of random records is taken from the data set having k number of records.

Step 2: Individual decision trees are constructed for each sample.

Step 3: Each decision tree will generate an output.

Step 4: Final output is considered based on Majority Voting or Averaging for Classification and regression, respectively.

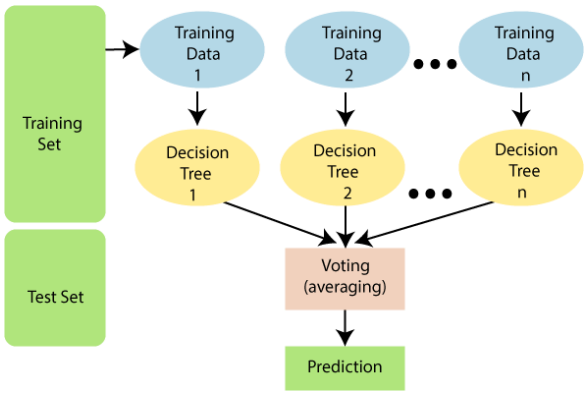

Figure 4.8 Random Forest Tree -Flow chart

(Source: *https://www.javatpoint.com/machine-learning-random-forest-algorithm*)

Important Features of Random Forest

1. Diversity- Not all attributes/variables/features are considered while making an individual tree; each tree is different.
2. Immune to the curse of dimensionality- Since each tree does not consider all the features, the feature space is reduced.

3. Parallelization - Each tree is created independently out of different data and attributes. This means we can fully use the CPU to build random forests.
4. Train-Test split- In a random forest, we don't have to segregate the data for train and testing.
5. Stability- Stability arises because the result is based on majority voting/ averaging. Difference Between Decision Tree & Random Forest: Random Forest is a collection of decision trees; still, there are many differences in their behavior.

Table 4.2 Difference between Decision tree and Random Forest

Sl.No	**Decision Trees**	**Random Forest**
1	Decision trees typically suffer from the problem of overfitting ifit's allowed to grow without any control.	Random forests are created from subsets of data, and the final output is based on average or majority ranking hence the problem of overfitting is taken care of.
2	A single decision tree is faster in computation.	It is comparatively slower.
3	When a data set with features is taken as input by a decision tree, it formulates some prediction rules.	Random forest randomly selects observations, builds a decision tree, and takes the average result. It doesn't use any set of formulas.

Thus, random forests are much more successful than decision trees only if the trees are diverse and acceptable.

4.6 MODEL PERFORMANCE INDEX

The accuracy of the predicted values with experimental data sets is evaluated through the model performance index viz., Correlation Coefficient (CC), Root Mean Square Error (RMSE), Scatter Index (SI), and Nash-Sutcliffe Efficiency (NSE). A model with minimum RMSE and SI maximum model efficiency and better CC is considered as better suited for the prediction of hydrodynamic parameters of QBW.

4.6.1 Correlation Coefficient

A correlation coefficient (CC) shows statistical correlations between two or more random variables or observed data values. The CC has a range of 0 to 1. Range 1 demonstrates that the equation is linear, accurately describing the connection between x and y, with all data points falling on a line for which y increases as x increases and vice versa. But the value 0 indicates that there is no linear dependence between the variables.

$$CC(r) = \frac{\sum(x_i - x_m).(y_i - y_m)}{\sqrt{(x_i - x_m)^2}\sqrt{(y_i - y_m)^2}} \quad (4.25)$$

where r – correlation coefficient, x_i - value of x variable, x_m -mean value of x variable, y_i - value of y variable, and y_m -mean value of y variable.

4.6.2 Root Mean Square Error

One of the methods most frequently used to assess the accuracy of forecasts is the root mean square error, also known as root mean square deviation. It illustrates the Euclidean distance between measured true values and forecasts. When computations are made outside the data sample, the discrepancies are referred to as prediction errors rather than residuals. The RMSE combines the sizes of prediction errors for different times into a single indicator of predictive capacity. Since RMSE is scale-dependent, it should only be employed to evaluate the predicting errors of several models for a single variable and not between variables. The lowest RMSE results in the best model.

$$RMSE = \sqrt{\frac{\sum_{i=1}^{n} \|O_i - P_i\|^2}{N}} \quad (4.26)$$

Where O_i = observed or actual values, P_i = predicted values, and N = total number of data points.

4.6.3 Scatter Index

In statistics, the scatter or spread of data points indicates how stretched or squeezed a distribution is. Common measures of statistical dispersion are the variance, standard deviation, and interquartile range. Dispersion is contrasted with location or central tendency, which are the most used properties of distributions.

$$S.I = \frac{RMSE}{x_m} \quad (4.27)$$

where, SI = scattered Index, RMSE = Root mean square and X_m= mean of observation.

4.6.4 Nash-Sutcliffe Efficiency

It is also vital to test the model with various other performance evaluation indicators, such as the NSE, to determine how resilient the generated model is. NSE, a normalized statistic, establishes how much residual variance (noise) there is in relation to the variance of the measured data (information). The models' efficacy was evaluated using the Nash-Sutcliffe coefficient. The NSE range for a model might be between -1 and 1. An efficiency of 1 (NSE = 1) indicates that the estimate and the observations agree exactly. In contrast, NSE = 0 occurs when the observed mean is a better predictor than the model. An efficiency of zero (NSE = 0) denotes that the model predictions are as accurate as the mean of the observed data (described by the denominator). In general, the model is more accurate the closer the model efficiency is; near 1 is the mean of actual data.

$$NSE = 1 - \frac{\sum_{i=1}^{n}(O_i - P_i)^2}{\sum_{i=1}^{n}(O_i - O_m)^2} \qquad (4.28)$$

O_i – observed i^{th} value, P_i – predicted i^{th} value, and O_m- mean observed value.

4.7 SUMMARY

In this chapter, various CITs, such as ANN, ANFIS, SVM, and Deep Learning, are briefly described. Also, the procedures adopted in evaluating the models used in hydrodynamic parameters of QBW using CC, RMSE, SI, and NSE are presented.

CHAPTER 5

PREDICTION OF REFLECTION COEFFICIENT

5.1. GENERAL

The studies on quarter-circle breakwaters are limited since these structures have evolved in recent years. Hence, there is ample scope to study the Reflection coefficient (K_r) of QBW, particularly using soft computing techniques. This chapter discusses forecasting K_r by segregated data and adopting various soft computing models such as ANN, ANFIS, SVM, and Deep Learning and assessing the models.

5.2 REFLECTION COEFFICIENT (K_r)

The present study aims to predict the wave reflection coefficient due to quarter circle breakwater with different porosity using various computational intelligence techniques. The experimental data for analysis of Quarter Circle Breakwater (QCB) are taken from work of Binumol et al (2017). This particular study investigates the wave reflection, loss characteristics on an emerged seaside perforated quarter circle breakwater of three different radii 0.55 m, 0.575 m and 0.60 m with ratio of spacing to diameter of perforations (S/D) equal to 5, 4, 3, 2.5 and 2 for different water depths and wave conditions. The detail experimental parameters considered for the present are explained in Chapter 3.

The wave reflection coefficient (Kr) is defined as the ratio of reflected wave height (Hr) to incident wave height (Hi) for regular waves;

$$K_r = \frac{H_r}{H_i} \tag{5.1}$$

Where K_r – coefficient of reflection, H_r – reflected wave height, and H_i – Incident wave height.

The prediction of the reflection coefficient is studied considering the predominating parameters obtained from the principal component analysis. Accordingly, the predominant variables such as the Radius of the structure (R), depth of water in front

of the structure (d), incident wave height (H_i), and wave period (T). Wave steepness (H_i/gT^2) which is prominent among the non-dimensional parameter, is also considered.

5.2.1 Data separation for prediction of Reflection coefficient, K_r

From the literature survey, it was observed that the available data was segregated for training and testing the network while employing different soft computing techniques. The entire available dataset consists of 252 data sets for each condition and is called global data (GD). From this global data, 177 data sets, i.e., 70% are considered for training, and the remaining 30%, i.e., 75, are used for testing the network for each S/D ratio.

5.3 PREDICTION OF REFLECTION COEFFICIENT (Kr) OF A PERFORATED QBW USING ARTIFICIAL NEURAL NETWORK (ANN).

5.3.1 Using dimensional parameters

The selection of updated methods to train the network is a crucial step in the neural network technique. This is because the network's performance greatly depends on the methods used. Four distinct quarter-circle breakwaters with different perforations (S/D=2,3,4 and 5) are used to study wave reflection using different soft computing techniques. For each condition of perforations, 252 data sets are collected by varying the radius of the breakwater and the water depth in front of it. Both structural parameters and non-dimensional wave parameters are given as input to the network.

In the present work, while using ANN, such as the Levenberg-Marquardt method and conjugate gradient are considered to train the network. The best ANN architecture was obtained on a trial-and-error basis. The network is fed with the Radius of the structure ®, depth of water in front of the structure (d), incident wave height (h), wave period (t), and wave steepness (hi/gT^2) as inputs to predict a single output by varying the number of neurons in the hidden layer, and a number of epochs. Better model performance indices (MPI) were attained with a 5-10-1 network at 200 epochs, and the results of the same are presented in Tables 5.1 to 5.4 for different perforations on the curved surface of the breakwater. Scattered plots of actual Vs. predicted reflection coefficient (K_r) is shown in Figure 5.1.to 5.8.

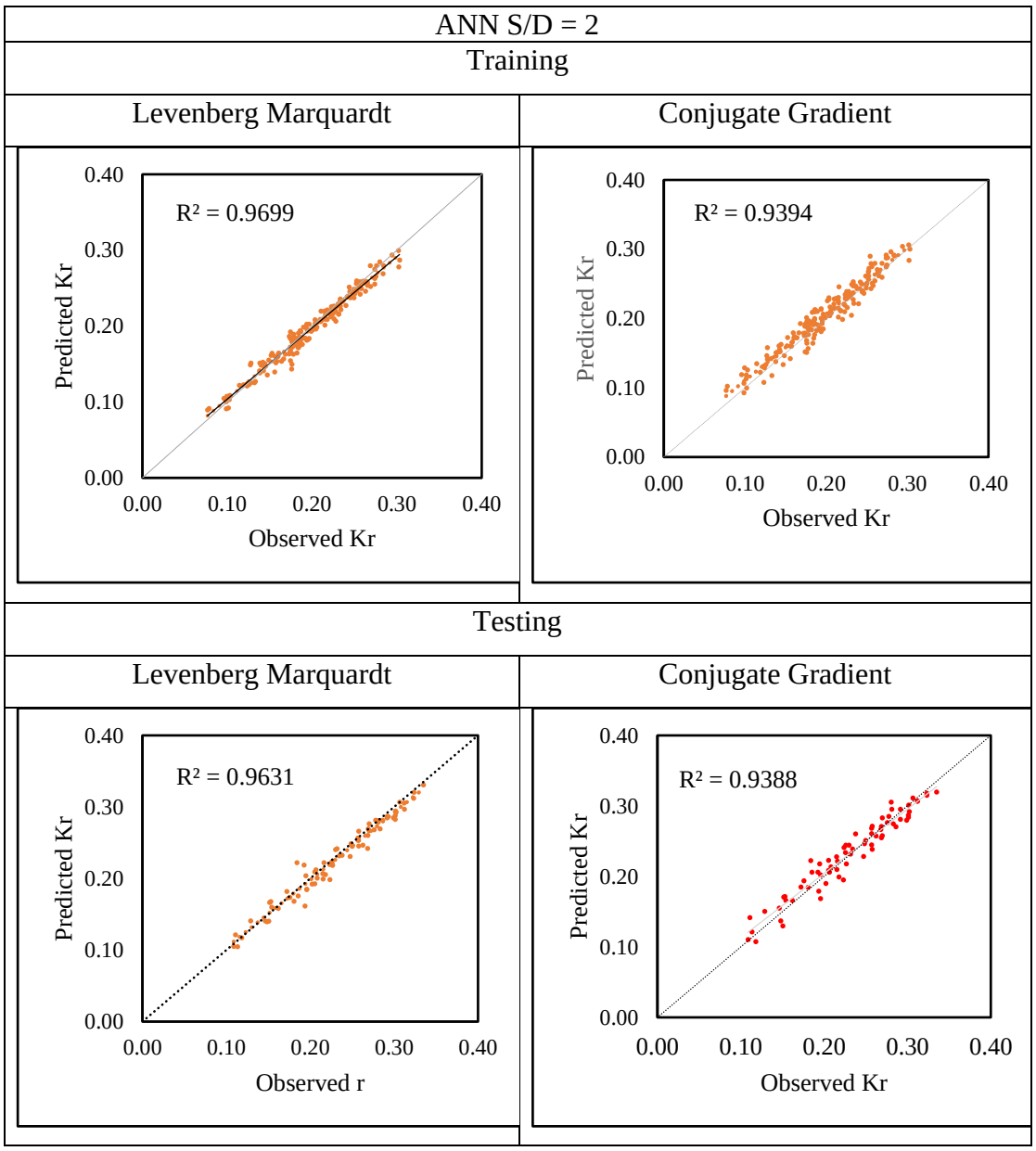

Figure 5.1 Scattered Plot between Observed and Predicted Values of K_r (ANN S/D=2).

Table 5.1 Model Performance Indices using ANN by dimensional parameters.

Model Performance Index (MPI) Parameters	ANN S/D=2			
	Training		Testing	
	Levenberg Marquardt	Conjugate Gradient	Levenberg Marquardt	Conjugate Gradient
CC	0.984	0.969	0.981	0.968
RMSE	0.014	0.019	0.011	0.014
SI	4.968	6.573	5.046	6.209
NSE	0.973	0.967	0.959	0.937

Figure 5.1 indicates a scatter plot of observed vs. predicted K_r; comparing the MPI values and their model performance index tabulated in Table 5.1, it is observed that the coefficient of correlation (CC) obtained by the LM algorithm is better compared to the CG algorithm. The value of CC obtained by the LM method in training is 0.984 as compared to a value of 0.969 in the CG method. While in testing, the CC value was found to be 0.981 and 0.968 for LM and CG methods, respectively. The values for RMSE in training were 0.014 for the LM method against 0.019 for the CG method, while in testing, it was 0.011 and 0.014, respectively. The value for SI in training and testing was 4.968 and 5.046 for the LM method, respectively, and 6.573 and 6.209 for the CG method, respectively. The lower values for RMSE and SI in the CG method as compared to the LM method further indicate that the accuracy is more for the CG method. The values for NSE from Table 5.1 show that the LM method has greater values, hence emphasizing the accuracy of the LM method.

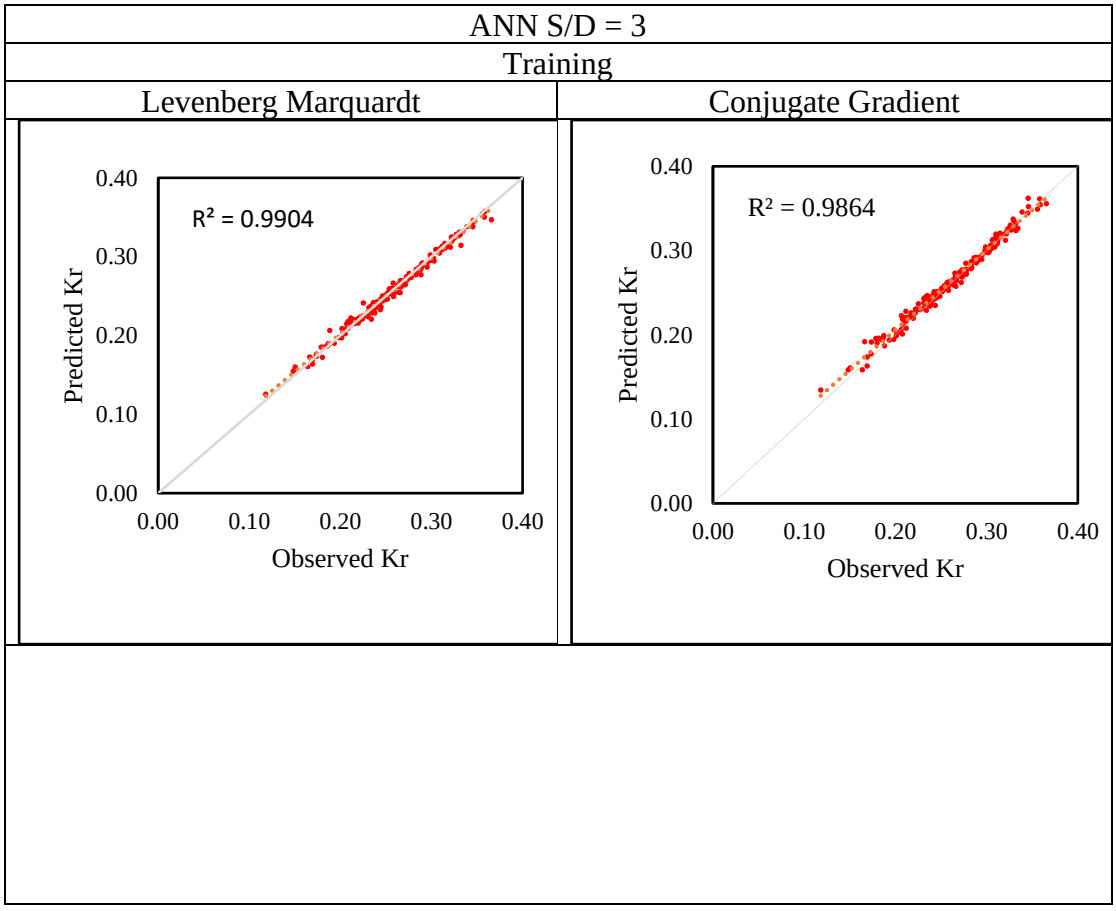

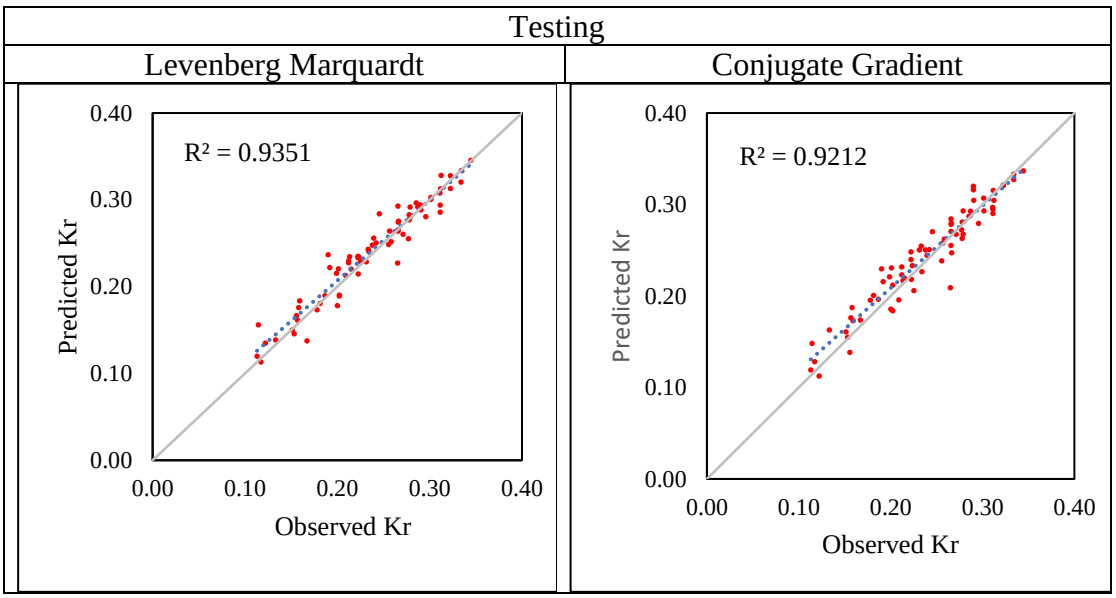

Figure 5.2 Scattered Plot between Observed and Predicted Values of K_r (ANN S/D=3)

Table 5.2 Model Performance Indices using ANN by dimensional parameters

Model Performance Index (MPI) Parameters	ANN S/D=3			
	Training		Testing	
	Levenberg Marquardt	Conjugate Gradient	Levenberg Marquardt	Conjugate Gradient
CC	0.995	0.992	0.967	0.959
RMSE	0.004	0.006	0.015	0.017
SI	1.891	2.492	6.505	7.238
NSE	0.989	0.981	0.928	0.908

From Figure 5.2, plots of observed vs. predicted Kr and from able 5.2 coefficients of correlation (CC) obtained from the LM method is superior to the CG method. In comparison to a value of 0.995 in the LM technique, the value of CC obtained by the CG method in training is 0.992. Testing revealed that the CC values for the LM and CG methods were 0.967 and 0.959, respectively. The RMSE values were 0.004 and 0.006 during training and 0.015 and 0.017 during testing for both LM and CG methods, respectively. Whereas the scattered Index were 1.891 and 2.492, during training and 6.505 and 7.238, during testing, respectively. The greater accuracy of the LM approach is further supported by the lower RMSE and SI values in comparison to the CG method. With the LM method, the NSE value varied from 0.989 in training and 0.928 in testing versus 0.981 in training and 0.908 in testing for CG, demonstrating that the LM

approach has higher values, highlighting its improved accuracy as compared to the CG method.

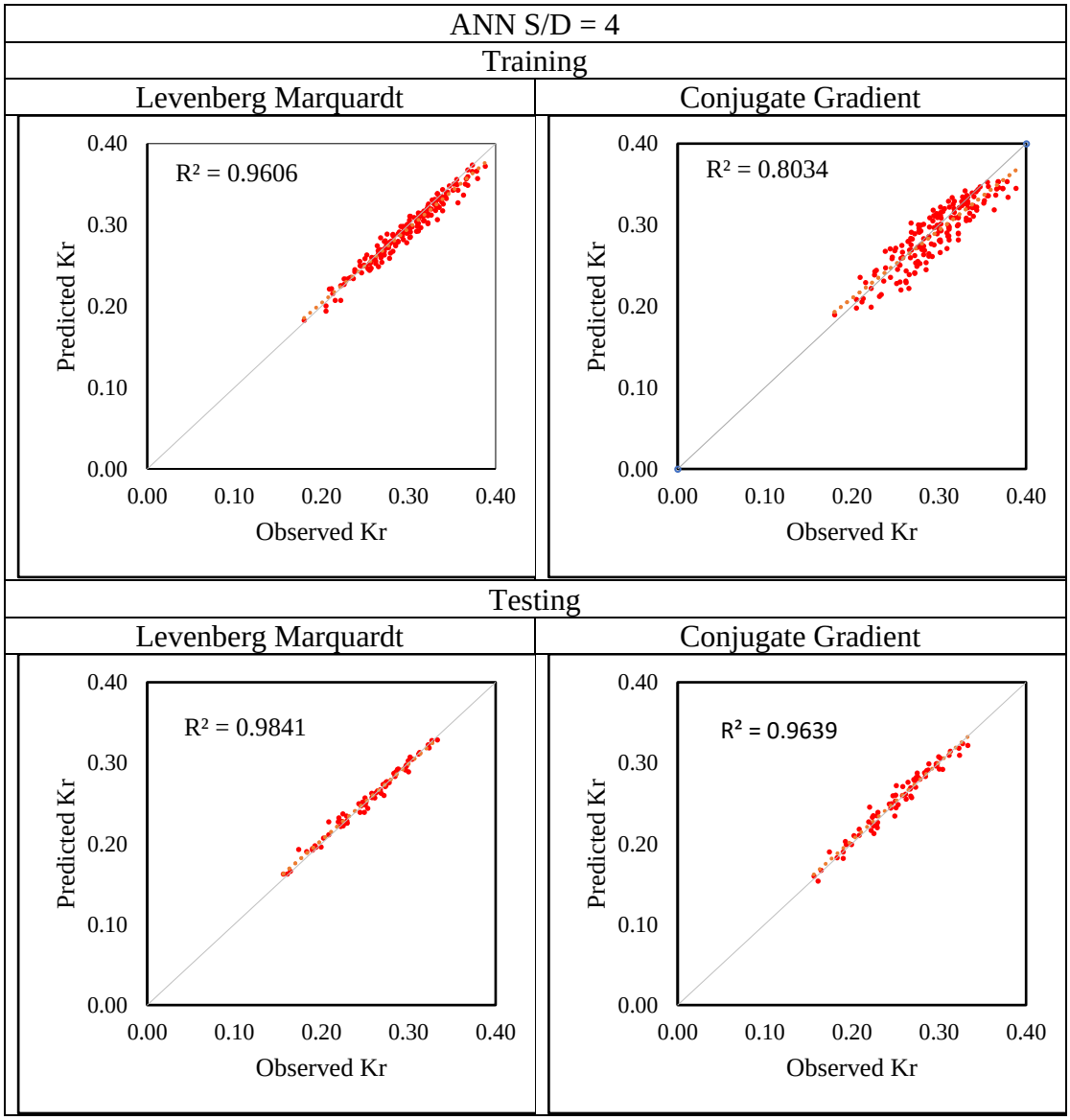

Figure 5.3 Scattered Plot between Observed and Predicted Values of K_r (ANN S/D=4)

Table 5.3 Model Performance Indices by dimensional parameters

Model Performance Index (MPI) Parameters	ANN S/D=4			
	Training		Testing	
	Levenberg Marquardt	Conjugate Gradient	Levenberg Marquardt	Conjugate Gradient
CC	0.980	0.896	0.991	0.981

RMSE	0.007	0.009	0.005	0.008
SI	3.076	6.435	2.230	3.257
NSE	0.950	0.781	0.997	0.995

It can be observed from Figure 5.3 and Table 5.3 that the LM coefficient of correlation (CC) obtained from LM is superior to the CG method when comparing the plots of observed vs. anticipated K_r. The CC value attained by the LM approach in training is 0.980 compared to a value of 0.896 in the CG method. As a result of testing, it was obtained that the CC values for the LM and CG approaches were, respectively, 0.991 and 0.981. Results for RMSE for the LM approach and CG method in training were 0.007 and 0.009, respectively, while they were 0.005 and 0.008 in testing. The values for SI in training and testing for the LM methodology were 3.076 and 2.230, respectively, while for the CG method, they were 6.435 and 3.257, respectively. The RMSE and SI values compared to the CG method further demonstrate the higher accuracy of the LM method. The results for NSE in Table 5.3 show that the LM approach has higher values, showing its better accuracy when compared to the CG method: 0.950 in training and 0.997 in testing for LM, with 0.781 in training and 0.995 in testing for CG.

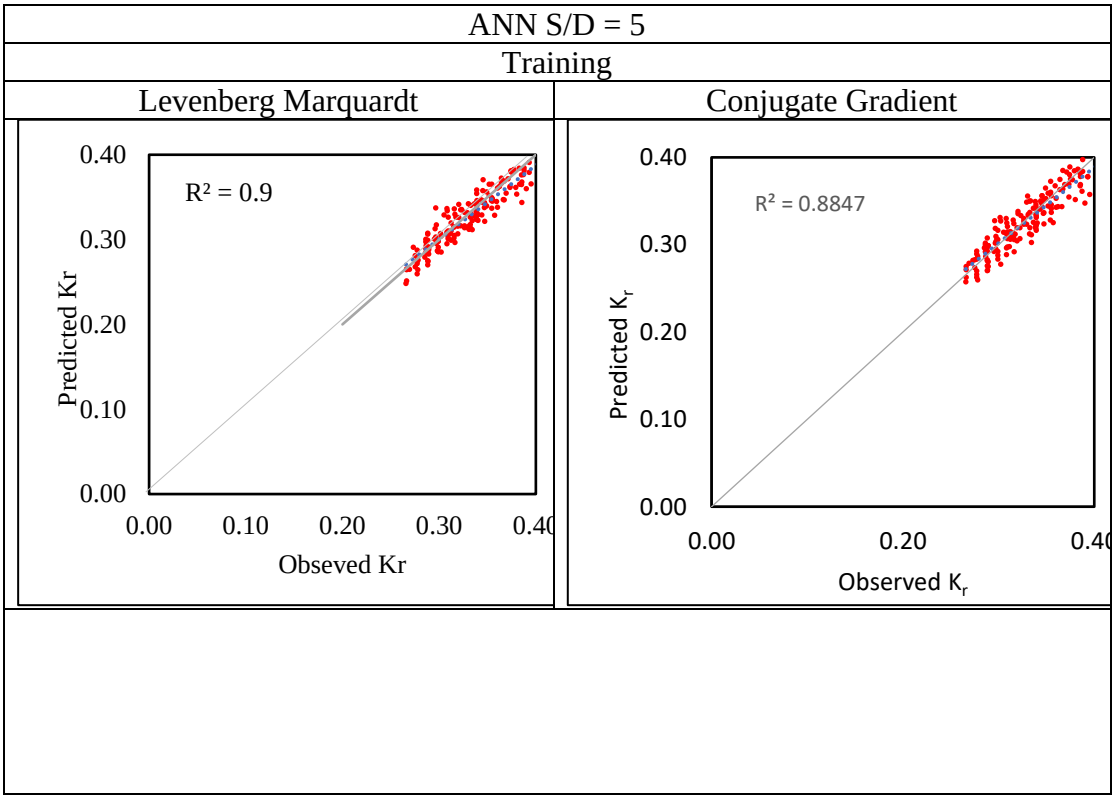

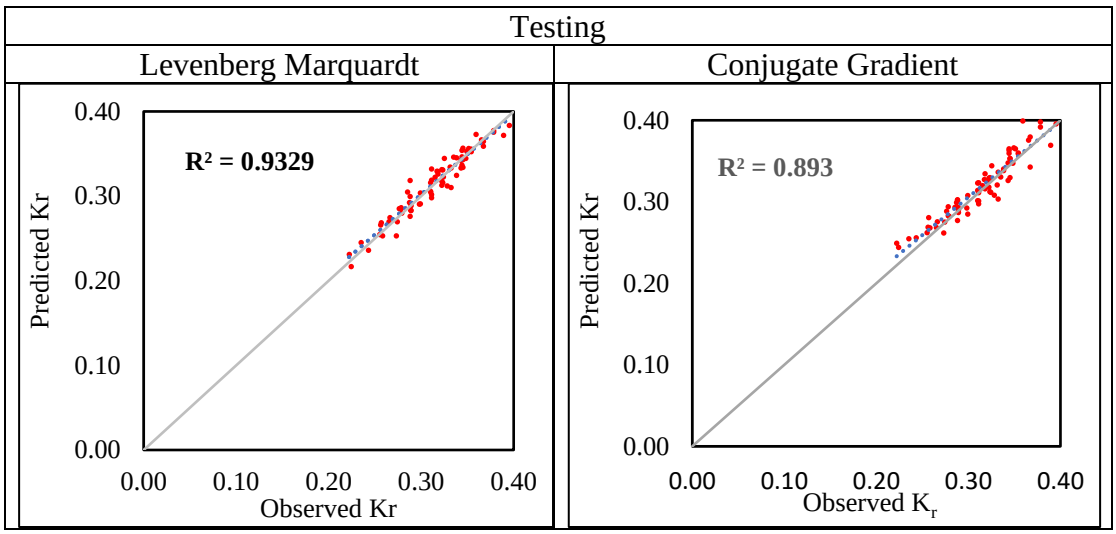

Figure 5.4 Scattered Plot between Observed and Predicted Values of K_r (ANN S/D=5)

Table 5.4 Model Performance Indices using ANN by dimensional parameters

Model Performance Index (MPI) Parameters	ANN S/D=5			
	Training		Testing	
	Levenberg Marquardt	Conjugate Gradient	Levenberg Marquardt	Conjugate Gradient
CC	0.948	0.940	0.966	0.945
RMSE	0.001	0.001	0.010	0.013
SI	4.140	4.318	3.203	4.419
NSE	0.889	0.860	0.931	0.869

From the plots shown in Figure 5.4, observed vs. anticipated K_r, and from Table 5.4, it can be shown that the LM approach's coefficient of correlation (CC) is superior to the CG method. The values of the model performance index during training, the LM method achieved a CC value of 0.948 as opposed to the CG technique's 0.940. The CC values for the LM and CG methods were found to be 0.966 and 0.945, respectively, as a result of testing. In training, the RMSE for the LM technique and the CG method were 0.001 and 0.001, respectively, whereas, in testing, they were 0.010 and 0.013, respectively. For the LM method, the values for SI were 4.140 and 3.203 in training and testing, respectively, while for the CG method, they were 4.318 and 4.419 in training and testing, respectively. Further evidence of the improved accuracy of the LM method comes from the lower RMSE and SI values as compared to the CG method. The LM method has higher values for NSE than the CG method, demonstrating

improved accuracy: 0.889 in training and 0.931 in testing for LM vs. 0.860 in training and 0.869 in testing for CG.

Table 5.5 Comparison of Model Performance Index using ANN by LM algorithm using dimensional parameters

	CC		RMSE		SI		NSE	
	Training	Testing	Training	Testing	Training	Testing	Training	Testing
S/D=2	0.984	0.981	0.014	0.011	4.968	5.046	0.973	0.959
S/D=3	0.995	0.967	0.004	0.015	1.891	6.505	0.989	0.928
S/D=4	0.980	0.991	0.007	0.005	3.076	2.230	0.950	0.997
S/D=5	0.948	0.966	0.001	0.010	4.140	3.203	0.889	0.931

Comparison of Model Performance Indices for different S/d ratios of perforated QBW models using ANN by LM algorithm is presented in Table 5.5.

5.3.2 Using non-dimensional parameters

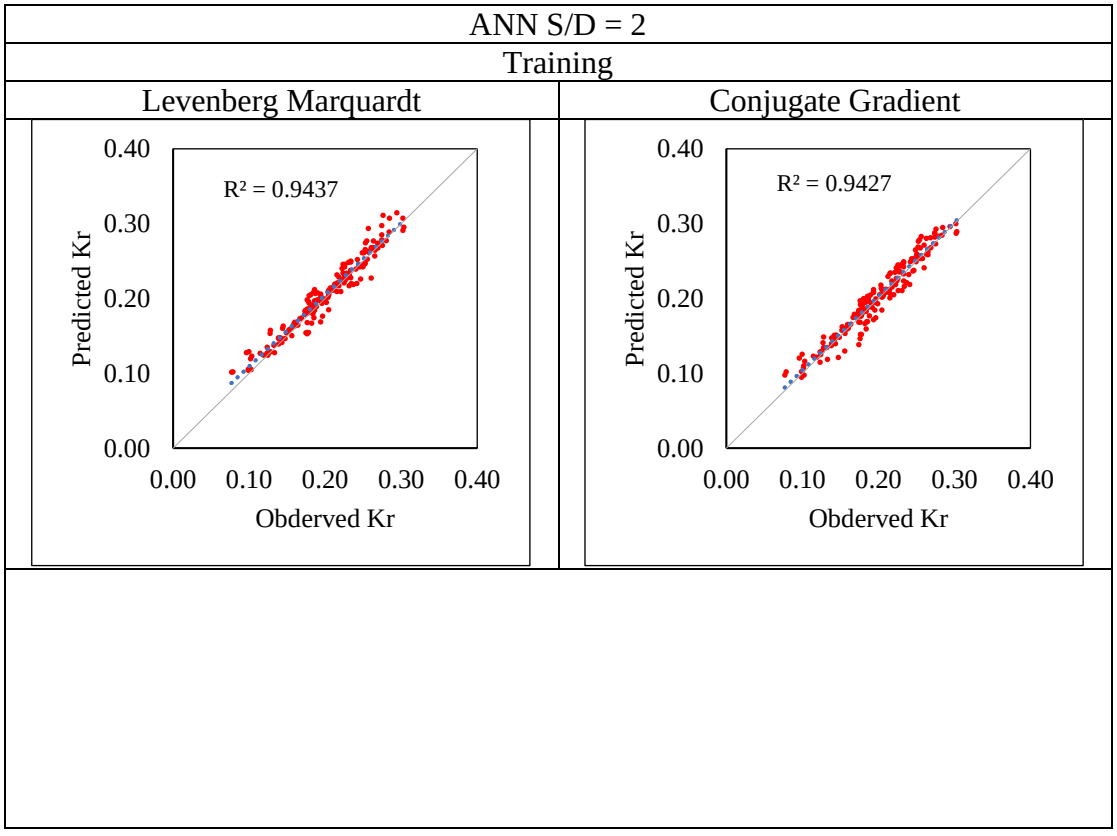

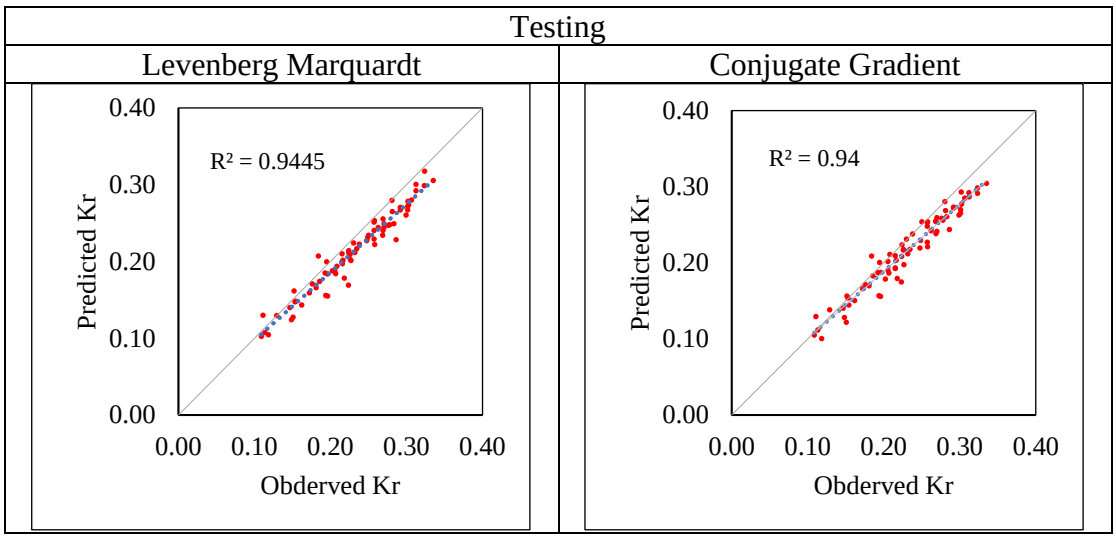

Figure 5.5 Scattered Plot between Observed and Predicted Values of K_r (ANN S/D=2)

Table 5.6 Model Performance Indices using ANN by non-dimensional parameters

Model Performance Index (MPI) Parameters	ANFIS S/D=2			
	Training		Testing	
	Levenberg Marquardt	Conjugate Gradient	Levenberg Marquardt	Conjugate Gradient
CC	0.9714	0.9709	0.9719	0.9695
RMSE	0.0495	0.0511	0.1193	0.1234
SI	0.0279	0.0289	0.1549	0.1602
NSE	0.9213	0.8954	0.9117	0.8923

On comparing the observed and predicted K_r, it can be shown that the LM approach's coefficient of correlation (CC) is superior to the CG method. The values of the model performance index that were found are shown in Table 5.6. During training, the LM method achieved a CC value of 0.9714 as opposed to the CG technique's 0.9709. The CC values for the LM and CG methods were found to be 0.9719 and 0.9695, respectively, as a result of testing. In training, the RMSE for the LM technique and the CG method were 0.0495 and 0.0511, respectively, whereas, in testing, they were 0.1193 and 0.1234, respectively. For the LM method, the values for SI were 0.0279 and 0.1549 in training and testing, respectively, while for the CG method, they were 0.0289 and 0.1602 in training and testing, respectively. Further evidence of the improved accuracy of the LM method comes from the lower RMSE and SI values as compared to the CG

method. The LM method has higher values for NSE than the CG method, demonstrating improved accuracy: 0.8954 in training and 0.8923 in testing for CG vs. 0.9213 in training and 0.9117 in testing for LM.

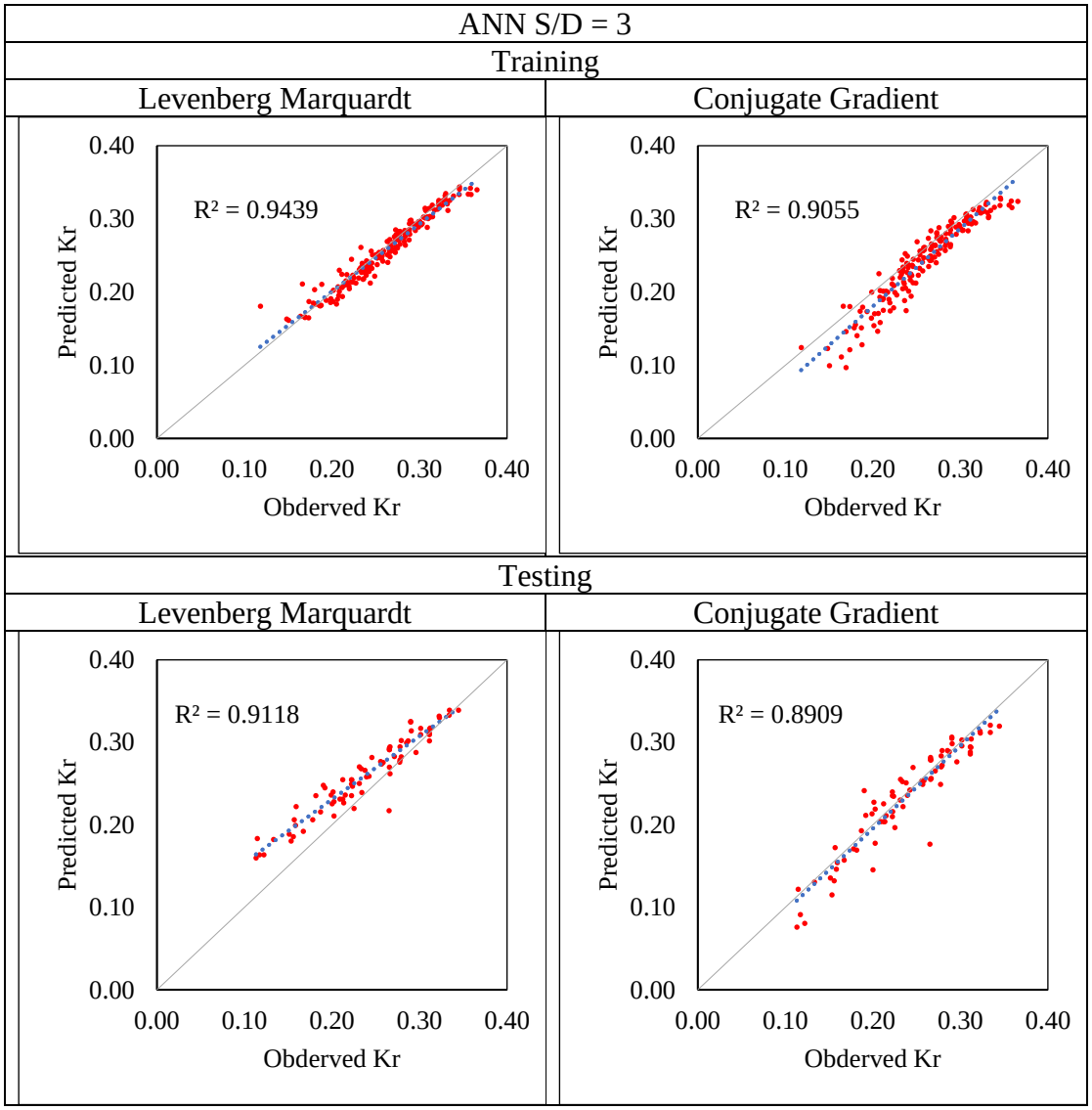

Figure 5.6 Scattered Plot between Observed and Predicted Values of K_r (ANN S/D=3)

Table 5.7 Model Performance Indices using ANN by non-dimensional parameters

Model Performance Index (MPI) Parameters	ANFIS S/D=3			
	Training		Testing	
	Levenberg Marquardt	Conjugate Gradient	Levenberg Marquardt	Conjugate Gradient

CC	0.9715	0.9516	0.9549	0.9439
RMSE	0.0231	0.0682	0.0322	0.0541
SI	0.0131	0.0385	0.0418	0.0703
NSE	0.9113	0.8938	0.9025	0.8812

It can be shown that the LM approach's coefficient of correlation (CC) is superior to the CG method when comparing the plots of observed vs. anticipated K_r. The model performance index values that were obtained are listed in Table 5.7. The CC value attained by the LM approach in training is 0.9715 compared to a value of 0.9516 in the CG method. As a result of testing, it was obtained that the CC values for the LM and CG approaches were, respectively, 0.9549 and 0.9439. Results for RMSE for the LM approach and CG method in training were 0.0231 and 0.0682, respectively, while they were 0.0322 and 0.0541 in testing. The values for SI in training and testing for the LM methodology were 0.0131 and 0.0418, respectively, while for the CG method, they were 0.0385 and 0.0703, respectively. The RMSE and SI values compared to the CG method further demonstrate the higher accuracy of the LM method. The results for NSE in Table 5.7 show that the LM approach has higher values, showing its better accuracy when compared to the CG method: 0.8938 in training and 0.8812 in testing for CG, with 0.9113 in training and 0.9025 in testing for LM.

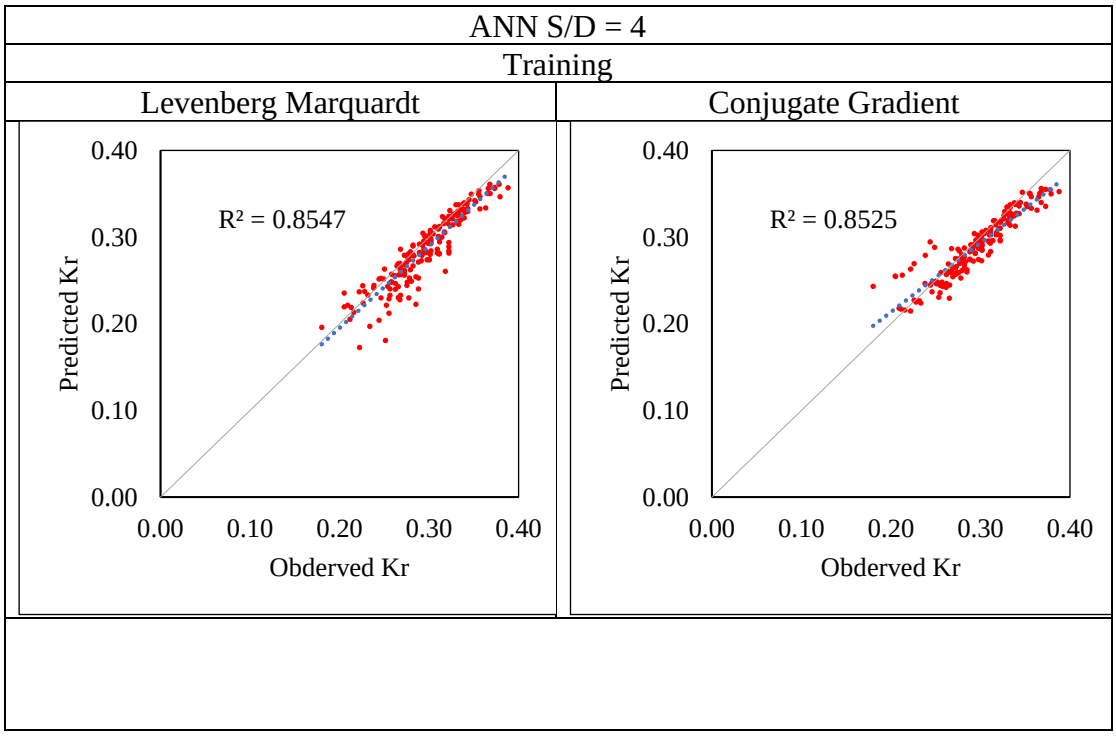

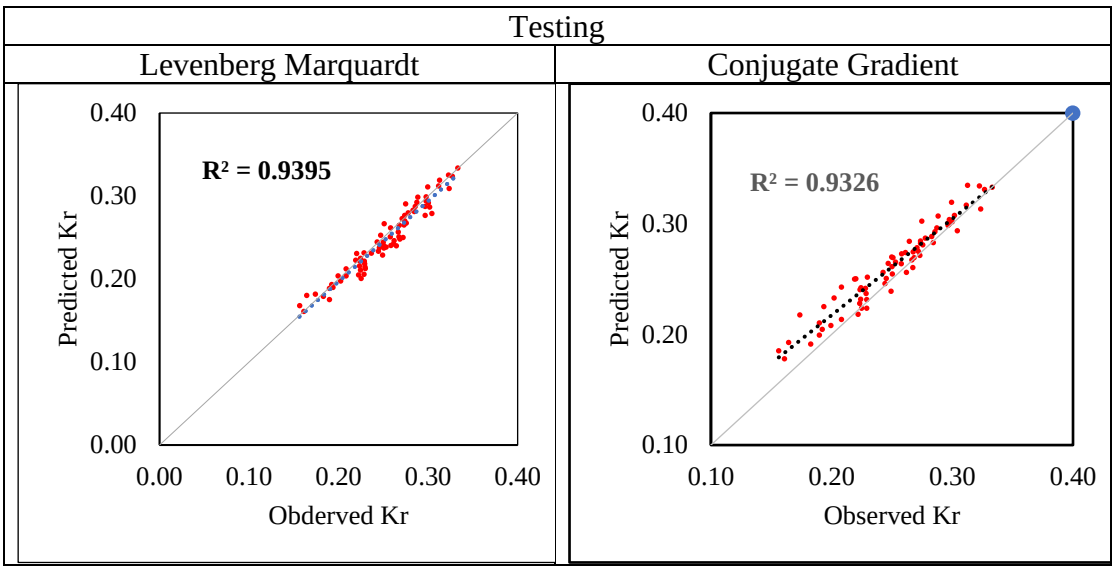

Figure 5.7 Scattered Plot between Observed and Predicted Values of K_r (ANN S/D=4)

Table 5.8 Model Performance Indices using ANN by non-dimensional parameters

Model Performance Index (MPI) Parameters	ANN S/D=4			
	Training		Testing	
	Levenberg Marquardt	Conjugate Gradient	Levenberg Marquardt	Conjugate Gradient
CC	0.9203	0.9233	0.9975	0.9654
RMSE	0.0314	0.0826	0.0382	0.0841
SI	0.0003	0.0005	0.0005	0.1092
NSE	0.9271	0.8832	0.9136	0.8783

It can be shown that the LM approach's coefficient of correlation (CC) is superior to the CG method when comparing the plots of observed vs. anticipated K_r. The model performance index values that were obtained are listed in Table 5.8. The CC value attained by the LM approach in training is 0.9203 compared to a value of 0.9233 in the CG method. As a result of testing, it was obtained that the CC values for the LM and CG approaches were, respectively, 0.9975 and 0.9654. Results for RMSE for the LM approach and CG method in training were 0.0314 and 0.0826, respectively, while they were 0.0382 and 0.0841 in testing. The values for SI in training and testing for the LM methodology were 0.0003 and 0.0005, respectively, while for the CG method, they were 0.0005 and 0.1092, respectively. The RMSE and SI values compared to the CG method further demonstrate the higher accuracy of the LM method. The results for NSE

in Table 5.8 show that the LM approach has higher values, showing its better accuracy when compared to the CG method: 0.8832 in training and 0.8783 in testing for CG, with 0.9271 in training and 0.9136 in testing for LM.

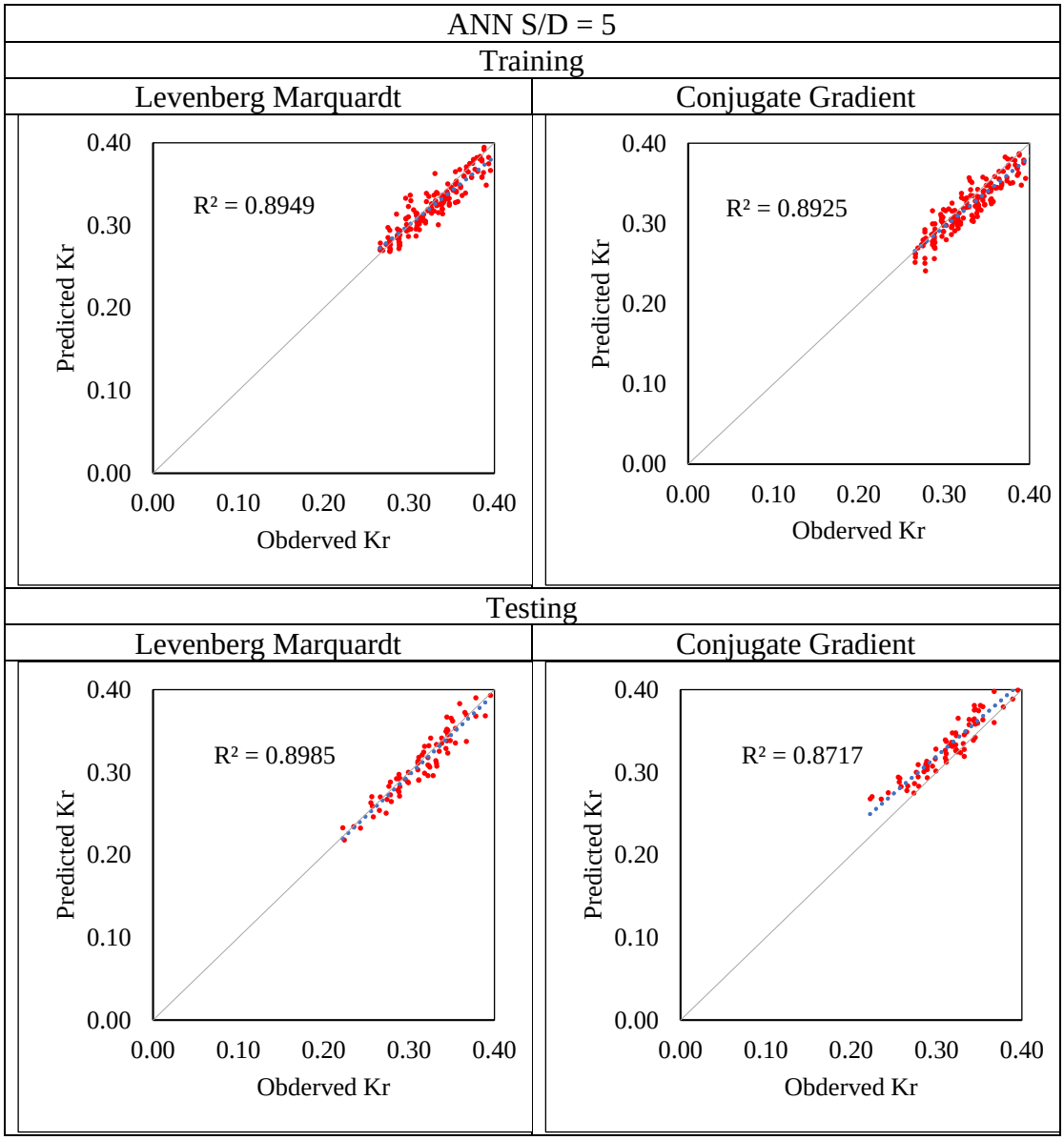

Figure 5.8 Scattered Plot between Observed and Predicted Values of K_r (ANN S/D=5)

Table 5.9 Model Performance Indices using ANN by non-dimensional parameters

Model Performance Index (MPI) Parameters	ANN S/D=5			
	Training		Testing	
	Levenberg Marquardt	Conjugate Gradient	Levenberg Marquardt	Conjugate Gradient
CC	0.9459	0.9447	0.9479	0.9336
RMSE	0.0006	0.0719	0.0006	0.0722
SI	0.0003	0.0406	0.0008	0.0938
NSE	0.9640	0.8375	0.9588	0.8214

It can be shown that the LM approach's coefficient of correlation (CC) is superior to the CG method when comparing the plots of observed vs. anticipated K_r. The model performance index values that were obtained are listed in Table 5.9. The CC value attained by the LM approach in training is 0.9459 compared to a value of 0.9447 in the CG method. As a result of testing, it was obtained that the CC values for the LM and CG approaches were, respectively, 0.9479 and 0.9336. Results for RMSE for the LM approach and CG method in training were 0.0006 and 0.0719, respectively, while they were 0.0006 and 0.0722 in testing. The values for SI in training and testing for the LM methodology were 0.0003 and 0.0406, respectively, while for the CG method, they were 0.0008 and 0.0938, respectively. The RMSE and SI values compared to the CG method further demonstrate the higher accuracy of the LM method. The results for NSE in Table 5.9 show that the LM approach has higher values, showing its better accuracy when compared to the CG method: 0.8375 in training and 0.8214 in testing for CG, with 0.9640 in training and 0.9588 in testing for LM.

Table 5.10 Comparison of Model Performance Index using ANN by LM algorithm Using non-dimensional parameters

	CC		RMSE		SI		NSE	
	Training	Testing	Training	Testing	Training	Testing	Training	Testing
S/D=2	0.9714	0.9719	0.0495	0.1193	0.0279	0.1549	0.9213	0.9117
S/D=3	0.9715	0.9549	0.0231	0.0322	0.0131	0.0418	0.9113	0.9025
S/D=4	0.9203	0.9975	0.0314	0.0382	0.0003	0.0005	0.9271	0.9136

S/D=5	0.9459	0.9479	0.0006	0.0006	0.0003	0.0008	0.9640	0.9588

Comparison of Model Performance Indices for different S/D ratios of perforated QBW models using ANN by LM algorithm is presented in Table 5.10.

5.4 PREDICTION OF REFLECTION COEFFICIENT (K_r) OF A PERFORATED QBW USING ADAPTIVE NEURO-FUSSY INFERENCE SYSTEM (ANFIS)

5.4.1 Using Dimensional Parameters

The training data supplied to create the input membership function for the ANFIS model with removing clustering comprised of 5 inputs and 1 output data. As the total dataset comprises 4 different wave heights, the number of clusters is set to 4. An improvement factor is set as 0.001 between the two consecutive iterations, and the maximum iterations count was set to 25. The exponent of the partition matrix component m=1.2 was found to be the best, with the lowest error. The Gumbel's and Linear membership functions are considered in the present study. The results are shown in Table 5.10 - 5.13, and plots are shown in Figures 5.9 to 5.12 for different S/D ratios of perforations.

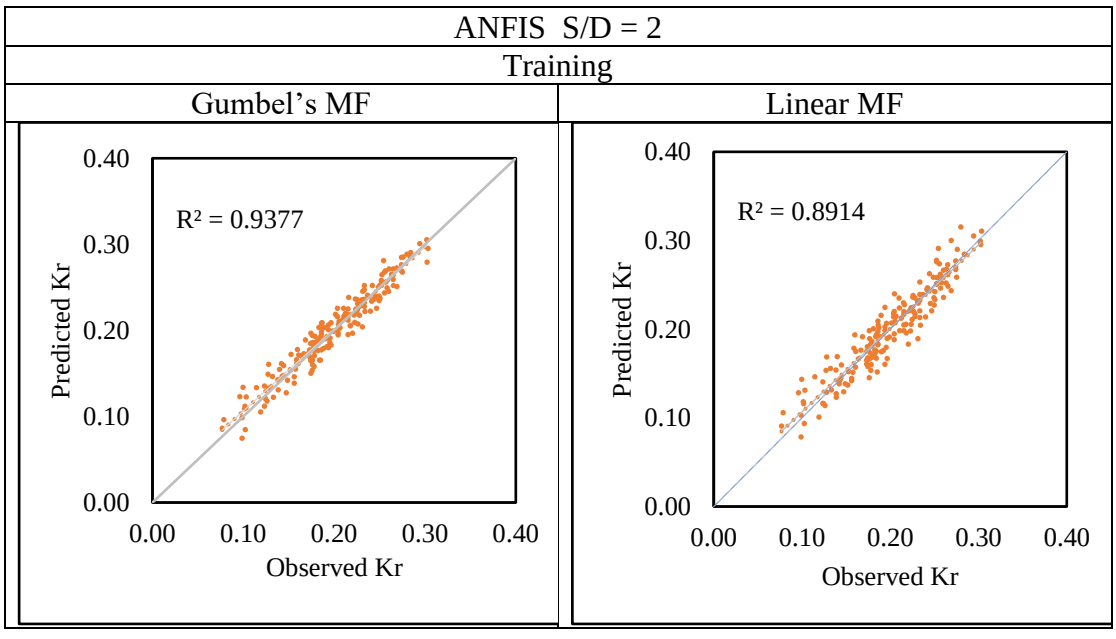

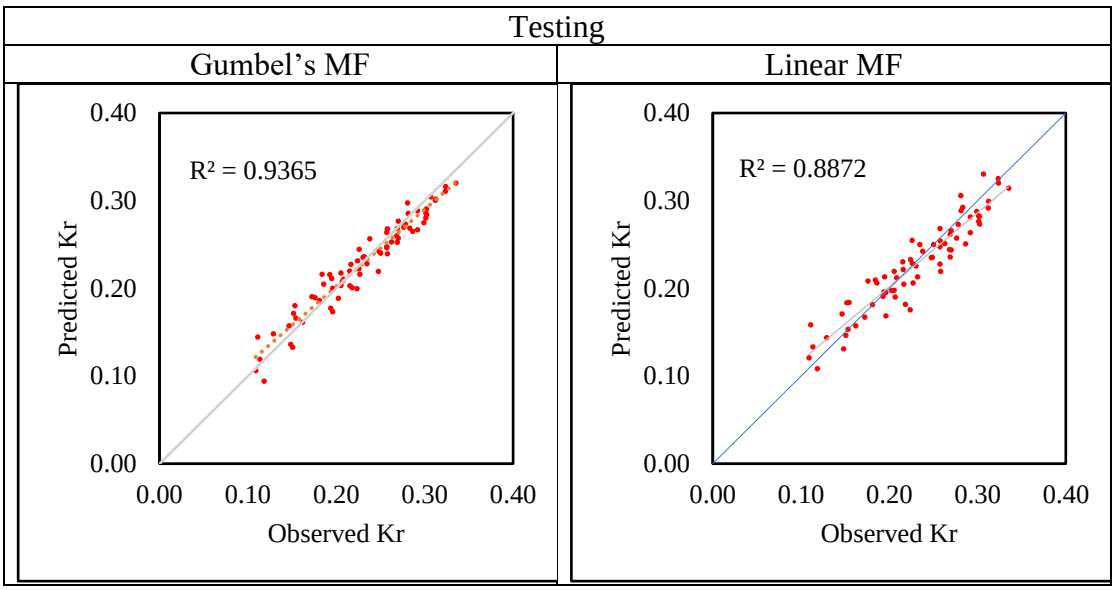

Figure 5.9 Scattered Plot between Observed and Predicted Values of K_r (ANFIS S/D=2)

Table 5.11 Model Performance Indices using ANFIS by dimensional parameters

Model Performance Index (MPI) Parameters	ANFIS S/D=2			
	Training		Testing	
	Gumbel's MF	Linear MF	Gumbel's MF	Linear MF
CC	0.968	0.944	0.967	0.942
RMSE	0.013	0.017	0.015	0.019
SI	6.316	8.371	6.441	8.199
NSE	0.937	0.888	0.933	0.883

From the plots of observed vs. anticipated K_r, it can be shown that **G**umbel's MF approach's coefficient of correlation (CC) is superior to the Linear MF method. The values of the model performance index that were found are shown in Table 5.11. During training, Gumbel's MF strategy achieved a CC value of 0.968 as opposed to the Linear MF technique's 0.944. The CC values during testing using Gumbel's MF and Linear MF were found to be 0.967 and 0.942, respectively. In training, the RMSE for Gumbel's MF technique and the Linear MF method were 0.013 and 0.017, respectively, whereas, in testing, they were 0.015 and 0.019, respectively. For Gumbel's MF method, the values for SI were 6.316 and 6.441 in training and testing, while for the Linear MF method, they were 8.371 and 8.199 in training and testing,

respectively. Further evidence of the improved accuracy of Gumbel's MF approach comes from the lower RMSE and SI values as compared to the Linear MF method. The Gumbel's MF method has higher values for NSE than the Linear MF method, demonstrating improved accuracy: 0.937 in training and 0.933 in testing, 0.888 in training, and 0.883 in testing.

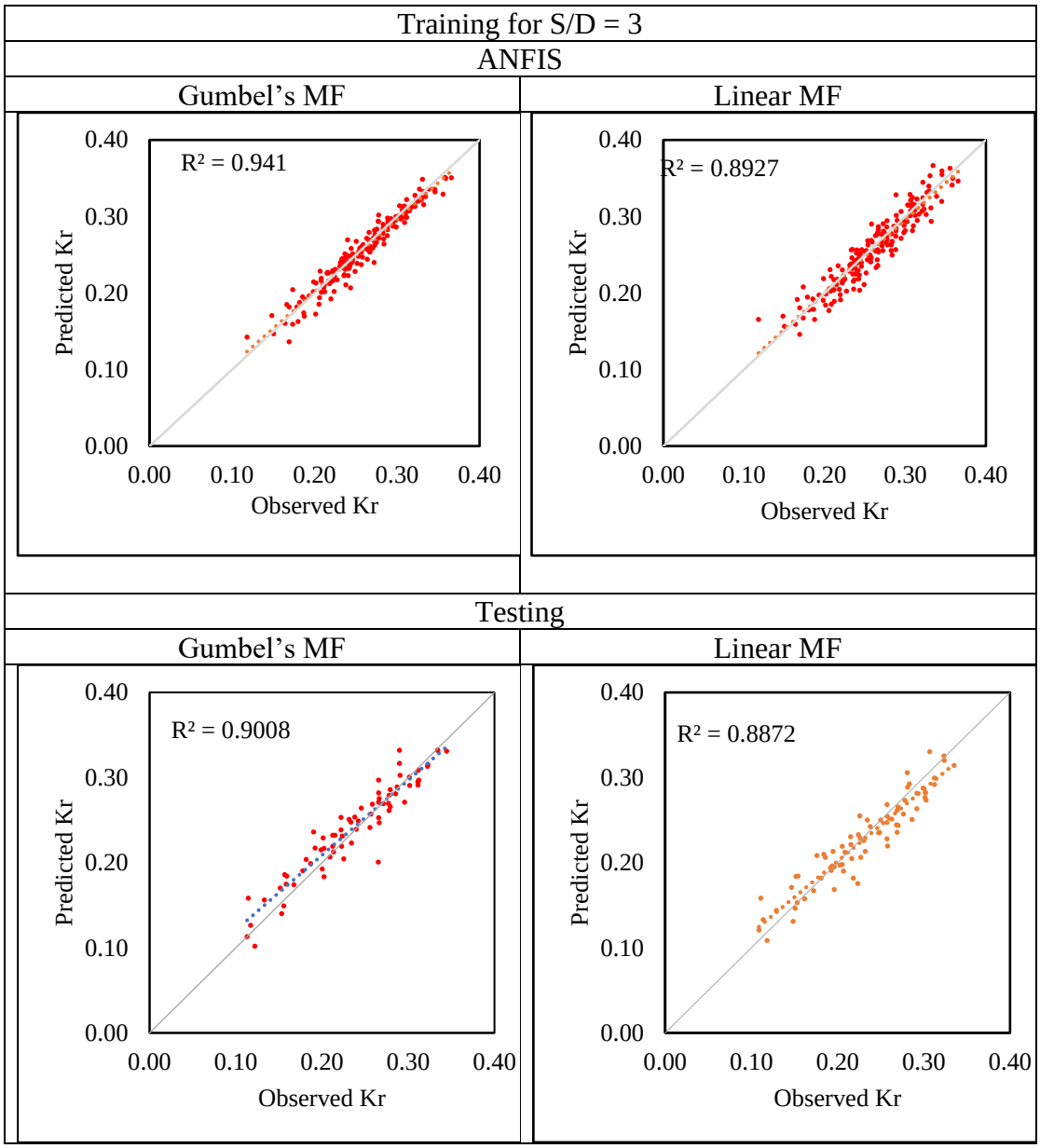

Figure 5.10 Scattered Plot between Observed and Predicted Values of K_r (ANFIS S/D=3)

From Figure 5.10, on comparing the plots of observed vs. predicted Kr, it can be seen that the Linear MF approach's coefficient of correlation (CC) is superior to Gumbel's

MF method. Table 5.12 lists the model performance index values that were obtained. In comparison to a value of 0.970 in Gumbel's MF technique, the value of CC obtained by the Linear MF method in training is 0.944. Testing revealed that the CC values for Gumbel's MF and Linear MF methods were, respectively, 0.949 and 0.942. The results for RMSE were 0.011 for the Linear MF technique in training and 0.016 for the Gumbel's MF method, whereas they were 0.018 and 0.024, respectively, in testing. For Gumbel's MF technique, the values for SI in training and testing were 4.519 and 7.980, respectively, and 6.245 and 10.278, respectively, for the Linear MF method. The greater accuracy of Gumbel's MF approach is further supported by the lower RMSE and SI values in comparison to the Linear MF method. The numbers for NSE in the Table 5.12 are 0.940 in training and 0.888 in testing for Gumbel's MF versus 0.885 in training and 0.846 in testing for Linear MF, demonstrating that the Gumbel's MF approach has higher values, highlighting its improved accuracy as compared to the Linear MF method.

Table 5.12 Model Performance Indices using ANFIS

Model Performance Index (MPI) Parameters	ANFIS S/D=3			
	Training		Testing	
	Gumbel's MF	Linear MF	Gumbel's MF	Linear MF
CC	0.970	0.944	0.949	0.942
RMSE	0.011	0.016	0.018	0.024
SI	4.519	6.245	7.980	10.278
NSE	0.940	0.885	0.888	0.846

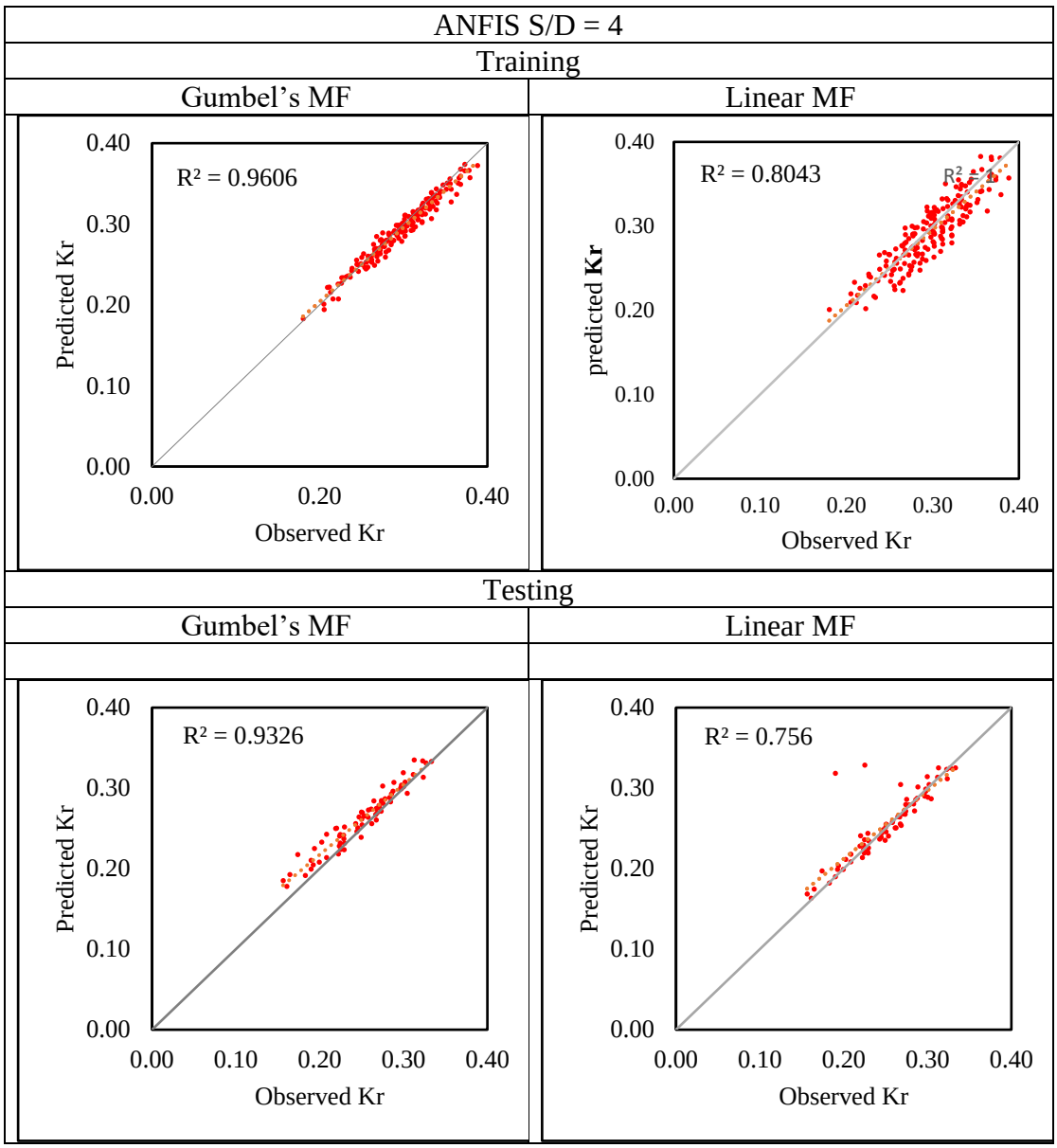

Figure 5.11 Scattered Plot between Observed and Predicted Values of K_r (ANFIS S/D=4)

Table 5.13 Model Performance Indices using ANFIS

Model Performance Index (MPI) Parameters	ANFIS S/D=4			
	Training		Testing	
	Gumbel's MF	Linear MF	Gumbel's MF	Linear MF
CC	0.980	0.897	0.965	0.869
RMSE	0.018	0.022	0.015	0.021
SI	6.382	7.757	6.065	8.502

NSE	0.784	0.682	0.983	0.966

On Comparing the plots of observed vs. predicted K_r from Figure 5.11, it is observed that the coefficient of correlation (CC) obtained by Gumbel's MF method is better compared to the Linear MF method. The model performance index values obtained are tabulated in Table 5.13. The value of CC obtained by Gumbel's MF method in training is 0.980 as compared to a value of 0.897 in the Linear MF method. In testing, the CC value was found to be 0.965 and 0.869 for Gumbel's MF and Linear MF methods, respectively. The values for RMSE in training were 0.018 for Gimbel's MF method against 0.022 for the Linear MF method, while in testing, it was 0.015 and 0.021, respectively. The value for SI in training and testing was 6.382 and 6.065 for Gumbel's MF method, respectively, and 7.757 and 8.502 for the Linear MF method, respectively. The lower values for RMSE and SI in the Linear MF method as compared to the Linear MF method further indicate that the accuracy is more for Gumbel's MF method. The values for NSE 0.784 and 0.983 in training and testing, respectively, for Gumbel's MF and 0.682 and 0.966 for training and testing, respectively for Linear MF, show that Gumbel's MF method has greater values, hence emphasizing the accuracy over Gumbel's MF method.

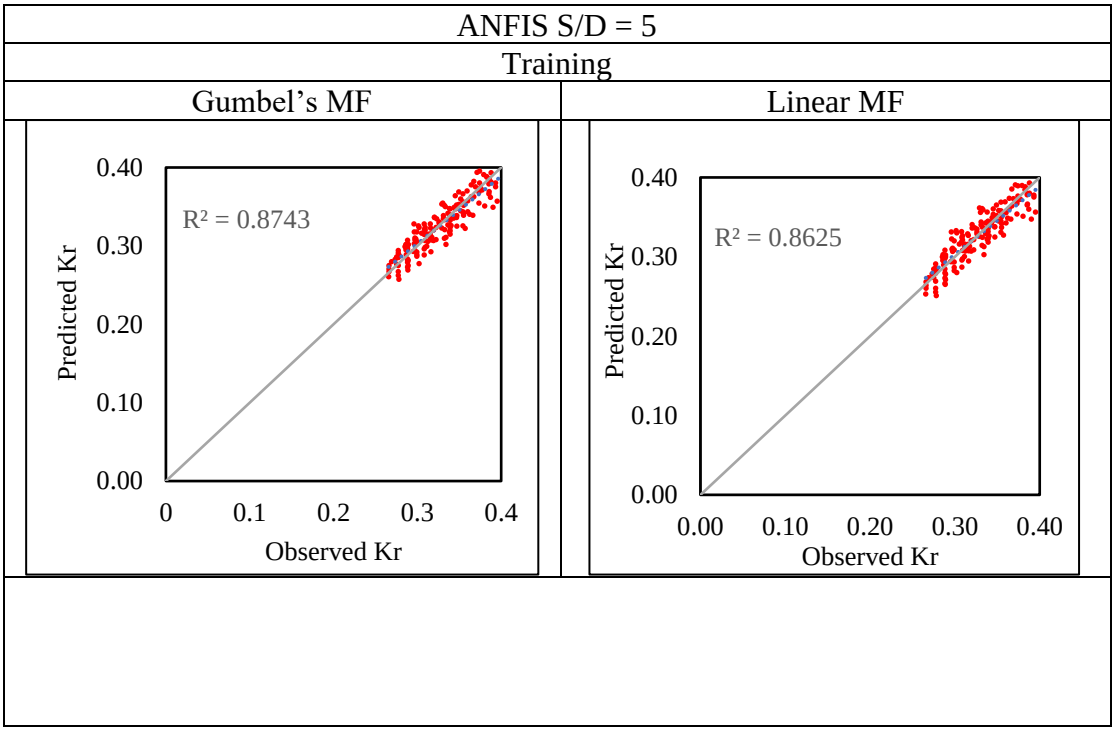

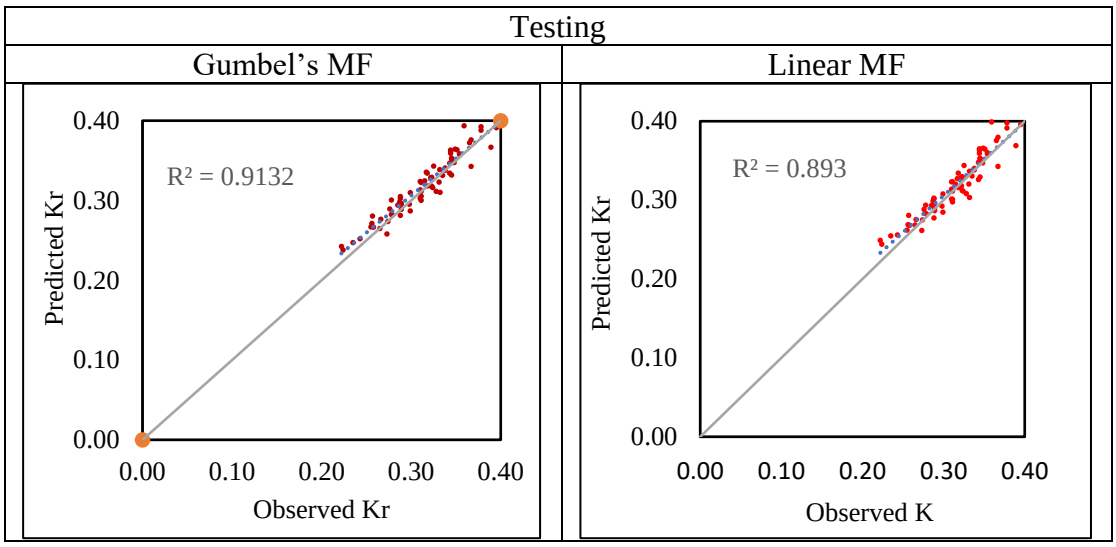

Figure 5.12 Scattered Plot between Observed and Predicted Values of K_r (ANFIS S/D=5)

Table 5.14 Model Performance Indices using ANFIS by dimensional parameters

Model Performance Index (MPI) Parameters	ANFIS S/D=5			
	Training		Testing	
	Gumbel's MF	Linear MF	Gumbel's MF	Linear MF
CC	0.954	0.928	0.956	0.945
RMSE	0.015	0.016	0.012	0.014
SI	4.469	4.665	3.959	4.302
NSE	0.872	0.860	0.895	0.876

From Figure 5.12, it can be seen that Gumbel's MF approach's coefficient of correlation (CC) is superior to the Linear MF method when comparing the plots of observed vs. predicted K_r. The model performance index values that were obtained are listed in Table 5.14. The CC value attained by Gumbel's MF approach in training is 0.954 compared to a value of 0.928 in the Linear MF technique. During testing, it was found that the CC values for Gumbel's MF and Linear MF methods were 0.956 and 0.945, respectively. Results for RMSE for the Gumbel's MF approach and Linear MF method in training were 0.015 and 0.016, respectively, while they were 0.012 and 0.014 for testing. The values for SI during training and testing for Gumbel's MF methodology were 4.469 and 3.959, respectively, while for the Linear MF method, they were 4.665 and 4.302,

respectively. The reduced RMSE and SI values compared to the Linear MF method further demonstrate the higher accuracy of Gumbel's MF method. The results for NSE in Table 5.14 show that Gumbel's MF approach has higher values, showing its better accuracy when compared to the linear MF method: 0.872 in training and 0.895 in testing for Gumbel's MF with 0.860 in training and 0.876 in testing for Linear MF.

Table 5.15 Comparison of Model Performance Index obtained from ANFIS by Gumbel's using Dimensional parameters

	CC		RMSE		SI		NSE	
	Training	Testing	Training	Testing	Training	Testing	Training	Testing
S/D=2	0.9680	0.967	0.013	0.015	6.316	6.441	0.937	0.933
S/D=3	0.970	0.949	0.011	0.018	4.519	7..980	0.940	0.888
S/D=4	0.980	0.965	0.018	0.015	6.382	6.065	0.784	0.983
S/D=5	0.954	0.956	0.015	0.012	4.469	3.959	0.872	0.895

Comparison of Model Performance Indices for different S/d ratios of perforated QBW models using ANN by LM algorithm is presented in Table 5.15.

5.4.2 Using Non-Dimensional Parameters

ANFIS S/D = 2

Training

Gumbel's MF

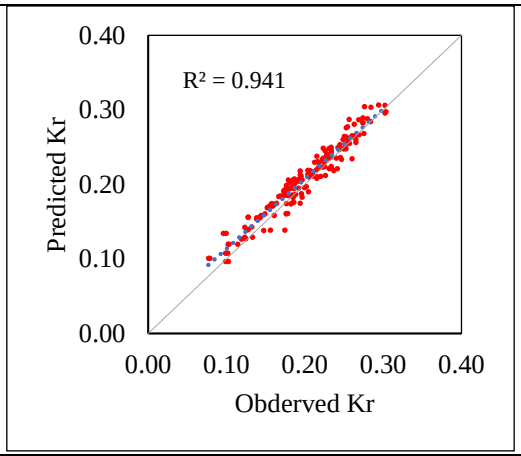

Linear MF

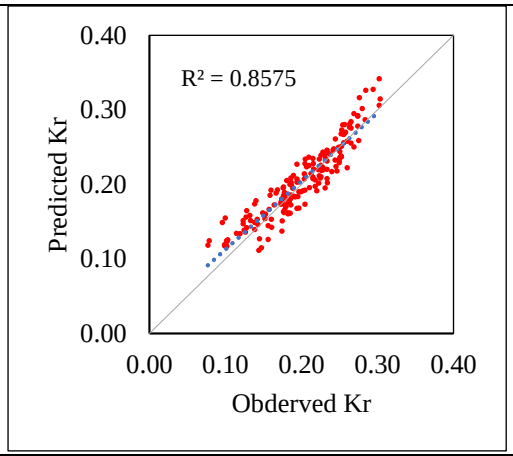

Testing

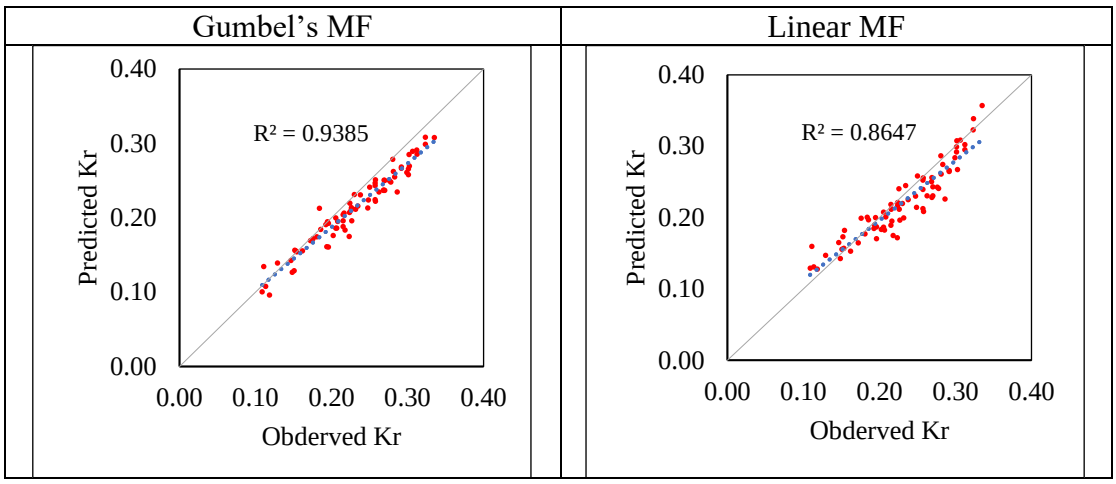

Figure 5.13 Scattered Plot between Observed and Predicted Values of K_r (ANFIS S/D=2)

Table 5.16 Model Performance Indices using ANFIS by non-dimensional Parameters

Model Performance Index (MPI) Parameters	ANFIS S/D=2			
	Training		Testing	
	Gumbel's MF	Linear MF	Gumbel's MF	Linear MF
CC	0.9700	0.9260	0.9688	0.9298
RMSE	0.0485	0.0496	0.0504	0.1245
SI	0.0274	0.0280	0.0654	0.1617
NSE	0.875	0.859	0.885	0.865

Figure 5.13 show the plot of observed Vs. predicted $K_{r;}$ from Table 5.16, it can be seen that Gumbel's MF approach's coefficient of correlation (CC) is superior to the Linear MF method. The CC value attained by Gumbel's MF approach in training is 0.9700 compared to a value of 0.9260 in the Linear MF technique. During testing, it was found that the CC values for Gumbel's MF and Linear MF methods were 0.9688 and 0.9298, respectively. Results for RMSE for the Gumbel's MF approach and Linear MF method in training were 0.0485 and 0.0496, respectively, while they were 0.0504 and 0.1245 for testing. The values for SI during training and testing for Gumbel's MF methodology were 0.0274 and 0.0654, respectively, while for the Linear MF method, they were 0.0280 and 0.1617, respectively. The reduced RMSE and SI values compared to the

Linear MF method further demonstrate the higher accuracy of Gumbel's MF method. The results for NSE in Table 5.16 show that Gumbel's MF approach has higher values, showing its better accuracy when compared to the linear MF method: 0.859 in training and 0.865 in testing for Linear MF with 0.875 in training and 0.885 in testing for Gumbel's MF.

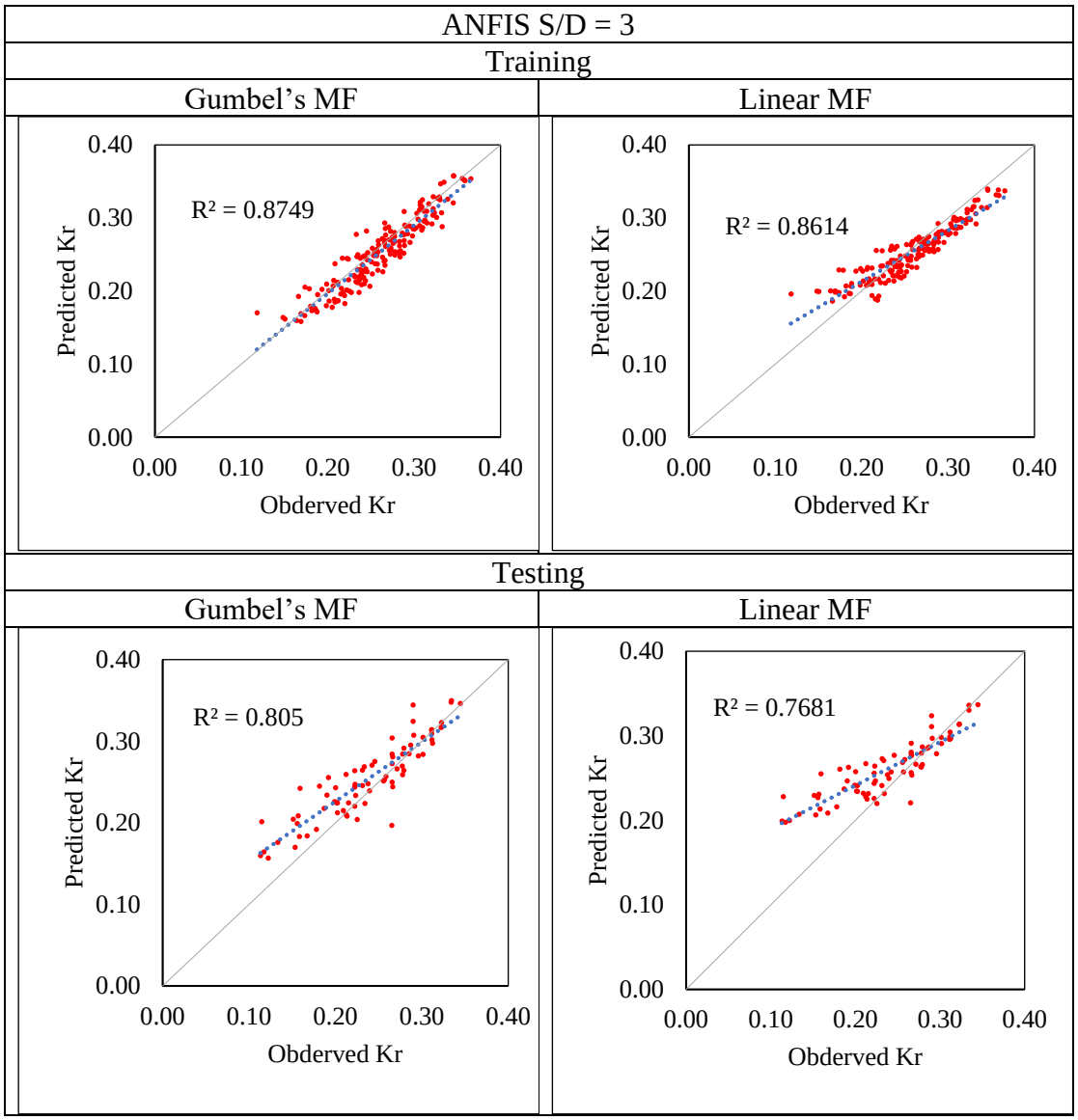

Figure 5.14 Scattered Plot between Observed and Predicted Values of K_r (ANFIS S/D=3)

Table 5.17 Model Performance Indices using ANFIS by non-dimensional Parameters

Model Performance Index (MPI) Parameters	ANFIS S/D=3			
	Training		Testing	
	Gumbel's MF	Linear MF	Gumbel's MF	Linear MF
CC	0.9337	0.9281	0.9219	0.8764
RMSE	0.0348	0.0392	0.0302	0.0862
SI	0.0197	0.0221	0.0392	0.1119
NSE	0.921	0.893	0.8992	0.881

Comparing the plots of observed vs. anticipated K_r, it can be shown that Gumbel's MF approach's coefficient of correlation (CC) is superior to the Linear MF method. The values of the model performance index that were found are shown in Table 5.17. During training, Gumbel's MF strategy achieved a CC value of 0.9337 as opposed to the Linear MF technique's 0.9281. The CC values during testing using Gumbel's MF and Linear MF were found to be 0.9219 and 0.8764, respectively. In training, the RMSE for Gumbel's MF technique and the Linear MF method were 0.0348 and 0.0392, respectively, whereas, in testing, they were 0.0302 and 0.0862, respectively. For Gumbel's MF method, the values for SI were 0.0197 and 0.0392 in training and testing, while for the Linear MF method, they were 0.0221 and 0.1119 in training and testing, respectively. Further evidence of the improved accuracy of Gumbel's MF approach comes from the lower RMSE and SI values as compared to the Linear MF method. The Gumbel's MF method has higher values for NSE than the Linear MF method, demonstrating improved accuracy: 0.8932 in training and 0.8811 in testing, and 0.921 training and 0.8992 in testing by Gumbel's MF.

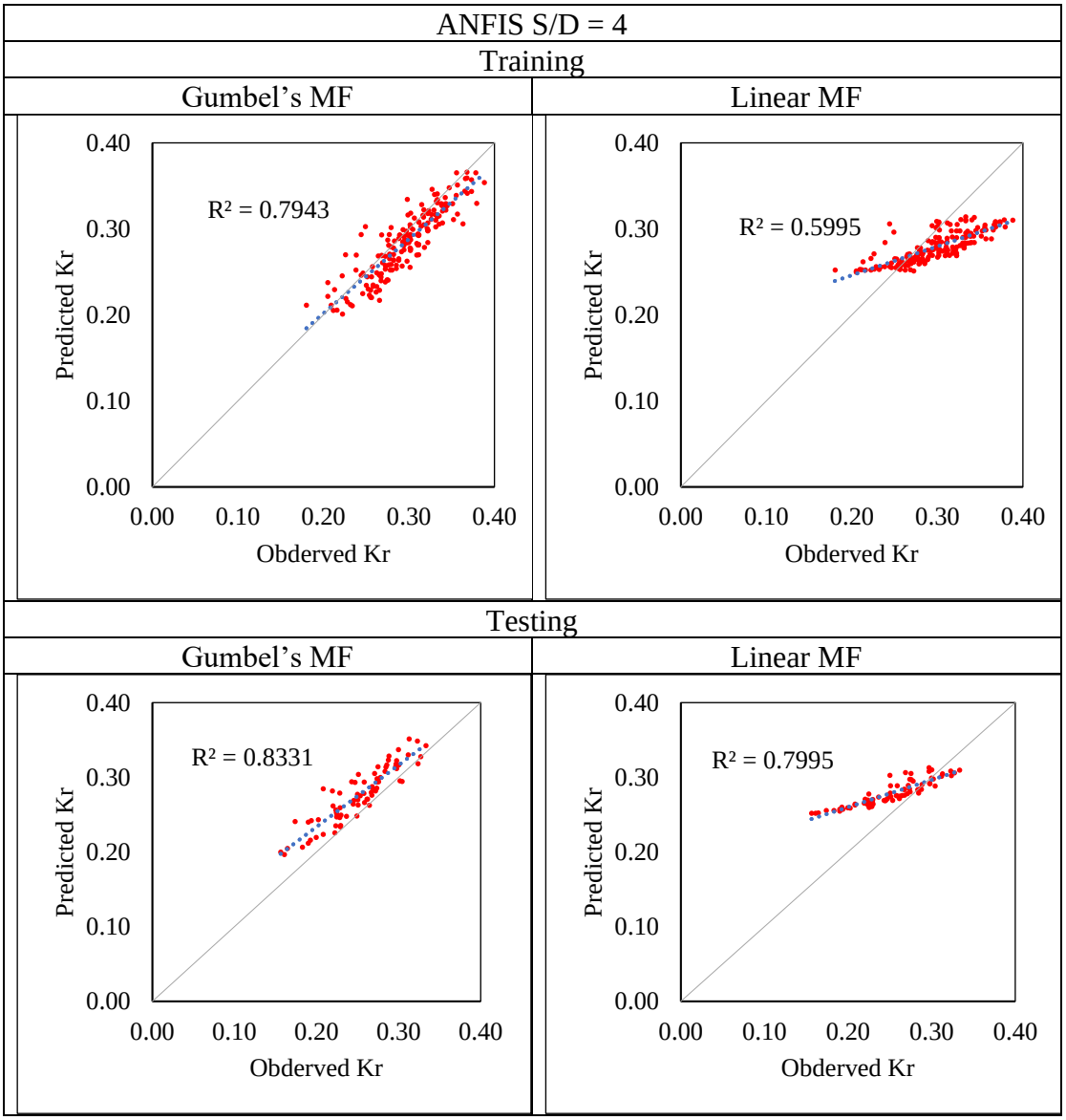

Figure 5.15 Scattered Plot between Observed and Predicted Values of K_r (ANFIS S/D=4)

Table 5.18 Model Performance Indices by non-dimensional parameters

Model Performance Index (MPI) Parameters	ANFIS S/D=4			
	Training		Testing	
	Gumbel's MF	Linear MF	Gumbel's MF	Linear MF
CC	0.8912	0.7743	0.9127	0.8941
RMSE	0.0354	0.0826	0.0313	0.0865
SI	0.0002	0.0005	0.0407	0.1124
NSE	0.927	0.883	0.913	0.895

From Figure 5.15, it can be seen that Gumbel's MF approach's coefficient of correlation (CC) is superior to the Linear MF method when comparing the plots of observed vs. predicted K_r. The model performance index values that were obtained are listed in Table 5.18. The CC value attained by Gumbel's MF approach in training is 0.8912 compared to a value of 0.7743 in the Linear MF technique. During testing, it was found that the CC values for Gumbel's MF and Linear MF methods were 0.9127 and 0.8941, respectively. Results for RMSE for the Gumbel's MF approach and Linear MF method in training were 0.0354 and 0.0826, respectively, while they were 0.0313 and 0.0865 for testing. The values for SI during training and testing for Gumbel's MF methodology were 0.0002 and 0.0407, respectively, while for the Linear MF method, they were 0.0005 and 0.1124, respectively. The reduced RMSE and SI values compared to the Linear MF method further demonstrate the higher accuracy of Gumbel's MF method. The results for NSE in Table 5.18 show that Gumbel's MF approach has higher values, showing its better accuracy when compared to the linear MF method: 0.927 in training and 0.913 in testing for Gumbel's MF with 0.883 in training and 0.895 in testing for Linear MF.

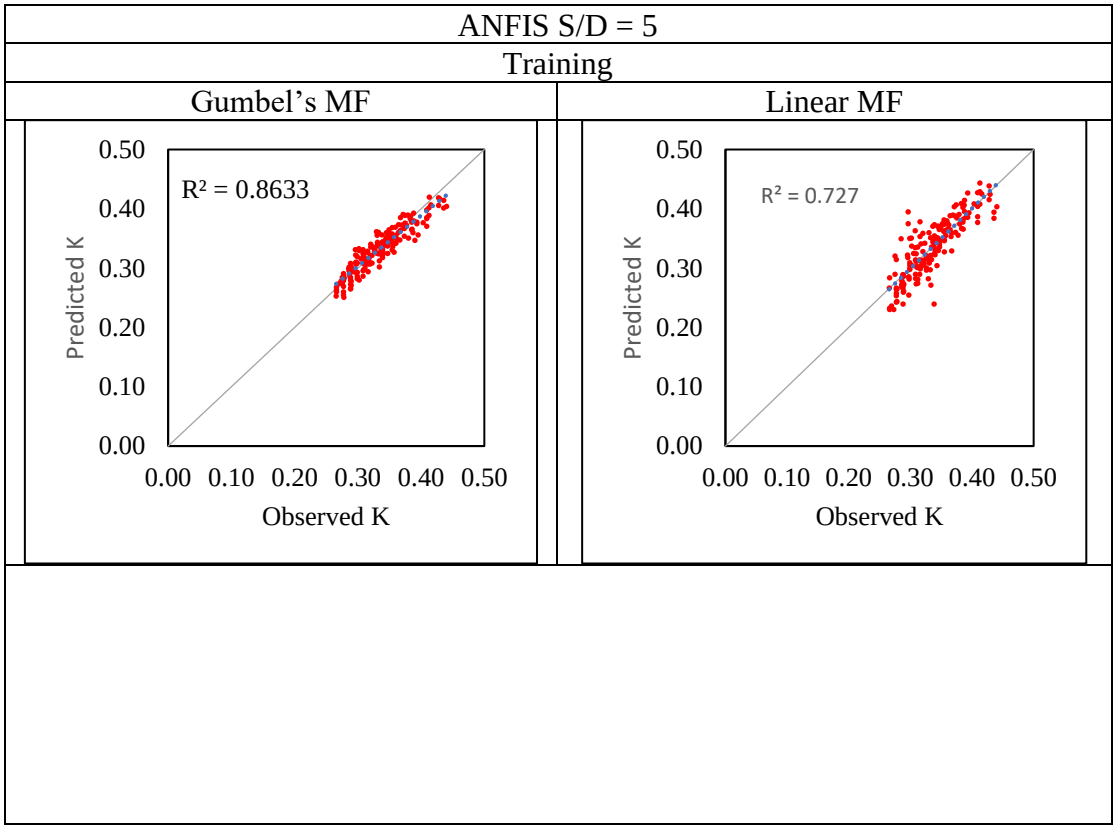

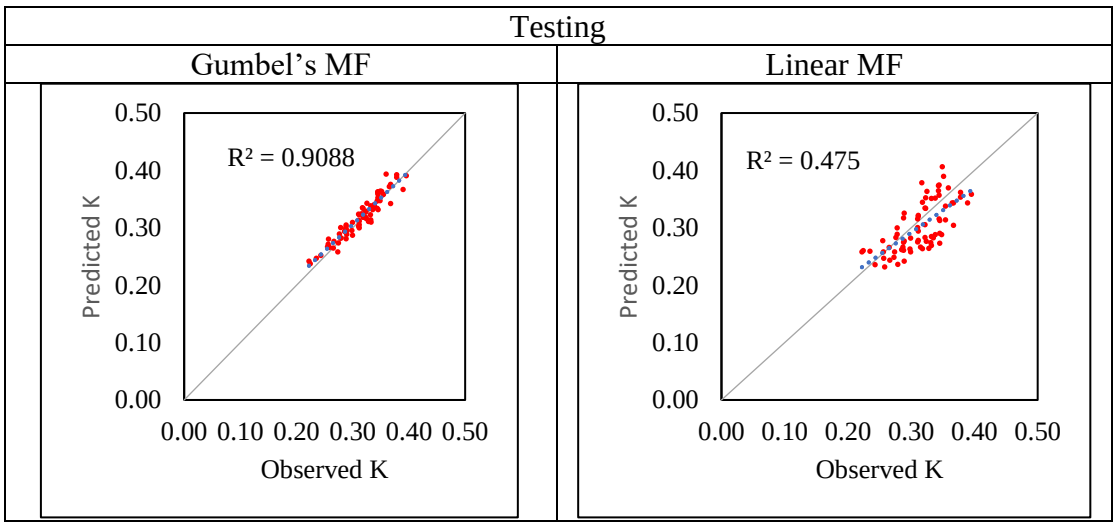

Figure 5.16 Scattered Plot between Observed and Predicted Values of K_r (ANFIS S/D=5)

Table 5.19 Model Performance Indices using ANFIS by non-dimensional Parameters

Model Performance Index (MPI) Parameters	ANFIS S/D=5			
	Training		Testing	
	Gumbel's MF	Linear MF	Gumbel's MF	Linear MF
CC	0.9291	0.8214	0.9451	0.8854
RMSE	0.0458	0.0556	0.0487	0.0572
SI	0.0259	0.0314	0.0633	0.0743
NSE	0.874	0.862	0.938	0.867

From Figure 5.16, it can be seen that Gumbel's MF approach's coefficient of correlation (CC) is superior to the Linear MF method when comparing the plots of observed vs. predicted K_r. The model performance index values that were obtained are listed in Table 5.19. The CC value attained by Gumbel's MF approach in training is 0.9291 compared to a value of 0.8214 in the Linear MF technique. During testing, it was found that the CC values for Gumbel's MF and Linear MF methods were 0.9451 and 0.8854, respectively. Results for RMSE for the Gumbel's MF approach and Linear MF method in training were 0.0458 and 0.0556, respectively, while they were 0.0487 and 0.0572 for testing. The values for SI during training and testing for Gumbel's MF methodology

were 0.0259 and 0.0633, respectively, while for the Linear MF method, they were 0.0314 and 0.0743, respectively. The reduced RMSE and SI values compared to the Linear MF method further demonstrate the higher accuracy of Gumbel's MF method. The results for NSE in Table 5.19 show that Gumbel's MF approach has higher values, showing its better accuracy when compared to the linear MF method: 0.862 in training and 0.867 in testing for Linear MF with 0.874 in training and 0.938 in testing for Gumbel's MF.

Table 5.20 Comparison of Model Performance Index obtained from ANFIS by Gumbel's using non-dimensional parameters

	CC		RMSE		SI		NSE	
	Training	Testing	Training	Testing	Training	Testing	Training	Testing
S/D=2	0.9700	0.9688	0.0485	0.0504	0.0274	0.0654	0.875	0.885
S/D=3	0.9337	0.9219	0.0348	0.0302	0.0197	0.0392	0.921	0.8992
S/D=4	0.8912	0.9127	0.0354	0.0313	0.0002	0.0407	0.927	0.913
S/D=5	0.9291	0.9451	0.0458	0.0487	0.0259	0.0633	0.874	0.938

Comparison of Model Performance Indices for different S/d ratios of perforated QBW models using ANN by LM algorithm is presented in Table 5.20.

5.5 PREDICTION OF REFLECTION COEFFICIENT (K_r) OF A PERFORATED QBW USING SUPPORT VECTOR MODEL (SVM)

5.5.1 Using Dimensional Parameters

The effectiveness of the SVM models hinges on careful kernel parameter selection. When creating SVM models, parameters are initially randomly searched by coarse search to fine search by trial-and-error method to identify the approximate optimal values. Then, the near-optimal values are fine-tuned to identify the precise optimal values using the K-fold cross-validation optimization technique. The present study considers the value of d (degree) for a Sigmoidal kernel function and Gaussian kernel function as 5 and 3, respectively. For different S/D ratios of perforations on the sea side

face of QBW, the number of support vectors for predicting the wave reflection coefficient is the same for both kernel functions.

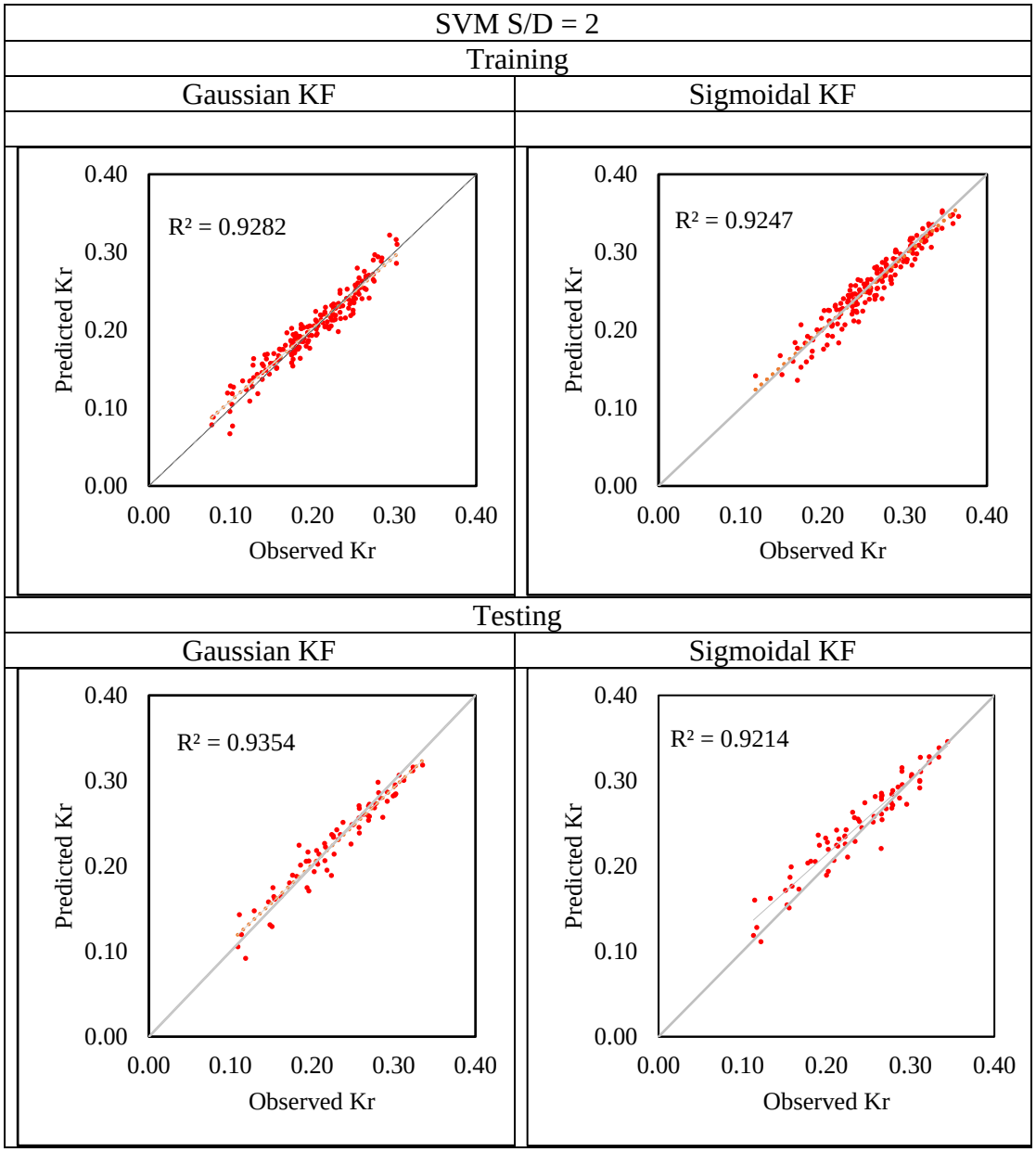

Figure 5.17 Scattered Plot between Observed and Predicted Values of K_r (SVM S/D=2)

Table 5.21 Model Performance Indices using SVM by dimensional parameters

Model Performance Index (MPI) Parameters	SVM S/D=2			
	Training		Testing	
	Gaussian KF	Sigmoidal KF	Gaussian KF	Sigmoidal KF
CC	0.963	0.961	0.967	0.959
RMSE	0.013	0.014	0.014	0.015
SI	6.389	6.788	6.382	6.639
NSE	0.985	0.927	0.934	0.928

When comparing the plots of observed vs. anticipated K_r, it can be shown that the Sigmoidal KF approach's coefficient of correlation (CC) is superior to the Gaussian KF method. The values of the model performance index that were found are shown in Table 5.21. During training, the Gaussian KF strategy achieved a CC value of 0.963 as opposed to the Sigmoidal KF technique's 0.961. The CC values for the Gaussian KF and Sigmoidal KF techniques were found to be, respectively, 0.967 and 0.959 as a result of testing. In training, the RMSE for the Gaussian KF technique and the Sigmoidal KF method were 0.013 and 0.014, respectively, whereas in testing, they were 0.014 and 0.015, respectively. For the Gaussian KF method, the values for SI were 6.389 and 6.382 in training and testing, respectively, while for the Sigmoidal KF method, they were 6.788 and 6.639 in training and testing, respectively. Further evidence of the improved accuracy of the Gaussian KF approach comes from the lower RMSE and SI values as compared to the Sigmoidal KF method. The Gaussian KF method has higher values for NSE than the Sigmoidal KF method, demonstrating improved accuracy: 0.985 in training and 0.934 in testing for Gaussian KF vs. 0.927 in training and 0.928 in testing for Sigmoidal KF.

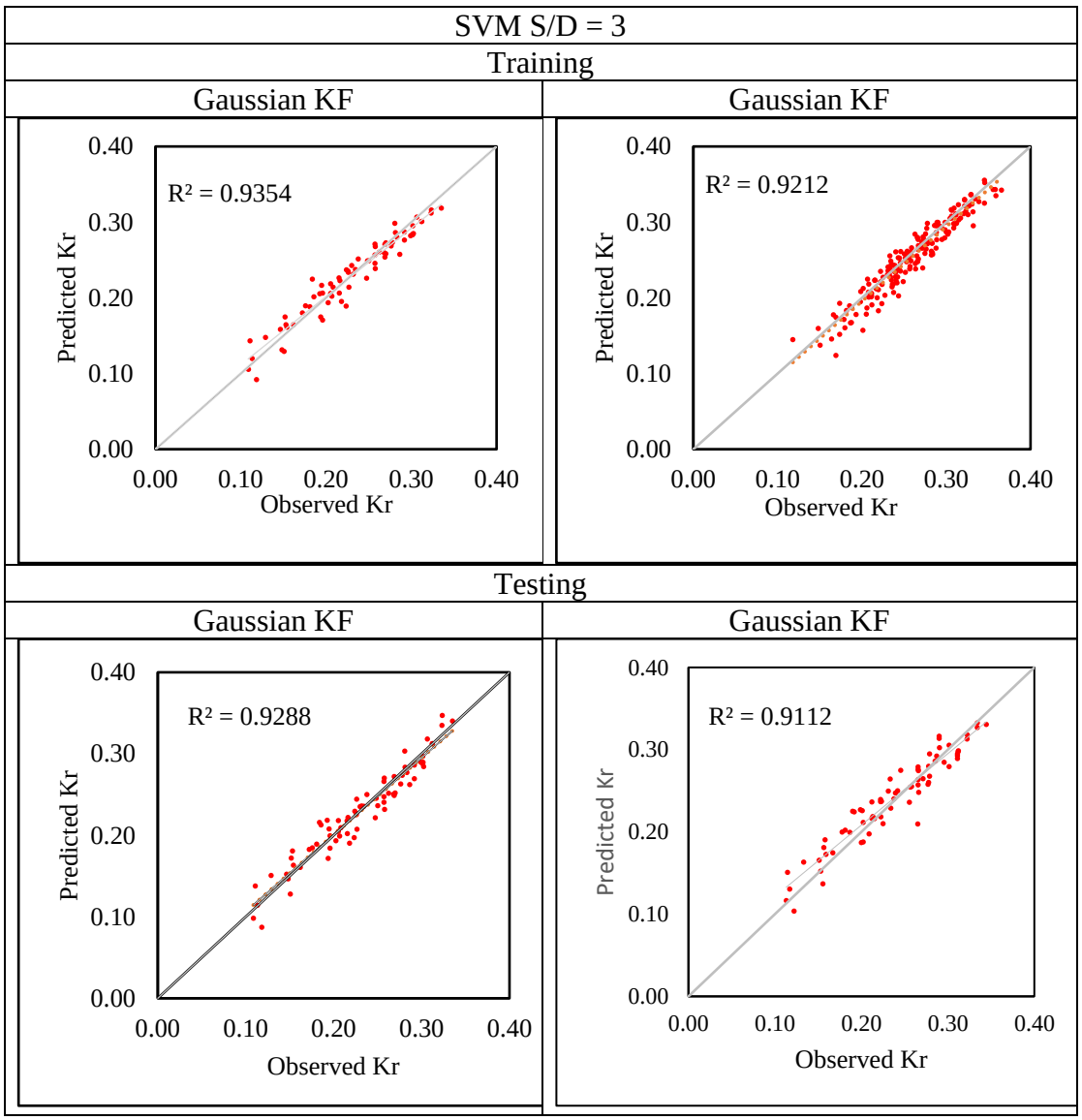

Figure 5.18 Scattered Plot between Observed and Predicted Values of K_r (SVM S/D=3)

Table 5.22 Model Performance Indices using SVM by dimensional parameters

Model Performance Index (MPI) Parameters	SVM S/D=3			
	Training		Testing	
	Gaussian KF	Sigmoidal KF	Gaussian KF	Sigmoidal KF
CC	0.966	0.959	0.963	0.954
RMSE	0.012	0.013	0.017	0.019

SI	5.119	5.140	7.546	7.236
NSE	0.946	0.922	0.901	0.889

On comparing the plots of observed vs. predicted Kr, it can be seen that the Gaussian KF approach's coefficient of correlation (CC) is superior to the Gaussian KF method. Table 5.22 lists the model performance index values that were obtained. In comparison to a value of 0.966 in the Gaussian KF technique, the value of CC obtained by the Sigmoidal KF method in training is 0.959. Testing revealed that the CC values for the Gaussian KF and Sigmoidal KF methods were, respectively, 0.963 and 0.954. The results for RMSE were 0.012 for the Gaussian KF and 0.013 for the Sigmoidal KF method during training, whereas they were 0.017 and 0.019, respectively, in testing. For the Gaussian KF technique, the values for SI in training and testing were 5.119 and 7.546, respectively, and 5.140 and 7.236, respectively, for Sigmoidal KF. The greater accuracy of the Gaussian KF approach is further supported by the lower RMSE and SI values in comparison to the Sigmoidal KF method. The numbers for NSE in Table 5.22, 0.946 in training and 0.901 in testing for Gaussian KF versus 0.922 in training and 0.889 in testing for Sigmoidal KF, demonstrate that the Gaussian KF approach has higher values, highlighting its improved accuracy as compared to the Sigmoidal KF method.

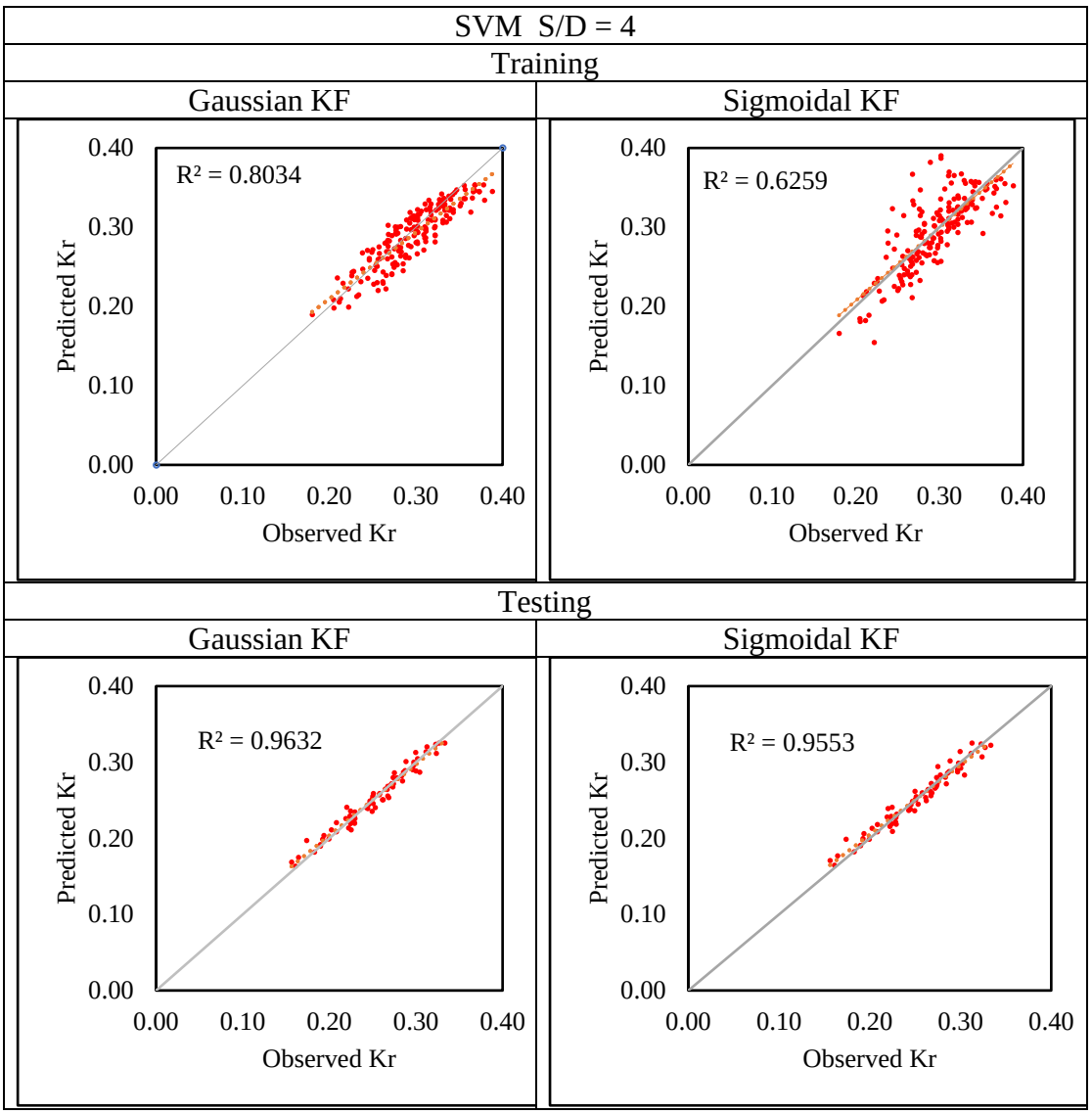

Figure 5.19 Scattered Plot between Observed and Predicted Values of K_r (SVM S/D=4)

Table 5.23 Model Performance Indices using SVM by dimensional parameters

Model Performance Index (MPI) Parameters	SVM S/D=4			
	Training		Testing	
	Gaussian KF	Sigmoidal KF	Gaussian KF	Sigmoidal KF
CC	0.896	0.791	0.981	0.977
RMSE	0.028	0.046	0.007	0.009
SI	9.863	15.581	3.212	3.560
NSE	0.882	0.748	0.994	0.991

Comparing the plots of observed vs. predicted K_r, it is observed that the coefficient of correlation (CC) obtained by the Gaussian KF method is better compared to the Sigmoidal KF method. The model performance index values obtained are tabulated in Table 5.23. The value of CC obtained by the Gaussian KF method in training is 0.896 as compared to a value of 0.791 in the Sigmoidal KF method. In testing, the CC value was found to be 0.981 and 0.977 for Gaussian KF and Sigmoidal KF methods, respectively. The values for RMSE in training were 0.028 for the Gaussian KF method against 0.046 for the Sigmoidal KF method, while in testing, it was 0.007 and 0.009, respectively. The value for SI in training and testing was 9.863 and 3.212 for the Gaussian KF method, respectively, and 15.581 and 3.560 for the Sigmoidal KF method, respectively. The lower values for RMSE and SI in the Gaussian KF method as compared to the Sigmoidal KF method further indicate that the accuracy is more for the Gaussian KF method. The values for NSE 0.882 and 0.994 in training and testing, respectively, for Gaussian KF and 0.748 and 0.991 for training and testing, respectively for Sigmoidal KF, show that Gaussian KF method has greater values, hence emphasizing the accuracy over Sigmoidal KF method.

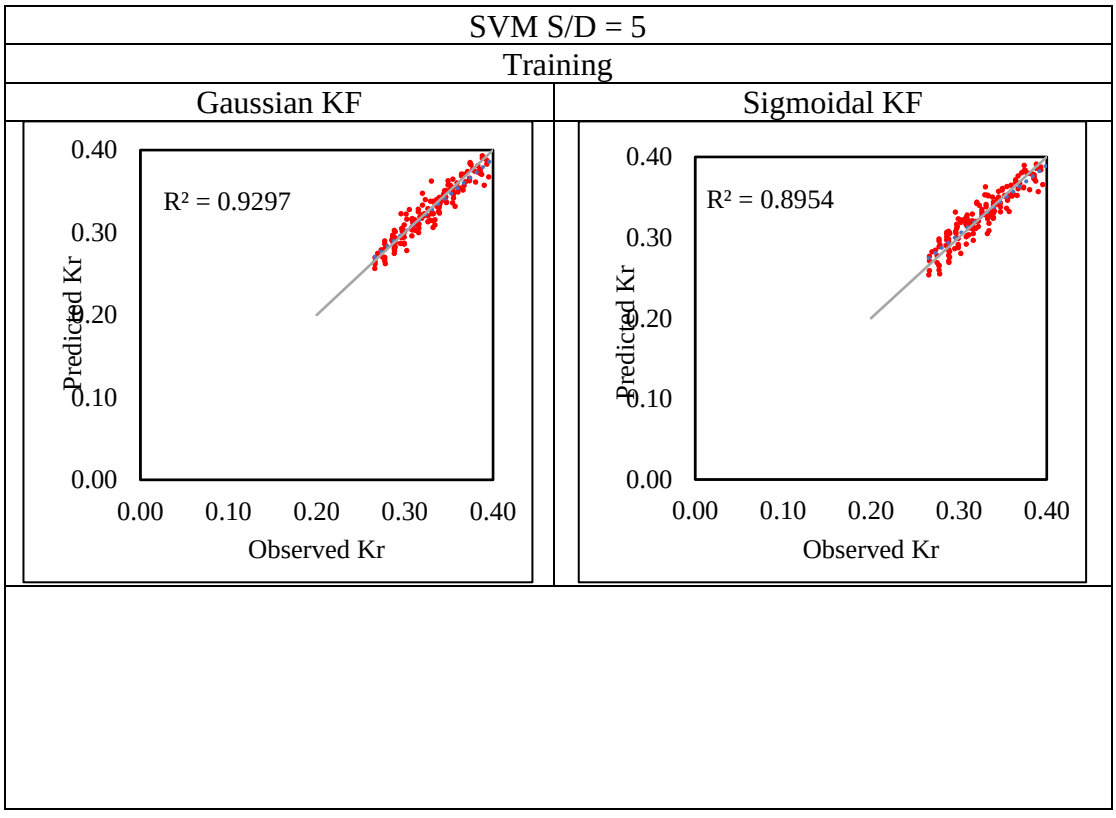

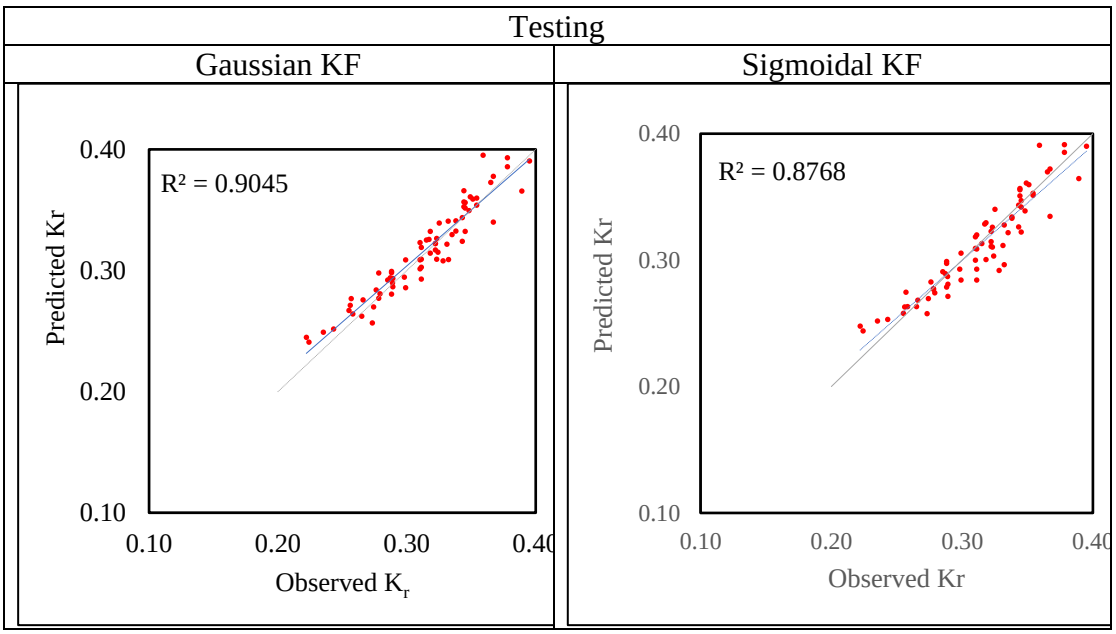

Figure 5.20 Scattered Plot between Observed and Predicted Values of K_r (SVM S/D=5)

Table 5.24 Model Performance Indices using SVM by dimensional parameters

Model Performance Index (MPI) Parameters	SVM S/D=5			
	Training		Testing	
	Gaussian KF	Sigmoidal KF	Gaussian KF	Sigmoidal KF
CC	0.964	0.946	0.951	0.936
RMSE	0.011	0.013	0.012	0.014
SI	3.471	4.075	3.894	4.338
NSE	0.923	0.893	0.897	0.874

It can be seen that the Gaussian KF approach's coefficient of correlation (CC) is superior to the Gaussian KF method when comparing the plots of observed vs. anticipated K_r. The model performance index values that were obtained are listed in Table 5.24. The CC value attained by the Gaussian KF approach in training is 0.964 compared to a value of 0.946 in the Sigmoidal KF technique. As a result of testing, it was obtained that the CC values for the Gaussian KF and Sigmoidal KF approaches were, respectively, 0.951 and 0.936. Results for RMSE for the Gaussian KF approach and Sigmoidal KF method in training were 0.011 and 0.013, respectively, while they were 0.012 and 0.014 in testing. The values for SI in training and testing for the Gaussian KF method were 3.471 and 3.894, respectively, while for the Sigmoidal KF

method, they were 4.075 and 4.338, respectively. The RMSE and SI values compared to the Gaussian KF method further demonstrate the higher accuracy of the Gaussian KF approach. The results for NSE in Table 5.24 show that the Gaussian KF approach has higher values, showing its better accuracy when compared to the Sigmoidal KF method: 0.923 in training and 0.897 in testing for Gaussian KF with 0.893 in training and 0.874 in testing for Sigmoidal KF.

Table 5.25 Comparison of Model Performance Indices Obtained from SVM by Gaussian kernel using dimensional parameters

	CC		RMSE		SI		NSE	
	Training	Testing	Training	Testing	Training	Testing	Training	Testing
S/D=2	0.963	0.967	0.013	0.014	6.389	6.382	0.985	0.934
S/D=3	0.966	0.963	0.012	0.017	5.119	7.546	0.946	0.901
S/D=4	0.896	0.981	0.028	0.007	9.863	3.212	0.882	0.994
S/D=5	0.964	0.951	0.011	0.012	3.471	3.894	0.923	0.897

Comparison of Model Performance Indices for different S/d ratios of perforated QBW models using SVM by Gaussian kernel is presented in Table 5.25.

5.5.2 Using Non-Dimensional Parameters

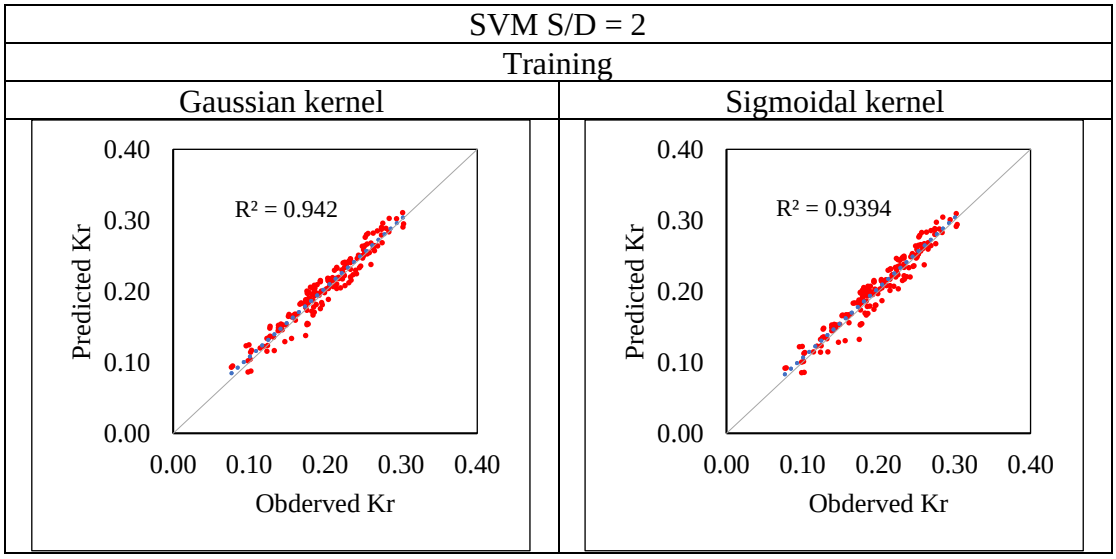

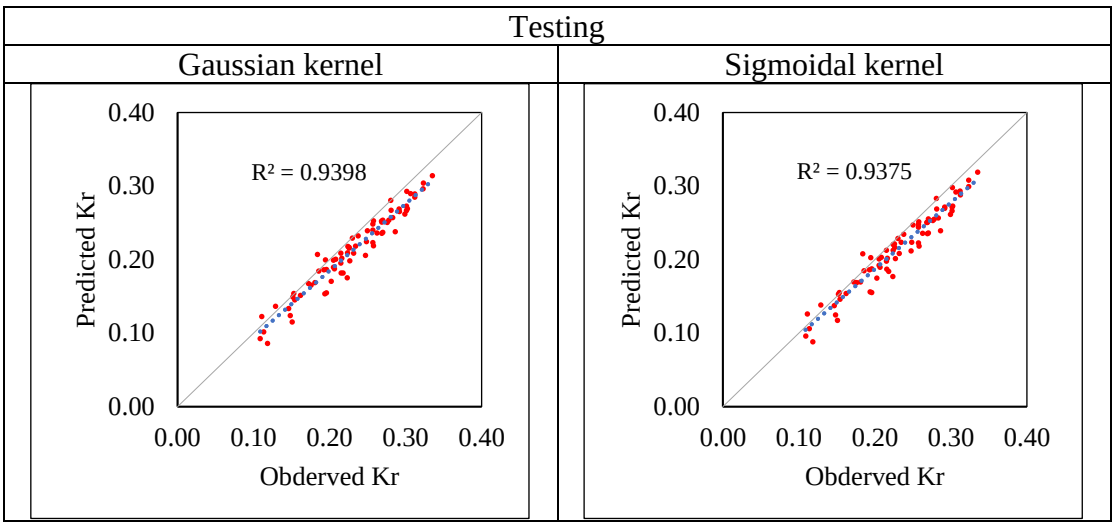

Figure 5.21 Scattered Plot between Observed and Predicted Values of K_r (SVM S/D=2)

Table 5.26 Model Performance Indices using SVM by non-dimensional parameters

Model Performance Index (MPI) Parameters	SVM S/D=2			
	Training		Testing	
	Gaussian kernel	Sigmoidal kernel	Gaussian kernel	Sigmoidal kernel
CC	0.970	0.969	0.969	0.968
RMSE	0.0511	0.0503	0.1339	0.1348
SI	0.0289	0.0284	0.1739	0.1751
NSE	0.963	0.892	0.912	0.896

It can be seen that the Gaussian KF approach's coefficient of correlation (CC) is superior to the Gaussian KF method when comparing the plots of observed vs. anticipated K_r. The model performance index values that were obtained are listed in Table 5.26. The CC value attained by the Gaussian KF approach in training is 0.970 compared to a value of 0.969 in the Sigmoidal KF technique. As a result of testing, it was obtained that the CC values for the Gaussian KF and Sigmoidal KF approaches were, respectively, 0.969 and 0.968. Results for RMSE for the Gaussian KF approach and Sigmoidal KF method in training were 0.0511 and 0.0503, respectively, while they were 0.1339 and 0.1348 in testing. The values for SI in training and testing for the Gaussian KF method were 0.0289 and 0.1739, respectively, while for the Sigmoidal KF method, they were 0.0284 and 0.1751, respectively. The RMSE and SI values

compared to the Gaussian KF method further demonstrate the higher accuracy of the Gaussian KF approach. The results for NSE in Table 5.26 show that the Gaussian KF approach has higher values, showing its better accuracy when compared to the Sigmoidal KF method: 0.963 in training and 0.912 in testing for Gaussian KF with 0.892 in training and 0.896 in testing for Sigmoidal KF.

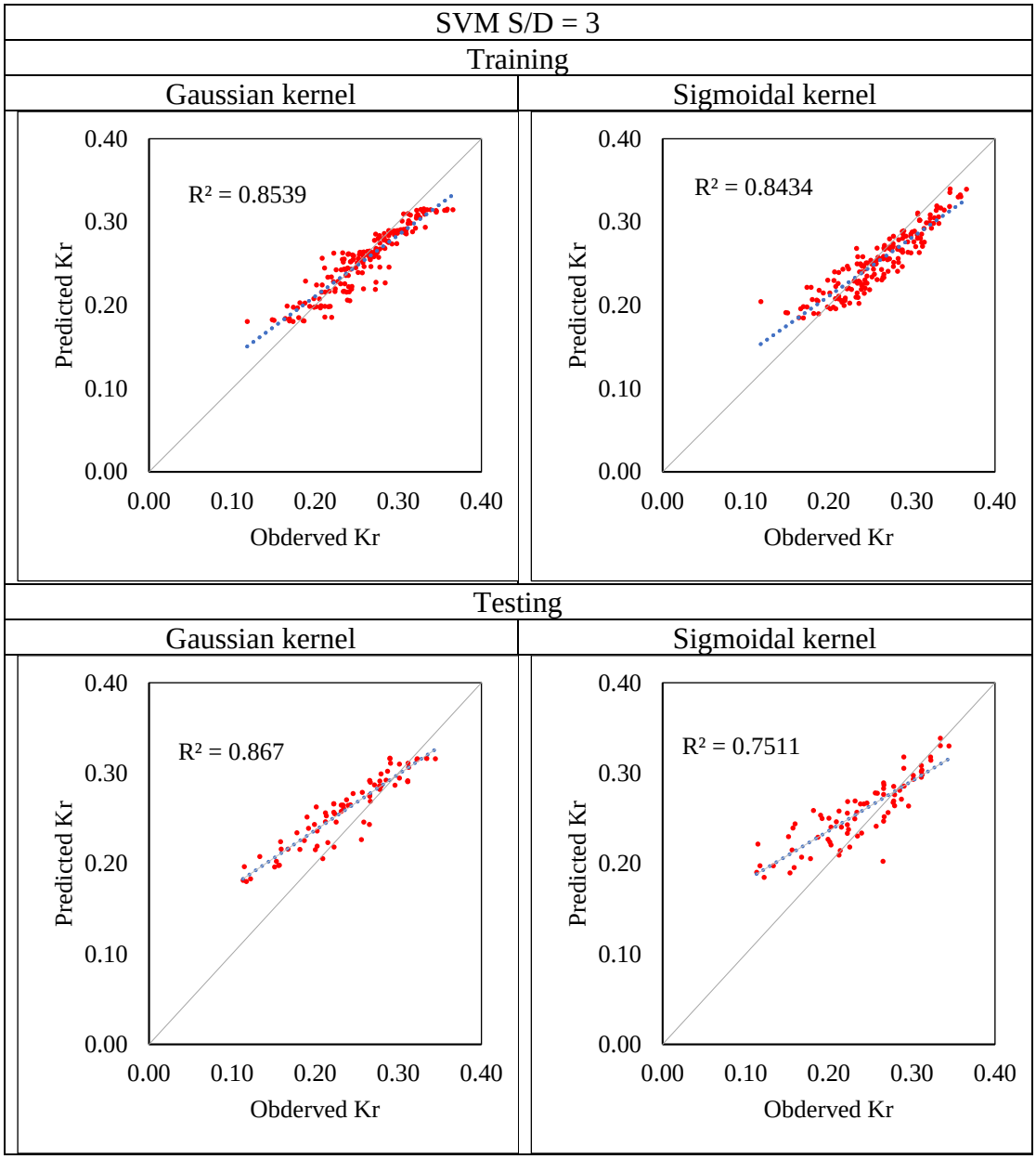

Figure 5.22 Scattered Plot between Observed and Predicted Values of K_r (SVM S/D=3)

Table 5.27 Model Performance Indices using SVM by non-dimensional parameters

Model Performance Index (MPI) Parameters	SVM S/D=3			
	Training		Testing	
	Gaussian kernel	Sigmoidal kernel	Gaussian kernel	Sigmoidal kernel
CC	0.9241	0.9186	0.9311	0.8666
RMSE	0.0324	0.0403	0.0256	0.0311
SI	0.0183	0.0227	0.0332	0.0404
NSE	0.941	0.915	0.928	0.898

Comparing the plots of observed vs. predicted K_r, it is observed that the coefficient of correlation (CC) obtained by the Gaussian KF method is better compared to the Sigmoidal KF method. The model performance index values obtained are tabulated in Table 5.27. The value of CC obtained by the Gaussian KF method in training is 0.9241 as compared to a value of 0.9186 in the Sigmoidal KF method. In testing, the CC value was found to be 0.9311 and 0.8666 for Gaussian KF and Sigmoidal KF methods, respectively. The values for RMSE in training were 0.0324 for the Gaussian KF method against 0.0403 for the Sigmoidal KF method, while in testing, it was 0.0256 and 0.0311, respectively. The value for SI in training and testing was 0.0183 and 0.0332 for the Gaussian KF method, respectively, and 0.0227 and 0.0404 for the Sigmoidal KF method, respectively. The lower values for RMSE and SI in the Gaussian KF method as compared to the Sigmoidal KF method further indicate that the accuracy is more for the Gaussian KF method. The values for NSE 0.941 and 0.928 in training and testing, respectively, for Gaussian KF and 0.915 and 0.898 for training and testing, respectively for Sigmoidal KF, show that the Gaussian KF method has greater values, hence emphasizing the accuracy over Sigmoidal KF method.

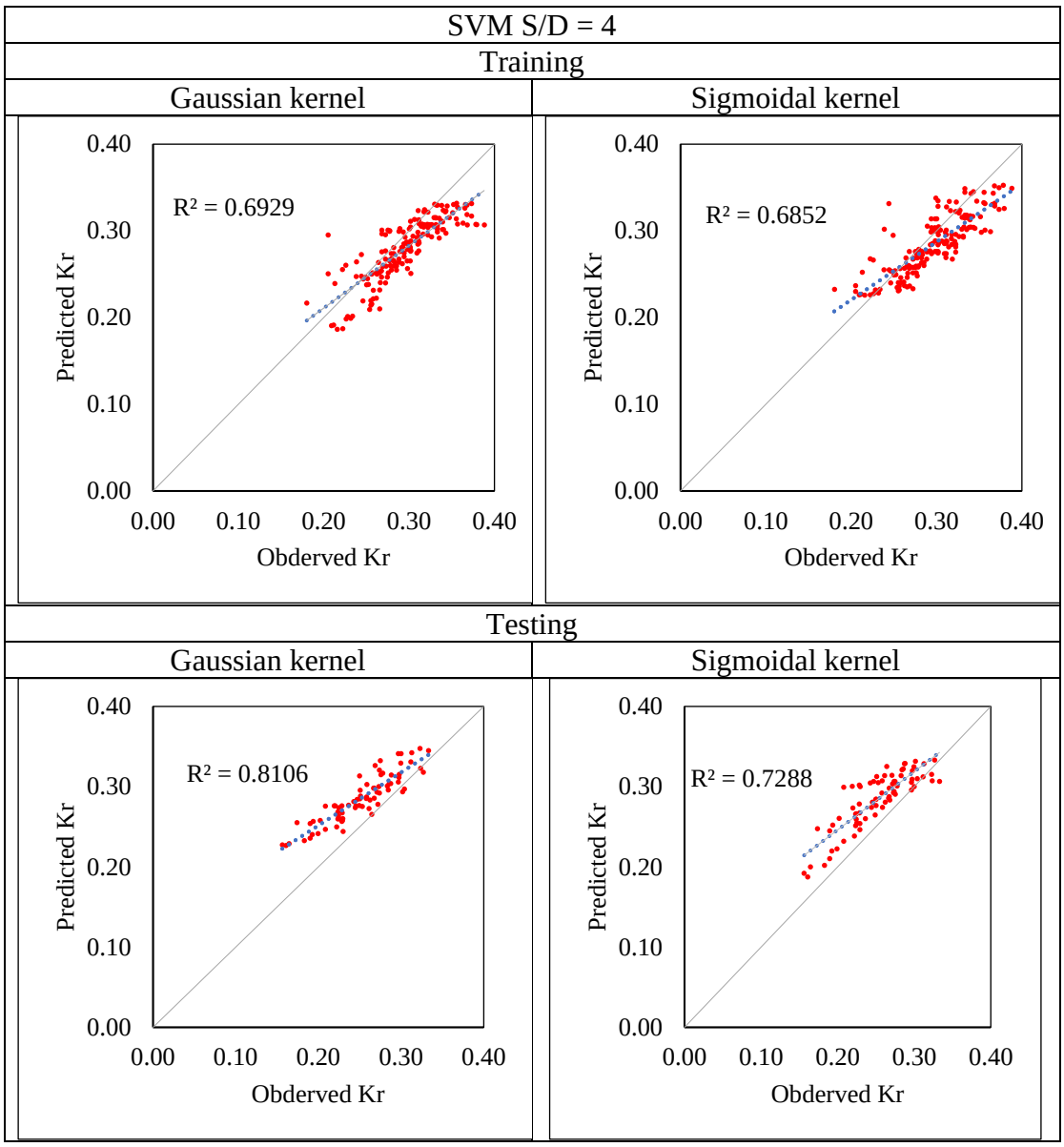

Figure 5.23 Scattered Plot between Observed and Predicted Values of K_r (SVM S/D=4)

Table 5.28 Model Performance Indices using SVM by non-dimensional parameters

Model Performance Index (MPI) Parameters	SVM S/D=4			
	Training		Testing	
	Gaussian kernel	Sigmoidal kernel	Gaussian kernel	Sigmoidal kernel
CC	0.8324	0.8277	0.9003	0.8537
RMSE	0.0669	0.0994	0.0652	0.1005
SI	0.0004	0.0006	0.0847	0.1305
NSE	0.912	0.817	0.931	0.846

When comparing the plots of observed vs. predicted Kr, it can be seen that the Gaussian KF approach's coefficient of correlation (CC) is superior to the Gaussian KF method. Table 5.28 lists the model performance index values that were obtained. In comparison to a value of 0.8324 in the Gaussian KF technique, the value of CC obtained by the Sigmoidal KF method in training is 0.8277. Testing revealed that the CC values for the Gaussian KF and Sigmoidal KF methods were, respectively, 0.9003 and 0.8537. The results for RMSE were 0.0669 for the Gaussian KF and 0.0994 for the Sigmoidal KF method during training, whereas they were 0.0652 and 0.1005, respectively, in testing. For the Gaussian KF technique, the values for SI in training and testing were 0.0004 and 0.0847, respectively, and 0.0006 and 0.1305, respectively, for Sigmoidal KF. The greater accuracy of the Gaussian KF approach is further supported by the lower RMSE and SI values in comparison to the Sigmoidal KF method. The numbers for NSE in Table 5.28, 0.912 in training and 0.931 in testing for Gaussian KF versus 0.817 in training and 0.846 in testing for Sigmoidal KF, demonstrate that the Gaussian KF approach has higher values, highlighting its improved accuracy as compared to the Sigmoidal KF method.

SVM S/D = 5	
Training	
Gaussian kernel	Sigmoidal kernel
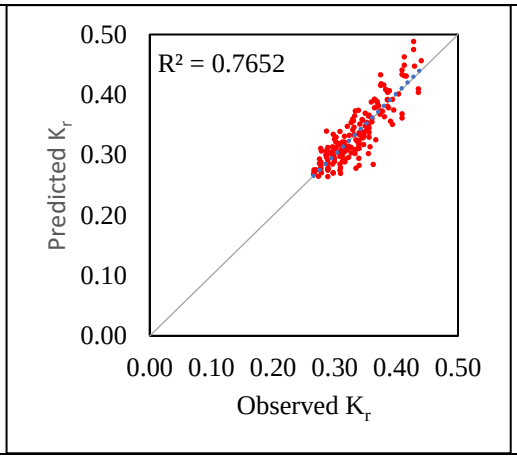	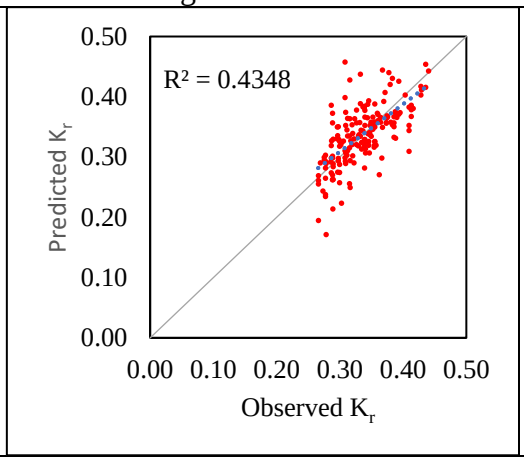
Testing	
Gaussian kernel	Sigmoidal kernel

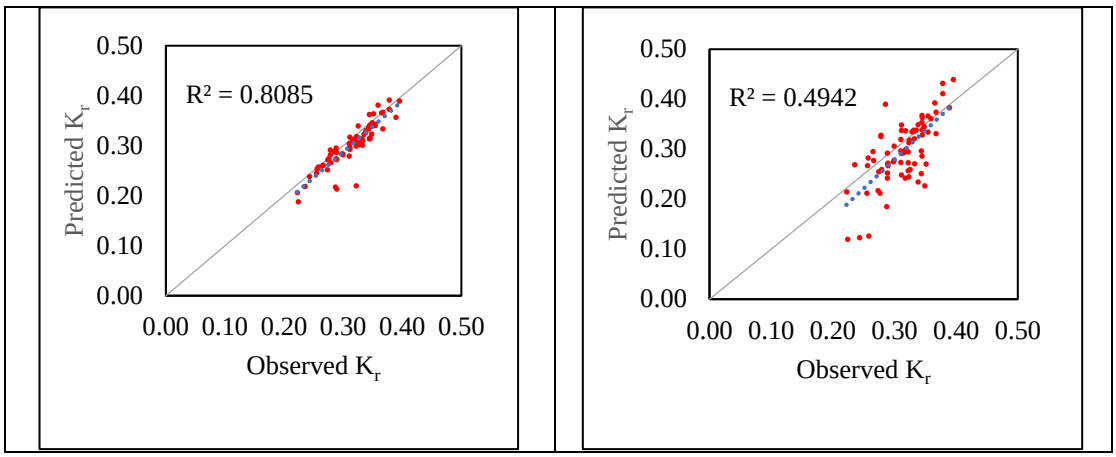

Figure 5.24 Scattered Plot between Observed and Predicted Values of K_r (SVM S/D=5)

Table 5.29 Model Performance Indices using SVM by non-dimensional parameters

Model Performance Index (MPI) Parameters	SVM S/D=5			
	Training		Testing	
	Gaussian kernel	Sigmoidal kernel	Gaussian kernel	Sigmoidal kernel
CC	0.8802	0.6323	0.8992	0.7031
RMSE	0.0458	0.0556	0.0487	0.0572
SI	0.0259	0.0314	0.0633	0.0743
NSE	0.913	0.889	0.897	0.871

When comparing the plots of observed vs. anticipated K_r, it can be shown that the Sigmoidal KF approach's coefficient of correlation (CC) is superior to the Gaussian KF method. The values of the model performance index that were found are shown in Table 5.29. During training, the Gaussian KF strategy achieved a CC value of 0.8802 as opposed to the Sigmoidal KF technique's 0.6323. The CC values for the Gaussian KF and Sigmoidal KF techniques were found to be, respectively, 0.8992 and 0.7031 as a result of testing. In training, the RMSE for the Gaussian KF technique and the Sigmoidal KF method were 0.0458 and 0.0556, respectively, whereas, in testing, they were 0.0487 and 0.0572, respectively. For the Gaussian KF method, the values for SI were 0.0259 and 0.0633 in training and testing, respectively, while for the Sigmoidal KF method, they were 0.0314 and 0.0743 in training and testing, respectively. Further evidence of the improved accuracy of the Gaussian KF approach comes from the lower RMSE and SI values as compared to the Sigmoidal KF method. The Gaussian KF

method has higher values for NSE than the Sigmoidal KF method, demonstrating improved accuracy: 0.913 in training and 0.897 in testing for Gaussian KF vs. 0.889 in training and 0.871 in testing for Sigmoidal KF.

Table 5.30 Comparison of Model Performance Index obtained from SVM by Gaussian kernel using non-dimensional parameters

	CC		RMSE		SI		NSE	
	Training	Testing	Training	Testing	Training	Testing	Training	Testing
S/D=2	0.970	0.969	0.0511	0.1339	0.0289	0.1739	0.963	0.912
S/D=3	0.924	0.931	0.0324	0.0256	0.0883	0.0332	0.941	0.928
S/D=4	0.983	0.900	0.0669	00652	0.0004	0.0847	0.912	0.931
S/D=5	0.880	0.899	0.0458	0.0487	0.0259	0.0633	0.913	0.897

Comparison of Model Performance Indices for different S/d ratios of perforated QBW models using SVM by Gaussian kernel is presented in Table 5.30.

5.6 PREDICTION OF REFLECTION COEFFICIENT (K_r) OF A PERFORATED QBW USING DEEP LEARNING MODEL

Deep Learning is a type of machine learning method based on learning data representations in deep learning methods, such as deep artificial neural networks, which use multiple processing layers to discover patterns and structures in very large data sets. Each layer learns a concept from the data that subsequent layers build on; the higher the level, the more abstract the concepts that are learned. Deep learning does not depend on prior data processing and automatically extracts features. To use a simple example, a deep neural network tasked with interpreting shapes would learn to recognize simple edges in the first layer and then add recognition of the more complex shapes composed of those edges in subsequent layers. There is no hard and fast rule for how many layers are needed to constitute deep learning, but most experts agree that more than two layers are required. Using a similar principle, the following predictions are carried out.

5.6.1 Using Dimensional Parameters

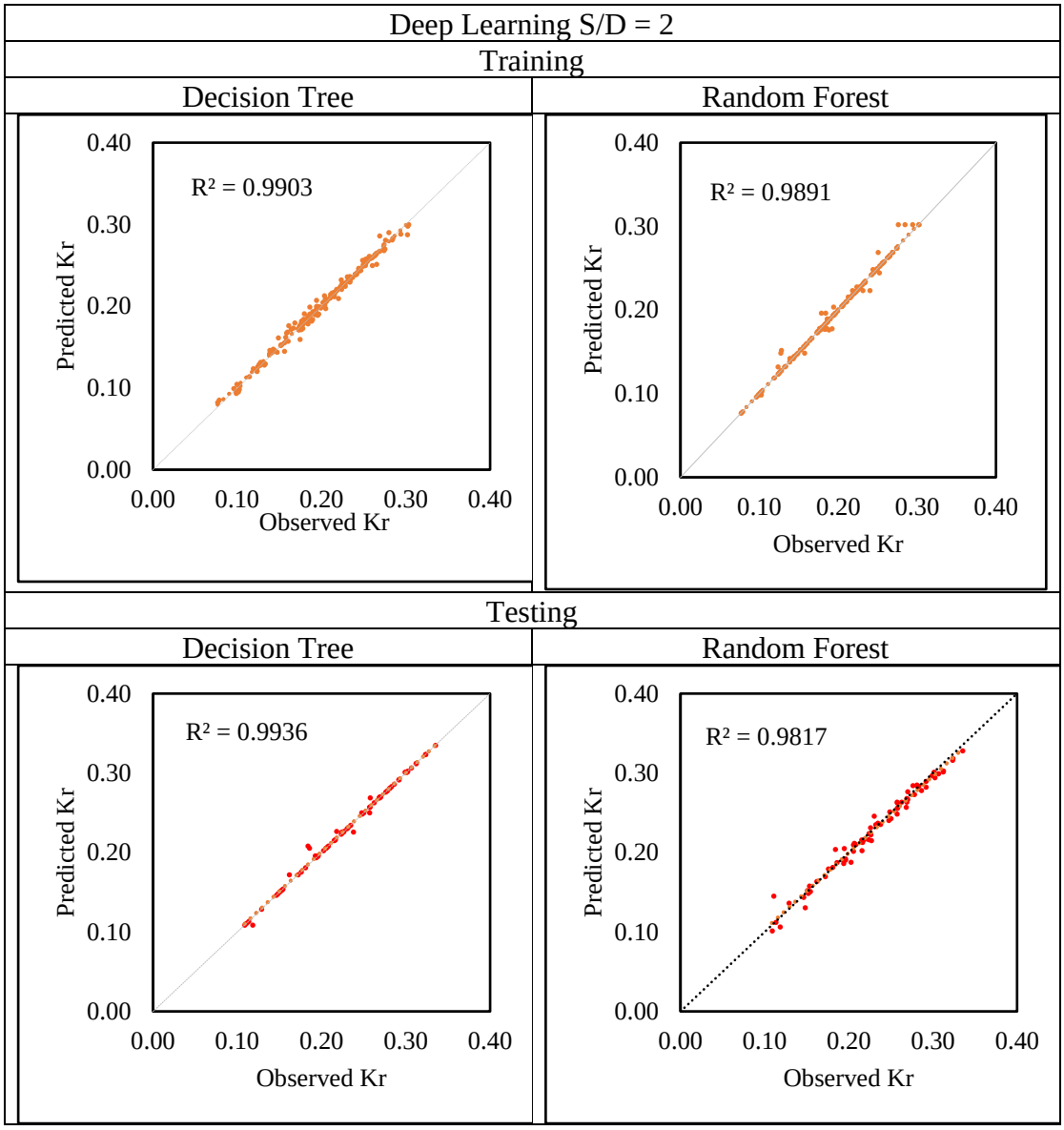

Figure 5.25 Scattered Plot between Observed and Predicted Values of K_r (Deep Learning S/D=2)

Table 5.31 Model Performance Indices using Deep Learning by dimensional parameters

Model Performance Index (MPI) Parameters	Deep Learning S/D=2			
	Training		Testing	
	Decision Tree	Random Forest	Decision Tree	Random Forest
CC	0.995	0.994	0.996	0.990
RMSE	0.005	0.015	0.007	0.008

SI	2.503	3.474	2.020	3.420
NSE	0.991	0.990	0.993	0.981

Comparing the plots of observed vs. predicted Kr, it can be observed that the Decision Tree approach's coefficient of correlation (CC) is superior to the Random Forest method. Table 5.31 lists the model performance index values that were obtained. In comparison to a value of 0.995 in the Decision Tree technique, the value of CC obtained by the Random Forest method in training is 0.994. During testing, the CC values for the Decision Tree and Random Forest methods were, respectively, 0.966 and 0.990. The results for RMSE were 0.015 for the Random Forest method in training and 0.005 for the Decision Tree method, whereas they were 0.008 and 0.007, respectively, in testing. For the Decision Tree method, the values for SI in training and testing were 2.503 and 2.020, respectively, and 3.474 and 3.420, respectively, for the Random Forest method. The greater accuracy of the Random Forest approach is further supported by the lower RMSE and SI values in comparison to the Decision Tree method. The numbers for NSE, 0.991 in training and 0.993 in testing for Decision Tree versus 0.990 in training and 0.981 in testing for Random Forest, demonstrate that the Decision Tree approach has higher values, highlighting its improved accuracy as compared to the Decision Tree method.

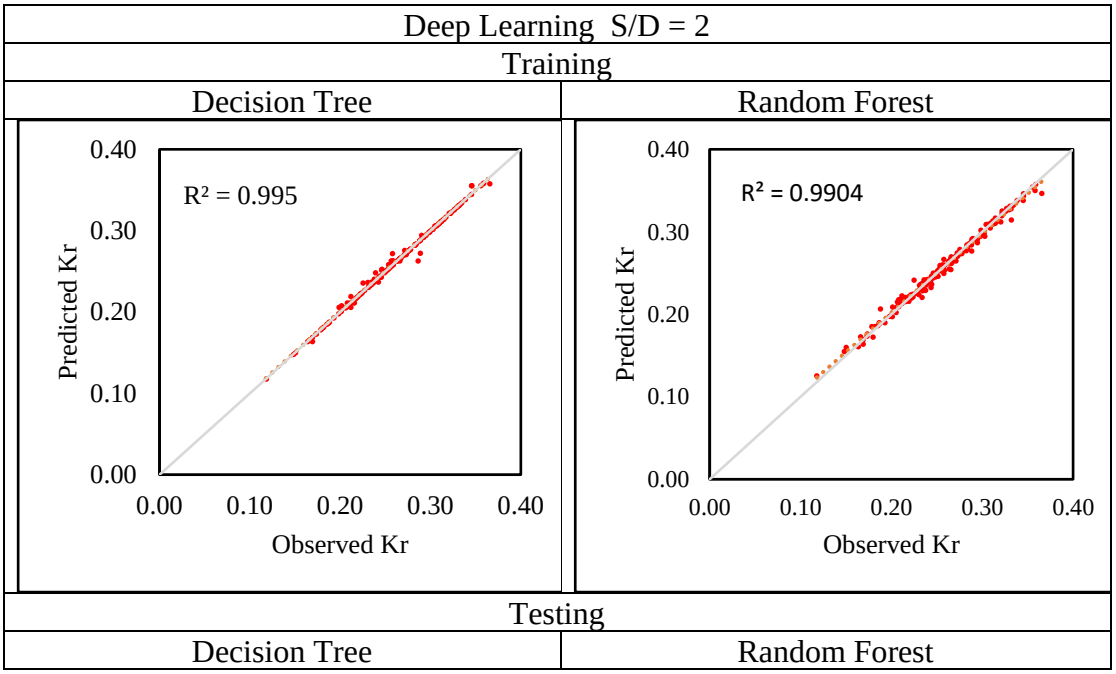

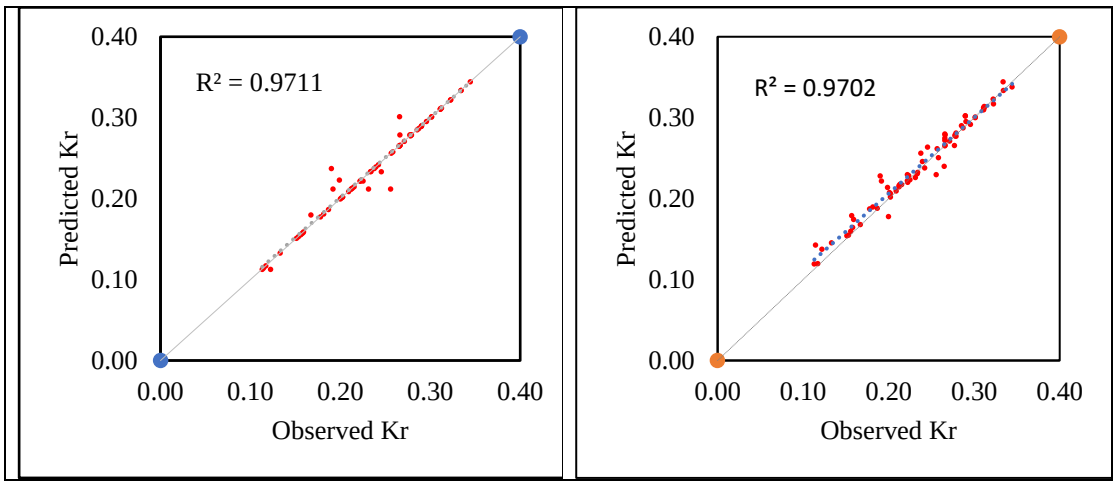

Figure 5.26 Scattered Plot between Observed and Predicted Values of K_r (Deep Learning S/D=3)

Table 5.32 Model Performance Indices using Deep Learning by dimensional parameters

Model Performance Index (MPI) Parameters	Deep Learning S/D=3			
	Training		Testing	
	Decision Tree	Random Forest	Decision Tree	Random Forest
CC	0.997	0.995	0.985	0.985
RMSE	0.002	0.003	0.009	0.010
SI	1.314	1.791	1.163	0.218
NSE	0.995	0.989	0.962	0.968

When comparing the plots of observed vs. predicted K_r, it can be seen that the Decision Tree approach's coefficient of correlation (CC) is superior to the Random Forest method. The values of the model performance index that were found are shown in Table 5.32. During training, the Random Forest strategy achieved a CC value of 0.995 as opposed to the Decision Tree technique's 0.997. The CC values for the Random Forest and Decision Tree techniques were found to be, respectively, 0.985 and 0.985 as a result of testing. In training, the RMSE for the Decision Tree technique and the Random Forest method were 0.002 and 0.003, respectively, whereas, in testing, they were 0.009 and 0.010, respectively. For the Random Forest methodology, the values for SI were 1.791 and 0.218 in training and testing, respectively, while for the Decision Tree method, they were 1.314 and 0.463 in training and testing, respectively. The improved accuracy of the Decision tree approach comes from the lower RMSE and SI values as

compared to the Decision Tree method. The Decision Tree method has higher values for NSE than the Random Forest method, demonstrating improved accuracy: 0.995 in training and 0.962 in testing for Decision Tree vs. 0.989 in training and 0.968 in testing for Random Forest.

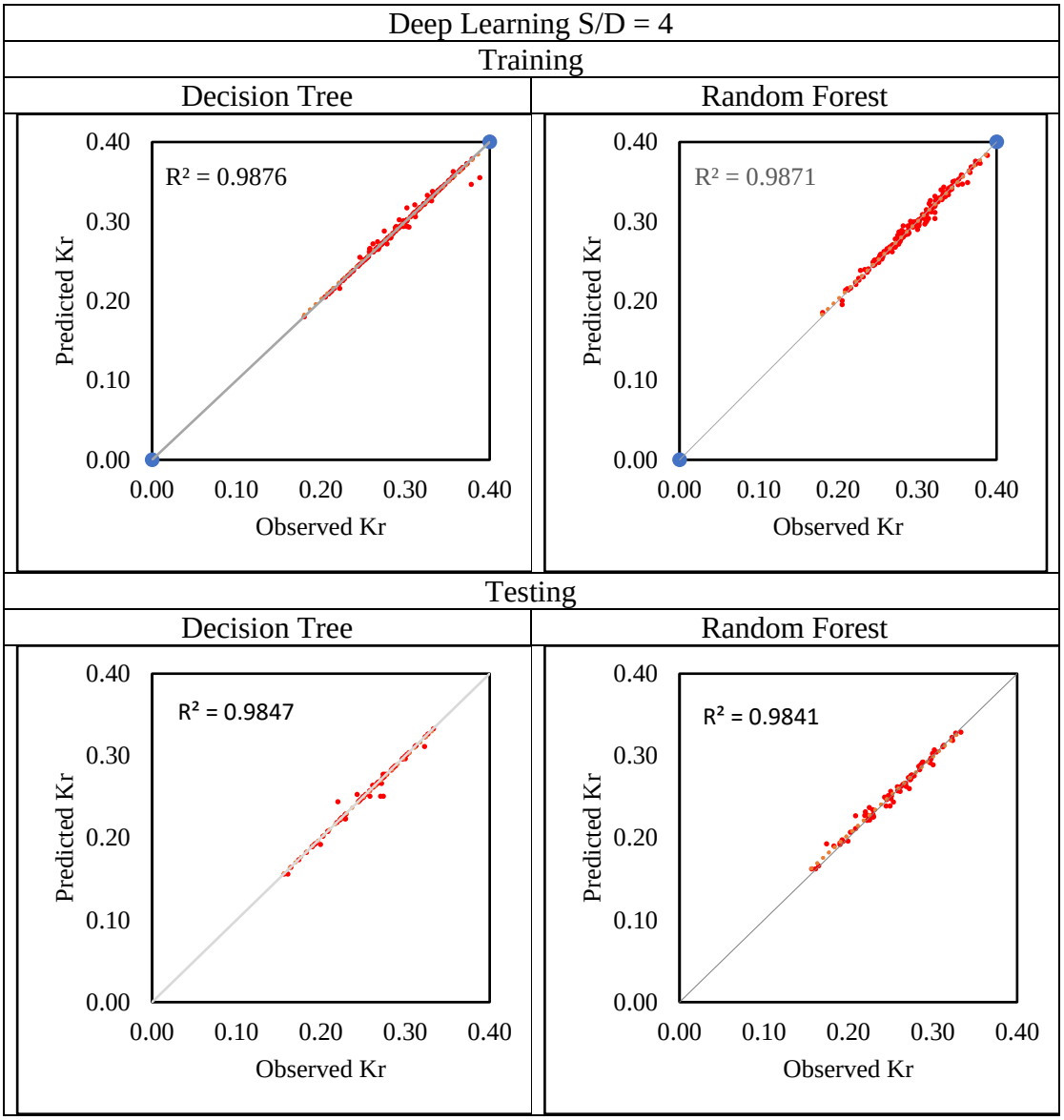

Figure 5.27 Scattered Plot between Observed and Predicted Values of K_r (Deep Learning S/D=4)

Table 5.33 Model Performance Indices using Deep Learning by dimensional parameters

Model Performance	Deep Learning S/D=4	
	Training	Testing

Index (MPI) Parameters	Decision Tree	Random Forest	Decision Tree	Random Forest
CC	0.993	0.988	0.992	0.989
RMSE	0.004	0.005	0.005	0.006
SI	1.539	1.569	1.637	1.712
NSE	0.988	0.986	0.998	0.997

It can be seen that the Decision Tree approach's coefficient of correlation (CC) is superior to the Random Forest method when comparing the plots of observed vs. anticipated K_r. The model performance index values are listed in Table 5.33. The CC value attained by the Random Forest approach in training is 0.988 compared to a value of 0.993 in the Decision Tree technique. As a result of testing, it was found that the CC values for the Decision Tree and Random Forest were 0.992 and 0.989. Results for RMSE for the Random Forest approach and Decision Tree method in training were 0.004 and 0.005, respectively, while they were 0.005 and 0.006 in testing. The values for SI in training and testing for the Decision tree method were 1.539 and 1.637, respectively, while for the Random Forest method, they were 1.569 and 1.712, respectively. The RMSE and SI values, when compared to the Random Forest method, the Decision Tree demonstrate higher accuracy of the approach. The results for NSE in Table 5.33 show that the Decision tree approach has higher values, showing it has better accuracy compared to the Random Forest method. The NSE values for training and testing are 0.988 and 0.998 in the decision tree and 0.986 in training, and 0.997 in testing for Random Forest.

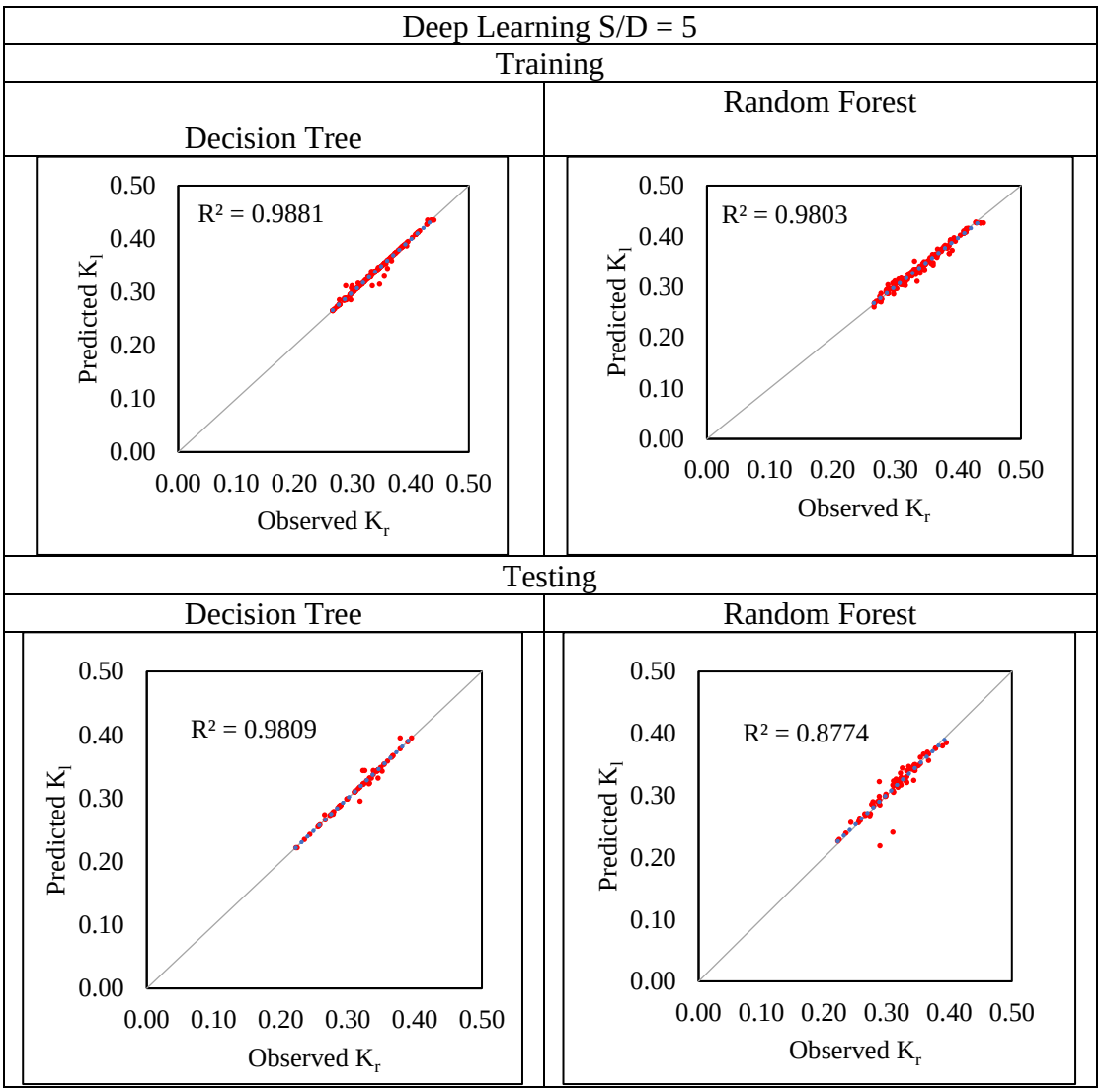

Figure 5.28 Scattered Plot between Observed and Predicted Values of K_r (Deep Learning S/D=5)

Table 5.34 Model Performance Indices using Deep Learning by dimensional parameters

Model Performance Index (MPI) Parameters	Deep Learning S/D=5			
	Training		Testing	
	Decision Tree	Random Forest	Decision Tree	Random Forest
CC	0.991	0.962	0.962	0.937
RMSE	0.004	0.006	0.005	0.007
SI	1.332	1.737	1.860	2.307
NSE	0.988	0.981	0.974	0.971

On comparing the plots of observed vs. predicted Kr, it can be seen that the Decision Tree approach's coefficient of correlation (CC) is superior to the Random Forest method. Table 5.34 lists the model performance index values that were obtained. In comparison to a value of 0.991 in the Decision Tree method, the value of CC obtained by the Random Forest method in training is 0.962. Testing revealed that the CC values for the Random Forest and Decision Tree methods were, respectively, 0.937 and 0.962. The results for RMSE were 0.006 for the Random Forest method in training and 0.004 for the Decision Tree method, whereas, during testing, they were 0.007 and 0.005, respectively. For the Random Forest method, the values for SI in training and testing were 1.737 and 2.307, respectively, and 1.332 and 1.860, respectively, for the Decision Tree method. The greater accuracy of the Decision Tree method is further supported by the lower RMSE and SI values in comparison to the Random Forest method. The numbers for NSE in Table 5.34, 0.988 in training and 0.974 in testing for Decision Tree versus 0.981 in training and 0.971 in testing for Random Forest, demonstrate that the Decision Tree method has higher values, highlighting its improved accuracy as compared to the Random Forest method.

Table 5.35 Comparison of Model Performance Indices obtained for Deep Learning by Decision Tree using dimensional parameters

	CC		RMSE		SI		NSE	
	Training	Testing	Training	Testing	Training	Testing	Training	Testing
S/D=2	0.995	0.996	0.005	0.007	2.503	2.020	0.991	0.993
S/D=3	0.997	0.985	0.002	0.009	1.314	1.163	0.995	0.962
S/D=4	0.993	0.992	0.004	0.005	1.539	1.637	0.998	0.998
S/D=5	0.962	0.962	0.004	0.005	1.332	1.860	0.988	0.974

Comparison of Model Performance Indices for different S/d ratios of perforated QBW models using ANN by LM algorithm is presented in Table 5.35.

5.6.2 Using Non-Dimensional Parameters

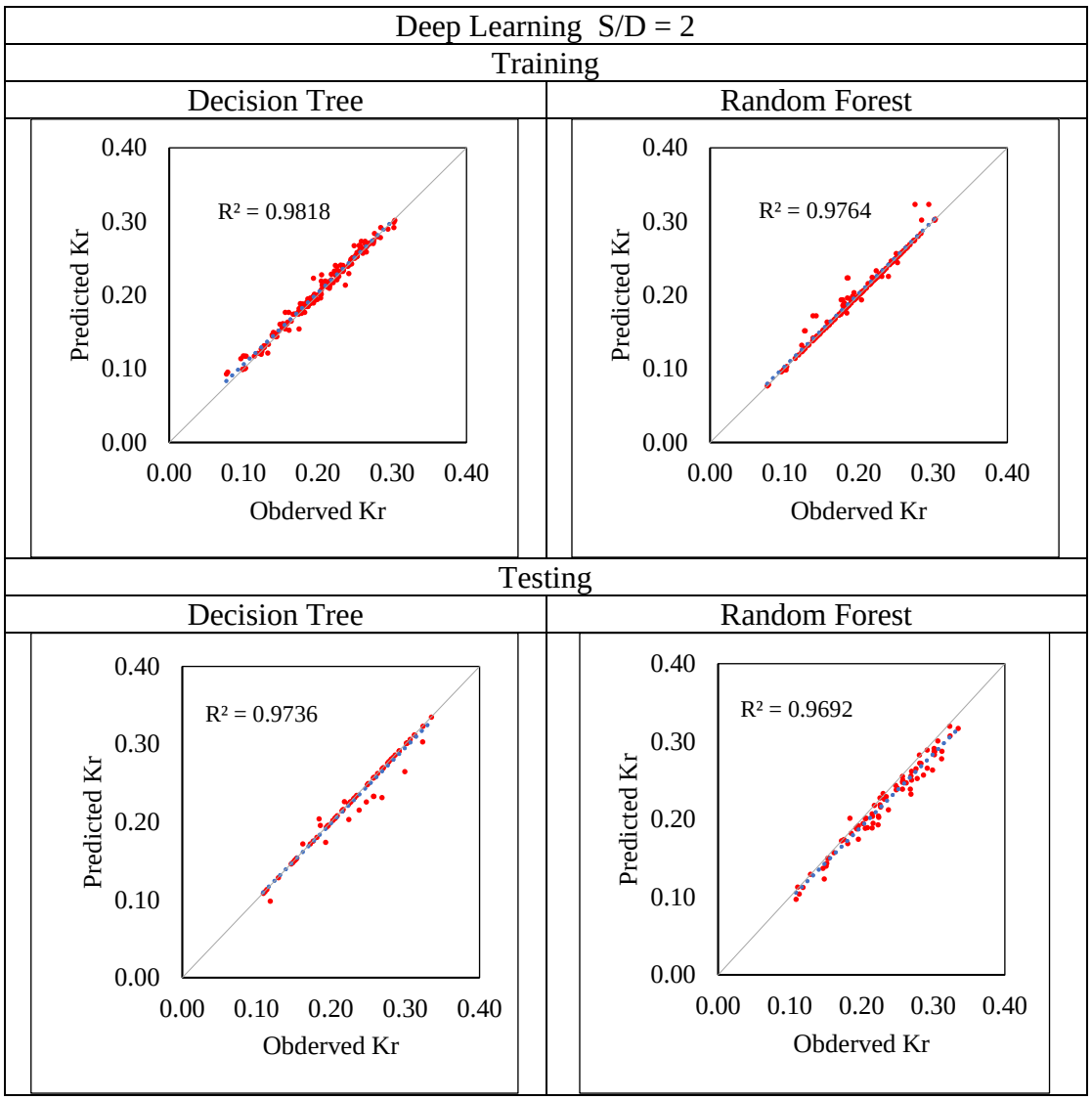

Figure 5.29 Scattered Plot between Observed and Predicted Values of K_r (DL S/D=2)

Table 5.36 Model Performance Indices Deep Learning by non-dimensional parameters

Model Performance Index (MPI) Parameters	Deep Learning S/D=2			
	Training		Testing	
	Decision Tree	Random Forest	Decision Tree	Random Forest
CC	0.9908	0.9881	0.9867	0.9845
RMSE	0.0495	0.0505	0.0864	0.1379
SI	0.0279	0.0285	0.0488	0.1791
NSE	0.988	0.981	0.974	0.971

On comparing the plots of observed vs. predicted Kr, it can be seen that the Random Forest approach's coefficient of correlation (CC) is superior to the Decision Tree method. Table 5.36 lists the model performance index values that were obtained. In comparison to a value of 0.9908 in the Decision Tree method, the value of CC obtained by the Random Forest method in training is 0.9881. Testing revealed that the CC values for the Random Forest and Decision Tree methods were, respectively, 0.9867 and 0.9845. The results for RMSE were 0.0505 for the Random Forest method in training and 0.0495 for the Decision Tree method, whereas, during testing, they were 0.1379 and 0.0864, respectively. For the Random Forest method, the values for SI in training and testing were 0.0285 and 0.1791, respectively, and 0.0279 and 0.0488, respectively, for the Decision Tree method. The greater accuracy of the Decision Tree method is further supported by the lower RMSE and SI values in comparison to the Random Forest method. The numbers for NSE in Table 5.36, 0.988 in training and 0.974 in testing for Decision Tree versus 0.981 in training and 0.971 in testing for Random Forest, demonstrate that the Decision Tree method has higher values, highlighting its improved accuracy as compared to the Random Forest method.

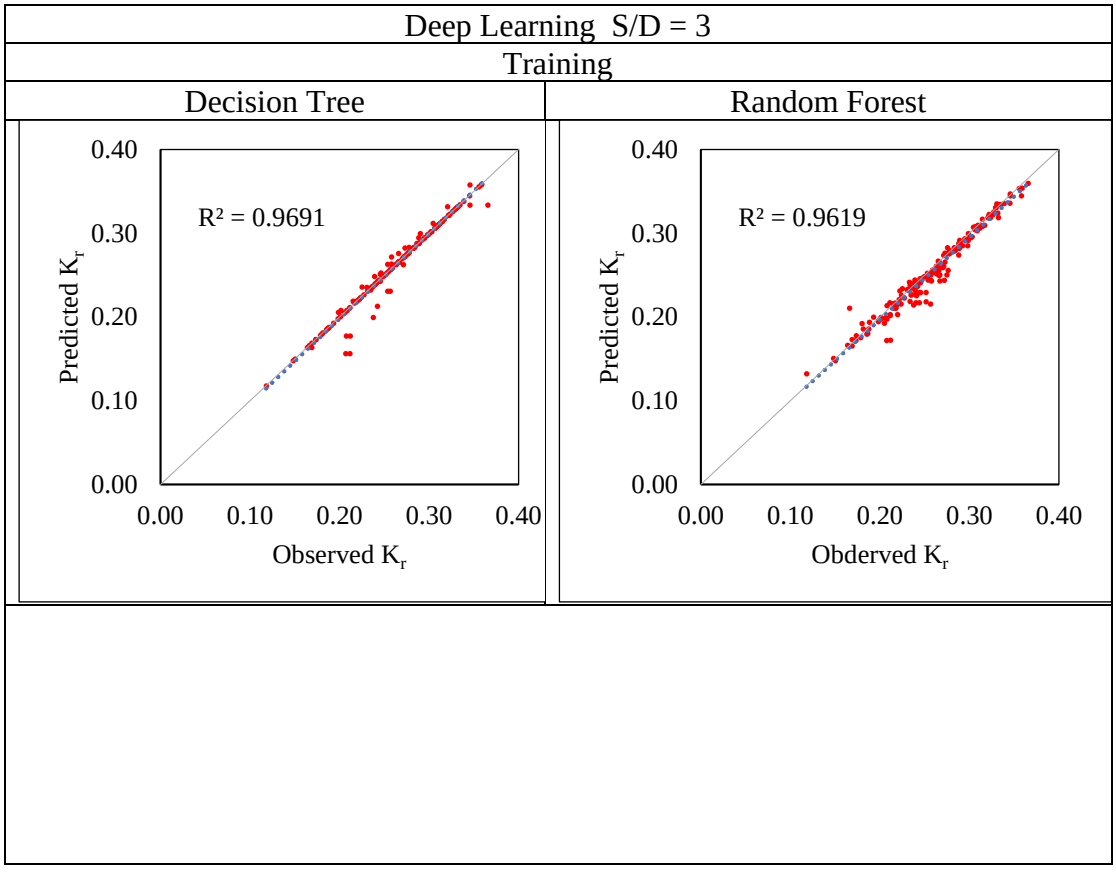

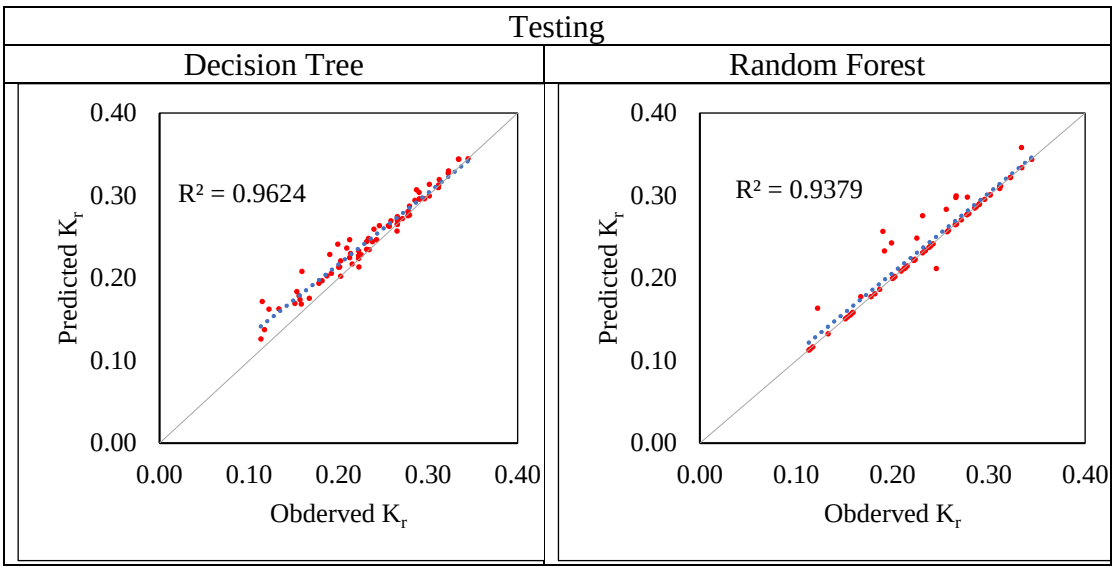

Figure 5.30 Scattered Plot between Observed and Predicted Values of K_r (DL S/D=3)

Table 5.37 Model Performance Indices Deep Learning by non-dimensional parameters

Model Performance Index (MPI) Parameters	Deep Learning S/D=3			
	Training		Testing	
	Decision Tree	Random Forest	Decision Tree	Random Forest
CC	0.9844	0.9807	0.9810	0.9684
RMSE	0.0511	0.0712	0.0475	0.0536
SI	0.0288	0.0402	0.0617	0.0696
NSE	0.988	0.986	0.998	0.997

In comparison to a value given in Table 5.37, 0.9844 in the Decision Tree method, the value of CC obtained by the Random Forest method in training is 0.9807. Testing revealed that the CC values for the Decision Tree and Random Forest methods were, respectively, 0.9810 and 0.9684. The results for RMSE were 0.0712 for the Random Forest method in training and 0.0511 for the Decision Tree method, whereas, during testing, they were 0.0536 and 0.0475, respectively. For the Random Forest method, the values for SI in training and testing were 0.0402 and 0.0696, respectively, and 0.0288 and 0.0617, respectively, for the Decision Tree method. The greater accuracy of the Decision Tree method is further supported by the lower RMSE and SI values in comparison to the Random Forest method. The numbers for NSE in the Table5.37,

0.988 in training and 0.998 in testing for Decision Tree versus 0.986 in training and 0.997 in testing for Random Forest, demonstrate that the Decision Tree method has higher values, highlighting its improved accuracy as compared to the Random Forest method.

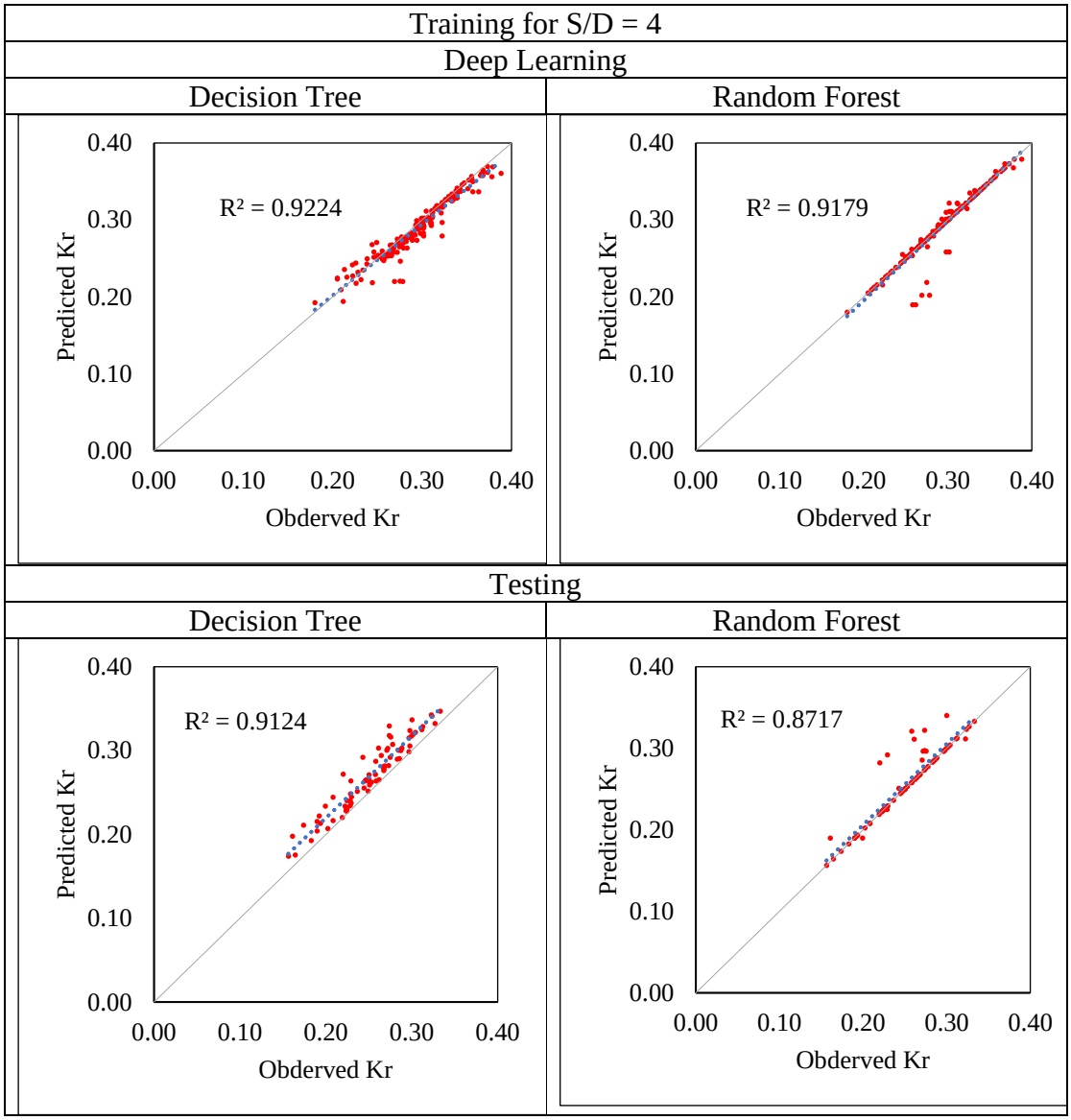

Figure 5.31 Scattered Plot between Observed and Predicted Values of K_r (DL S/D=4)

Table 5.38 Model Performance Indices Deep Learning by non-dimensional parameters

Model Performance Index (MPI) Parameters	Deep Learning S/D=4			
	Training		Testing	
	Decision Tree	Random Forest	Decision Tree	Random Forest
CC	0.9604	0.9581	0.9552	0.9336
RMSE	0.1051	0.1219	0.1036	0.1036
SI	0.0006	0.0007	0.1345	0.1345
NSE	0.995	0.989	0.962	0.968

In comparison to a value given in Table 5.38, 0.9604 in the Decision Tree method, the value of CC obtained by the Random Forest method in training is 0.9581. Testing revealed that the CC values for the Decision Tree and Random Forest were, respectively, 0.9552 and 0.9336. The results for RMSE were 0.1219 for the Random Forest method in training and 0.1051 for the Decision Tree method, whereas, during testing, they were 0.1036 and 0.1036, respectively. For the Random Forest method, the values for SI in training and testing were 0.0007 and 0.1345, respectively, and 0.0006 and 0.1345, respectively, for the Decision Tree method. The greater accuracy of the Decision Tree method is further supported by the lower RMSE and SI values in comparison to the Random Forest method. The numbers for NSE in Table 5.38, 0.995 in training and 0.962 in testing for Decision Tree versus 0.989 in training and 0.968 in testing for Random Forest, demonstrate that the Decision Tree method has higher values, highlighting its improved accuracy as compared to the Random Forest method.

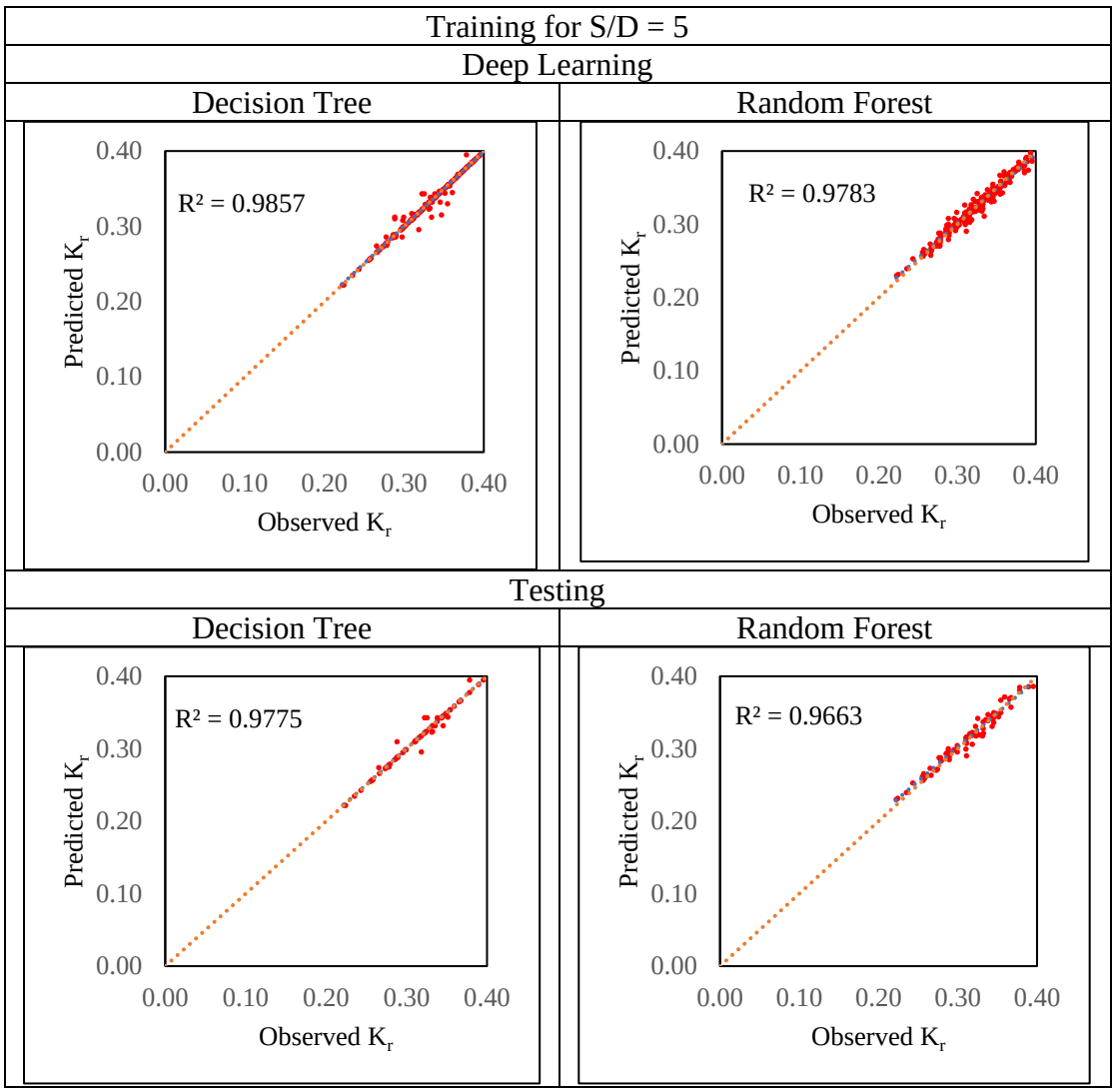

Figure 5.32 Scattered Plot between Observed and Predicted Values of K_r (DL S/D=5)

Table 5.39 Model Performance Indices for Deep Learning by non-dimensional parameters

Model Performance Index (MPI) Parameters	Deep Learning S/D=5			
	Training		Testing	
	Decision Tree	Random Forest	Decision Tree	Random Forest
CC	0.9928	0.9891	0.9886	0.9830
RMSE	0.0792	0.0802	0.0975	0.1026
SI	0.0447	0.0453	0.1267	0.1332
NSE	0.993	0.984	0.958	0.961

In comparison to the value given in Table 5.39, the value of 0.9928 in the Decision Tree method, the value of CC obtained by the Random Forest method in training is 0.9891. Testing revealed that the CC values for the Decision Tree and Random Forest were, respectively, 0.9886 and 0.9830. The results for RMSE were 0.0802 for the Random Forest method in training and 0.0792 for the Decision Tree method, whereas, during testing, they were 0.1026 and 0.0975, respectively. For the Random Forest method, the values for SI in training and testing were 0.0453 and 0.1332, respectively, and 0.0447 and 0.1267, respectively, for the Decision Tree method. The greater accuracy of the Decision Tree method is further supported by the lower RMSE and SI values in comparison to the Random Forest method. The numbers for NSE in Table 5.39, 0.993 in training and 0.958 in testing for Decision Tree versus 0.984 in training and 0.961 in testing for Random Forest, demonstrate that the Decision Tree method has higher values, highlighting its improved accuracy as compared to the Random Forest method.

Table 5.40 Comparison of Model Performance Indices obtained for Deep Learning by Decision Tree using non-dimensional parameters

	CC		RMSE		SI		NSE	
	Training	Testing	Training	Testing	Training	Testing	Training	Testing
S/D=2	0.9908	0.9867	0.0495	0.0864	0.0279	0.0488	0.988	0.974
S/D=3	0.9844	0.9810	0.0511	0.0175	0.0288	0.0617	0.988	0.998
S/D=4	0.9604	0.9552	0.1051	0.1036	0.0006	01345	0.995	0.962
S/D=5	0.9928	0.9886	0.0795	0.0975	0.0447	0.1267	0.993	0.958

Comparison of Model Performance Indices for different S/d ratios of perforated QBW models using deep learning by Decision Tree algorithm are presented in Table 5.40.

5. 7 PREDICTION OF REFLECTION COEFFICIENT OF NON-PERFORATED QBW USING NON-DIMENSIONAL PARAMETERS

The ANN and ANFIS models were chosen to understand the effectiveness of soft computing techniques in predicting the reflection coefficient of a non-perforated quarter circle breakwater spaced at S/D=2. Two non-dimensional input parameters were considered: wave steepness (H_i/gT^2) and relative water depth (d/hs). The Artificial

neural network is a collection of small processing units, or neurons, that communicate by delivering analogue signals. These impulses pass between neurons *via* weighted connections, and each neuron collects the information and generates solutions based on an internal activation system. This solution is used as informationfor other neurons. The learning process is achieved by modifying the weights of the connectionsbetween units. The model forecasted results are correlated to the targets during the training procedure. The inaccuracy is calculated by obtaining the appropriate weight adjustments to minimize errors by back-propagation. The Neural Network (NN) models stop iterating when inaccuracies exceed the goal error. The weights are changed to reduce the disparity between thedesired and the computed outputs in response to this error signal. Adjusting weights is repeateduntil the appropriate level of precision between the target values and calculated results is achieved. The consequences are frozen after learning. The ANN is then supplied with a data setto validate the performance of the computed outputs. The experimental data for this ANN model performance is used from the physical model work of Binumol et al. (2017). ANFIS is a neuro-fuzzy technique where the ANN is fused with fuzzy logic principles, and hence it has significant performance11. The fuzzy system employs flexible 'if-then rules that can be applied to modelling human knowledge and reasoning without precise quantitative measures. It is possible to model complex non-linear systems using fuzzy rule-based models with high computational speed. For modelling, The grid partition method generates the optimum fuzzy rules in an ANFIS model with built-in two membership functions for each variable with 100 epochs. Different membership functions considered are the Linear membership function (lrmf), trapezoidal- membership function (trapmf), generalized bell-membership function (gbellmf), and Gaussian membership function (gaussmf). The model results are compared with experimental results by usingstatistical measures such as Root Mean Square Error (RMSE), Scatter Index (SI), and Nash- Sutcliffe Efficiency (NSE) between target output and network predicted outcome is illustrated in Table 5.40.

Table 5.41: Statistical parameters for ANN models for predicting K_r of non-perorated QBW

Network	RMSE		CC		SI		NSE	
	Training	Testing	Training	Testing	Training	Testing	Training	Testing
2-1-1	0.0623	0.0719	0.954	0.968	0.1471	0.1697	0.913	0.916
2-2-1	0.0588	0.0661	0.959	0.972	0.1388	0.1560	0.923	0.929
2-3-1	0.0516	0.0630	0.968	0.972	0.1220	0.1486	0.940	0.935
2-4-1	0.0511	0.0629	0.97	0.969	0.1206	0.1484	0.943	0.936
2-5-1	0.0516	0.0702	0.968	0.965	0.1219	0.1658	0.940	0.920
2-6-1	0.0502	0.0675	0.97	0.968	0.1186	0.1592	0.944	0.926

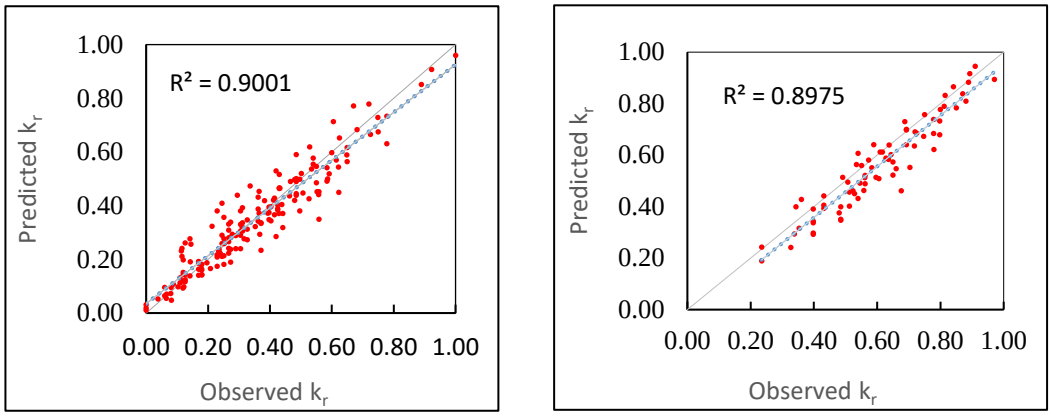

Figure 5.33 Scatter plots for training and testing dataset of 2-1-1ANN model, non-perforated QBW

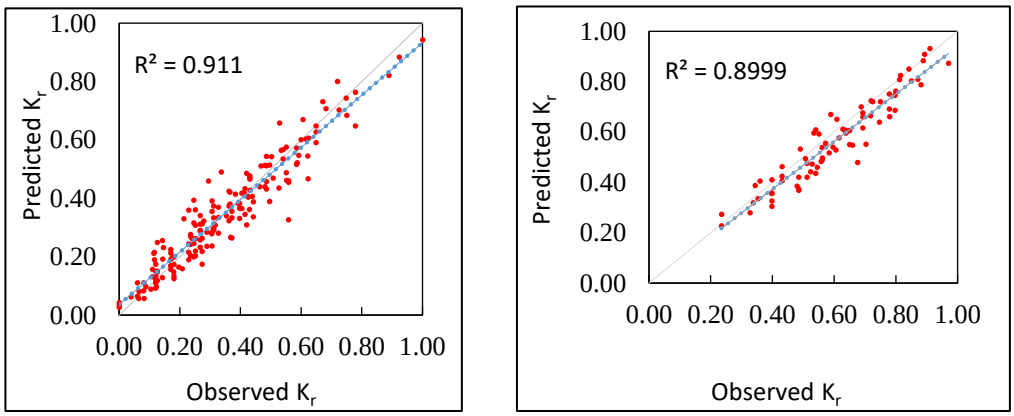

Figure 5.34 Scatter plot for training and testing dataset of ANN 2-2-1 model for non-perforated QBW

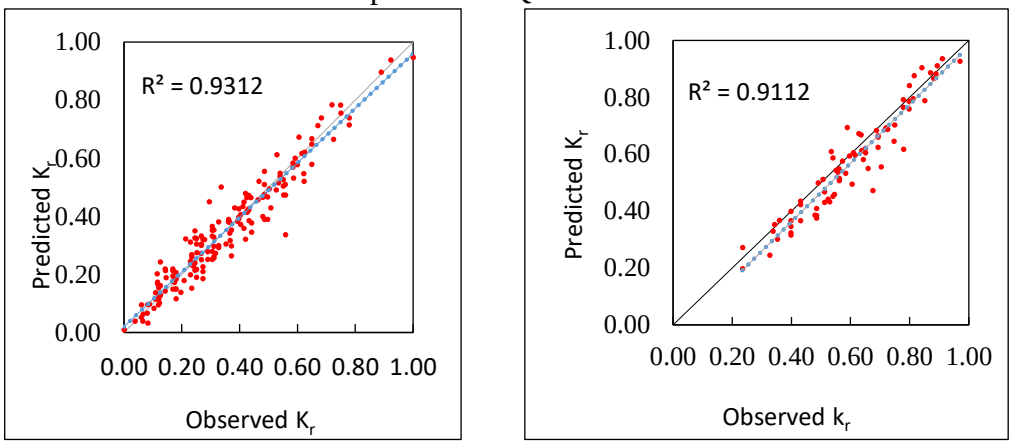

Fig. 5.35 Scatter plots for training and testing dataset of ANN 2-3-1 model, non-perforated QBW

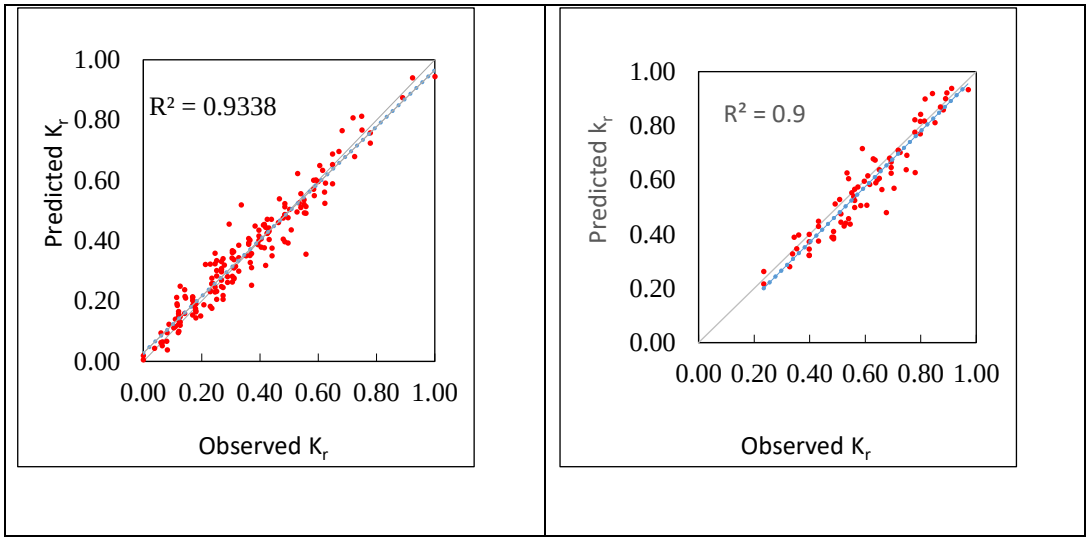

Fig. 5.36 Scatter plots for training and testing dataset of ANN 2-4-1 model for non-perforated QBW

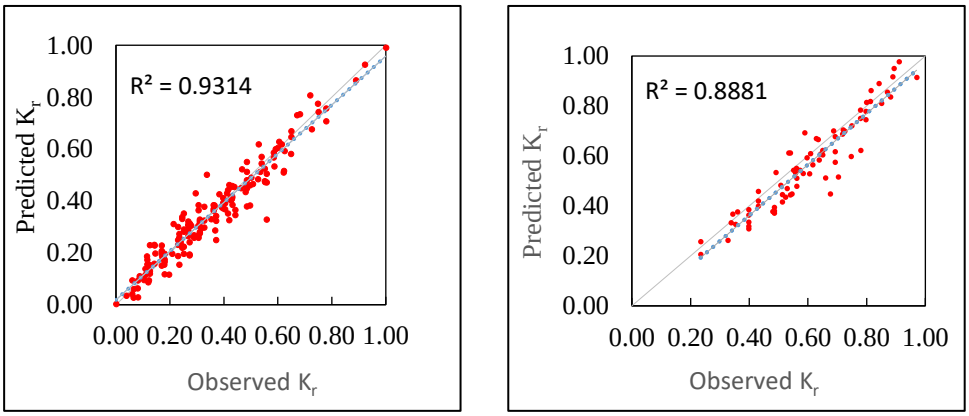

Fig. 5.37 Scatter plots for training and testing dataset of ANN 2-5-1 model for non-perforated QBW

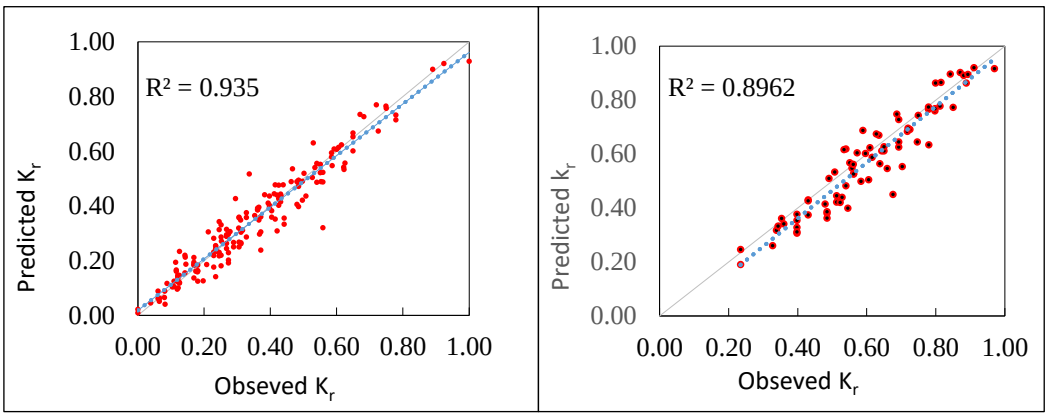

Fig. 5.38 Scatter plots for training and testing dataset of ANN 2-6-1 model for non-perforated QBW

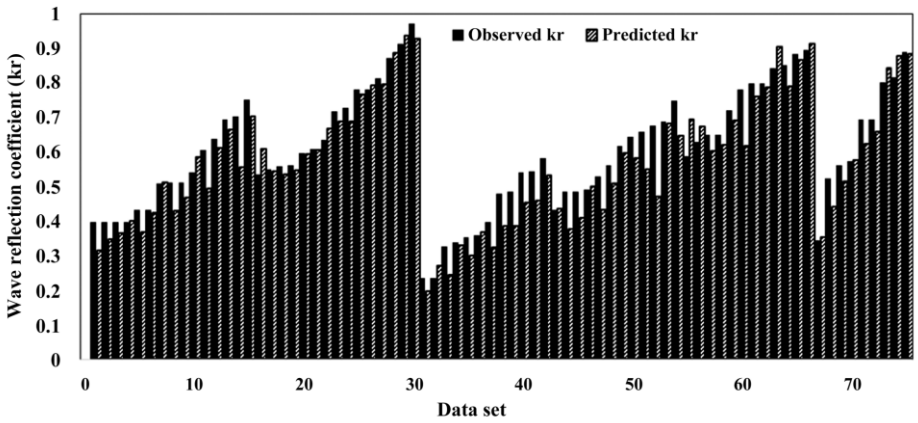

Figure 5.39 Comparison of Kr predicted values by ANN 2-3 -1 with observed Values for non-perforated QBW

Table 5.42— Statistical measures for ANFIS model for non-perforated QBW

Statistical parameters	Functions							
	Linear		Trapezoidal		Gumbell		Gaussian	
	Training	Testing	Training	Testing	Training	Testing	Training	Testing
RMS	0.0574	0.0636	0.05625	0.0645	0.05151	0.0648	0.05130	0.0643
NSE	0.926	0.934	0.929	0.932	0.941	0.932	0.941	0.933
CC	0.961	0.971	0.962	0.971	0.969	0.971	0.968	0.971
SI	0.1354	0.1502	0.1328	0.1522	0.1216	0.1529	0.1211	0.1518

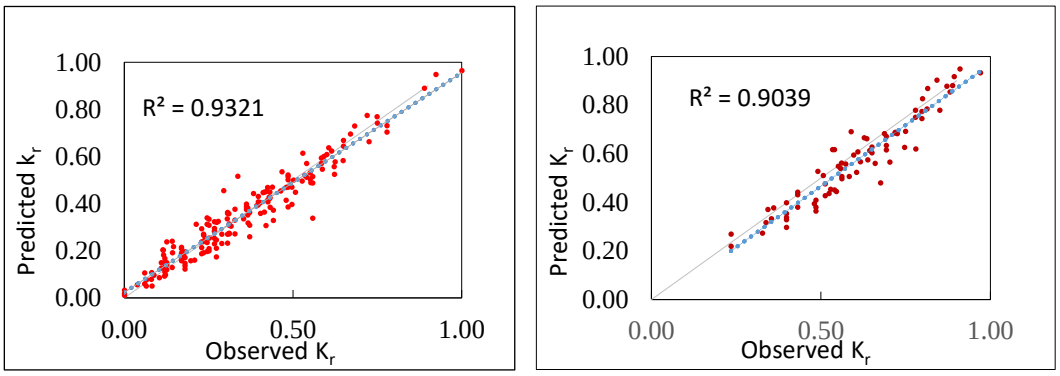

Fig. 5.40 Scatter plots for training and testing data of ANFIS model of non-perforated QBW

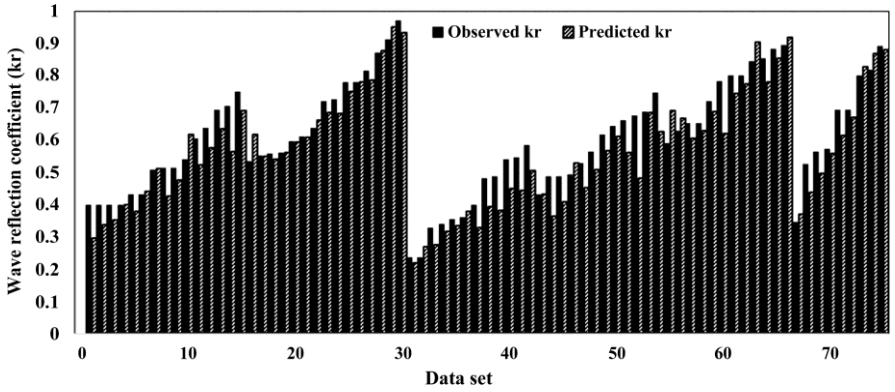

Figure 5.41 Comparison of K_r predicted values using ANFIS with observed Values for training and testing of non-perforated QBW.

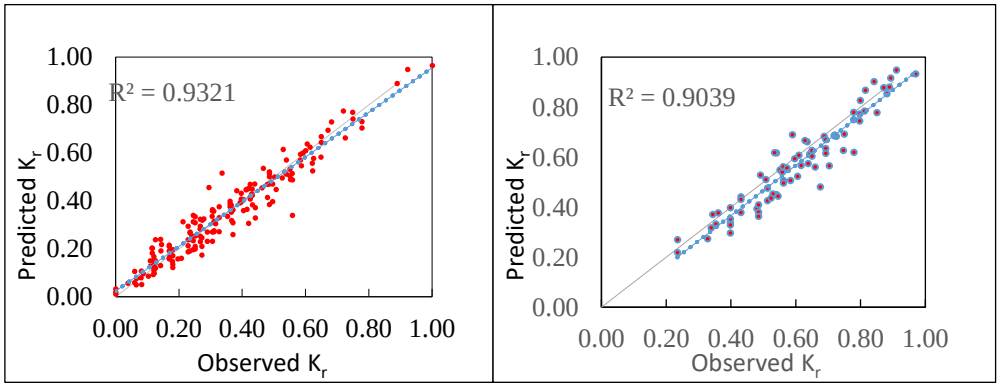

Fig 5.42 Scatter plots for training and testing of ANFIS model for Linear MF non-perforated QBW

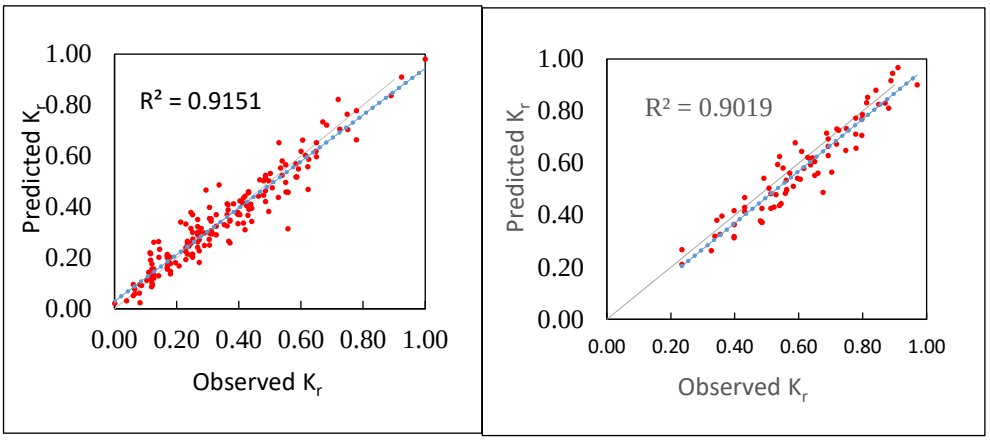

Fig 5.43 Scatter plots for training and testing of ANFIS model for Trapezoidal MF non-perforated QBW

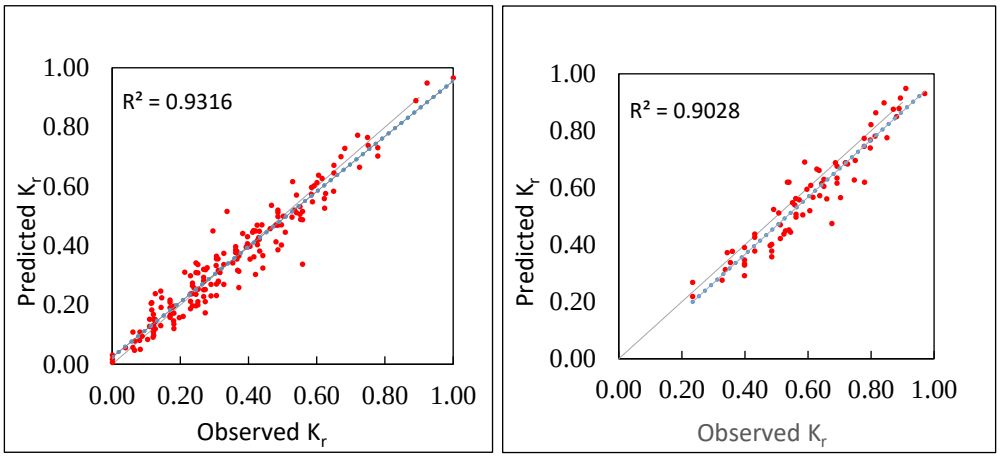

Fig 5.44 Scatter plots for training and testing of ANFIS model for Gumbel's MF non-perforated QBW

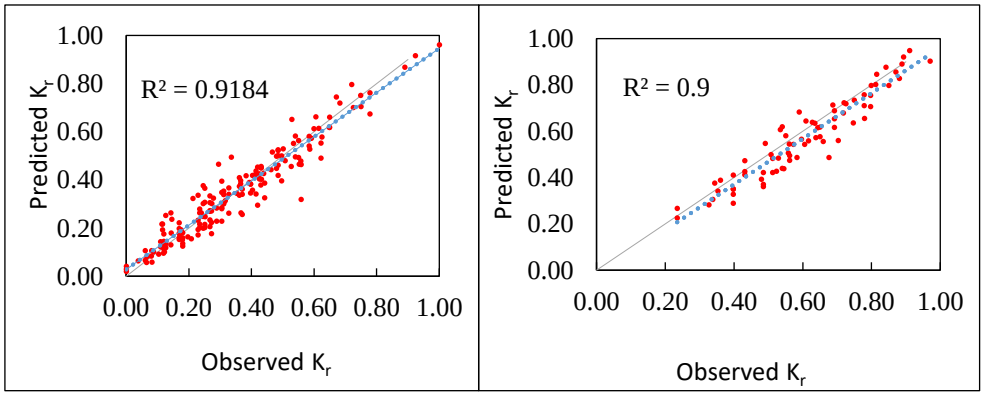

Fig 5.45 Scatter plots for training and testing of ANFIS model for Gaussian MF non-perforated QBW

The study's outcome involves the prediction of the reflection coefficient (Kr) of a non-perforated QBW by adopting ANN and ANFIS approaches. From the interpretation of the results, the following conclusions were drawn. The training and testing efficiency of the 2-3-1 ANN model correlates well with CC for training equal to 0.968 and for testing to 0.972. Also, the RMSE, SI & NSE values obtained were 0.0630, 0.1486 & 0.935, respectively. However, with ANFIS model correlates well with CC for training was 0.969, and for testing, 0.971. Also, the RMSE, SI & NSE values obtained for testing sets were 0.0643, 0.1518 & 0.933, respectively. Considering these results, further studies were continued by taking more input variables to assess the hydrodynamic performance of QBW.

5.8 SUMMARY

This approach of predicting Kr for available experimental data is successfully presented. Prediction is reasonably good for all the cases with 5 input parameters, including wave steepness. The maximum K_r value obtained from experimental data is 0.44. Initially the Prediction of reflection coefficient (Kr) carried out for non-perforated QBW using ANN and ANFIS models. ANN model 2-3-1 performed better, indicating the Coefficient of Correlation (CC) for training equal to 0.968 and for testing to 0.972 compared to other networks. Out of the four soft computing methods considered for the study with different methods and functions, the decision tree of the deep learning method outperformed in predicting the reflection coefficient near the actual experimental value with a correlation of 0.995 and a minimum error of 0.005. Also, the RMSE, SI & NSE values obtained were 0.0630, 0.1486 & 0.935, respectively. The ANFIS model with Gumbel's membership function correlates well with CC for training, which was 0.969, and for testing, 0.971. Also, the RMSE, SI & NSE values obtained for testing sets were 0.05151, 0.11216 & 0.941, respectively.

CHAPTER 6

PREDICTION OF LOSS COEFFICIENT

6.1 GENERAL

In wave–structure interaction problems, energy balance relations are frequently constructed and used to confirm the accuracy of the computational results obtained from numerical approaches. These energy identities are also utilized to gather qualitative information on many different kinds of relevant physical characteristics. The energy identity for rigid structures is well known to be;

$$K_r^2 + K_t^2 = 1$$

where K_r and K_t are the corresponding reflection and transmission coefficients. (ref: Santanu Koley & Kottala Panduranga (2021))

This energy identity will stay true even if we use flexible barriers. As a result of the structural porosity, a significant percentage of the incoming wave energy is generally lost when a wave passes through a porous structure. Therefore, the energy identity will be changed into;

$$K_r^2 + K_t^2 + K_l = 1$$

Where K_r- reflection coefficiwnt, K_l - loss coefficient and K_t – transmission coefficient (ref: Santanu Koley & Kottala Panduranga (2021))

The studies on quarter-circle breakwaters are in the primitive stage, and the practical applications are on a trial basis. Hence, there is plenty of opportunities to understand the loss coefficient (K_l) QBW. Conducting laboratory studies every time is time-consuming and uneconomical. Therefore, CIM is adopted to predict the loss coefficient (K_l) of a QBW. The loss coefficient is obtained using the energy balance equation from the available experimental data and is utilized in the present study.

The chapter discusses data segregation, the prediction of K_l using different soft computing models,and the assessment of the models.

6.2 LOSS COEFFICIENT (K_l)

In recent years for the protection of various marine facilities, massive, porous constructions like rubble mound breakwaters are now being utilized in harbours.

However, due to the huge demand for coastal marine development, there is a lot of demand for rubble material. In order to overcome this, QBW with porosity is being considered. These types of breakwaters are able to disperse a portion of the energy of the incoming waves because of the presence of structural porosity. This method aids in creating a calm area on the lee side of these breakwaters.

In the present study, available experimental data (Binumol, 2017) on perforated quarter circle breakwater of various radii with different porosities and water depth in front of the structure is utilized to predict the loss coefficient due to the QBW. The experimental parameters taken into account are listed in Chapter 3. The predominating parameters, such as the Radius of the structure (R), depth of water in front of the structure (d), incident wave height (H_i), wave period (T), and wave steepness (H_i/gT^2), are considered as input.

6.2.1 Data separation/segregation for prediction of loss coefficient, K_l

For the prediction of K_l using various soft computing techniques, data is to be separated/segregated for training and testing, respectively.

1. The data segregation procedure for the typical case of wave height
2. The entire dataset consisting of 252 data sets is called global data (GD) and issorted in the increasing order of wave heights (H_i).

70% of the data consisting of 177 data is used for training, and the remaining30%, i.e., 75 data sets, are used for testing and contain an entire range of values.

6.3 PREDICTION OF LOSS COEFFICIENT (K_l) OF A PERFORATED QBW USING ARTIFICIAL NEURAL NETWORK (ANN).

6.3.1 Using Dimensional parameters

In the neural network approach, network training is important and largely depends on the methods selected to train the network. The hydrodynamic performance of a quarter-circle breakwater using ANN, ANFIS, SVM, and deep learning methods is adopted for four S/D ratios (i.e., S/D=2,3,4 and 5) of perforation on its curved surface. The input parameters for the soft computing models taken into consideration include the structure's radius, depth in front of it, incident wave height, period, and steepness. In

the current research, the ANN network is trained using modern techniques such as the Levenberg-Marquardt method and conjugate gradient (Wilamoski et al., 2001). The network is trained for both dimensional and non-dimensional parameters, and a single output is predicted (either K_r or K_l) by adjusting the number of neurons in the only set hidden layer. The optimum ANN architecture was arrived by trial and error, and it is 5-10-1. The results of the same are reported, the results by dimensional parameters as input for various S/D ratios are listed in Tables 6.1 to 6.4, and dispersed model-predicted K_l plots are displayed in Figures 6.1 to 6.4.

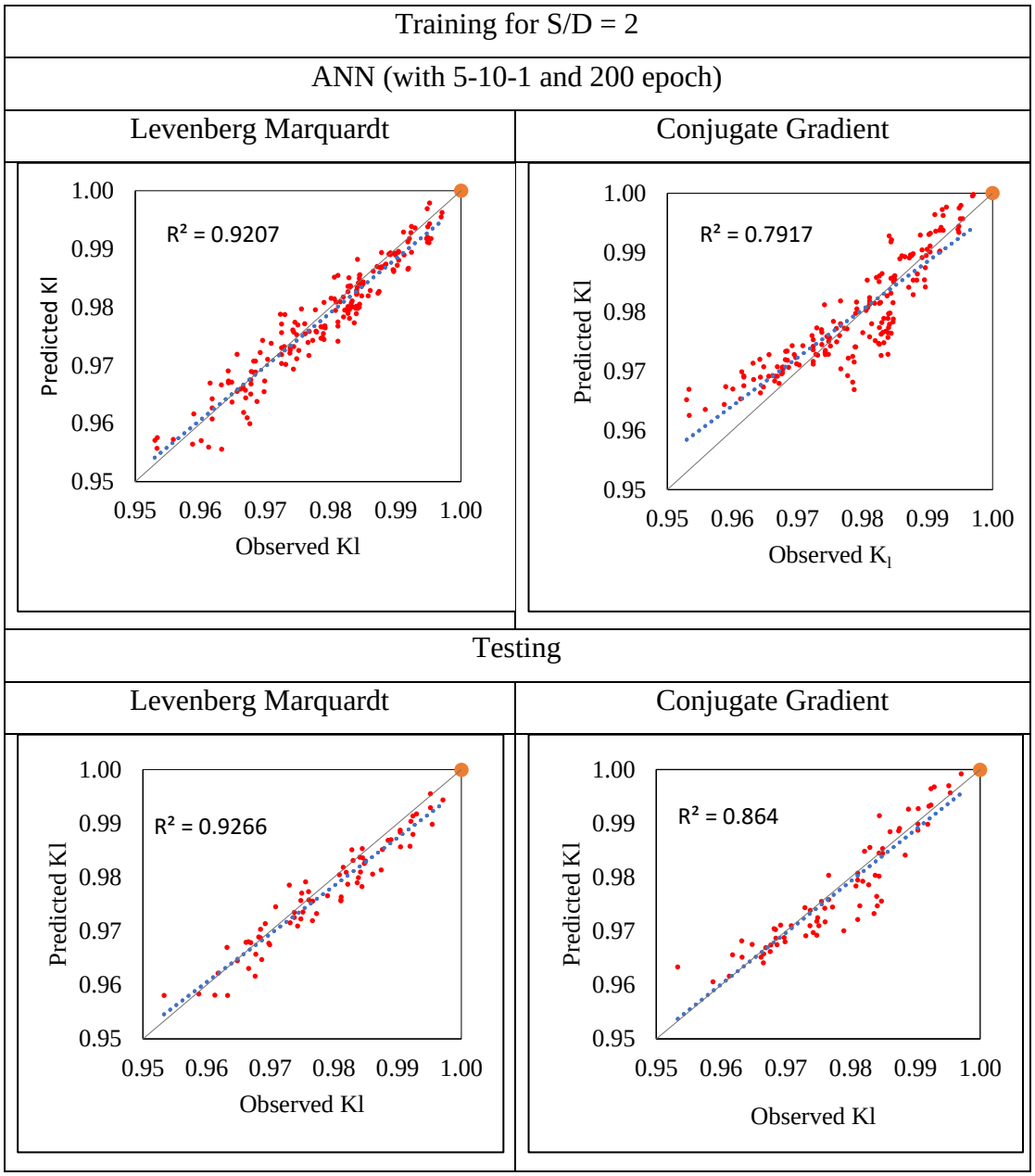

Figure 6.1 Scattered Plot between Observed and Predicted Values of K_l (ANN S/D=2)

Table 6.1 Model Performance Indices for ANN using dimensional parameters

Model Performance Index (MPI) Parameters	ANN S/D=2			
	Training		Testing	
	Levenberg Marquardt	Conjugate Gradient	Levenberg Marquardt	Conjugate Gradient
CC	0.959	0.889	0.963	0.929
RMSE	0.302	0.505	1.249	1.2731
SI	0.171	0.285	1.482	1.6531
NSE	0.982	0.946	0.968	0.925

Comparing the plots shown in Figure 6.1 of observed vs. predicted K_l and MPI values tabulated in Table 6.1, it is observed that the coefficient of correlation (CC) obtained by the LM method is better compared to the CG method. The value of CC obtained by the LM method in training is 0.959 as compared to a value of 0.889 in the CG method. In testing, the CC value was found to be 0.963 and 0.929 for LM and CG methods, respectively. The values for RMSE in training were 0.302 for the LM method against 0.505 for the CG method, while in testing, it was 1.249 and 1.273, respectively. The value for SI in training and testing was 0.171 and 1.482 for the LM method, respectively, and 0.285 and 1.653 for the CG method, respectively. The lower values for RMSE and SI in the LM method as compared to the CG method further indicate that the accuracy is more for the LM method. The values for NSE from Table 6.1 show that the LM method has greater values, hence emphasizing the accuracy over the LM method.

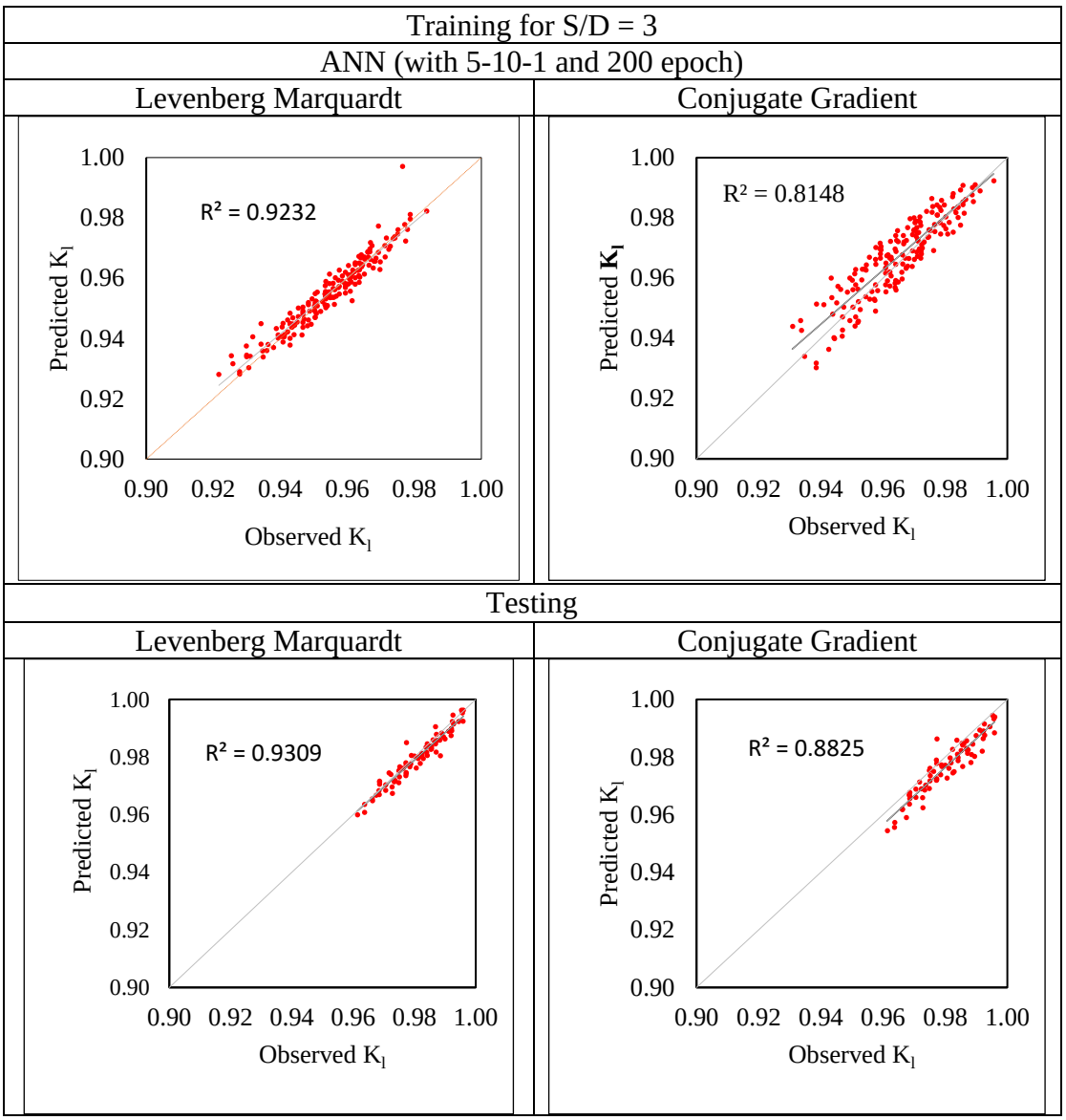

Figure 6.2 Scattered Plot between Observed and Predicted Values of K_l (ANN S/D=3)

Table 6.2 Model Performance Indices for ANN using dimensional parameters

Model Performance Index (MPI)	ANN S/D=3			
	Training		Testing	
	Levenberg Marquardt	Conjugate Gradient	Levenberg Marquardt	Conjugate Gradient
CC	0.961	0.902	0.965	0.939
RMSE	0.104	0.135	0.076	0.087
SI	0.059	0.076	0.043	0.113
NSE	0.959	0.909	0.984	0.893

When comparing the plots of observed vs. predicted K_l, it can be seen that the LM approach's coefficient of correlation (CC) is superior to the CG method. Table 6.2 lists the model performance index values that were obtained. In comparison to a value of 0.961 in the LM technique, the value of CC obtained by the CG method in training is 0.902. Testing revealed that the CC values for the LM and CG methods were, respectively, 0.965 and 0.939. The results for RMSE were 0.104 for the LM technique in training and 0.135 for the CG method, whereas they were 0.076 and 0.087, respectively, in testing. For the LM technique, the values for SI in training and testing were 0.059 and 0.043, respectively, and 0.076 and 0.113, respectively, for the CG method. The greater accuracy of the LM approach is further supported by the lower RMSE and SI values in comparison to the CG method. The numbers for NSE in Table 6.2, 0.959 in training and 0.984 in testing for LM versus 0.909 in training and 0.893 in testing for CG, demonstrate that the LM approach has higher values, highlighting its improved accuracy as compared to the CG method.

Training for S/D = 4

ANN (with 5-10-1 and 200 epoch)

Levenberg Marquardt	Conjugate Gradient

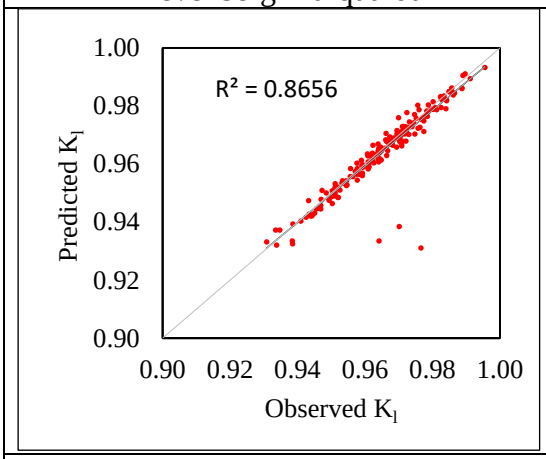

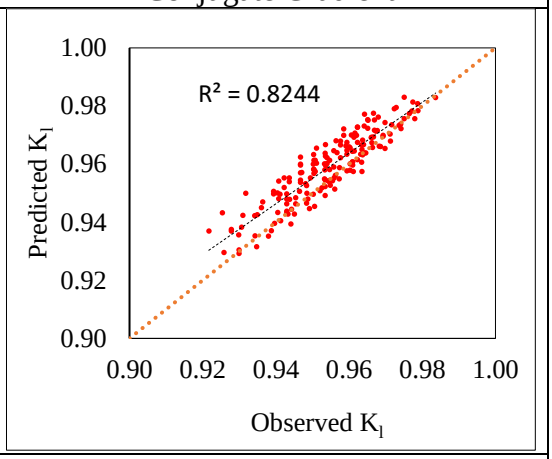

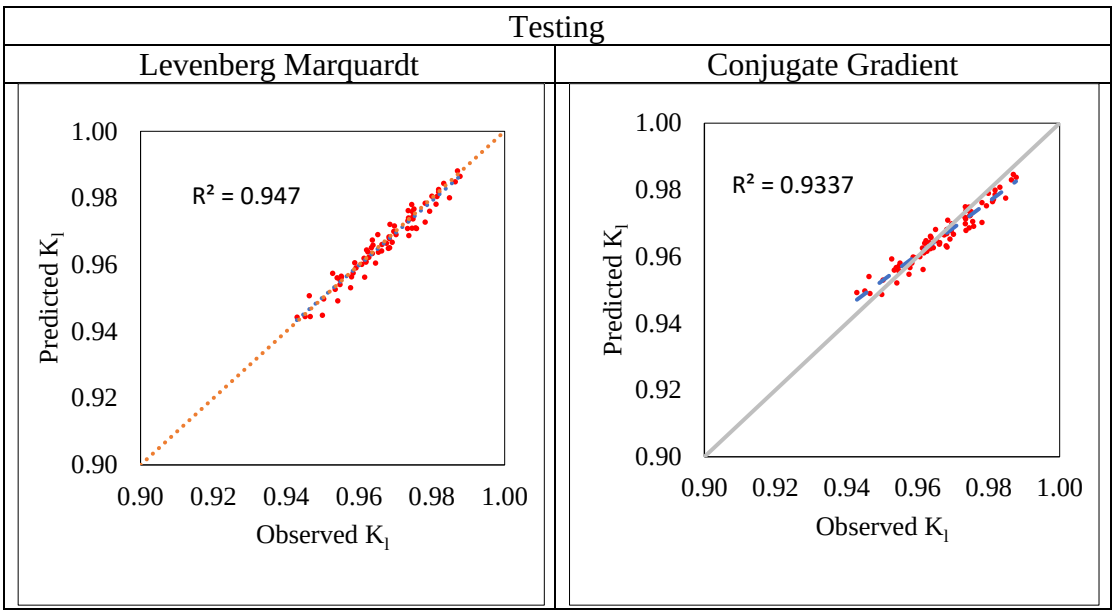

Figure 6.3 Scattered Plot between Observed and Predicted Values of K_l (ANN S/D=4)

Table 6.3 Model Performance Indices for ANN using dimensional parameters

Model Performance Index (MPI)	ANN S/D=4			
	Training		Testing	
	Levenberg Marquardt	Conjugate Gradient	Levenberg Marquardt	Conjugate Gradient
CC	0.931	0.907	0.973	0.966
RMSE	0.112	0.161	0.021	0.135
SI	0.063	0.091	0.012	0.175
NSE	0.931	0.928	0.912	0.846

It can be seen from Figure 6.3 that coefficient of correlation (CC) obtained by the LM approach is superior to the CG method. The model performance index values that were obtained are listed in Table 6.3. The CC value attained by the LM approach in training is 0.931 compared to a value of 0.907 in the CG technique. As a result of testing, it was obtained that the CC values for the LM and CG approaches were, respectively, 0.973 and 0.966. Results for RMSE for the LM and CG method in training were 0.112 and 0.161, respectively, while they were 0.021 and 0.135 in testing. The values for SI in training and testing for the LM methodology were 0.063 and 0.012, respectively, while for the CG method, they were 0.091 and 0.175, respectively. The smaller RMSE and SI values compared to the CG method further demonstrate the higher accuracy of the

LM approach. The results for NSE in Table 6.3 show that the LM approach has higher values, showing its better accuracy when compared to the CG method: 0.931 in training and 0.912 in testing, for CG 0.928 in training, and 0.846 in testing for LM.

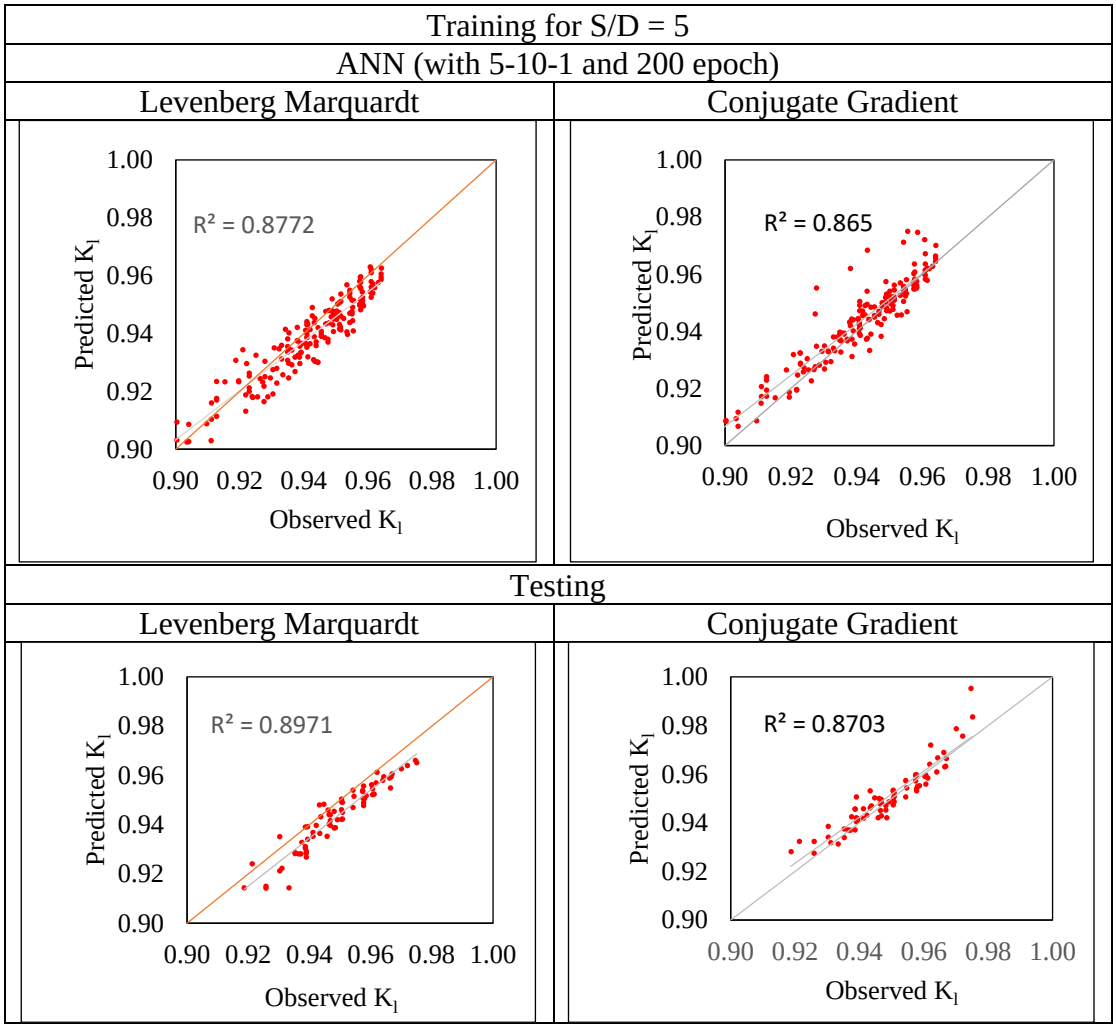

Figure 6.4 Scattered Plot between Observed and Predicted Values of K_l (ANN S/D=5)

Table 6.4 Model Performance Indices for ANN using dimensional parameters

Model Performance Index (MPI)	ANN S/D=5			
	Training		Testing	
	Levenberg Marquardt	Conjugate Gradient	Levenberg Marquardt	Conjugate Gradient
CC	0.936	0.930	0.947	0.933
RMSE	0.184	0.279	0.281	0.384
SI	0.104	0.158	0.159	0.177
NSE	0.943	0.936	0.967	0.951

From the plots shown in Figure 6.4, the observed vs. anticipated K_l, it can be seen that the coefficient of correlation (CC) obtained by LM is superior to the CG method. The values of the model performance index that were found are shown in Table 6.4. During training, the LM achieved a CC value of 0.936 as opposed to the CG of 0.930. The CC values for the LM and CG methods were found to be, respectively, 0.947 and 0.933 as a result of testing. In training, the RMSE for the LM and the CG method were 0.184 and 0.279, respectively, whereas, in testing, they were 0.281 and 0.384, respectively. For the LM, the values for SI were 0.104 and 0.159 in training and testing, respectively, while for the CG method, they were 0.158 and 0.177 in training and testing, respectively. Further evidence of the improved accuracy of the LM approach comes from the lower RMSE and SI values as compared to the CG method. The LM method has higher values for NSE than the CG method, demonstrating improved accuracy: 0.943 in training and 0.967 in testing for LM vs. 0.936 in training and 0.951 in testing for CG.

Table 6.5 Comparison of Model Performance Indices obtained from ANN by LM algorithm using dimensional parameters

	CC		RMSE		SI		NSE	
	Training	Testing	Training	Testing	Training	Testing	Training	Testing
S/D=2	0.959	0.963	0.302	1.249	0.171	1.482	0.982	0.968
S/D=3	0.961	0.965	0.104	0.076	0.059	0.043	0.959	0.984
S/D=4	0.931	0.736	0.112	0.021	0.063	0.012	0.931	0.912
S/D=5	0.936	0.947	0.184	0.281	0.104	0.159	0.943	0.967

Comparison of Model Performance Indices for different S/d ratios of perforated QBW models using ANN by LM algorithm is presented in Table 6.5.

6.3.2 Using Non-Dimensional parameters

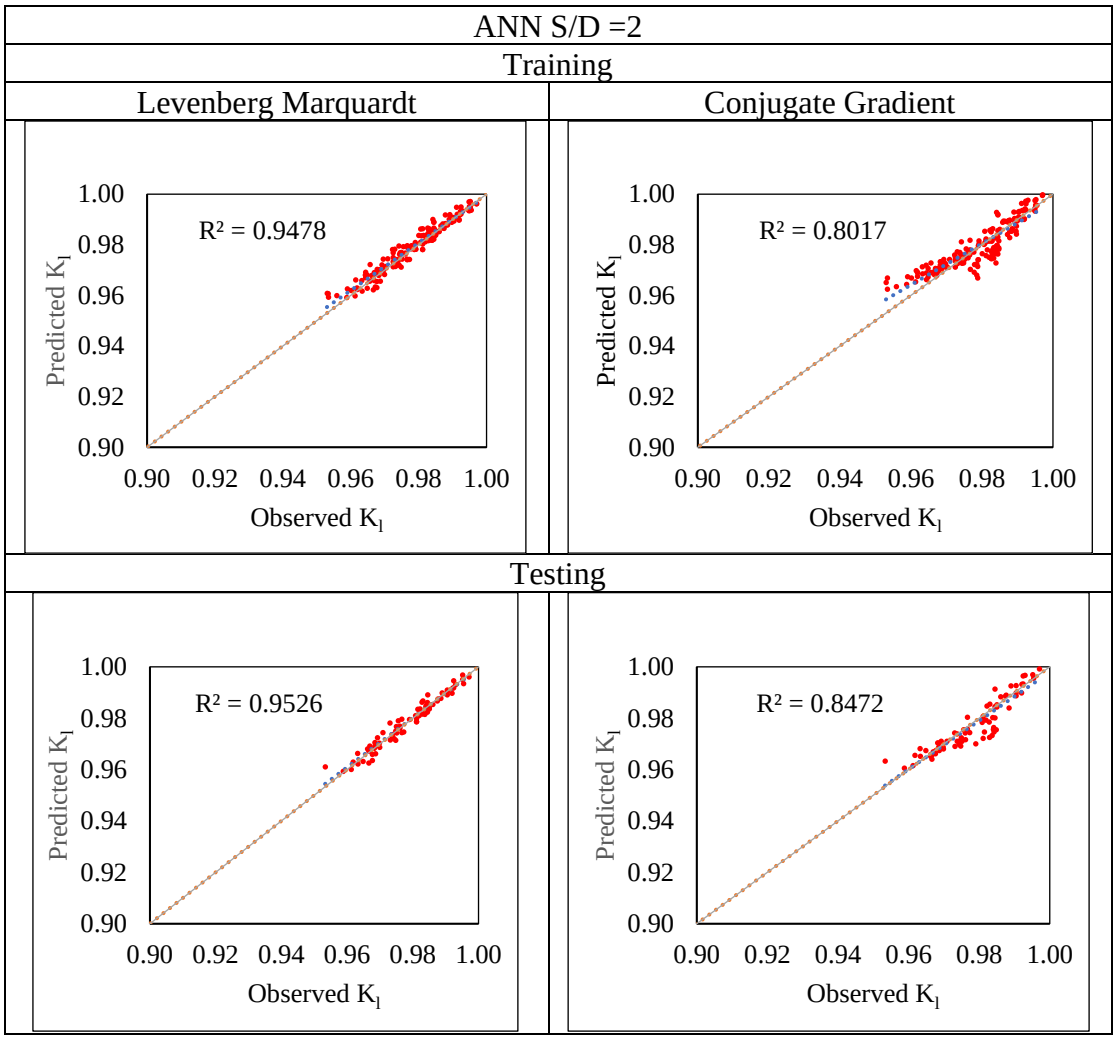

Figure 6.5 Scattered Plot between Observed and Predicted Values of K_l (ANN S/D=2)

Table 6.6 Model Performance Indices for ANN using non-dimensional parameters

Model Performance Index (MPI)	ANN S/D=2			
	Training		Testing	
	Levenberg Marquardt	Conjugate gradoemt	Levenberg Marquardt	Conjugate gradoemt
CC	0.9736	0.8954	0.9765	0.9204
RMSE	0.0485	0.0511	0.1193	0.1243
SI	0.0274	0.0289	0.1549	0.1602
NSE	0.973	0.941	0.952	0.961

When comparing the values of MPI values between the observed vs. anticipated K_l is shown in Table 6.6, the coefficient of correlation (CC) obtained by the LM method is

superior to the CG method. During training, the LM achieved a CC value of 0.9736 as compared to the CG method's 0.8954. The CC values for the LM and CG were found to be, respectively, 0.9765 and 0.9204 as a result of testing. In training, the RMSE for the LM technique and the CG method were 0.0485 and 0.0511, respectively, whereas, in testing, they were 0.1193 and 0.1243, respectively. For the LM, the values for SI were 0.0274 and 0.1549 in training and testing, respectively, while for the CG method, they were 0.0289 and 0.1602 in training and testing, respectively. Further evidence of the improved accuracy of the LM approach comes from the lower RMSE and SI values as compared to the CG method. The LM method has higher values for NSE than the CG method, demonstrating improved accuracy: 0.973 in training and 0.952 in testing for LM vs. 0.941 in training and 0.961 in testing for LM.

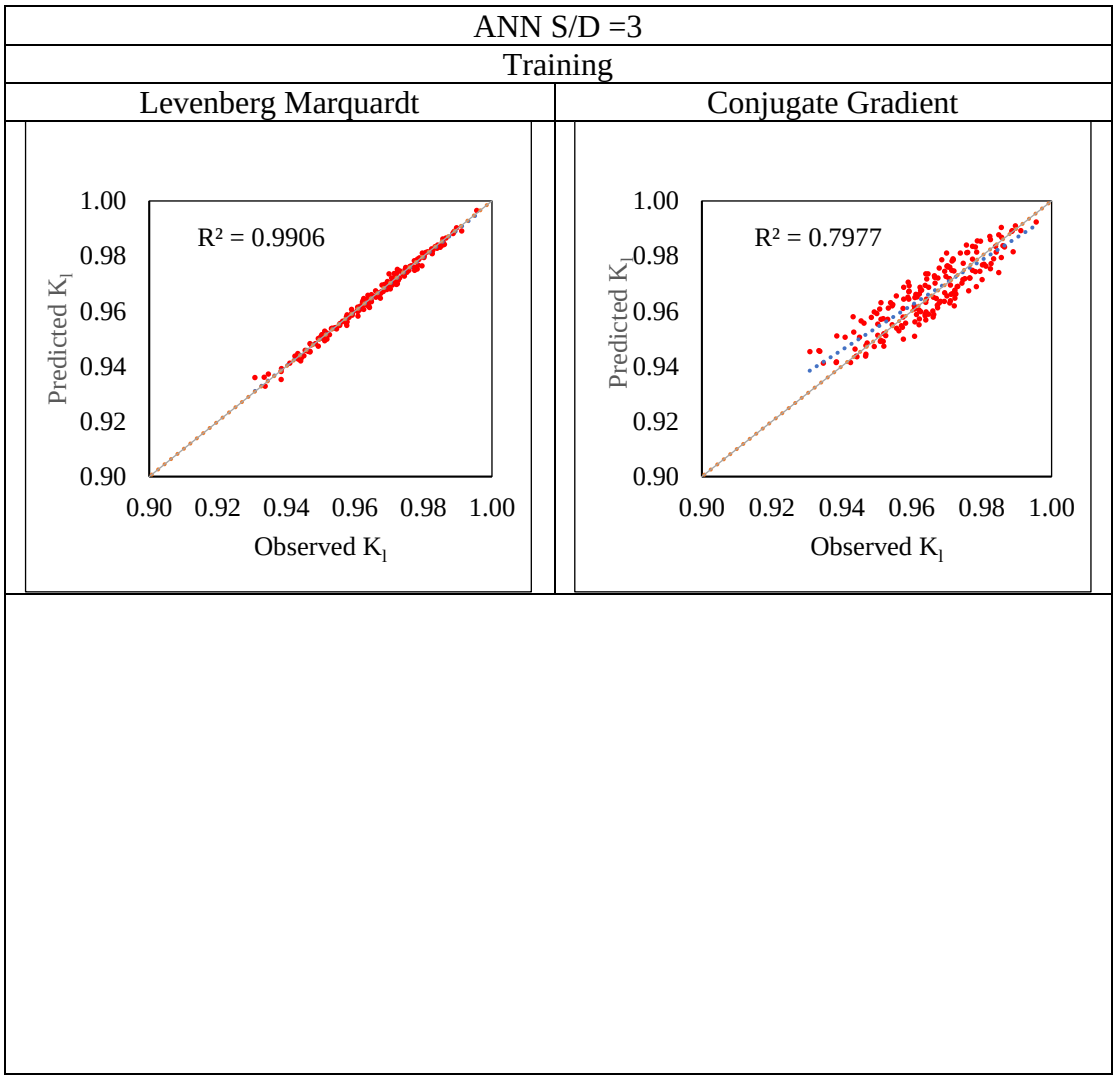

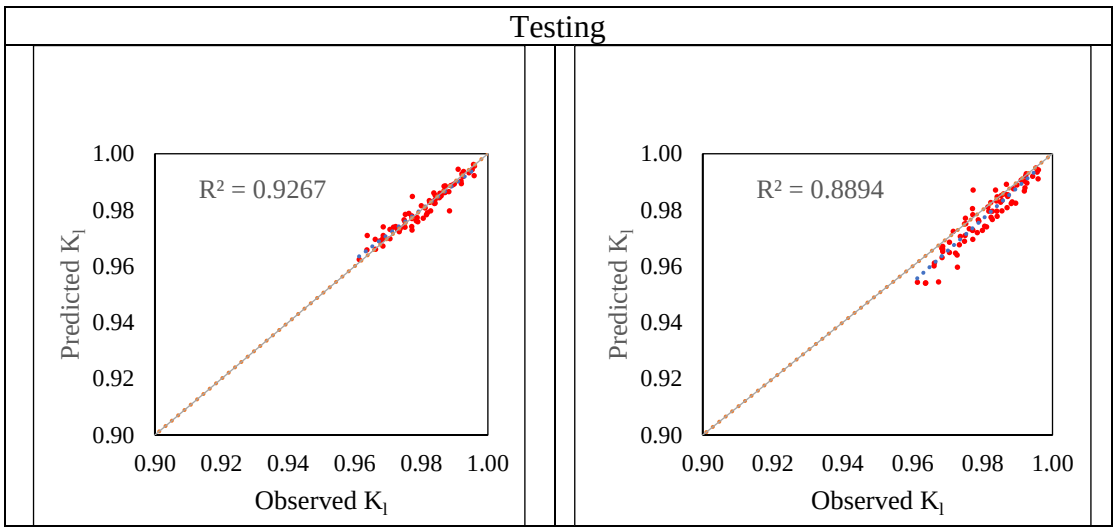

Figure 6.6 Scattered Plot between Observed and Predicted Values of K_l (ANN /D=2)

Table 6.7 Model Performance Indices for ANN using non-dimensional parameters

Model Performance Index (MPI)	ANN S/D=3			
	Training		Testing	
	Levenberg Marquardt	Conjugate gradoemt	Levenberg Marquardt	Conjugate gradoemt
CC	0.9953	0.8931	0.9626	0.9431
RMSE	0.0018	0.0455	0.0259	0.0303
SI	0.0001	0.0003	0.0001	0.0002
NSE	0.987	0.964	0.975	0.929

From the MPIs tabulated in Table 6.7, it can be seen that the LM approach's coefficient of correlation (CC) is superior to the CG method. During training, the LM achieved a CC value of 0.9953 as opposed to the CG's 0.8931. The CC values for the LM and CG techniques were found to be, respectively, 0.9626 and 0.9431 as a result of testing. In training, the RMSE for the LM and the CG method were 0.0018 and 0.0455, respectively, whereas, in testing, they were 0.0259 and 0.0303, respectively. For the LM method, the values for SI were 0.0001 and 0.0001 in training and testing, respectively, while for the CG method, they were 0.0003 and 0.0002 in training and testing, respectively. Further evidence of the improved accuracy of the LM comes from the lower RMSE and SI values as compared to the CG method. The LM method has higher values for NSE than the CG method, demonstrating improved accuracy: 0.987 in training and 0.975 in testing for LM vs. 0.964 in training and 0.929 in testing for CG.

ANN S/D =4

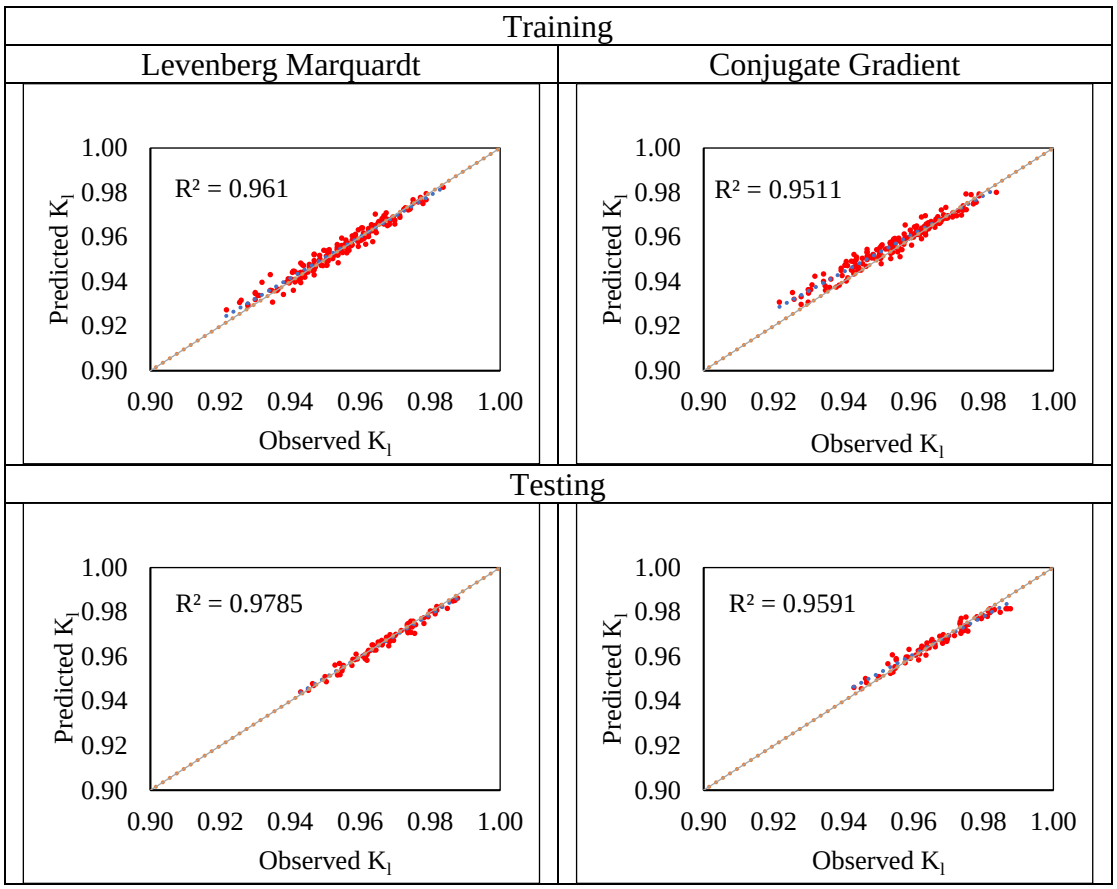

Figure 6.7 Scattered Plot between Observed and Predicted Values of K_l (ANN S/D=4)

Table 6.8 Model Performance Indices for ANN using non-dimensional parameters

Model Performance Index (MPI)	ANN S/D=4			
	Training		Testing	
	Levenberg Marquardt	Conjugate gradiemt	Levenberg Marquardt	Conjugate gradiemt
CC	0.9803	0.9752	0.9891	0.9793
RMSE	0.0826	0.1201	0.0841	0.0933
SI	0.0005	0.0007	0.1092	0.1211
NSE	0.983	0.956	0.968	0.937

From the values tabulated in Table 6.8 between the observed vs. Predicted K_l and MPI tabulated, it can be observed that the coefficient of correlation (CC) by LM is superior to the CG method. During training, the LM achieved a CC value of 0.9803 as opposed to the CG of 0.9752. The CC values from LM and CG were found to be, respectively, 0.9891 and 0.9793 as a result of testing. In training, the RMSE for the CG technique

and the LM method were 0.1201 and 0.0826, respectively, whereas, in testing, they were 0.0933 and 0.0841, respectively. For the CG methodology, the values for SI were 0.0007 and 0.1211 in training and testing, respectively, while for the LM method, they were 0.0005 and 0.1092 in training and testing, respectively. Further evidence of the improved accuracy of the LM approach comes from the lower RMSE and SI values as compared to the CG method. The LM method has higher values for NSE than the CG method, demonstrating improved accuracy: 0.983 in training and 0.968 in testing for LM vs. 0.956 in training and 0.937 in testing for CG.

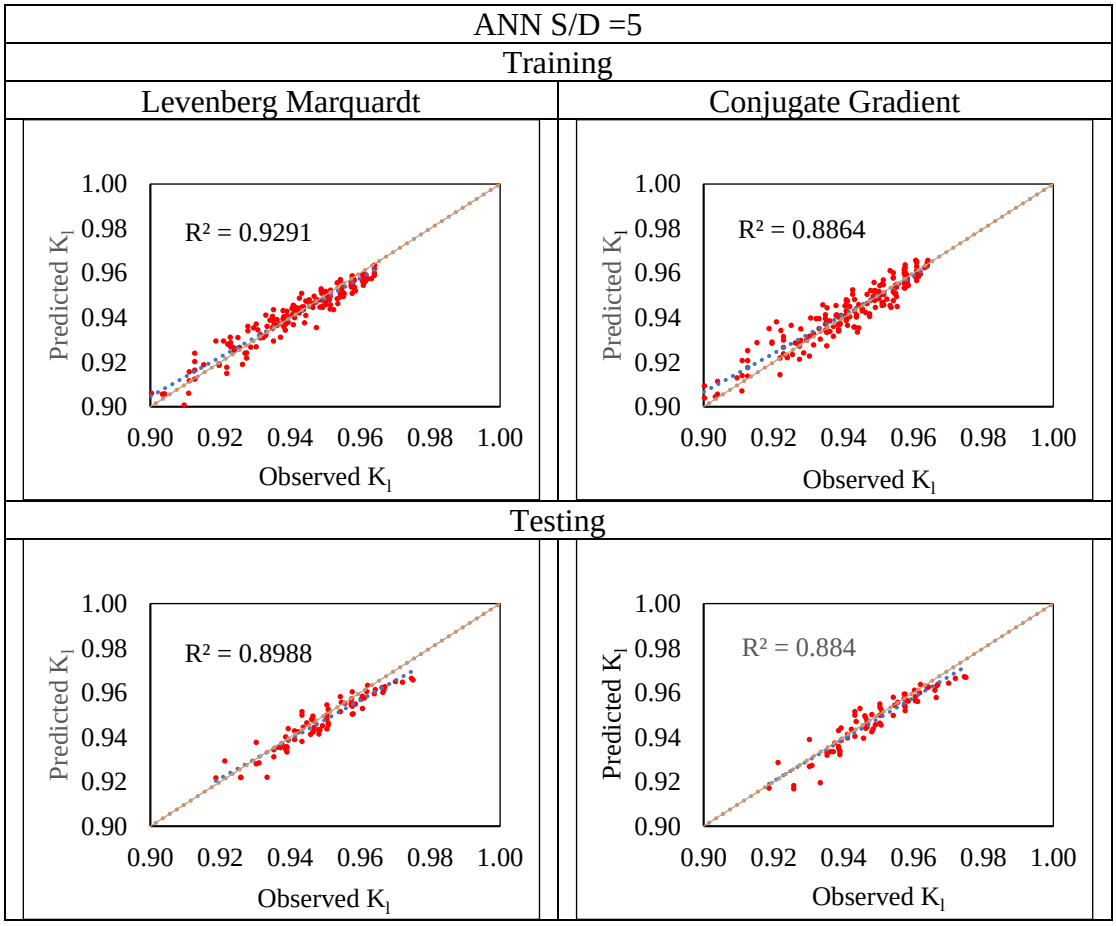

Figure 6.8 Scattered Plot between Observed and Predicted Values of K_l (ANN S/D=5)

Table 6.9 Model Performance Indices for ANN using non-dimensional parameters

Model Performance Index (MPI)	ANN S/D=5			
	Training		Testing	
	Levenberg Marquardt	Conjugate gradoemt	Levenberg Marquardt	Conjugate gradoemt
CC	0.9639	0.9415	0.9481	0.9402
RMSE	0.0719	0.0930	0.0722	0.0987
SI	0.0406	0.0526	0.0938	0.1282
NSE	0.958	0.893	0.951	0.912

By comparing the plots of observed vs. anticipated K_l and MPI values tabulated in Table 6.9, it can be seen that the coefficient of correlation (CC) by LM is superior to the CG method. During training, the LM achieved a CC value of 0.9639 as compared to the CG's 0.9415. The CC values for the LM and CG were found to be 0.9481 and 0.9402, respectively, during testing. The RMSE for the LM and the CG method during training were 0.0719 and 0.0930, respectively, whereas, in testing, they were 0.0722 and 0.0987, respectively. For the CG, the values for SI were 0.0526 and 0.1282 in training and testing, respectively, while for the LM method, they were 0.0406 and 0.0938 in training and testing, respectively. Further evidence of the improved accuracy of the LM approach comes from the lower RMSE and SI values as compared to the CG method. The LM has higher values for NSE than the CG method, demonstrating improved accuracy: 0.958 in training and 0.951 in testing for LM vs. 0.893 in training and 0.912 in testing for CG.

Table 6.10 Comparison of Model Performance Index obtained from ANN by Levenberg Marquardt algorithm using non-dimensional parameters

	CC		RMSE		SI		NSE	
	Training	Testing	Training	Testing	Training	Testing	Training	Testing
S/D=2	0.981	0.984	0.0485	0.1193	0.0274	0.1549	0.973	0.952
S/D=3	0.956	0.949	0.0018	0.0259	0.0001	0.0001	0.909	0.893
S/D=4	0.936	0.967	0.0826	0.0841	0.0005	0.1092	0.931	0.846
S/D=5	0.929	0.932	0.0719	0.0722	0.0406	0.0722	0.958	0.951

Table 6.10 compares the model performance index obtained by ANN using the Levenberg Marquardt algorithm for different perforations of QBW, QBW with S/D =3 Outperformed compared to other conditions of perforation.

6.4 PREDICTION OF LOSS COEFFICIENT (K_l) OF A PERFORATED QBW USING ADAPTIVE NEURO-FUZZY INFERENCE SYSTEM (ANFIS)

6.4.1 Using Dimensional Parameters

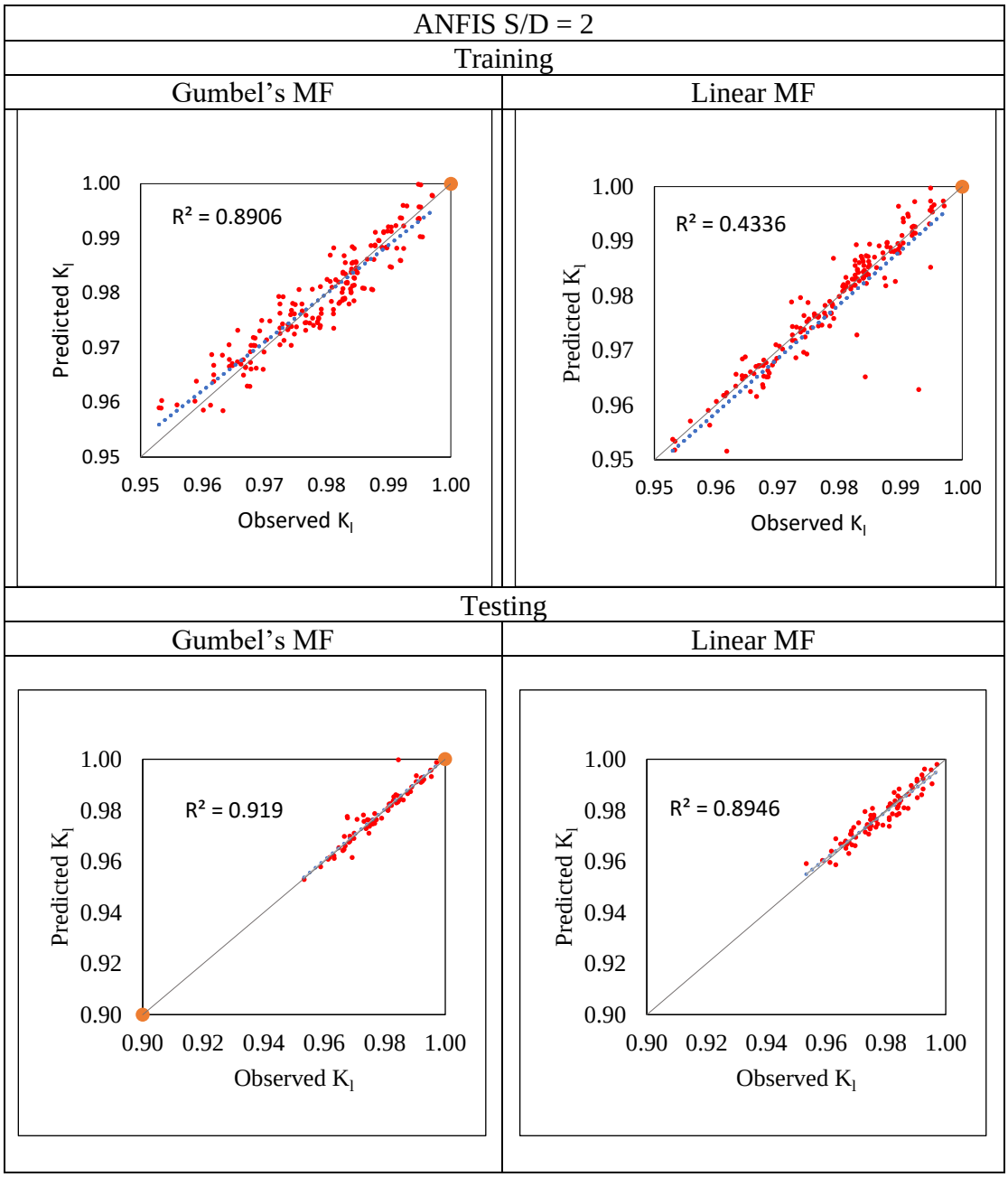

Figure 6.9 Scattered Plot between Observed and Predicted Values of K_l (ANFIS S/D=2)

Table 6.11 Model Performance Indices for ANFIS using dimensional parameters

Model Performance Index (MPI)	ANFIS S/D=2			
	Training		Testing	
	Gumbel's MF	Linear MF	Gumbel's MF	Linear MF
CC	0.913	0.658	0.958	0.946
RMSE	2.891	4.562	2.937	3.422
SI	1.634	2.581	3.814	4.444
NSE	0.897	0.861	0.923	0.917

When comparing the plots of observed vs. anticipated K_r and MPIs, it can be seen that Gumbel's MF's coefficient of correlation (CC) is superior to the coefficient obtained using Linear MF. The values of the model performance index that were found are shown in Table 6.11. During training, the Linear MF strategy achieved a CC value of 0.658 as compared to Gumbel's MF technique's 0.913. The CC values for the Linear MF and Gumbel's MF techniques were found to be, respectively, 0.946 and 0.958 as a result of testing. In training, the RMSE for the Linear MF technique and Gumbel's MF method were 4.562 and 2.891, respectively, whereas, in testing, they were 3.422 and 2.937, respectively. For the Linear MF, the values for SI were 2.581 and 4.444 in training and testing, respectively, while for the Gumbel's MF method, they were 1.634 and 3.814 in training and testing, respectively. Further evidence of the improved accuracy of Gumbel's MF approach comes from the lower RMSE and SI values as compared to Gumbel's MF method. The Gumbel's MF has higher values for NSE than the Linear MF method, demonstrating improved accuracy: 0.897 in training and 0.923 in testing for Gumbel's MF vs. 0.861 in training and 0.917 in testing for Linear MF.

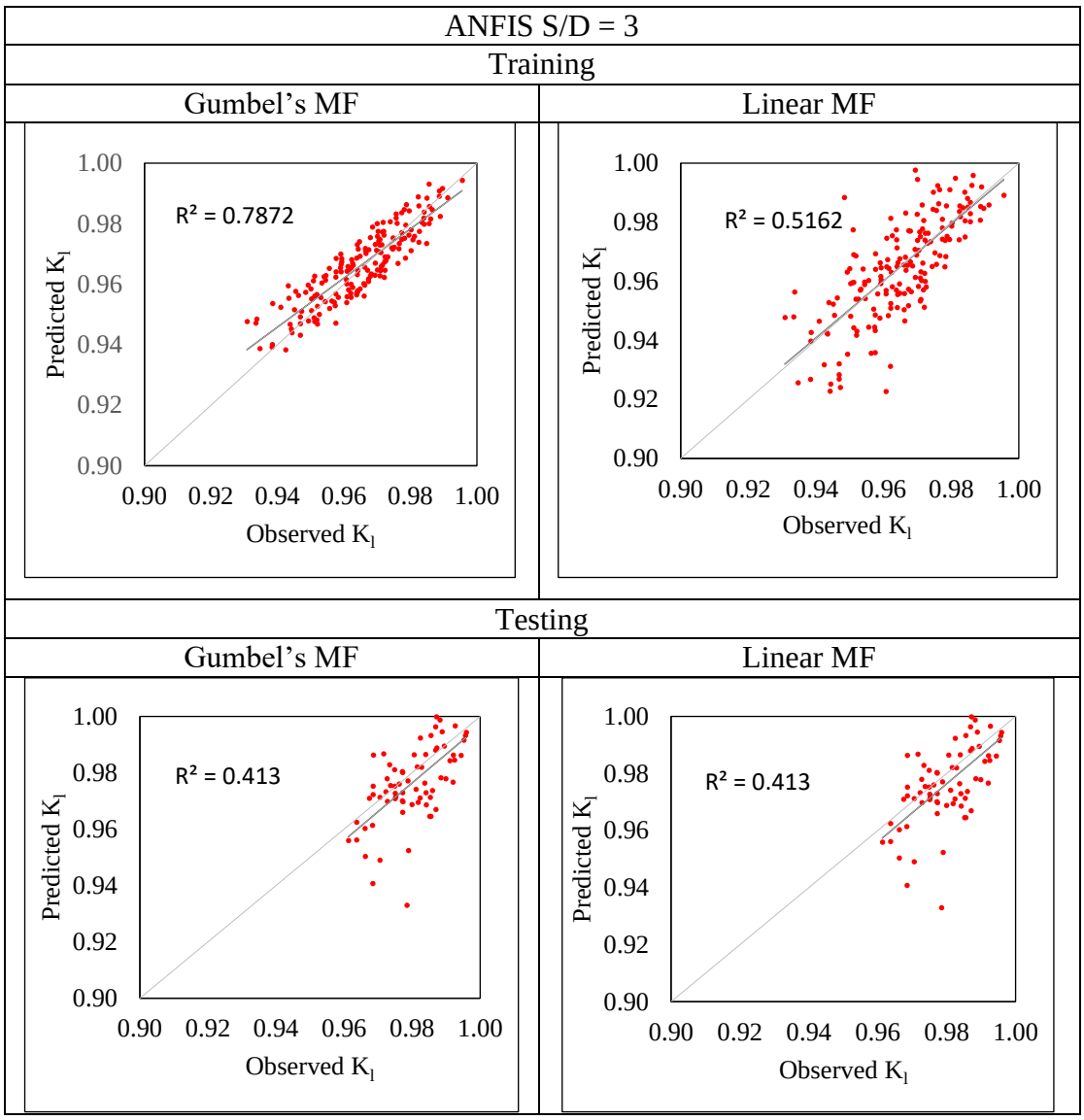

Figure 6.10 Scattered Plot between Observed and Predicted Values of K_l (ANFIS S/D=3)

Table 6.12 Model Performance Indices for ANFIS using dimensional parameters

Model Performance Index (MPI)	ANFIS S/D=3			
	Training		Testing	
	Gumbel's MF	Linear MF	Gumbel's MF	Linear MF
CC	0.887	0.784	0.643	0.643
RMSE	4.931	6.417	5.137	5.483
SI	2.786	3.625	6.671	7.121
NSE	0.832	0.804	0.912	0.891

By comparing the plots of observed vs. predicted K_l and MPI from Table 6.12, it can be seen that Gumbel's MF coefficient of correlation (CC) is superior to the Linear MF method. In comparison to a value of 0.887 in Gumbel's MF, the value of CC obtained by the Linear MF method in training is 0.784 during training. While testing, the CC values for the Linear MF and Gumbel's MF methods were, respectively, 0.643 and 0.643. The results for RMSE were 6.417 for the Linear MF technique in training and 4.931 for the Gumbel's MF method, whereas they were 5.483 and 5.137, respectively, in testing. For the Linear MF technique, the values for SI in training and testing were 3.625 and 7.121, respectively, and 2.786 and 6.671, respectively, for Gumbel's MF method. The greater accuracy of the Gumbel/s MF approach is further supported by the lower RMSE and SI values in comparison to the Linear MF method. The NSE is 0.804 in training and 0.891 in testing for Linear MF versus 0.832 in training and 0.912 in testing for Gumbel's MF, demonstrating that the Gumbel's MF approach has higher values, highlighting its improved accuracy as compared to the Linear MF method.

ANFIS S/D = 4

Training

Gumbel's MF

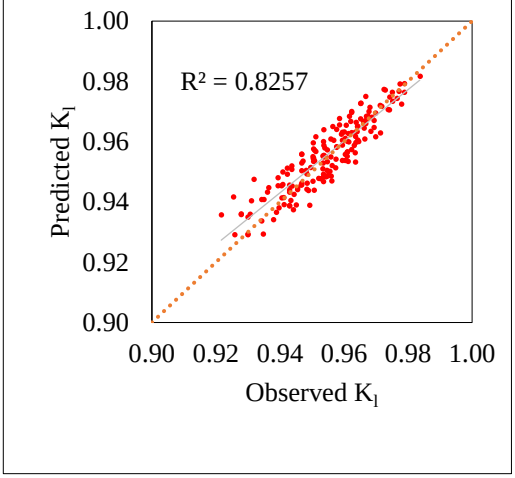

Linear MF

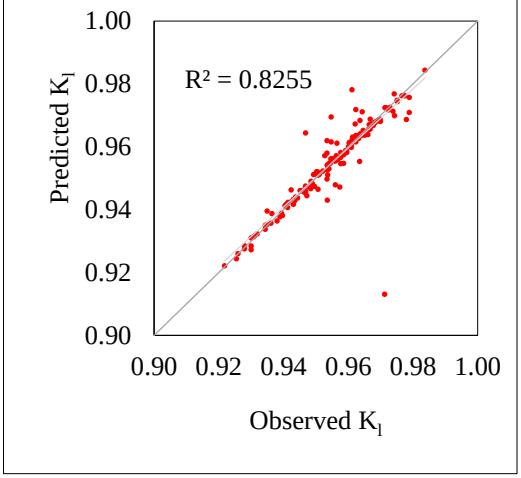

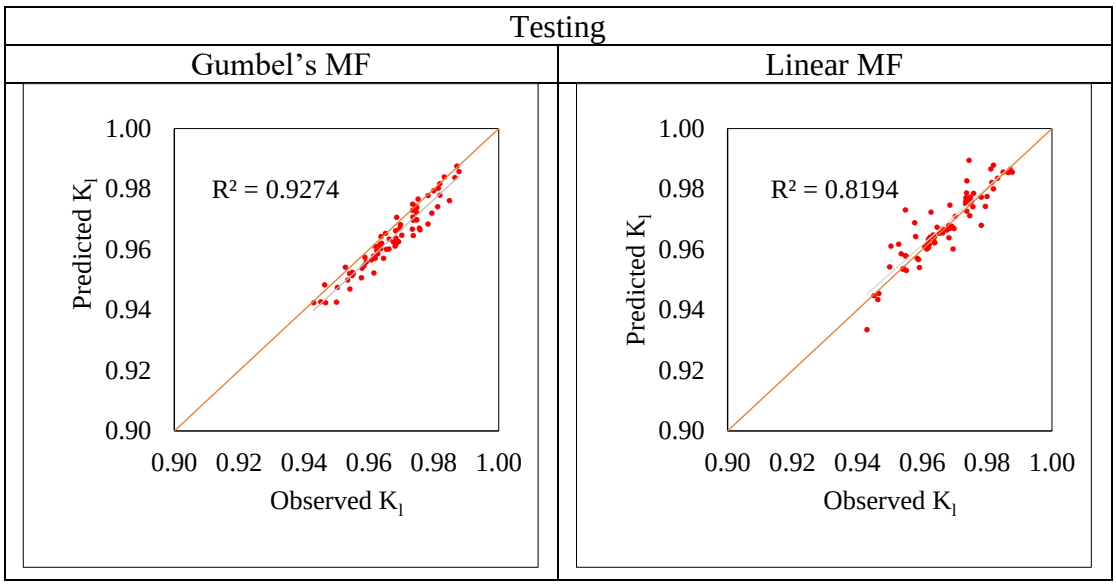

Figure 6.11 Scattered Plot between Observed and Predicted Values of K_l (ANFIS S/D=2)

Table 6.13 Model Performance Indices for ANFIS using dimensional parameters

Model Performance Index (MPI)	ANFIS S/D=4			
	Training		Testing	
	Gumbel's MF	Linear MF	Gumbel's MF	Linear MF
CC	0.918	0.908	0.963	0.905
RMSE	4.438	5.723	3.183	4.917
SI	2.055	3.668	5.731	6.385
NSE	0.897	0.853	0.846	0.872

Comparing the plots of observed vs. predicted K_l, it is observed that the coefficient of correlation (CC) obtained by Gumbel's MF method is better compared to the Linear MF method. The model performance index values obtained are tabulated in Table 6.13. The value of CC obtained by the Linear MF method in training is 0.908 as compared to a value of 0.918 in Gumbel's MF method. In testing, the CC value was found to be 0.905 and 0.963 for Linear MF and Gumbel's MF method, respectively. The values for RMSE in training were 5.723 for the Linear MF method against 4.438 for Gumbel's MF method, while in testing, it was 4.917 and 3.183, respectively. The value for SI in training and testing was 3.668 and 6.385 for the Linear MF method, respectively, and 2.055 and 5.731 for Gumbel's MF method, respectively. The lower values for RMSE and SI in Gumbel's MF method as compared linear MF method further indicate that

the accuracy is more for Gumbel's MF method. The values for NSE are 0.853 and 0.872 in training and testing, respectively, for Linear MF and 0.897 and 0.846 for training and testing, respectively, for Gumbel's MF, showing that Gumbel's MF method has greater values; hence emphasizing the accuracy over Gumbel's MF method.

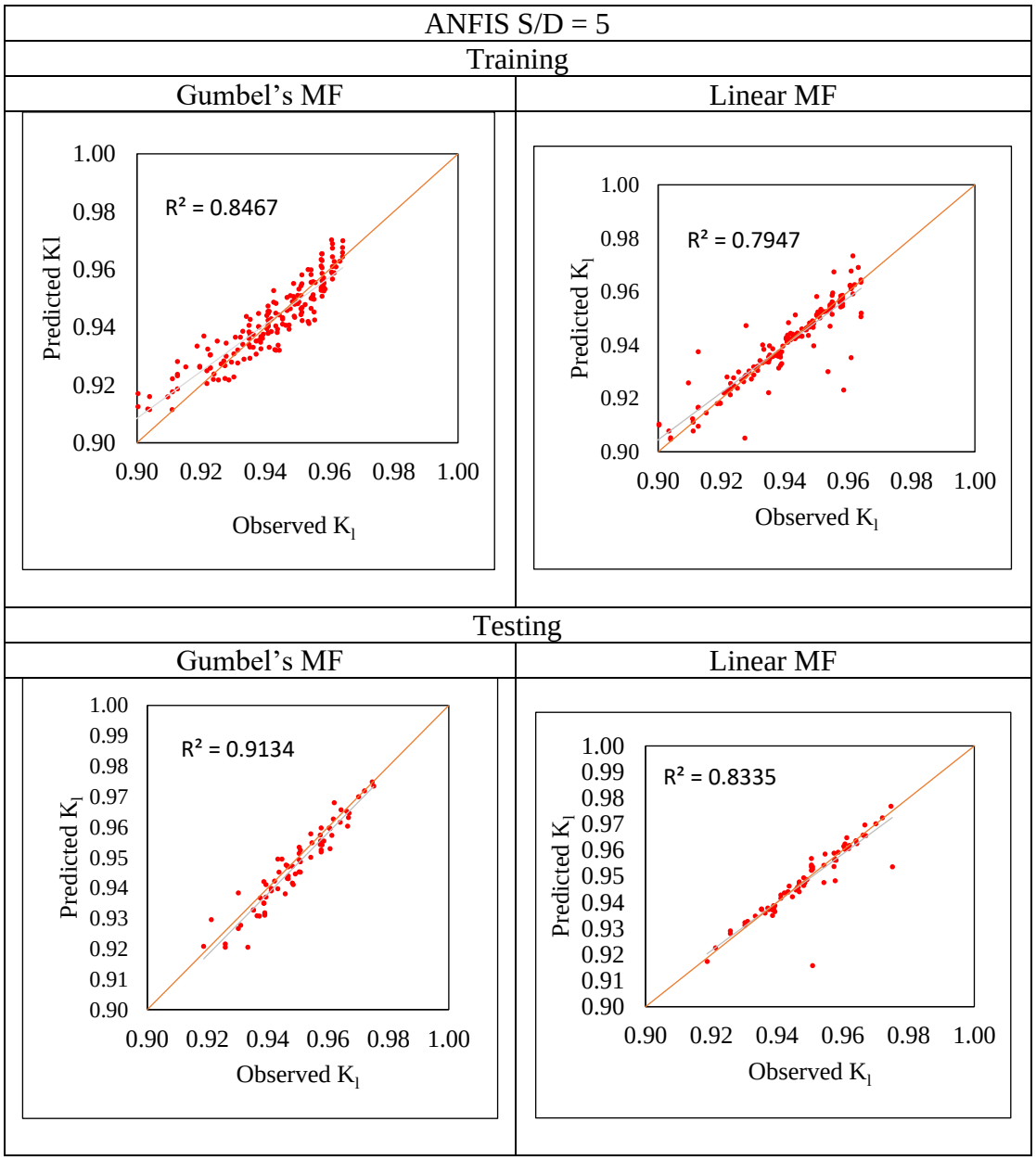

Figure 6.12 Scattered Plot between Observed and Predicted Values of K_l (ANFIS S/D=2)

Table 6.14 Model Performance Indices for ANFIS using dimensional parameters

Model Performance Index (MPI)	ANFIS S/D=5			
	Training		Testing	
	Gumbel's MF	Linear MF	Gumbel's MF	Linear MF
CC	0.919	0.891	0.956	0.913
RMSE	4.963	5.814	4.791	5.804
SI	2.804	3.284	6.538	7.222
NSE	0.899	0.893	0.852	0.844

It can be seen that Gumbel's MF approach's coefficient of correlation (CC) is superior to the Linear MF method when comparing the plots of observed vs. anticipated K_l. The model performance index is listed in Table 6.14. The CC value attained by the Linear MF approach in training is 0.891 compared to a value of 0.919 in Gumbel's MF technique. As a result of testing, it was obtained that the CC values for the Linear MF and Gumbel's MF approaches were, respectively, 0.913 and 0.956. Results for RMSE for the Linear MF approach and Gumbel's MF method in training were 5.814 and 4.963, respectively, while they were 5.804 and 4.791 in testing. The values for SI in training and testing for the Linear MF were 3.284 and 7.222, respectively, while for the Gumbel's MF, they were 2.804 and 6.538, respectively. The reduced RMSE and SI values compared to the Linear MF method further demonstrate the higher accuracy of Gumbel's MF approach. The results for NSE indicate that Gumbel's MF approach has higher values, showing its better accuracy when compared to the Linear MF method: 0.893 in training and 0.844 in testing for Linear MF with 0.899 in training and 0.852 in testing for Gumbel's MF.

Table 6.15 Comparison of Model Performance Index obtained for ANFIS model with by Gumbel's MF using dimensional parameters.

	CC		RMSE		SI		NSE	
	Training	Testing	Training	Testing	Training	Testing	Training	Testing
S/D=2	0.913	0.958	2.891	2.937	1.634	3.814	0.897	0.923
S/D=3	0.887	0.643	4.931	5.137	2.786	6.671	0.832	0.912
S/D=4	0.918	0.963	4.438	3.183	2.055	4.731	0.897	0.846

S/D=5	0.919	0.956	4.963	4.791	2.804	6.538	0.899	0.852

Table 6.15 compares the model performance index obtained by ANFIS using Gumbel's membership function for different perforations of QBW, QBW with S/D, =3 performed better compared to other conditions.

6.4.2 Using Non-Dimensional parameters

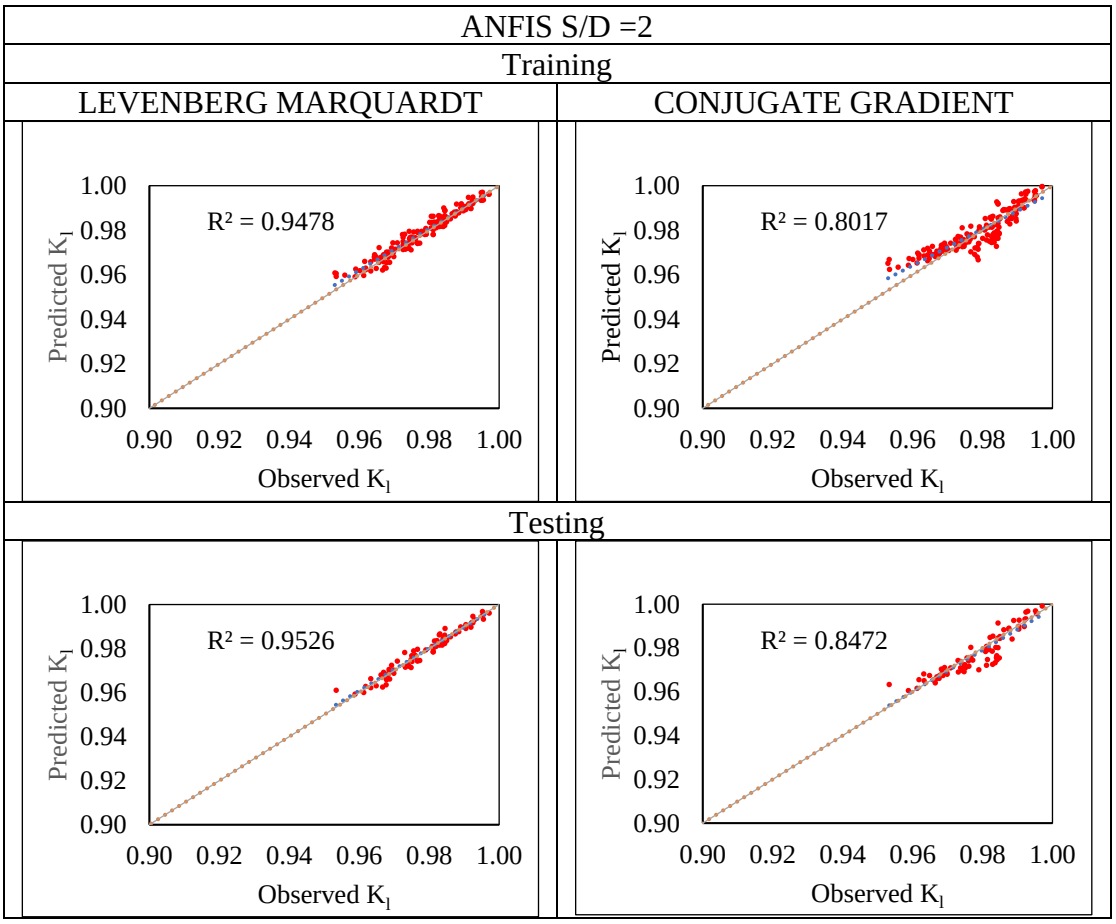

Figure 6.13 Scattered Plot between Observed and Predicted Values of K_l (ANFIS S/D=2)

Table 6.16 Model Performance Indices by ANFIS algorithm using non-dimensional parameters

Model Performance Index (MPI)	ANFIS S/D=2			
	Training		Testing	
	Gumbel's MF	Linear MF	Gumbel's MF	Linear MF
CC	0.9736	0.8954	0.9760	0.9204
RMSE	0.0503	0.0511	0.1234	0.1339
SI	0.0284	0.0289	0.1602	0.1739

NSE	0.903	0.873	0.945	0.921

By comparing the MPI, it can be seen that Gumbel's MF approach's coefficient of correlation (CC) is superior to the Linear MF method when comparing the plots of observed vs. anticipated K_l. The model performance index is listed in Table 6.16. The CC value attained by the Linear MF approach in training is 0.8954 compared to a value of 0.9736 in Gumbel's MF technique. As a result of testing, it was found that the CC values for the Linear MF and Gumbel's MF approaches were, respectively, 0.9204 and 0.9760. Results for RMSE for the Linear MF approach and Gumbel's MF method in training were 0.0511 and 0.0503, respectively, while they were 0.1339 and 0.1234 in testing. The values for SI in training and testing for the Linear MF were 0.0289 and 0.1739, respectively, while for the Gumbel's MF method, they were 0.0284 and 0.1602, respectively. The reduced RMSE and SI values compared to the Linear MF method further demonstrate the higher accuracy of Gumbel's MF approach. The results for NSE indicate that Gumbel's MF approach has higher values, showing its better accuracy when compared to the Linear MF method: 0.873 in training and 0.921 in testing for Linear MF with 0.903 in training and 0.945 in testing for Gumbel's MF.

ANFIS S/D =3

Training

LEVENBERG MARQUARDT

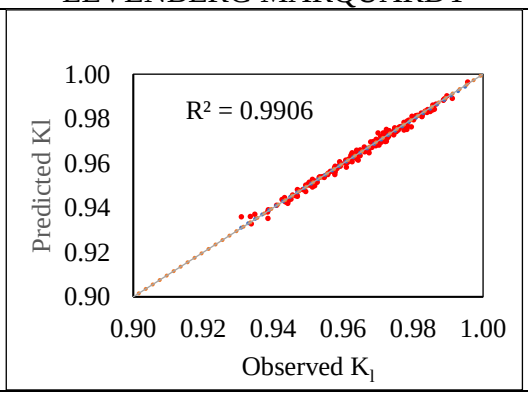

CONJUGATE GRADIENT

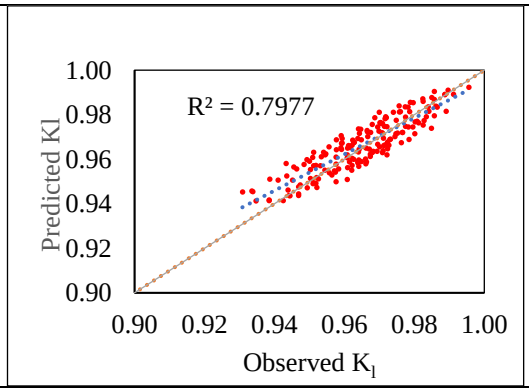

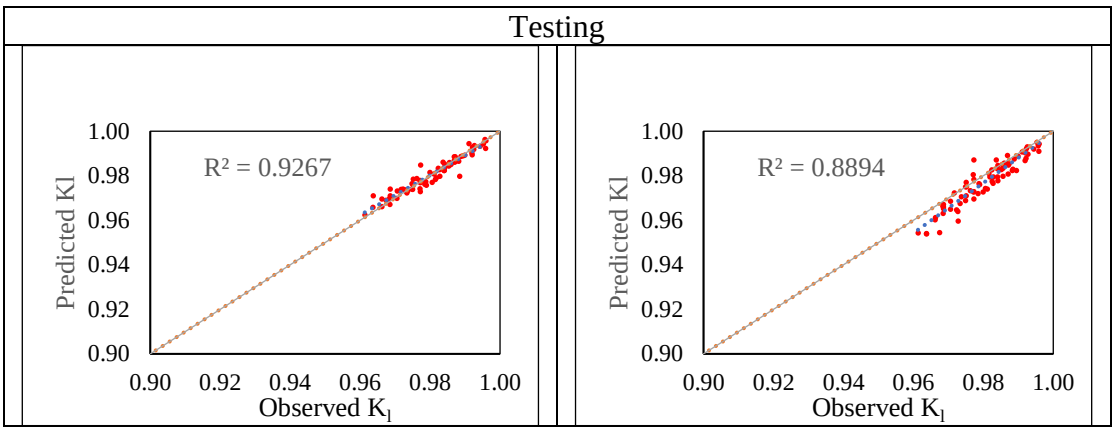

Figure 6.14 Scattered Plot between Observed and Predicted Values of K_l (ANFIS S/D=3)

Table 6.17 Model Performance Indices by ANFIS algorithm using non-dimensional parameters

Model Performance Index (MPI)	ANFIS S/D=3			
	Training		Testing	
	Gumbel's MF	Linear MF	Gumbel's MF	Linear MF
CC	0.9953	0.8931	0.9626	0.9431
RMSE	0.0362	0.0480	0.0221	0.0306
SI	0.0204	0.0271	0.0287	0.0398
NSE	0.891	0.841	0.922	0.912

By comparing the above-tabulated values of MPIs computed using Gumbel's and Linear membership functions, it can be observed that Gumbel's MF approach's coefficient of correlation (CC) is superior to the Linear MF method. The CC value attained by the Linear MF approach in training is 0.8931 compared to a value of 0.9953 in Gumbel's MF technique. On testing, it was found that the CC values for the Linear MF and Gumbel's MF approaches were, respectively, 0.9431 and 0.9626. Results for RMSE for the Linear MF approach and Gumbel's MF method in training were 0.0480 and 0.0362, respectively, while they were 0.0306 and 0.0221 in testing. The values for SI in training and testing for the Linear MF were 0.0271 and 0.0398, respectively, while for the Gumbel's MF method, they were 0.0204 and 0.0287, respectively. The reduced RMSE and SI values compared to the Linear MF method further demonstrate the higher accuracy of Gumbel's MF approach. The results for NSE indicate that Gumbel's MF

approach has higher values, showing its better accuracy when compared to the Linear MF method: 0.841 in training and 0.912 in testing for Linear MF with 0.891 in training and 0.922 in testing for Gumbel's MF.

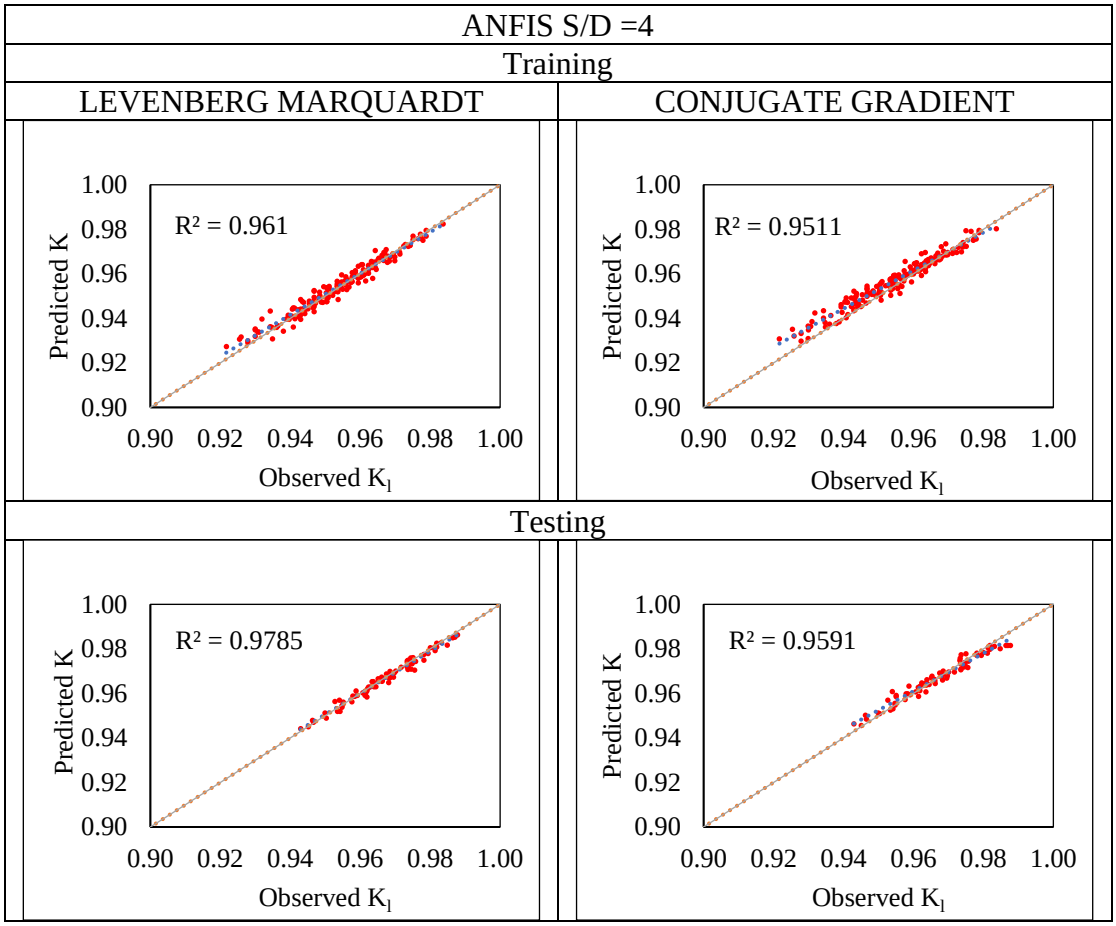

Figure 6.15 Scattered Plot between Observed and Predicted Values of K_l (ANFIS S/D=4)

Table 6.18 Model Performance Indices by ANFIS algorithm using non-dimensional parameters

Model Performance Index (MPI)	ANFIS S/D=4			
	Training		Testing	
	Gumbel's MF	Linear MF	Gumbel's MF	Linear MF
CC	0.9803	0.9752	0.9891	0.9793
RMSE	0.0332	0.0922	0.0313	0.0865
SI	0.0002	0.0005	0.0407	0.1124

NSE	0.936	0.921	0.935	0.928

From the above MPI values computed using Gumbel's and Linear membership functions tabulated in Table 6.18, it can be observed that Gumbel's MF approach's coefficient of correlation (CC) is superior to the Linear MF method. The CC value attained by the Linear MF approach in training is 0.9752 compared to a value of 0.9803 in Gumbel's MF technique. On testing, it was found that the CC values for the Linear MF and Gumbel's MF approaches were, respectively, 0.9793 and 0.9891. Results for RMSE for the Linear MF approach and Gumbel's MF method in training were 0.0922 and 0.0332, respectively, while they were 0.0865 and 0.0313 in testing. The values for SI in training and testing for the Linear MF were 0.0005 and 0.1124, respectively, while for the Gumbel's MF method, they were 0.0002 and 0.0407, respectively. The reduced RMSE and SI values compared to the Linear MF method further demonstrate the higher accuracy of Gumbel's MF approach. The results for NSE indicate that Gumbel's MF approach has higher values, showing its better accuracy when compared to the Linear MF method: 0.921 in training and 0.928 in testing for Linear MF with 0.936 in training and 0.935 in testing for Gumbel's MF.

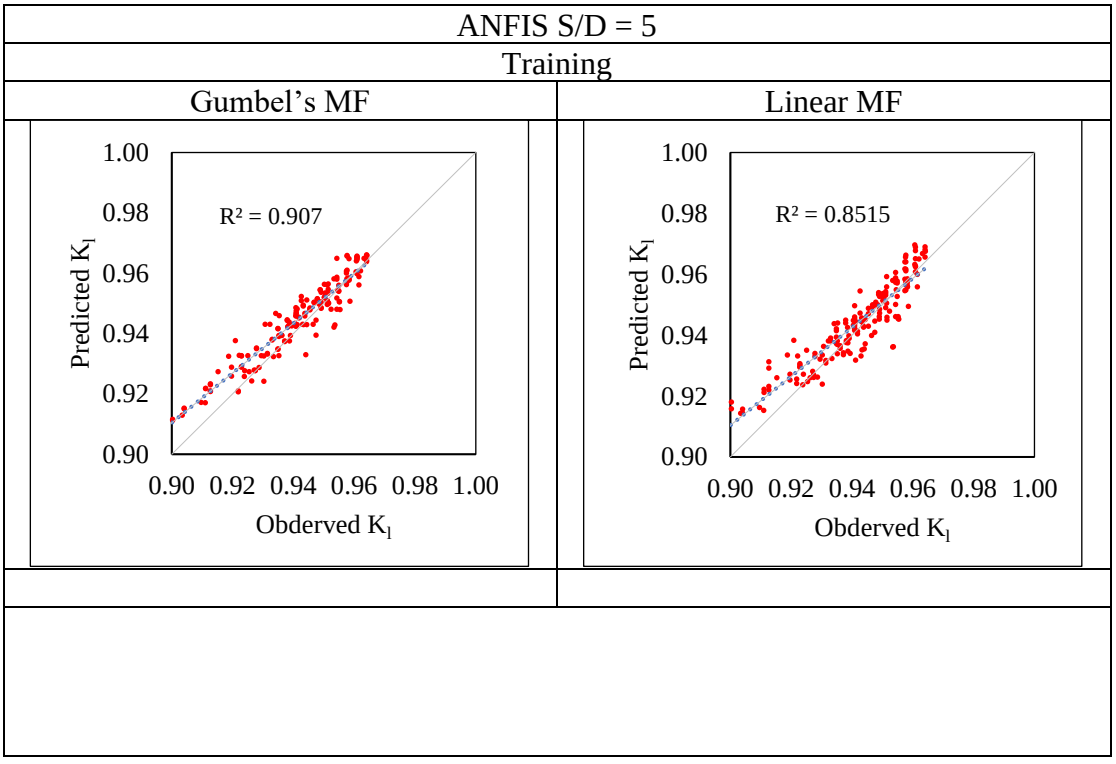

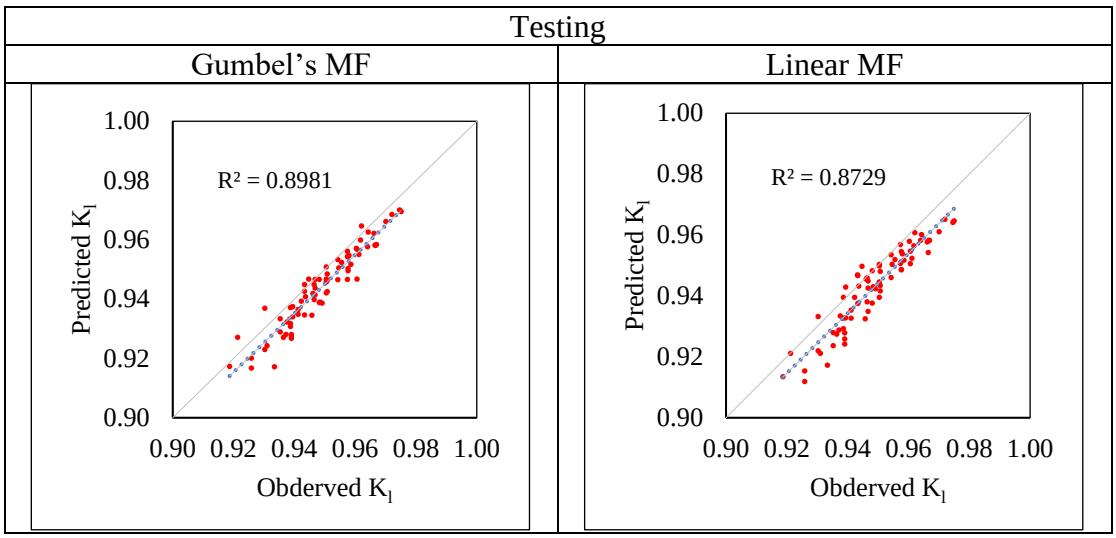

Figure 6.16 Scattered Plot between Observed and Predicted Values of K_l (ANFIS S/D=5)

Table 6.19 Model Performance Indices by ANFIS algorithm using non-dimensional parameters

Model Performance Index (MPI)	ANFIS S/D=5			
	Training		Testing	
	Gumbel's MF	Linear MF	Gumbel's MF	Linear MF
CC	0.952	0.923	0.948	0.934
RMSE	0.0581	0.0843	0.0433	0.0836
SI	0.0328	0.0476	0.0562	0.1069
NSE	0.983	0.893	0.921	0.919

Comparing the MPI values tabulated in Table 6.19, computed using Gumbel's and Linear membership functions, indicates that Gumbel's MF approach's coefficient of correlation (CC) is superior to the Linear MF method. The CC value attained by the Linear MF approach in training is 0.923 compared to a value of 0.952 in Gumbel's MF technique. On testing, it was found that the CC values for the Linear MF and Gumbel's MF approaches were, respectively, 0.934 and 0.948. Results for RMSE for the Linear MF approach and Gumbel's MF method in training were 0.0843 and 0.0581, respectively, while they were 0.0836 and 0.0433 in testing. The values for SI in training and testing for the Linear MF were 0.0476 and 0.1069, respectively, while for the Gumbel's MF method, they were 0.0328 and 0.0562, respectively. The reduced RMSE and SI values compared to the Linear MF method further demonstrate the higher accuracy of Gumbel's MF approach. The results for NSE indicate that Gumbel's MF

approach has higher values, showing its better accuracy when compared to the Linear MF method: 0.893 in training and 0.919 in testing for Linear MF with 0.983 in training and 0.921 in testing for Gumbel's MF.

Table 6.20 Model Performance Index obtained for ANFIS algorithm by Gumbel's MF using non-Dimensional parameters

	CC		RMSE		SI		NSE	
	Training	Testing	Training	Testing	Training	Testing	Training	Testing
S/D=2	0.976	0.976	0.0503	0.1234	0.0284	0.1602	0.903	0.945
S/D=3	0.948	0.938	0.0362	0.0221	0.0204	0.0287	0.891	0.922
S/D=4	0.934	0.957	0.0332	0.0313	0.0002	0.0407	0.936	0.935
S/D=5	0.952	0.948	0.0581	0.0433	0.0328	0.0562	0.983	0.921

From Table 6.20, comparing the model performance index obtained by SVM using the decision tree for different perforations of QBW, QBW with S/D=3 is found to be better.

6.5 PREDICTION OF LOSS COEFFICIENT (K_l) OF A PERFORATED QBW USING SUPPORT VECTOR METHOD (SVM)

6.5.1 Using Dimensional parameters

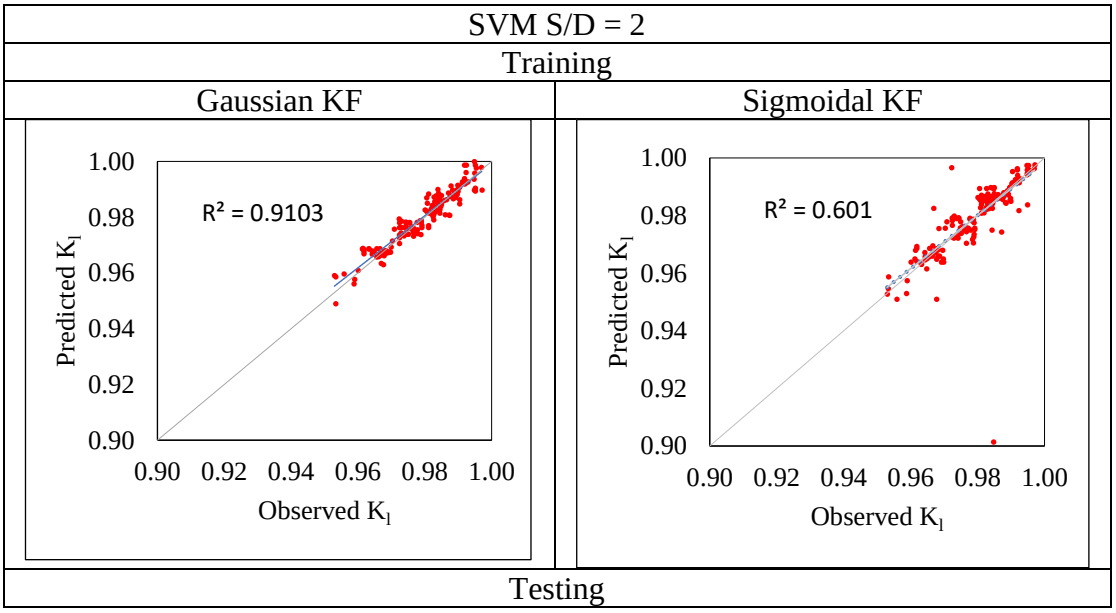

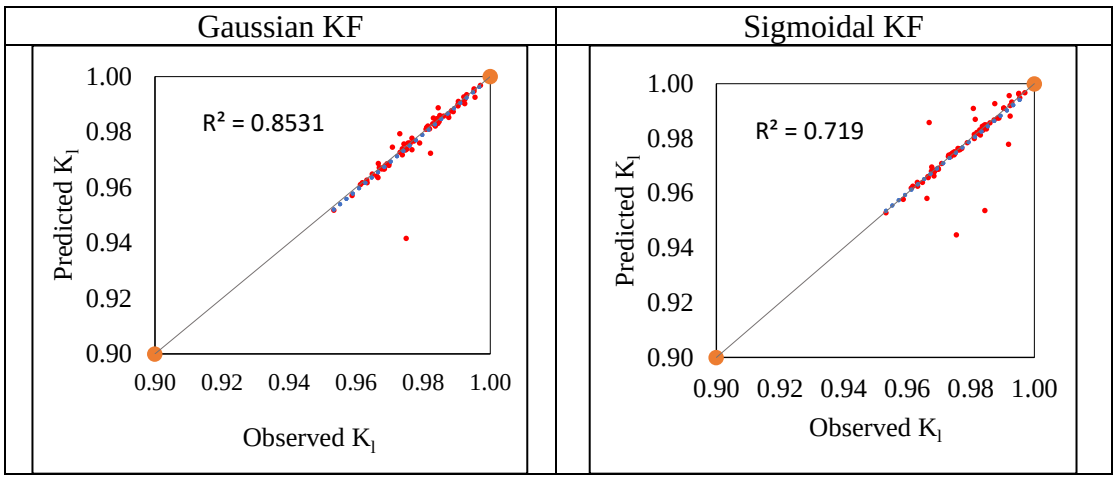

Figure 6.17 Scattered Plot between Observed and Predicted Values of K_l (SVM S/D=2)

Table 6.21 Model Performance Indices by SVM algorithm using dimensional parameters

Model Performance Index (MPI)	SVM S/D=2			
	Training		Testing	
	Gaussian KF	Sigmoidal KF	Gaussian KF	Sigmoidal KF
CC	0.954	0.775	0.924	0.848
RMSE	3.784	3.193	4.184	3.971
SI	1.804	2.137	5.157	5.433
NSE	0.931	0.889	0.912	0.904

On comparing the plots of observed vs. anticipated K_r and MPI values tabulated above in Table 6.21, it can be seen that the Gaussian KF approach's coefficient of correlation (CC) is superior to the Sigmoidal KF method. During training, the Gaussian KF achieved a CC value of 0.954 as opposed to the Sigmoidal KF of 0.775. The CC values for the Gaussian KF and Sigmoidal KF techniques were found to be, respectively, 0.924 and 0.848 while testing. The RMSE values during training for the Gaussian KF and the Sigmoidal KF were 3.784 and 3.193, respectively, whereas, during testing, they were 4.184 and 3.971, respectively. For the Gaussian KF, the values for SI were 1.804 and 5.157 in training and testing, respectively, while for the Sigmoidal KF method, they were 2.137 and 5.433 in training and testing, respectively. Further evidence of the improved accuracy of the Gaussian KF approach comes from the lower RMSE and SI values as compared to the Gaussian KF method. The Gaussian KF methodology has higher values for NSE than the Gaussian KF method, demonstrating improved

accuracy: 0.931 in training and 0.912 in testing for Gaussian KF vs. 0.889 in training and 0.904 in testing for Sigmoidal KF.

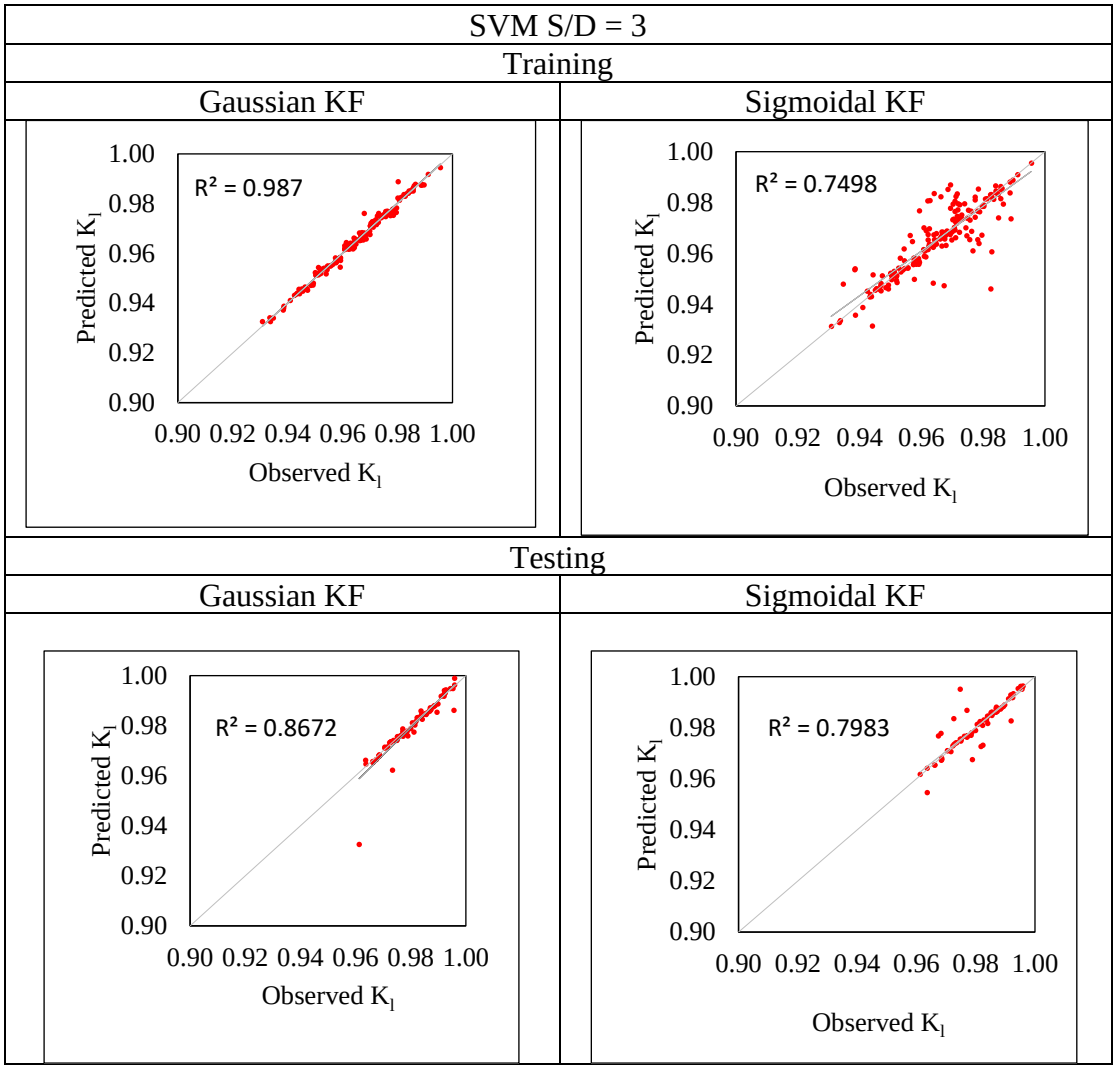

Figure 6.18 Scattered Plot between Observed and Predicted Values of K_l (SVM S/D=2)

Table 6.22 Model Performance Indices by SVM algorithm using dimensional parameters

Model Performance Index (MPI)	SVM S/D=3			
	Training		Testing	
	Gaussian KF	Sigmoidal KF	Gaussian KF	Sigmoidal KF
CC	0.993	0.865	0.913	0.893
RMSE	3.657	2.893	3.184	3.131
SI	2.066	1.634	4.135	4.066
NSE	0.941	0.917	0.932	0.912

Comparing the MPI values tabulated above in Table 6.22, computed using Gaussian KF and Sigmoidal KF, indicates the Gaussian KF approach's coefficient of correlation (CC) is superior to the Sigmoidal KF method. The CC value attained by the Sigmoidal KF approach in training is 0.865 compared to a value of 0.993 in the Gaussian KF. On testing, it was found that the CC values for the Sigmoidal KF and Gaussian KF approaches were, respectively, 0.893 and 0.913. Results for RMSE for the Sigmoidal KF approach and Gaussian KF in training were 2.893 and 3.657, respectively, while they were 3.131 and 3.184 in testing. The values for SI in training and testing for the Sigmoidal KF were 1.634 and 4.066, respectively, while for the Gaussian KF, they were 2.066 and 4.135, respectively. The reduced RMSE and SI values compared to the Sigmoidal KF further demonstrate the higher accuracy of the Gaussian KF. The results for NSE indicate that the Gaussian KF has higher values, showing its better accuracy when compared to the Sigmoidal KF: 0.917 in training and 0.912 in testing for Sigmoidal KF with 0.941 in training and 0.932 in testing for Gaussian KF.

SVM S/D = 4	
Training	
Gaussian KF	Sigmoidal KF
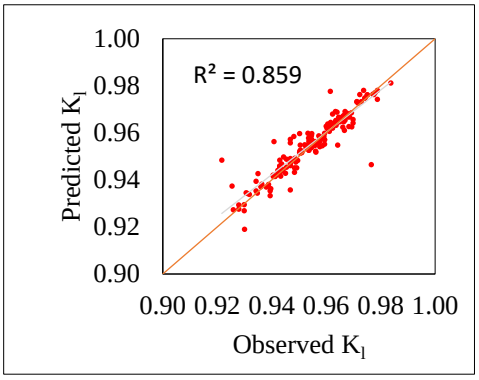	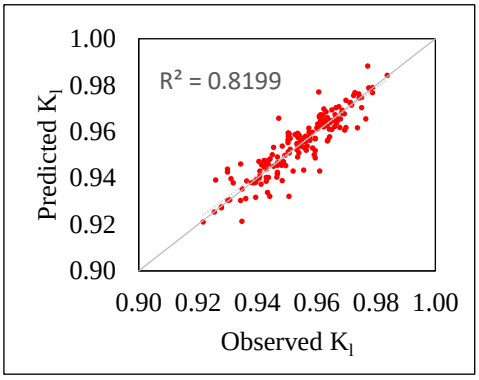

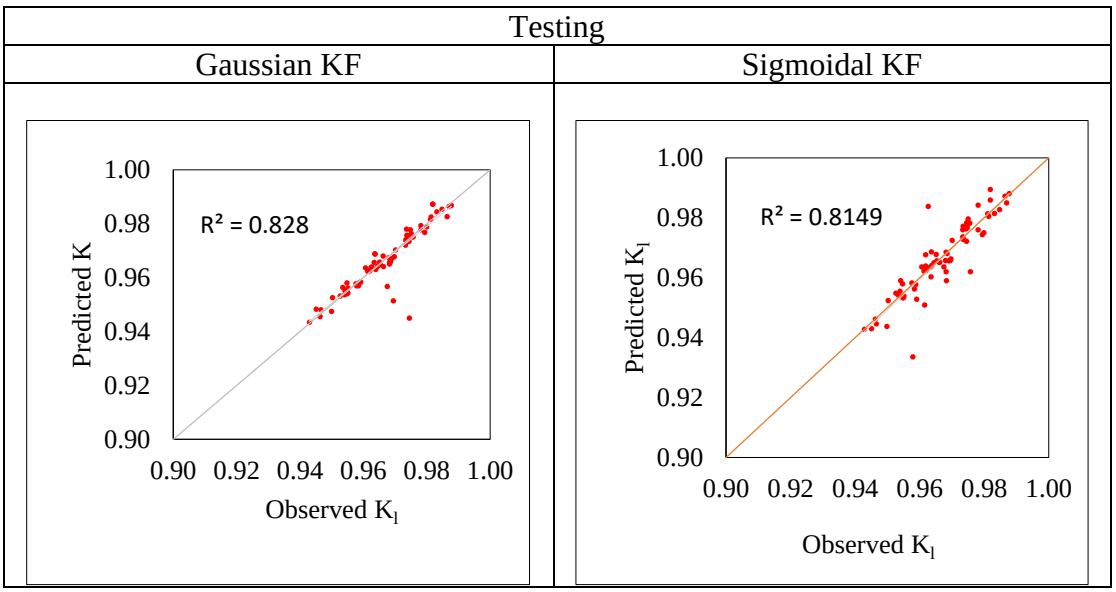

Figure 6.19 Scattered Plot between Observed and Predicted Values of K_l (SVM S/D=2)

Table 6.23 Model Performance Indices by SVM algorithm using dimensional parameters

Model Performance Index (MPI)	SVM S/D=4			
	Training		Testing	
	Gaussian KF	Sigmoidal KF	Gaussian KF	Sigmoidal KF
CC	0.946	0.930	0.940	0.935
RMSE	3.365	4.729	3.632	3.984
SI	2.166	2.406	4.174	5.716
NSE	0.951	0.924	0.932	0.917

From Table 6.23 comparing the MPI values of observed vs. predicted K_l, it is found that the coefficient of correlation (CC) obtained by the Gaussian KF method is better compared to the Sigmoidal KF method. The value of CC obtained by the Sigmoidal KF method in training is 0.930 as compared to a value of 0.946 in the Gaussian KF method. In testing, the CC value was found to be 0.935 and 0.940 for Sigmoidal KF and Gaussian KF, respectively. The values for RMSE in training were 4.729 for the Sigmoidal KF method against 3.365 for the Gaussian KF method, while in testing, it was 3.984 and 3.632, respectively. The value for SI in training and testing was 2.406 and 5.716 for the Sigmoidal KF method, respectively, and 2.166 and 4.174 for the Gaussian KF method, respectively. The lower values for RMSE and SI in the Gaussian KF method as compared to the Gaussian KF method further indicate that the accuracy

is more for the Gaussian KF method. The values for NSE were 0.924 and 0.917 in training and testing, respectively, for Sigmoidal KF and 0.951 and 0.932 in training and testing, respectively, for Gaussian KF. The Gaussian KF method has greater values, hence emphasizing the accuracy over the Gaussian KF method.

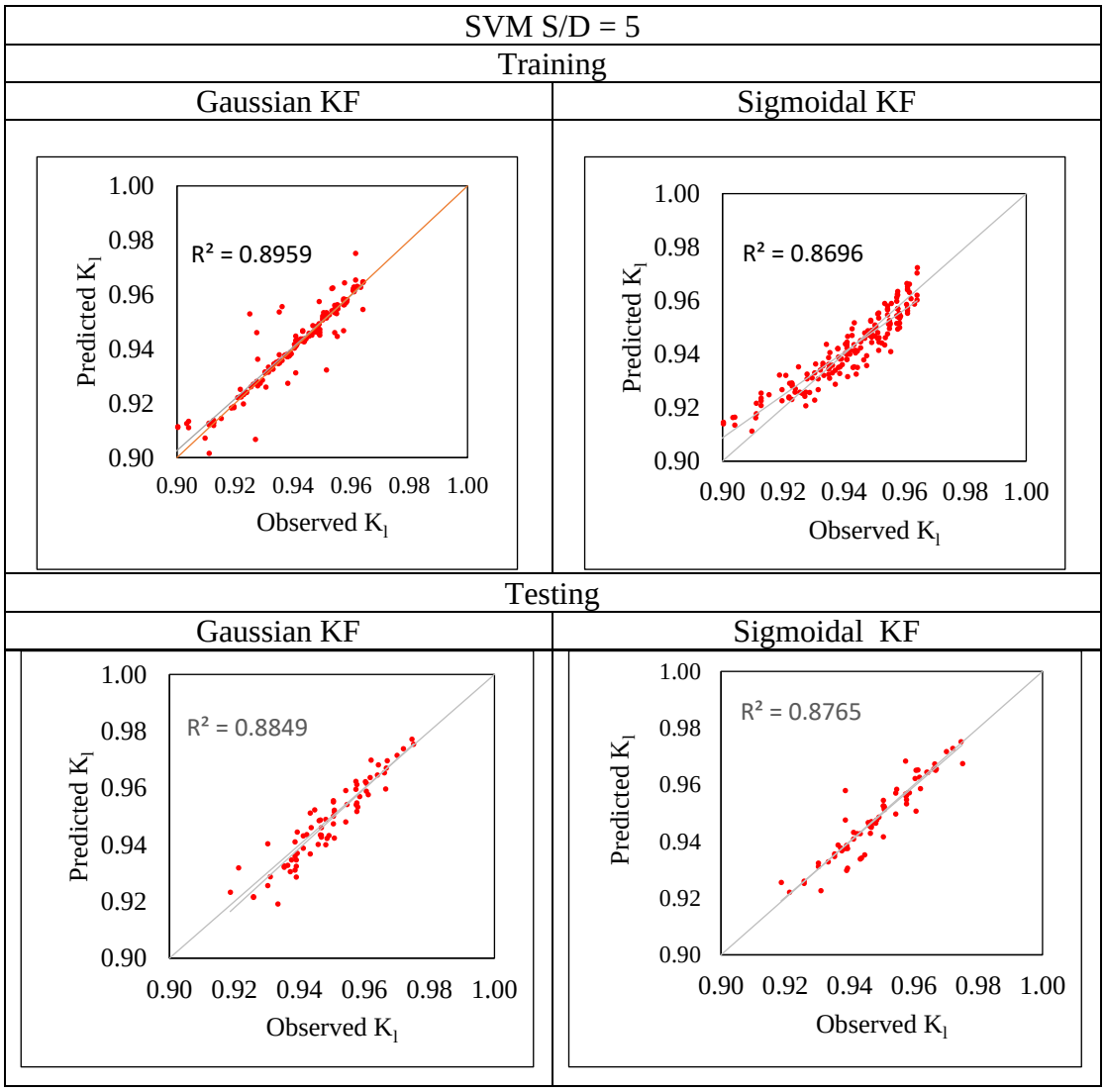

Figure 6.20 Scattered Plot between Observed and Predicted Values of K_l (SVM S/D=2)

Table 6.24 Model Performance Indices by SVM algorithm using dimensional parameters

Model Performance Index (MPI)	SVM S/D=5			
	Training		Testing	
	Gaussian KF	Sigmoidal KF	Gaussian KF	Sigmoidal KF
CC	0.9465	0.9325	0.9407	0.9362
RMSE	4.136	5.572	3.318	3.925
SI	2.502	2.583	4.088	5.318
NSE	0.972	0.913	0.919	0.917

The MPI values are tabulated in Table 6.24, and it can be observed that the Gaussian KF approach's coefficient of correlation (CC) is superior to the Sigmoidal KF method. The CC value attained by the Sigmoidal KF approach in training is 0.9325 compared to a value of 0.9465 in the Gaussian KF technique. As a result of testing, it was obtained that the CC values for the Sigmoidal KF and Gaussian KF approaches were, respectively, 0.9362 and 0.9407. Results for RMSE for the Sigmoidal KF approach and Gaussian KF method in training were 5.572 and 4.136, respectively, while they were 3.925 and 3.318 in testing. The values for SI in training and testing for the Sigmoidal KF were 2.583 and 5.318, respectively, while for the Gaussian KF method, they were 2.502 and 4.088, respectively. The reduced RMSE and SI values compared to the Gaussian KF method further demonstrate the higher accuracy of the Gaussian KF approach. The results for NSE in Table 6.24 show that the Gaussian KF approach has higher values, showing its better accuracy when compared to the Sigmoidal KF: 0.972 in training and 0.919 in testing for Gaussian KF with 0.913 in training and 0.917 in testing for Sigmoidal KF.

Table 6.25 Comparison of Model Performance Index obtained from SVM by Gaussian kernel function using Dimensional parameters

	CC		RMSE		SI		NSE	
	Training	Testing	Training	Testing	Training	Testing	Training	Testing
S/D=2	0.954	0.924	3.784	4.184	1.804	5.157	0.931	0.912
S/D=3	0.9953	0.913	3.657	3.184	2.066	4.135	0.941	0.932
S/D=4	0.946	0.940	3.365	3.362	2.166	4.174	0.951	0.932

S/D=5	0.932	0.941	4.136	3.318	2.502	4.088	0.972	0.919

Comparing the model performance index from Table 6.25, obtained by SVM using a decision tree for different perforations of QBW, QBW.

6.5.2 Using Non-Dimensional Parameters

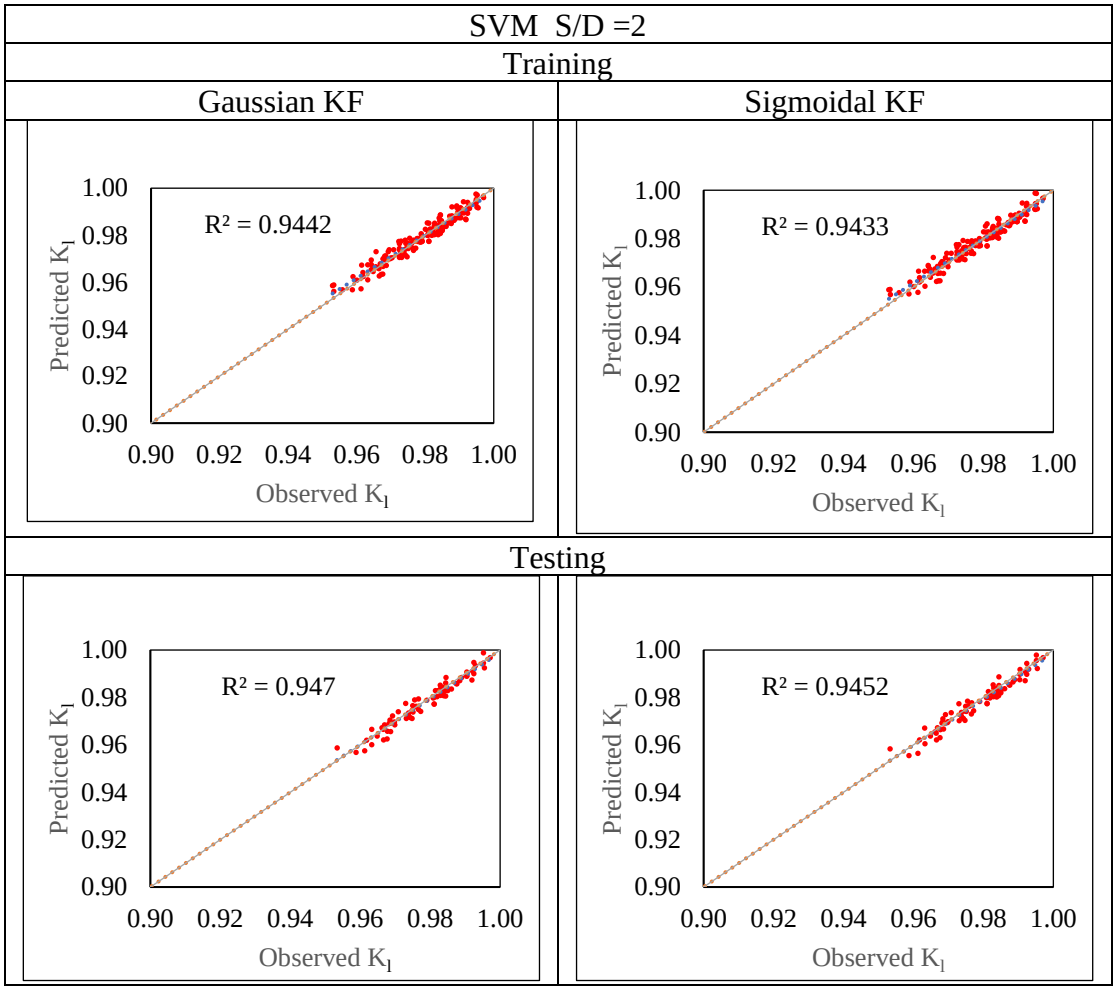

Figure 6.21 Scattered Plot between Observed and Predicted Values of K_l (SVM S/D=2)

Table 6.26 Model Performance Indices by SVM algorithm using non-dimensional parameters

Model Performance Index (MPI)	SVM S/D=2			
	Training		Testing	
	Gaussian kernel	Sigmoidal kernel	Gaussian kernel	Sigmoidal kernel
CC	0.9717	0.9712	0.9731	0.9722
RMSE	0.0505	0.0511	0.1348	0.3379
SI	0.0285	0.0289	0.1751	0.1791
NSE	0.953	0.927	0.915	0.899

The values tabulated in Table 6.26 above indicate that the Gaussian KF approach's coefficient of correlation (CC) is superior to the Sigmoidal KF method. The CC value attained by the Sigmoidal KF approach in training is 0.9712 compared to a value of 0.9717 in the Gaussian KF technique. As a result of testing, it was obtained that the CC values for the Sigmoidal KF and Gaussian KF approaches were, respectively, 0.9722 and 0.9731. Results for RMSE for the Sigmoidal KF approach and Gaussian KF method in training were 0.0511 and 0.0505, respectively, while they were 0.3379 and 0.1348 in testing. The values for SI in training and testing for the Sigmoidal KF were 0.0289 and 0.1791, respectively, while for the Gaussian KF method, they were 0.0285 and 0.1751, respectively. The reduced RMSE and SI values compared to the Gaussian KF method further demonstrate the higher accuracy of the Gaussian KF approach. The results for NSE in Table 6.26 show that the Gaussian KF approach has higher values, showing its better accuracy when compared to the Sigmoidal KF: 0.953 in training and 0.915 in testing for Gaussian KF with 0.927 in training and 0.899 in testing for Sigmoidal KF.

SVM S/D =3

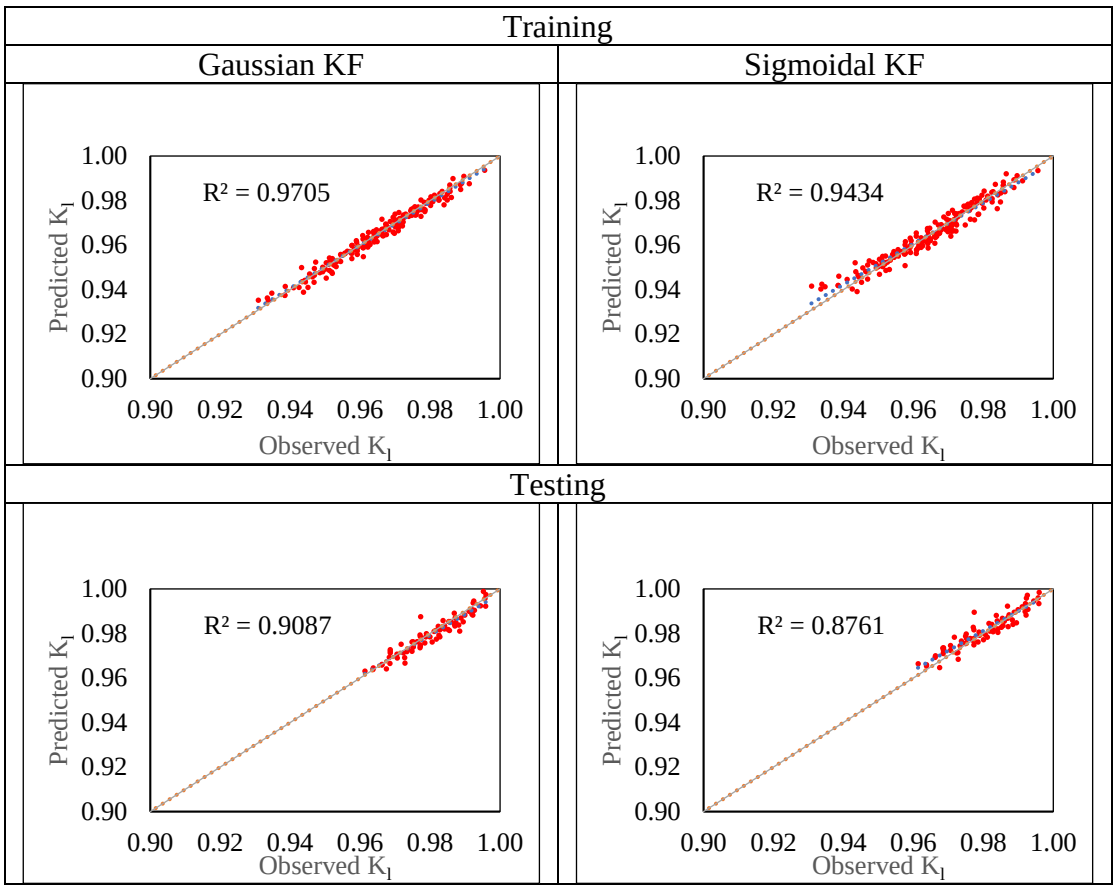

Figure 6.22 Scattered Plot between Observed and Predicted Values of K_l (SVM S/D=2)

Table 6.27 Model Performance Indices by SVM algorithm using non-dimensional parameters

Model Performance Index (MPI)	SVM S/D=3			
	Training		Testing	
	Gaussian kernel	Sigmoidal kernel	Gaussian kernel	Sigmoidal kernel
CC	0.9851	0.9712	0.9533	0.9360
RMSE	0.0362	0.0387	0.0240	0.0251
SI	0.0207	0.0216	0.0311	0.0323
NSE	0.948	0.939	0.953	0.944

Comparing the values tabulated in Table 6.27 above indicate that the Gaussian KF approach's coefficient of correlation (CC) is superior to the Sigmoidal KF method. The CC value attained by the Sigmoidal KF approach in training is 0.9712 compared to a value of 0.9851 in the Gaussian KF technique. As a result of testing, it was obtained that the CC values for the Sigmoidal KF and Gaussian KF approaches were, respectively, 0.9360 and 0.9533. Results for RMSE for the Sigmoidal KF approach and Gaussian KF method in training were 0.0387 and 0.0362, respectively, while they were

0.251 and 0.0240 in testing. The values for SI in training and testing for the Sigmoidal KF were 0.0216 and 0.0323, respectively, while for the Gaussian KF method, they were 0.0207 and 0.0311, respectively. The reduced RMSE and SI values compared to the Gaussian KF method further demonstrate the higher accuracy of the Gaussian KF approach. The results for NSE in Table 6.27 show that the Gaussian KF approach has higher values, showing its better accuracy when compared to the Sigmoidal KF: 0.948 in training and 0.953 in testing for Gaussian KF with 0.939 in training and 0.944 in testing for Sigmoidal KF.

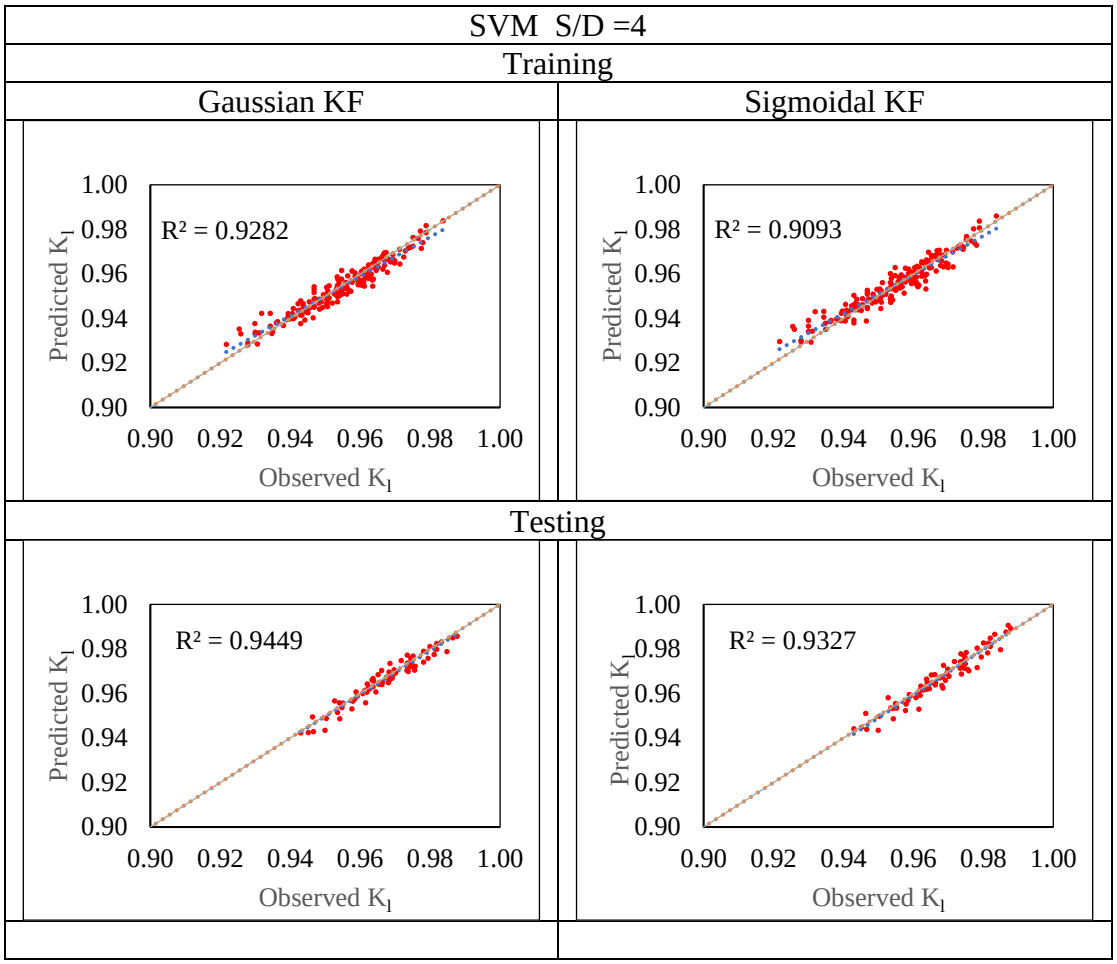

Figure 6.23 Scattered Plot between Observed and Predicted Values of K_l (SVM S/D=2)

Table 6.28 Model Performance Indices by SVM algorithm using non-dimensional parameters

Model Performance Index (MPI)	SVM S/D=4			
	Training		Testing	
	Gaussian kernel	Sigmoidal kernel	Gaussian kernel	Sigmoidal kernel
CC	0.9634	0.9535	0.9721	0.9657
RMSE	0.0669	0.0994	0.0652	0.1005
SI	0.0004	0.0006	0.0847	0.1305
NSE	0.957	0.948	0.939	0.931

Comparing the tabulated values from Table 6.28, it is observed that the Gaussian KF approach's coefficient of correlation (CC) is superior to the Sigmoidal KF method. The CC value attained by the Sigmoidal KF approach in training is 0.9535 compared to a value of 0.9634 in the Gaussian KF technique. As a result of testing, it was obtained that the CC values for the Sigmoidal KF and Gaussian KF approaches were, respectively, 0.9657 and 0.9721. Results for RMSE for the Sigmoidal KF approach and Gaussian KF method in training were 0.0994 and 0.0669, respectively, while they were 0.1005 and 0.0652 in testing. The values for SI in training and testing for the Sigmoidal KF were 0.0006 and 0.1305, respectively, while for the Gaussian KF method, they were 0.0669 and 0.0652, respectively. The reduced RMSE and SI values compared to the Gaussian KF method further demonstrate the higher accuracy of the Gaussian KF approach. The results for NSE in Table 6.28 show that the Gaussian KF approach has higher values, showing its better accuracy when compared to the Sigmoidal KF: 0.957 in training and 0.939 in testing for Gaussian KF with 0.948 in training and 0.931 in testing for Sigmoidal KF.

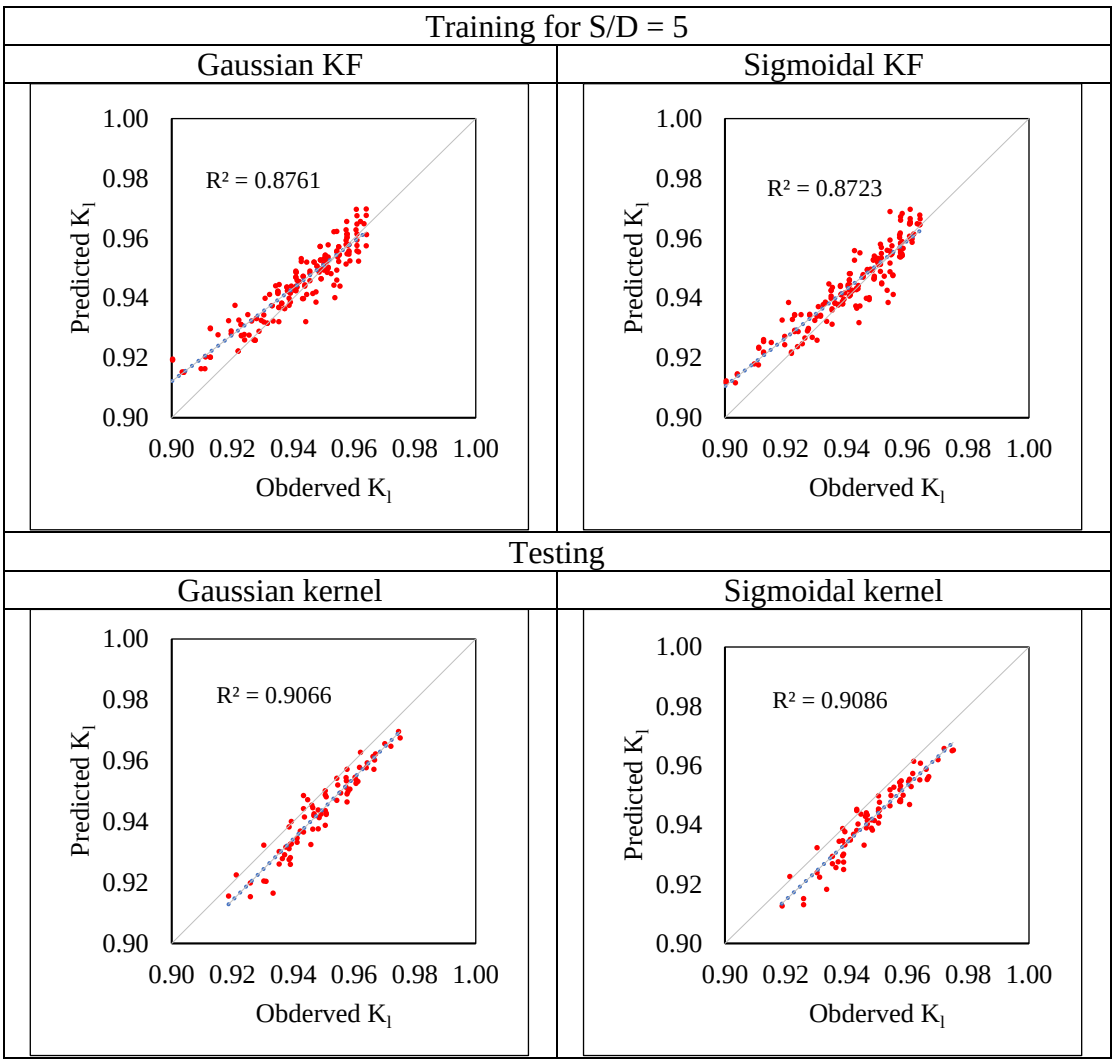

Figure 6.24 Scattered Plot between Observed and Predicted Values of K_l (SVM S/D=5)

Table 6.29 Model Performance Indices by SVM algorithm using non-dimensional parameters

Model Performance Index (MPI)	SVM S/D=5			
	Training		Testing	
	Gaussian kernel	Sigmoidal kernel	Gaussian kernel	Sigmoidal kernel
CC	0.936	0.934	0.952	0.953
RMSE	0.0458	0.0556	0.0487	0.0572
SI	0.0259	0.0314	0.0633	0.0743
NSE	0.965	0.943	0.954	0.921

From comparing the values tabulated in Table 6.29, it is observed that the Gaussian KF approach's coefficient of correlation (CC) is superior to the Sigmoidal KF method. The CC value attained by the Sigmoidal KF approach in training is 0.934 compared to a value of 0.936 in the Gaussian KF technique. As a result of testing, it was found that the CC values for the Sigmoidal KF and Gaussian KF approaches were, respectively, 0.953 and 0.952. Results for RMSE for the Sigmoidal KF approach and Gaussian KF method in training were 0.0556 and 0.0458, respectively, while they were 0.0572 and 0.0487 in testing. The values for SI in training and testing for the Sigmoidal KF were 0.0314 and 0.0743, respectively, while for the Gaussian KF method, they were 0.0259 and 0.0633, respectively. The reduced RMSE and SI values compared to the Gaussian KF method further demonstrate the higher accuracy of the Gaussian KF approach.
The results for NSE in Table 6.29 show that the Gaussian KF approach has higher values, showing its better accuracy when compared to the Sigmoidal KF: 0.965 in training and 0.9541 in testing for Gaussian KF with 0.943 in training and 0.921 in testing for Sigmoidal KF.

Table 6.30 Comparison of Model Performance Index obtained for SVM algorithm by Gaussian kernel function using non-dimensional parameters

	CC		RMSE		SI		NSE	
	Training	Testing	Training	Testing	Training	Testing	Training	Testing
S/D=2	0.973	0.975	0.0505	0.3348	0.0285	0.1751	0.953	0.915
S/D=3	0.952	0.940	0.0382	0.0251	0.0216	0.0326	0.948	0.953
S/D=4	0.941	0.962	0.0669	0.0652	0.0004	0.0847	0.957	0.939
S/D=5	0.936	0.952	0.0458	0.0487	0.0259	0.0633	0.965	0.954

Table 6.30 indicates a comparison of the model performance index obtained by SVM using the Gaussian kernel function for different perforations of a QBW.

6.6 PREDICTION OF LOSS COEFFICIENT (K_l) OF A PERFORATED QBW USING DEEP LEARNING METHOD

6.6.1 Using Dimensional parameters

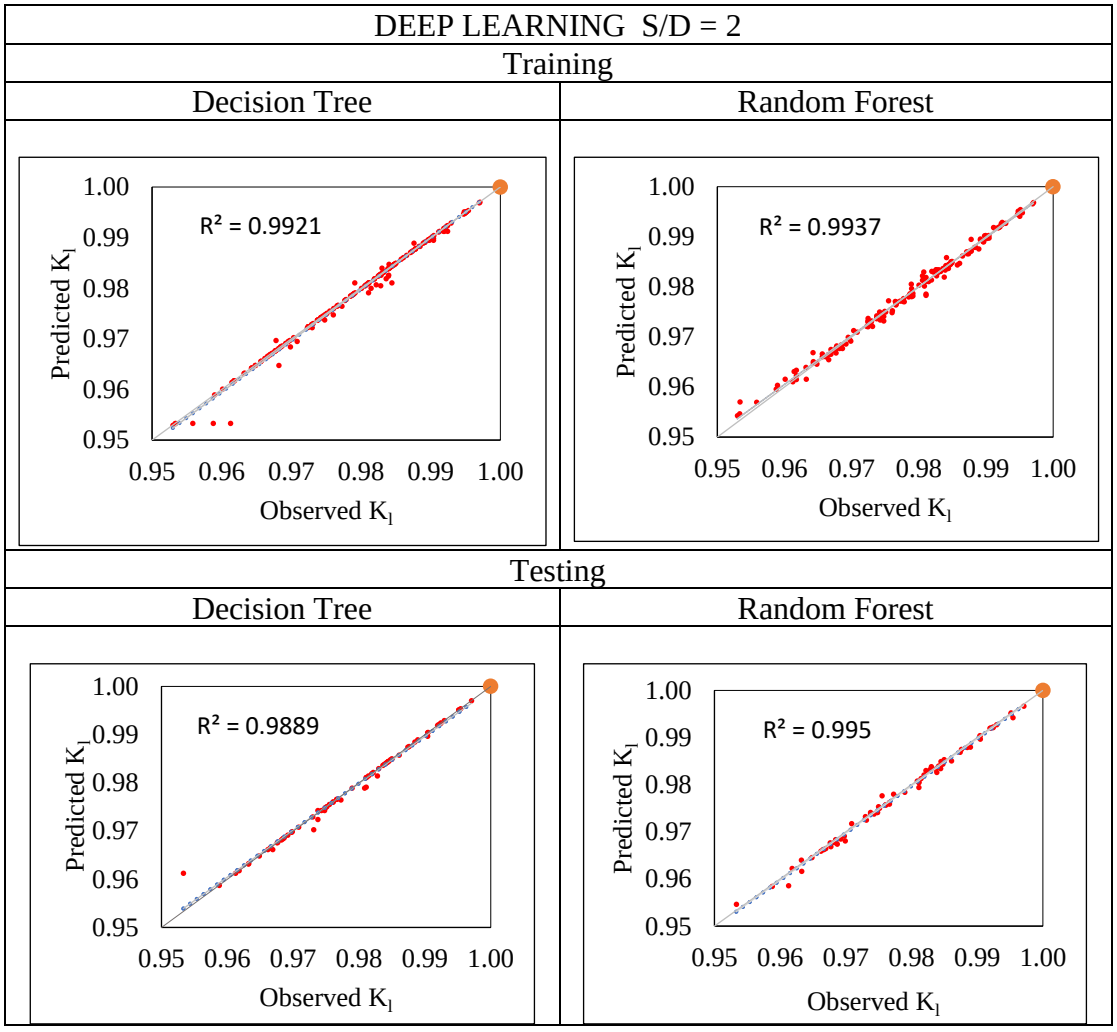

Figure 6.25 Scattered Plot between Observed and Predicted Values of K_l DL, S/D=2)

Table 6.31 Model Performance Indices for S/D=2 using dimensional parameters

Model Performance Index (MPI)	Deep Learning S/D=2			
	Training		Testing	
	Decision Tree	Random Forest	Decision Tree	Random Forest
CC	0.996	0.995	0.994	0.994
RMSE	0.0536	0.0967	0.0649	0.0667
SI	0.086	0.0546	0.097	0.0866
NSE	0.973	0.933	0.911	0.947

Comparing the values tabulated in Table 6.31 that the Decision Tree approach's coefficient of correlation (CC) is superior to the Random Forest method. The Coefficient of correlation during training and testing are 0.996 and 0.994 in the Decision Tree technique and 0.995 and 0.994 in the Random Forest method. The results for RMSE were 0.0967 for the Random Forest technique in training and 0.0536 for the Decision Tree method, whereas they were 0.0667 and 0.0649, respectively, in testing. For the Random Forest technique, the values for SI in training and testing were 0.0546 and 0.0866, respectively, and 0.086 and 0.097, respectively, for the Decision Tree method. The greater accuracy of the Random Forest approach is further supported by the lower RMSE and SI values in comparison to the Decision Tree method. The NSE is 0.933 in training and 0.947 in testing for Random Forest versus 0.973 in training and 0.911 in testing for Decision Tree, demonstrating that the Decision Tree approach has higher values, highlighting its improved accuracy as compared to the Random Forest method.

DEEP LEARNING S/D = 3	
Training	
Decision Tree	Random Forest
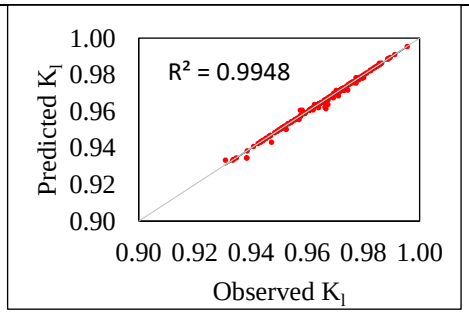	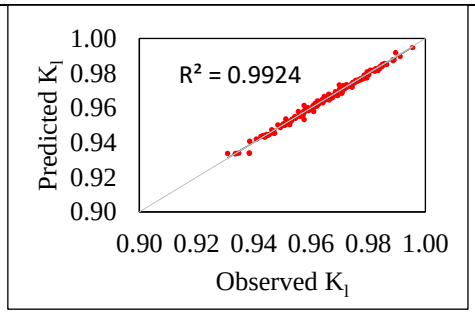

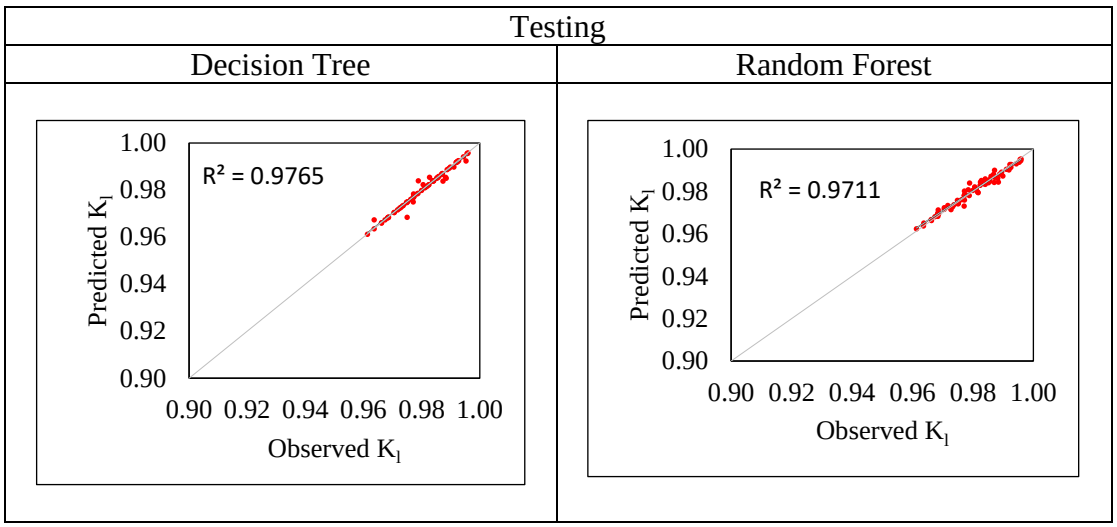

Figure 6.26 Scattered Plot between Observed and Predicted Values of K_l

Table 6.32 Model Performance Indices for S/D=3 using dimensional parameters

Model Performance Index (MPI)	Deep Learning S/D=3			
	Training		Testing	
	Decision Tree	Random Forest	Decision Tree	Random Forest
CC	0.997	0.996	0.988	0.985
RMSE	0.013	0..031	0.032	0.035
SI	0.015	0.063	0.045	0.048
NSE	0.966	0.943	0.963	0.951

The values of the model performance index that were found are shown in Table 6.32. By comparing the MPI values tabulated, it can be seen that the Decision Tree approach's coefficient of correlation (CC) is superior to the Random Forest method. During training, the Random Forest strategy achieved a CC value of 0.996 as opposed to the Decision Tree technique's 0.997. The CC values for the Random Forest and Decision Tree techniques were found to be, respectively, 0.985 and 0.988 as a result of testing. In training, the RMSE for the Random Forest technique and the Decision Tree method were 0.031 and 0.013, respectively, whereas, in testing, they were 0.035 and 0.032, respectively. For the Random Forest methodology, the values for SI were 0.063 and 0.048 in training and testing, respectively, while for the Decision Tree method, they were 0.015 and 0.045 in training and testing, respectively. The improved accuracy of the Random Forest approach comes from the lower RMSE and SI values as compared to the Decision Tree method. The Decision Tree has higher values for NSE than the

Random Forest method, demonstrating improved accuracy: 0.943 in training and 0.951 in testing for Random Forest vs. 0.966 in training and 0.963 in testing for Decision Tree.

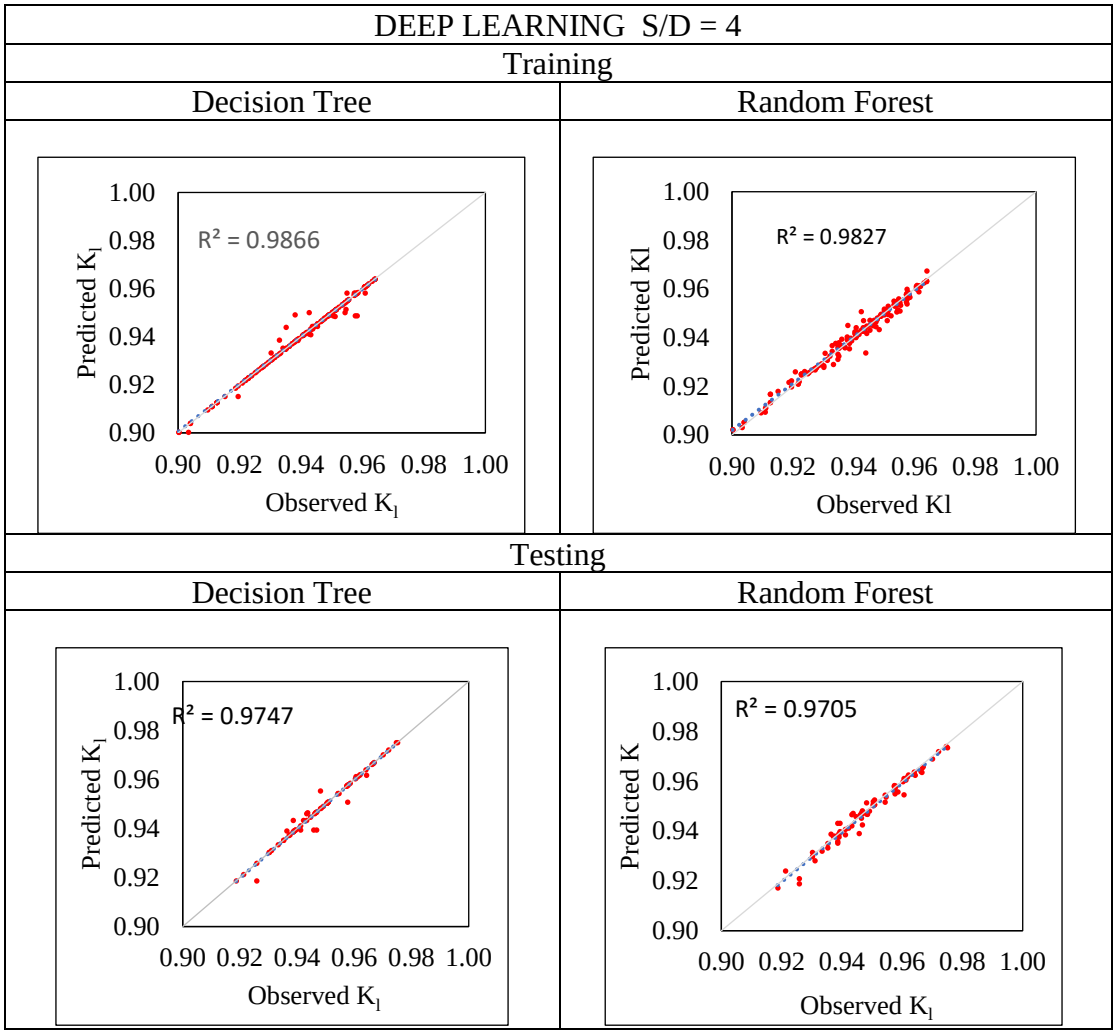

Figure 6.27 Scattered Plot between Observed and Predicted Values of K_l

Table 6.33 Model Performance Indices for S/D=4 using dimensional parameters

Model Performance Index (MPI)	Deep Learning S/D=4			
	Training		Testing	
	Decision Tree	Random Forest	Decision Tree	Random Forest
CC	0.993	0.991	0.987	0.988
RMSE	0.025	0.037	0.032	0.034
SI	0.014	0.018	0.043	0.041
NSE	0.971	0.952	0.948	0.935

From above Table 6.33, it can be observed that the Decision Tree approach's coefficient of correlation (CC) is superior to the Random Forest method. The CC value attained by the Random Forest approach in training is 0.991 compared to a value of 0.993 in the Decision Tree technique. During testing, it was found that the CC values for the Random Forest and Decision Tree approaches were, respectively, 0.988 and 0.987. Results for RMSE for the Random Forest approach and Decision Tree method in training were 0.037 and 0.025, respectively, while they were 0.034 and 0.032 in testing. The values for SI in training and testing for the Random Forest were 0.018 and 0.041, respectively, while for the Decision Tree method, they were 0.014 and 0.043, respectively. The reduced RMSE and SI values, when compared to the Decision Tree method, further demonstrate the higher accuracy of the Random Forest approach. The NSE values indicate the Decision Tree approach has higher values, showing it has better accuracy compared to the Random Forest method: 0.952 in training and 0.935 in testing for Random Forest with 0.971 in training and 0.948 in Random Forest in testing for Decision Tree.

<table>
<tr><td colspan="2">DEEP LEARNING S/D = 5</td></tr>
<tr><td colspan="2">Training</td></tr>
<tr><td>Decision Tree</td><td>Random Forest</td></tr>
<tr><td> 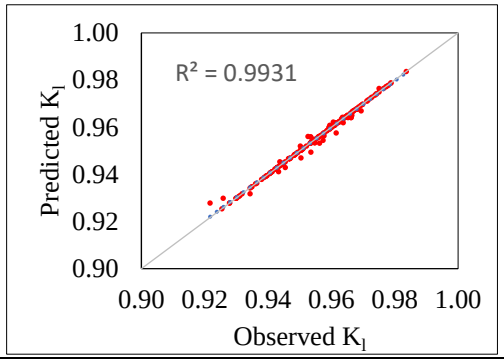
</td><td> 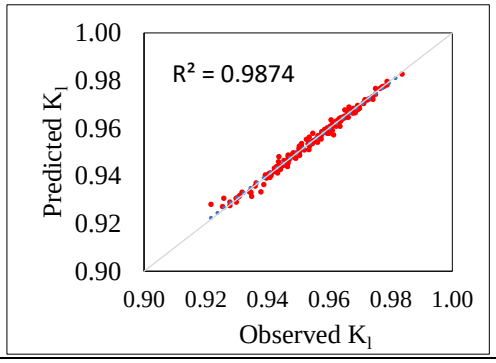
</td></tr>
<tr><td colspan="2">Testing</td></tr>
<tr><td>Decision Tree</td><td>Random Forest</td></tr>
<tr><td> 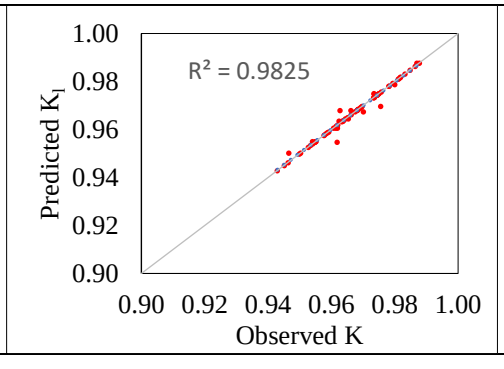
</td><td> 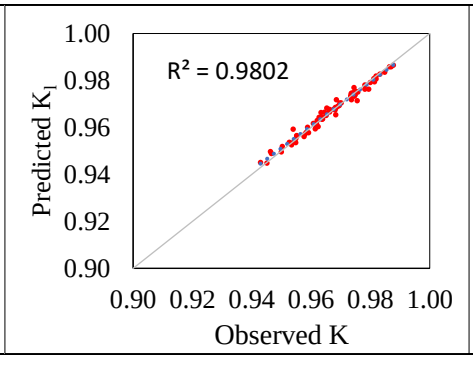
</td></tr>
</table>

Figure 6.28 Scattered Plot between Observed and Predicted Values of K_l (DL S/D=5)

Table 6.34 Model Performance Indices for S/D=5 using dimensional parameters

Model Performance Index (MPI)	DL S/D=5			
	Training		Testing	
	Decision Tree	Random Forest	Decision Tree	Random Forest
CC	0.998	0.996	0.992	0.991
RMSE	0.025	0.028	0.031	0.039
SI	0.014	0.016	0.041	0.045
NSE	0.967	0.958	0.957	0.943

On comparing the MPI values from Table 6.34, it can be seen that the Decision Tree approach's coefficient of correlation (CC) is superior to the Random Forest method. By comparing the CC value obtained from the Decision Tree technique is 0.998 as against 0.996 obtained by the Random Forest method while training. Testing revealed that the CC values for the Random Forest and Decision Tree methods were, respectively, 0.991 and 0.992. The results for RMSE were 0.028 for the Random Forest technique in training and 0.025 for the Decision Tree method, whereas they were 0.039 and 0.031, respectively, in testing. For the Random Forest technique, the values for SI in training and testing for Random Forest were 0.016 and 0.045, respectively, and 0.014 and 0.041, respectively, for the Decision Tree method. The greater accuracy of the Random Forest approach is further supported by the lower RMSE and SI values in comparison to the Decision Tree method. The NSE values are 0.958 in training and 0.943 in testing for Random Forest versus 0.967 in training and 0.957 in testing for Decision Tree, demonstrating that the Decision Tree approach has higher values, highlighting its improved accuracy as compared to the Random Forest method.

Table 6.35 Comparison of Model Performance Indices obtained for Deep Learning algorithm by Decision Tree using dimensional parameters

	CC		RMSE		SI		NSE	
	Training	Testing	Training	Testing	Training	Testing	Training	Testing
S/D=2	0.996	0.994	0.0536	0.0649	0.086	0.097	0.973	0.911
S/D=3	0.997	0.988	0.013	0.032	0.015	0.045	0.966	0.963

S/D=4	0.993	0.987	0.025	0.032	0.014	0.043	0.971	0.948
S/D=5	0.998	0.992	0.025	0.031	0.014	0.041	0.967	0.657

Table 6.35 show a comparison of the model performance index obtained by deep learning using a Decision Tree for different perforations of a QBW.

6.6.2 Using Non-Dimensional parameters

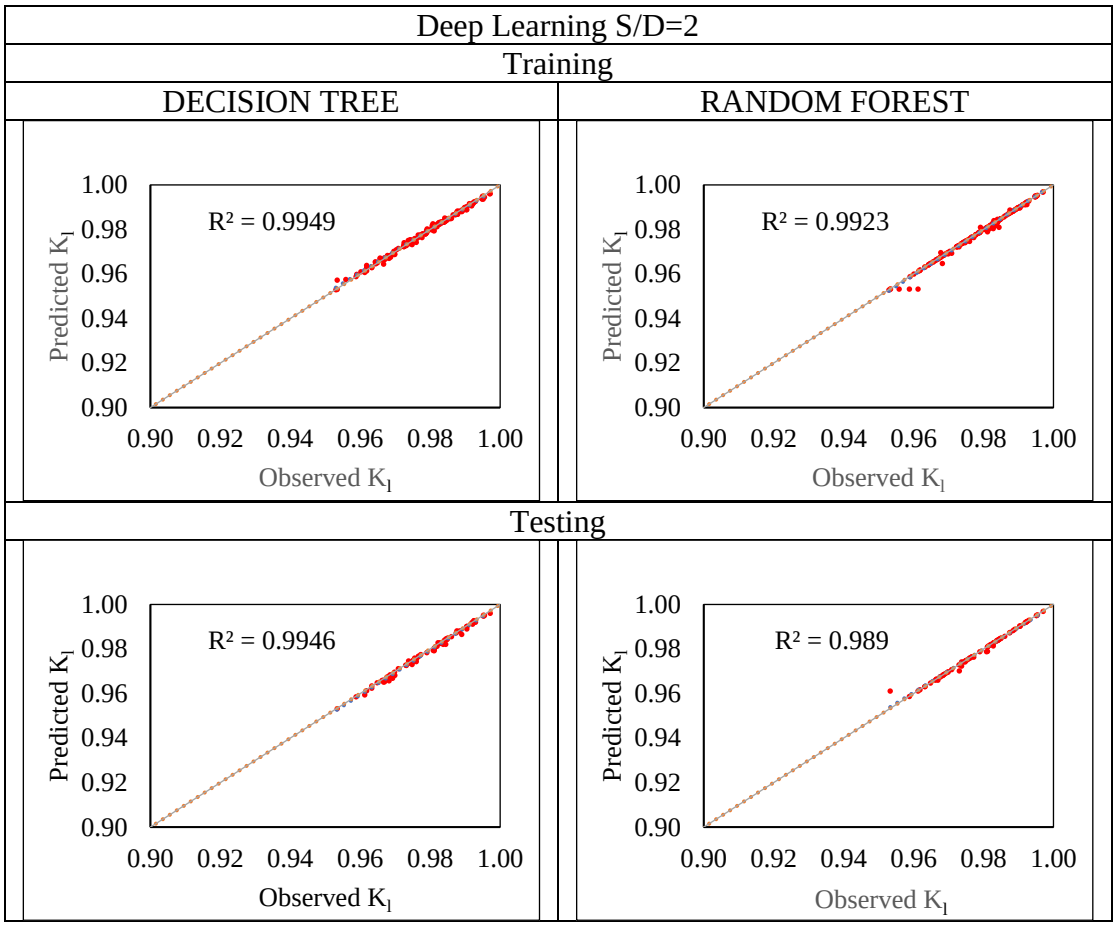

Figure 6.29 Scattered Plot between Observed and Predicted Values of K_l (DL S/D=2)

Table 6.36 Model Performance Indices S/D=2 using non-dimensional parameters

	Deep Learning S/D=2	
	Training	Testing

Model Performance Index (MPI)	Decision Tree	Random forest	Decision Tree	Random forest
CC	0.9974	0.9961	0.9973	0.9945
RMSE	0.049	0.051	0.056	0.077
SI	0.028	0.039	0.048	0.058
NSE	0.943	0.936	0.939	0.928

On comparing the MPI values from Table 6.36, it can be seen that the Decision Tree approach's coefficient of correlation (CC) is superior to the Random Forest method. By comparing the CC value obtained from the Decision Tree technique is 0.9974 as against 0.9961 obtained by the Random Forest method while training. Testing revealed that the CC values for the Decision Tree and Random Forest methods were, respectively, 0.9973 and 0.9945. The results for RMSE were 0.049 for the Decision Tree technique in training and 0.051 for the Random Forest method, whereas they were 0.056 and 0.077, respectively, in testing. For the Decision Tree technique, the values for SI in training and testing were 0.028 and 0.048, respectively, and 0.039 and 0.058, respectively, for the Random Forest method. The greater accuracy of the Decision Tree approach is further supported by the lower RMSE and SI values in comparison to the Decision Tree method. The NSE values are 0.943 in training and 0.939 in testing for Decision Tree versus 0.936 in training and 0.928 in testing for Random Forest, demonstrating that the Decision Tree approach has higher values, highlighting its improved accuracy as compared to the Random Forest method.

Deep Learning S/D =3

Training

DECISION TREE

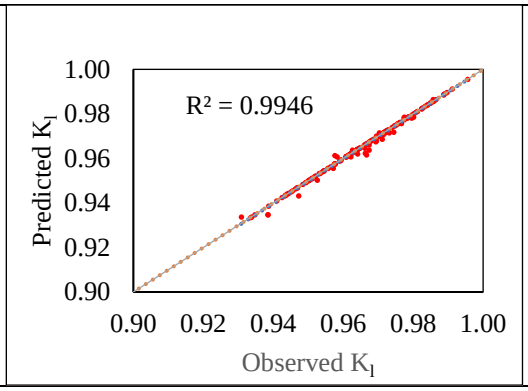

RANDOM FOREST

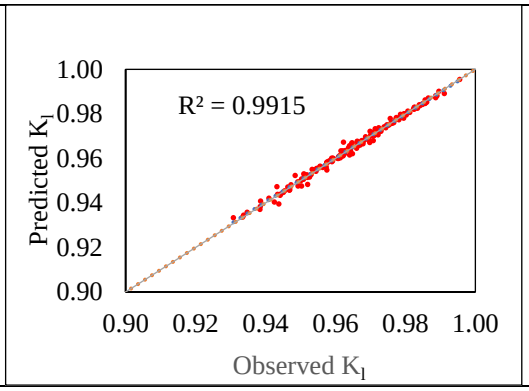

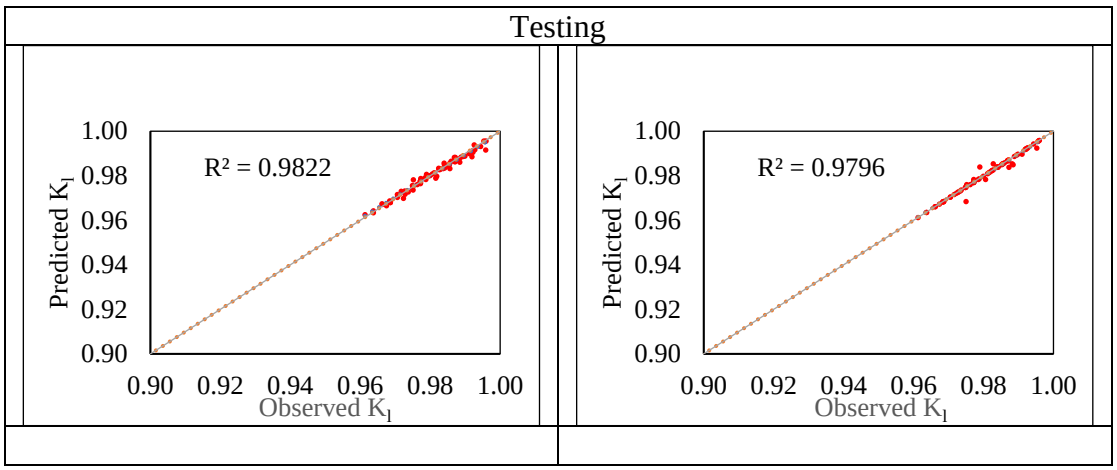

Figure 6.30 Scattered Plot between Observed and Predicted Values of K_l (DL S/D=3)

Table 6.37 Model Performance Indices for S/D-3 using non-dimensional parameters

Model Performance Index (MPI)	Deep Learning S/D=3			
	Training		Testing	
	Decision Tree	Random forest	Decision Tree	Random forest
CC	0.9973	0.9957	0.9911	0.9897
RMSE	0.048	0.049	0.037	0.033
SI	0.024	0.026	0.036	0.044
NSE	0.972	0.953	0.959	0.944

On comparing the MPI values, it can be seen in Table 6.37 that the Decision Tree approach's coefficient of correlation (CC) is superior to the Random Forest method. By comparing the CC value obtained from the Decision Tree technique is 0.9973 as against 0.9957 obtained by the Random Forest method while training. Testing revealed that the CC values for the Decision Tree and Random Forest methods were, respectively, 0.9911 and 0.9897. The results for RMSE were 0.048 for the Decision Tree technique in training and 0.049 for the Random Forest method, whereas they were 0.037 and 0.033, respectively, in testing. For the Decision Tree technique, the values for SI in training and testing were 0.024 and 0.036, respectively, and 0.026 and 0.044, respectively, for the Random Forest method. The greater accuracy of the Decision Tree approach is further supported by the lower RMSE and SI values in comparison to the

Decision Tree method. The NSE values are 0.972 in training and 0.959 in testing for Decision Tree versus 0.953 in training and 0.944 in testing for Random Forest, demonstrating that the Decision Tree approach has higher values, highlighting its improved accuracy as compared to the Random Forest method.

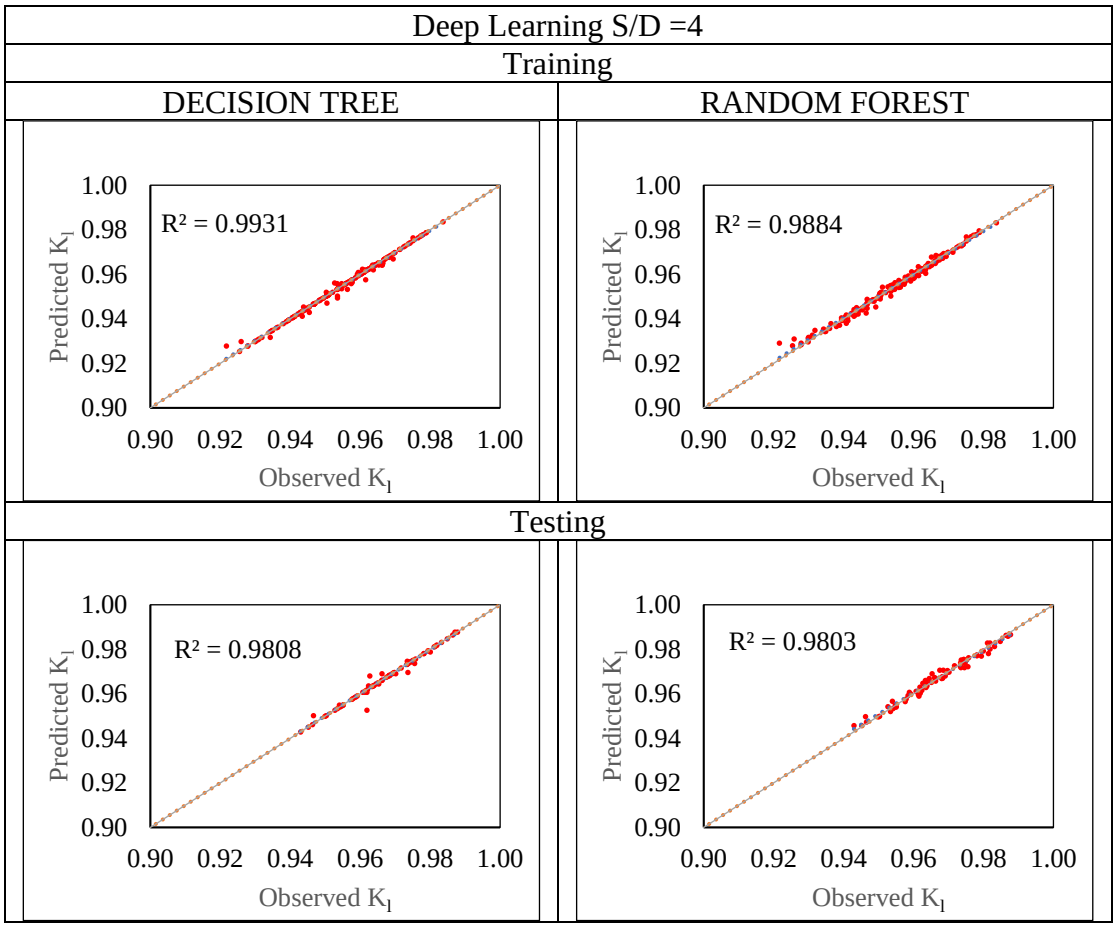

Figure 6.31 Scattered Plot between Observed and Predicted Values of K_l (DL S/D=4)

Table 6.38 Model Performance Indices for S/D-4 using non-dimensional parameters

Model Performance Index (MPI)	Deep Learning S/D=4			
	Training		Testing	
	Decision Tree	Random forest	Decision Tree	Random forest
CC	0.9965	0.9941	0.9903	0.9901
RMSE	0.105	0.121	0.104	0.109
SI	0.001	0.001	0.135	0.142
NSE	0.961	0.946	0.938	0.922

On comparing the MPI values from Table 6.38, it can be seen that the Decision Tree approach's coefficient of correlation (CC) is superior to the Random Forest method. By comparing the CC value obtained from the Decision Tree technique is 0.9965 as against 0.9941 obtained by the Random Forest method while training. Testing revealed that the CC values for the Decision Tree and Random Forest methods were, respectively, 0.9903 and 0.99901. The results for RMSE were 0.105 for the Decision Tree technique in training and 0.121 for the Random Forest method, whereas they were 0.104 and 0.109, respectively, in testing. For the Decision Tree technique, the values for SI in training and testing were 0.001 and 0.135, respectively, and 0.001 and 0.142, respectively, for the Random Forest method. The greater accuracy of the Decision Tree approach is further supported by the lower RMSE and SI values in comparison to the Decision Tree method. The NSE values are 0.961 in training and 0.938 in testing for Decision Tree versus 0.946 in training and 0.922 in testing for Random Forest, demonstrating that the Decision Tree approach has higher values, highlighting its improved accuracy as compared to the Random Forest method.

Deep Learning S/D = 5	
Training	
Decision Tree	Random Forest
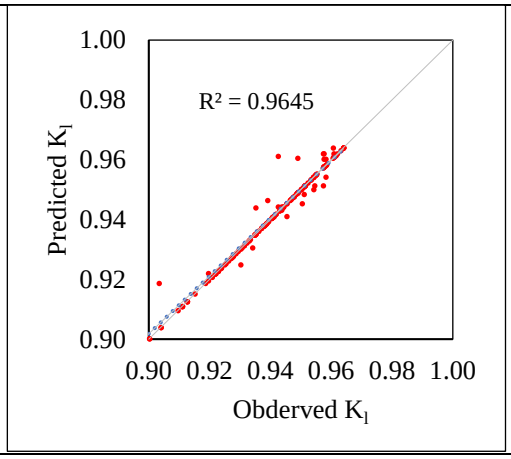	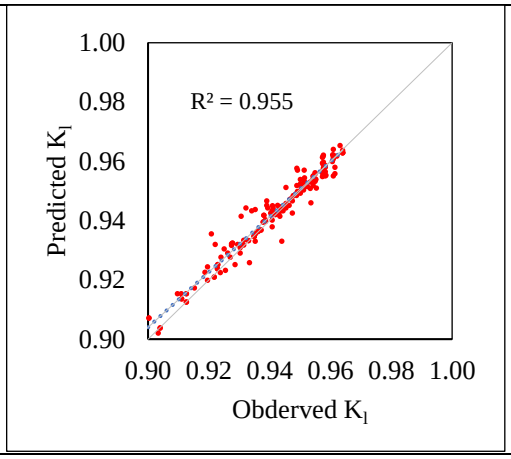

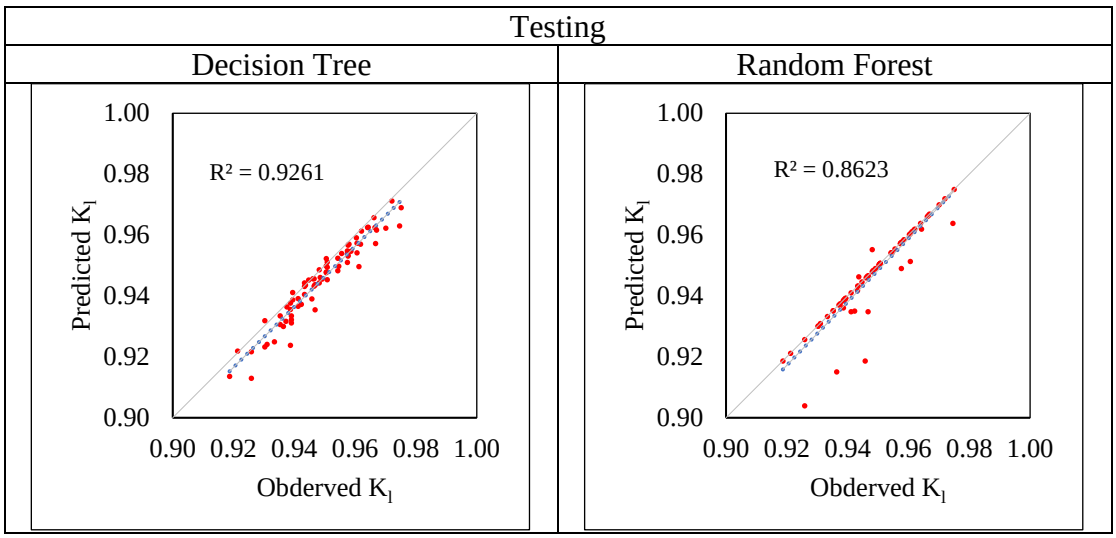

Figure 6.32 Scattered Plot between Observed and Predicted Values of K_l (DL S/D=5)

Table 6.39. Model Performance Indices for S/D=5 using non-dimensional parameters

Model Performance Index (MPI)	Deep Learning S/D=5			
	Training		Testing	
	Decision Tree	Random forest	Decision Tree	Random forest
CC	0.982	0.977	0.962	0.929
RMSE	0.079	0.080	0.097	0.103
SI	0.044	0.045	0.127	0.133
NSE	0.948	0.921	0.929	0.918

On comparing the MPI values from Table 6.39, it can be seen that the Decision Tree approach's coefficient of correlation (CC) is superior to the Random Forest method. By comparing the CC value obtained from the Decision Tree technique is 0.982 as against 0.977 obtained by the Random Forest method while training. Testing revealed that the CC values for the Decision Tree and Random Forest methods were, respectively, 0.962 and 0.929. The results for RMSE were 0.079 for the Decision Tree technique in training and 0.080 for the Random Forest method, whereas they were 0.097 and 0.103, respectively, in testing. For the Decision Tree technique, the values for SI in training and testing were 0.044 and 0.127, respectively, and 0.045 and 0.133, respectively, for the Random Forest method. The greater accuracy of the Decision Tree approach is further supported by the lower RMSE and SI values in comparison to the Decision Tree

method. The NSE values are 0.948 in training and 0.929 in testing for Decision trees versus 0.921 in training and 0.918 in testing for Random Forest, demonstrating that the Decision Tree approach has higher values, highlighting its improved accuracy as compared to the Random Forest method.

Table 6.40 Comparison of Model Performance Indices obtained for Deep Learning by Decision Tree using non-dimensional parameters

	CC		RMSE		SI		NSE	
	Training	Testing	Training	Testing	Training	Testing	Training	Testing
S/D=2	0.994	0.998	0.049	0.086	0.028	0.049	0.943	0.929
S/D=3	0.997	0.99	0.047	0.033	0.027	0.043	0.972	0.959
S/D=4	0.953	0.957	0.105	0.103	0.0006	0.135	0.961	0.938
S/D=5	0.982	0.962	0.079	0.097	0.044	0.127	0.948	0.929

Table 6.40 compares the model performance index obtained by deep learning using Decision Tree different perforations of a QBW.

6.7. SUMMARY

The proposed approach for predicting K_l from available experimental data is presented successfully. Prediction is highly accurate for all scenarios. The correlation coefficient obtained by experimental results is 0.997 with dimensional parameters and non-dimensional parameters for K_l. However, the decision tree of the deep learning approach outperformed the other three soft computing methods considered during the study, with a correlation of 0.997 and an RMSE of 0.326 with dimensional parameters as input and 0.997 and 0.047 with non-dimensional parameters as input in predicting the loss coefficient. From the model performance index, it is concluded that QBW with S/D=3 has performed better compared to other S/D ratios.

CHAPTER 7

SUMMARY & CONCLUSIONS

7.1 SUMMARY

In the present study, soft computing models are programmed to predict the hydraulic performance of emerged seaside perforated quarter circle breakwater by the conventional approach of data segregation has been successfully carried out. The study attempts to facilitate coastal engineers in predicting the hydraulic performance of emerged seaside perforated quarter circle breakwater to be installed in similar site conditions. Several cases considered are discussed in the previous chapters, based on which it is found that the Deep Learning method gave good results in most cases.

7.2 CONCLUSIONS

The present study uses various computational intelligence techniques: ANN, ANFIS, SVM, and Deep Learning models with 252 experimental data sets. Based on the present study, the following conclusions are drawn:

7.2.1 Reflection coefficient prediction

ANN model is tested using two methods, i.e., Levenberg-Marquardt and Conjugate gradient method, for predicting the Reflection coefficient. On comparing the results for S/D =2 condition CG(0.981) and CG (0.968); for S/D=3, CG(0.989) and CG (0.959); for S/D=4 CG(0.943) and CG (0.952); for S/D=5 CG(0.966) and CG(0.937), in most of the cases CG performed better. The ANFIS model is studied using two membership functions, i.e., Gumbel's and Linear. On comparing the results for S/D=2 condition Gumbel's (0.967) and Linear (0.942); for S/D=3 Gumbel's (0.969) and Linear (0.918); for S/D=4 Gumbel's (0.973) and Linear (0.966); for S/D=5 Gumbel's (0.945) and Linear (0.956), in most of the cases ANFIS model with Gumbel's membership function performed better.

With the SVM model, two kernel functions, i.e., Gaussian and Sigmoidal kernel, were considered in the present study. On comparing the results for S/D=2 condition Gaussian (0.964) and Sigmoidal (0.967); for S/D=3 condition Gaussian (0.979) and Sigmoidal

(0.959); for S/D=4 condition Gaussian (0.971) and Sigmoidal (0.954); for S/D=5 condition Gaussian (0.936) and Sigmoidal (0.951). In the case of the SVM model with a Gaussian kernel gave better prediction than the Sigmoidal kernel function.

In deep learning, two methods are considered, i.e., decision tree and Random- Forest, for S/D=2 condition decision tree (0.997) and Random-Forest (0.991); for S/D=3 condition decision tree (0.986) and Random Forest (0.985); for S/D=4 condition decision tree (0.992) and Random Forest (0.992); for S/D=5 condition decision tree (0.988) and Random Forest (0.983). In this method, both methods performed well. However, the decision tree gave more precise results.
Comparing the Conjugate Gradient method, Gumbel's Membership Function, Gaussian Kernel function, and decision tree – the decision tree has outperformed the other algorithms, both with dimensional and non-dimensional parameters as input.

7.2.2 Loss coefficient prediction

For predicting the Reflection coefficient, the ANN model is tested using two methods: Levenberg Marquardt and Conjugate gradient. When comparing the results for S/D =2 condition CG(0.923) and CG (0.975); S/D=3, CG(0.962) and CG (0.943); S/D=4 CG(0.979) and CG (0.968); S/D=5 CG(0.9514) and CG (0.9430), CG performed better in most cases.

Gumbel's and Linear membership functions are used in the ANFIS model. When comparing the results for S/D=2 condition Gumbel's (0.9592) and Linear (0.9446); S/D=3 Gumbel's (0.9792) and Linear (0.9274); S/D=4 Gumbel's (0.9729) and Linear (0.9630); and S/D=5 Gumbel's (0.9364) and Linear (0.9557), Gumbel's membership function performed better in most cases with ANFIS model.

SVM model, two kernel functions, i.e., Gaussian and Gaussian kernel, are considered in the study. On comparing the results for S/D=2 condition Gaussian (0.9592) and Gaussian (0.9719); for S/D=3 condition Gaussian (0.9531) and Gaussian (0.9363); for S/D=4 condition Gaussian (0.9743) and Gaussian (0.9689); for S/D=5 condition Gaussian (0.9319) and Gaussian (0.9450). In the case of SVM, the model Gaussian kernel gave a better prediction than the Gaussian kernel function.

In deep learning, two methods are considered, i.e., decision tree and Random- Forest, for S/D=2 condition decision tree (0.9944) and Random-Forest (0.9973); for S/D=3 condition decision tree (0.9897) and Random Forest (0.9911); for S/D=4 condition decision tree (0.9903) and Random Forest (0.9903); for S/D=5 condition decision tree (0.9885) and Random Forest (0.9830). In this method, both methods performed well. However, the decision tree gave much more precise results for all conditions of perforation. Deep learning approaches, as shown above, are much more effective in forecasting hydrodynamic performance, such as the Reflection coefficient and loss coefficient of QBW subjected to monochromatic waves.

7.3 CONTRIBUTIONS FROM THE STUDY

The study of the hydrodynamic parameters plays a very vital role in designing hydraulic structures such as breakwaters subjected to wave climate. From the study, it is found that soft computing techniques can be an effective tool to predict hydrodynamic parameters such as the Reflection coefficient (Kr) and loss coefficient (K_l) of a QBW subjected to waves action as against the conventional method of laboratory testing which is not only time-consuming but also uneconomical. The use of soft computing techniques over experimental methods is ideal if earlier data for similar situations/conditions is readily available, as these techniques are data-driven.

7.4 LIMITATIONS AND FUTURE SCOPE

The major limitation of the study is that models are site-specific and can be applied only if similar site conditions exist.

- The study can be undertaken by varying the percentage of data for training and testing networks.
- There is a scope to carry out a similar study for quarter circle breakwater employing other soft computing techniques like Extreme Learning Machines, Ant Colony optimization or Firefly optimization method, Convolution network, and recurrent network could be explored.
-

REFERENCES

Ana Gomes, José L. S. Pinho, Tiago Valente, José S. Antunes do Carmo andbArkal V. Hegde. (2020) Performance Assessment of a Semi-Circular Breakwater through CFD Modelling. J. Mar. Sci. Eng. 2020,vol. 8(3), pp 229; https://doi.org/10.3390/jmse8030226.

Afred Ultsch, Frank Röske (2002) Self-organizing feature maps predicting sea levels. Information Sciences, Volume 144(1-4), 125; https://doi.org/10.1016/S00200255(02)00203-7.

"Artificial Neural Network". (2021). https://www.javatpoint.com/artificial-neural-network (Apr. 4, 2022)

Alex J. Smola and Bernhard Scholkopf (2004) A tutorial on support vector regression, An extended version of this paper is available as Neuro COLT Technical Report TR-98-030. 0960-3174 C 2004 Kluwer Academic Publishers.

Aydogan, B., Ayat, B., Ozturk, M. N., Cevik E.O. and Yuksel, Y. (2010). Current velocity forecasting in straits with artificial neural networks, a case study: Strait of Istanbul. Ocean Engineering, vol.37, pp 443 – 453. https://doi.org/10.1016/j.oceaneng.2010.01.016

Bateni, S.M. and Jeng, D.S. (2007). Estimation of pile group scour using adaptive neuro-fuzzy approach. Ocean Engineering, vol.34, pp 1344-1354. https://doi.org/10.1016/j.oceaneng.2006.07.003

Beltrami, G.M. (2008). An ANN algorithm for automatic, real-time tsunami detection in deep-sea level measurement. Ocean Engineering, vol.35, pp 572-587. https://doi.org/10.1016/j.oceaneng.2007.11.009.

Binumol S, SubbaRao, Arkal Vittal Hegde (2015) Runup and Rundown Characteristics of an Emerged Seaside Perforated Quarter Circle Breakwater. Aquatic Procedia, Volume 4, 2015, pp 234-239 https://doi.org/10.1016/j.aqpro.2015.02.032

Binumol, S, Subba Rao, Hegde Arkal Vittal (2017) Sliding stability analysis of emerged quarter circle breakwater with varying seaside perforations. Indian journal of Geo-Marine science, IJMS Vol.46(07) [July 2017] pp 1428-1435 http://nopr.niscpr.res.in/handle/123456789/42234

Binumol, S (2017): Studies on The Effects Of An Emerged Impermeable And Seaside Perforated Quarter Circle Breakwater On Near Field Hydrodynamic. PhD thesis to NITK, Surathkal

Browne, M., Castelle, B., Strauss, D., Tomlinson, R., Blumenstein, M. and Lane, C. (2007). Near-shore swell estimation from a global wind-wave model: spectral process, linear and artificial neural network. Coastal Engineering, vol.54, pp 445- 460. https://doi.org/10.1016/j.coastaleng.2006.11.007

Čehovin, J., and Žagar, D. (2019). Determining rock armour stability under the stress of wave loading. Acta hydro technica, 32(56), 21-33. https://doi.org/10.15292/acta.hydro.2019.02

Cebada-Relea, A. J., López, M., & Aenlle, M. (2022). Time-domain numerical modelling of the connector forces in a modular pontoon floating breakwater under regular and irregular oblique waves. Ocean Engineering, 243, 110263.

Deo, M.C. and Jagdale, S.S. (2003). Prediction of breaking waves with neural networks. Ocean Engineering, vol.30, pp 1163-1178. https://doi.org/10.1016/S0029-8018(02)00086-0

Deo, M.C. and Naidu, S.C. (1999). Real time wave forecasting using neural networks. Ocean Engineering, vol.26, pp191-203.

https://doi.org/10.1016/S0029-8018(97)10025-7

Deo, M.C., Jha, A., Chaphekar A.S. and Ravikant, K. (2001). Neural networks for wave forecasting. Ocean Engineering, 28, 889-898. https://doi.org/10.1016/S0029-8018(00)00027-5 .

Deo, M C, Jagdale, S S (2003) Prediction of breaking waves with neural networks . Ocean Engineering, Volume 30, Issue 9, June 2003, Pages 1163-

1178. https://doi.org/10.1016/S0029-8018(02)00086-0

Dinakaran, G, Sundar, V, Sundaravadivelu, R, Graw, K U (2009) Effect of perforations and rubble mound height on wave transformation characteristics of surface piercing semicircular breakwaters. Ocean Engineering, Volume 36, Issues 15–16, November 2009, pp 1182-1198, https://doi.org/10.1016/j.oceaneng.2009.08.005

Dwarakish G.S, Nithyapriya B (2016) Application of soft computing techniques in

coastal study. Journal of Ocean Engineering and Science, vol -I, issue 4 pp 247-255. http:/doi.org/10.1016/j.joes.2016.06.004

Gaur, S. and Deo, M.C. (2008). Real-time wave forecasting using genetic programming. Ocean Engineering, 35, pp 1166-1172. https://doi.org/10.1016/j.oceaneng.2008.04.007

Goyal, R., Singh, K., & Hegde, A. V. (2014). Quarter Circular Breakwater: Prediction and Artificial Neural Network. Marine Technological Society Journal, vol.48, pp 1–7. http://idr.nitk.ac.in/jspui/handle/123456789/12719

Goyal, R., Singh, K., Hegde, A. V., & Thakur, G. S. (2015). Prediction of Hydrodynamic Characteristics of Quarter Circular Breakwater Using Stepwise Regression. International Journal of Ocean Climate Systems, 6(1), pp 47–54, Google Scholar.

Graw, K. U., Knapp, S., Sundar, V. & Sundaravadivelu, R. (1998). Dynamic pressures exerted on semicircular breakwater. Leipzig Annual Civil Engineering Report No.3, pp. 333-344.

Gunaydin, K. (2008). The estimation of monthly mean significant wave heights by using artificial neural network and regression methods. Ocean Engineering, vol.35, pp 1406-1415. https://doi.org/10.1016/j.oceaneng.2008.07.008

Gunn, S.R. (1998). Support vector machines for classification and regression. University of Southampton, Technical report, Image speech and intelligent Systems group. Google Scholar.

Han, D., Chan, L. and Zhu, N. (2007). Flood forecasting using support vector machines. Journal of Hydro informatics, vol.9, pp 267-276. https://doi.org/10.2166/hydro.2007.027

Harish, N., Lokesha., Mandal, S., Rao, S. & Patil, S.G. (2014). Parameter Optimization using GA in SVM to Predict Damage Level of Non-Reshaped

Berm Breakwater. International Journal of Ocean and Climate Systems.vol. 5, pp 79- 88. https://doi.org/10.1260/1759-3131.5.2.79

Harish, N., Mandal, S., Rao, S., and Patil, S. G. (2015). Particle Swarm Optimization based support vector machine for damage level prediction of non-reshaped berm breakwater. Applied Soft Computing, vol.27, pp 313–321. https://doi.org/10.1016/j.asoc.2014.10.041

Hashemi M.R., Ghadampour Z. and Neill S.P. (2010). Using an artificial neural network to model seasonal changes in beach profiles. Ocean Engineering, vol.37, pp 1345–1356. https://doi.org/10.1016/j.oceaneng.2010.07.004

Hegde, A. V., & Naseeb, S.M. (2014). Transmission performance of submerged semicircular breakwaters for different radii and submergence ratios. The International Journal of Ocean and Climate Systems,vol. 5(3), pp 151-161 https://doi.org/10.1260/1759-3131.5.3.151

Hegde, A. V., Ganesh, C., & Kumar, V. (2010). Hydrodynamic performance characteristics of semicircular breakwater wave run-up and run- down. Journal of Hydraulic Engineering.vol. 16, pp 99-108. https://doi.org/10.1080/09715010.2010.10515019

Hegde, A., Sharhabeel, P. S., & Mohan, S. (2015). Stability of a perforated quarter circle breakwater. International Journal of Ocean Climate Systems, vol.6, pp 185–194. Google Scholar.

Hegde, A.V., Mohan, S., Pinho, J. L. S., & Sharhabeel P. S., (2018). Physical model studies on the stability of emerged seaside perforated semicircular breakwaters. Indian Journal of Geo-Marine Sciences,vol. 47, pp 681-685, 0379-5136. https://hdl.handle.net/1822/58934.

Hodaei, S.M.R., Chamani, M.R., Moghim, M.N. et al (2016). l. Experimental study on reflection coefficient of curved perforated plate. J. Marine. Sci. Appl. vol. 15, pp 382–387 https://doi.org/10.1007/s11804-016-1383-5

“Hyperparameter Tuning for Support Vector Machines — C and Gamma Parameters”. (2022). https://towardsdatascience.com/hyperparameter-tuning-for-support-vector-machines-c-and-gamma-parameters-6a5097416167. (April 10, 2022).

Inman, D. L.(1974) Ancient and Modern Harbors: a Repeating Phylogeny. Proceedings of the 14th Coastal Engineering Conference, Copenhagen, Denmark, June 1974, American Society of Civil Engineers, Reston, VA, pp. 2049-2067.

Ippen, A.T. (1966). Estuary and Coastal hydrodynamics. McGraw-Hill Book Company, New York.

Issacson M. (1991). Measurement of regular wave reflection. ASCE Journal of Waterways, Port, Coastal and Ocean Engineering,vol.117, pp 553–569. https://doi.org/10.1061/(ASCE)0733-950X(1991)117:6(553)

Jabbari, E., & Talebi, O. (2011). Using artificial neural networks for estimation of scour at the head of vertical wall breakwater. Journal of Coastal Research, vol.64, pp 521–526. https://www.jstor.org/stable/26482227

Jain, P., & Deo, M. C. (2008). Artificial Neural Networks for Coastal and Ocean studies. Proceedings of 12th International Association for Computer Methods and Advances in Geomechanics, pp 1655–1663. http://dspace.library.iitb.ac.in/xmlui/handle/10054/679

James C Bedzek (1996)Computational Intelligence: Soft Computing and Fuzzy-Neuro Integration with Applications, 1998, Volume 162 ISBN : 978-3- 642-63796-4

Jang, J.S. R. (1993). ANFIS: Adaptive-Network-Based Fuzzy Inference System. IEEE Transactions on Systems, Man, and Cybernetics vol. 23, pp 665– 685. https://doi.org/10.1109/21.256541

Jang, J.S.R., Sun, C.T. and Mizutani, E. (1997). Neuro-Fuzzy and Soft Computing, PTR Prentice Hall, New York.

Jaran G.E.(1961) , A perforated vertical breakwater , The Dock and Harbour. Authority, Vol.41 no 486, pp. 394-398.

Jeng, D. S., Cha, D. and Blumenstein, M. (2004). Neural network for the prediction of wave induced liquefaction potential. Ocean Engineering, vol.31, pp 2073-2086 https://doi.org/10.1016/j.oceaneng.2004.05.006

Jiang, Zou, Q. & Zhang, N. (2017). Wave load on submerged quarter-circular and semicircular breakwaters under irregular waves. Coastal Engineering, vol.121, pp265–277. https://doi.org/10.1016/j.coastaleng.2016.11.006

Karla, R. and Deo, M.C. (2007). Derivation of coastal wind and wave parameters from offshore measurements of TOPEX satellite using ANN, Coastal Engineering vol.54, pp 187-196

https://doi.org/10.1016/j.coastaleng.2006.07.001

Karla, R., Deo, M.C., Kumar, R. and Agarwal, V. K. (2005). RBF network for spatial mapping of wave heights. Marine Structures, vol.18, pp 289-300. https://doi.org/10.1016/j.marstruc.2005.09.003

Kazeminezhad, M. H., Etemad-shahidi, A. and Mousvi, S. J. (2005). Application of fuzzy inference system in the prediction of wave parameters. Ocean Engineering, vol.32, 1709-1725.

https://doi.org/10.1016/j.oceaneng.2005.02.001

Kecman, V. (2001). Learning and Soft Computing, Support Vector Machines, Neural Networks, and Fuzzy Logic Models. The MIT Press, Cambridge, MA, USA.

Kim, D. H., Kim, Y. J., & Hur, D. S. (2014). Artificial neural network based breakwater damage estimation considering tidal level variation. Ocean Engineering, vol.87, pp 185–190.

https://doi.org/10.1016/j.oceaneng.2014.06.001

Koç, M. L., & Balas, C. E. (2012). Genetic algorithms based on logic-driven fuzzy neural networks for stability assessment of rubble-mound breakwaters. Applied Ocean Research, vol. 37, pp 211–219.

https://doi.org/10.1016/j.apor.2012.04.005

Koç, M. L., Balas, C. E., & Koç, D. İ. (2016). Stability assessment of rubble-mound breakwaters using genetic programming. Ocean Engineering, vol.111, pp 8–12. https://doi.org/10.1016/j.oceaneng.2015.10.058

Kosko, B. (2003). Neural Networks and Fuzzy Systems, A Dynamical System Approach to Machine Intelligence. Prentice Hall of India Private Limited, New Delhi.

Kundapura, Suman, Arkal, Vittal Hegde and Pinho, Jose L. S.(2019) Below the Data Range Prediction of Soft Computing Wave Reflection of Semicircular Breakwater. Journal of Marine Science and Application, Volume 18, Issue 2, pp.167-175 https://doi.org/ 10.1007/s11804-019-00088-4

Kuntoji, G., Rao, M., & Rao, S., (2018). Prediction of wave transmission over the submerged reef of tandem breakwater using PSO-SVM and PSO-ANN techniques. ISH Journal of Hydraulic Engineering, vol. 26(3), pp 283-290. https://doi:org/10.1080/09715010.2018.1482796

Lee, A., Kim, S. E., & Suh, K.D. (2015). Estimation of Stability Number of Rock Armor Using Artificial Neural Network Combined with Principal Component

Analysis. Procedia Engineering, vol.116, pp 149–154. https://doi.org/10.1016/j.proeng.2015.08.276

Lee, T.L. (2004). Back propagation neural network for long term tidal predictions. Ocean Engineering, vol.31, pp 225-238,

https://doi.org/10.1016/S0029-8018(03)00115-X

Lee, T.L. (2006). Neural network prediction of a storm surge. Ocean Engineering, vol.33, pp 483-494.

https://doi.org/10.1016/j.oceaneng.2005.04.012

Liang, S., Li, M. and Sun, Z. (2008). Prediction models for tidal level including strong meteorologic effects using neural network. Ocean Engineering, vol.35, pp 666-675. https://doi.org/10.1016/j.oceaneng.2007.12.006

Londhe, S.N. (2008). Soft computing approach for real-time estimation of missing wave heights. Ocean Engineering, vol.35,pp 1080-1089. https://doi.org/10.1016/j.oceaneng.2008.05.003

Londhe, S.N. and Deo, M.C. (2003). Wave tranquility studies using neural networks.Marine Structures, vol.16, pp 419-436.

https://doi.org/10.1016/j.marstruc.2003.09.001

“Machine Learning Random Forest Algorithm”. (2021). https://www.javatpoint.com/machine-learning-random-forest-algorithm, (May 10, 2022).

Mahjoobi, J. and Mosabbeb E.A. (2009). Prediction of significant wave height using regressive support vector machines Ocean Engineering, vol.36,pp 339-347. https://doi.org/10.1016/j.oceaneng.2009.01.001

Maia, Alexandre & Rodrigues, Armanda & Lemos, Rute & Capitão, Rui & Fortes, Conceição. (2017). A Web Platform for the Systematic Monitoring of Coastal Structures. Conference: 3rd International Conference on Geographical Information Systems Theory, Applications and Management I. doi:10.5220/0006335401020111

"Major Kernel Functions in Support Vector Machine (SVM)". (2021). https://www.geeksforgeeks.org/major-kernel-functions-in-support-vector-machine-svm. (Jan. 31, 2022).

Makarynskyy, O. (2004). Improving wave predictions with artificial neural networks.Ocean Engineering, vol.31, pp709-724. https://doi.org/10.1016/j.oceaneng.2003.05.003

Mandal, S., Rao, S. and Raju, D.H. (2005). Ocean wave parameters estimation using back propagation neural network. Marine Structures, vol.18, pp 301-318. https://doi.org/10.1016/j.marstruc.2005.09.002

Mandal, S. and Prabaharan, N. (2006). Ocean wave forecasting using recurrent neural network. Ocean Engineering, vol. 33, pp 1401-1410.

https://doi.org/10.1016/j.oceaneng.2005.08.007

Mohamed A Mohandas, Shafiqur Rehman, Tatal O. Halawani, (1998) A Neural Network approach for wind speed prediction, Renewable Energy,, vol. 3(3), 345–354. https://doi.org/10.1016/S0960-1481(98)00001-9

Mandal, S., Rao, S., Harish, N., & Lokesha (2012). Damage level prediction of non- reshaped berm breakwater using ANN, SVM, and ANFIS models. International Journal of Naval Architecture and Ocean Engineering, vol.4, pp 112–122. https://doi.org/10.2478/IJNAOE-2013-0082

Mase, H., Sakamoto, M., & Sakai, T., (1995). Neural network for stability analysis of rubblemound breakwaters. Journal of Waterway, Port, Coastal and Ocean Engineering, vol.121, pp 294–299.

https://doi.org/10.1061/(ASCE)0733-950X(1995)121:6(294)

Naithani and Deo (2005) Estimation of wave spectral shapes using ANN, Advances in Engineering Software, vol. 36, Issues 11–12, November–December 2005, Pages 750-756.

https://doi.org/10.1016/j.advengsoft.2005.03.021

Narayana Harish, Sukomal Mandal, Subba Rao, SG Patil (2015) Particle swarm optimization-based support vector machine for damage level prediction of non-reshaped berm breakwater. journal of Applied Soft Computing, vol.27 pp 313-321 https://doi.org/10.1016/j.asoc.2014.10.041.

Patil, S. G., Mandal, S., & Hegde, A. V. (2012). Genetic algorithm based support vector machine regression in predicting wave transmission of horizontally interlaced multi-layer moored floating pipe breakwater. Advances in Engineering Software, vol.45, pp 203–212.

https://doi.org/10.1016/j.advengsoft.2011.09.026

Patil, S. G., Mandal, S., Hegde, A. V., & Alavandar, S. (2011). Neuro-fuzzy based approach for wave transmission prediction of horizontally interlaced multilayer moored floating pipe breakwater. Ocean Engineering, vol.38, pp 186–196. https://doi.org/10.1016/j.oceaneng.2010.10.009

Per Brunn (1985) Design and Construction of Mounds for Breakwaters and Coastal Protection (Developments in Geotechnical Engineering) Publisher : Elsevier Science Ltd (1 February 1985) ISBN-10 : 0444423915 ISBN-13 : 978-0444423917

Pourzangbar, A., Losada, M. A., Saber, A., Ahari, L. R., Larroudé, P., Vaezi, M., and Brocchini, M. (2017b). Prediction of non-breaking wave induced scour depth at the trunk section of breakwaters using Genetic Programming and Artificial Neural Networks. Coastal Engineering,vol. 121, pp 107–118. https://doi.org/10.1016/j.coastaleng.2016.12.008

Prashanth Janardhan (2014). Parametric Studies On Stability Of Reshaped Berm Breakwater With Concrete Cubes As Armor Unit. https://www.researc https://www.researc huttp:/www. researchgate.net/publication/273694926_

Prashanth Janardhan (2014) Parametric studies on stability of reshaped berm breakwater with concrete cubes as armor unit. Ph DThesis, NITK, Surathkal.

Quinn, Alonzo DeF. (1972) Design and Construction of Ports and Marine Structures, Second Edition, Mc Graw-Hill Book Company, New York, N.Y., 611p.

Rajendra, K., Balaji, R. & Mukul, P. (2017). Review of Indian research on innovative breakwaters. India Journal of Geo-Marine Sciences, vol.46, pp 431–452. http://nopr.niscair.res.in/handle/123456789/40819

Raju, B., Hegde, A. V., & Chandrashekar, O. (2015). Computational Intelligence on Hydrodynamic Performance Characteristics of Emerged Perforated Quarter Circle Breakwater. Procedia Engineering, vol. 116, pp 118–124. https://doi.org/10.1016/j.proeng.2015.08.272.

Relea, Alejandro & López, Mario & Aenlle López, Manuel. (2022). Time-domain numerical modelling of the connector forces in a modular pontoon floating breakwater under regular and irregular oblique waves. Ocean Engineering. 243. 110263. 10.1016/j.oceaneng.2021.110263.

Rao, S. (2000). Studies on performance of perforated pile breakwater. Doctoral dissertation, Mangalore University, Mangalore, India.

Rao, S. Mandal, S. (2005). Hindcasting of storm waves using neural networks. Ocean Engineering vol.32, pp 667–684.

https://doi.org/10.1016/j.oceaneng.2004.09.003.

Rushi Goyal, Kriti Singh, Arkal Vittal Hegde and G.S. Thakur (2015) Prediction of Hydrodynamic Characteristics of Quarter Circular Breakwater Using Stepwise Regression. International Journal of Ocean and Climate Systems, Volume 6 · Number 1, pp 47-54 February 1, 2015 .

Santanu Koley & Kottala Panduranga (2021) Energy balance relations for flow through thick porous structures. International Journal of Computational Methods and Experimental Measurements, volume 9(1), pp 28-37 ISSN: 2046- 0546 (paper format), ISSN: 2046-0554 (online), http://www.witpress.com/journals DOI: 10.2495/CMEM-V9-N1-28-37

Shi, Yj., Wu, Ml., Jiang, Xl. et al. (2011) Experimental researches on reflective and transmitting performances of quarter circular breakwater under regular and irregular waves. China Ocean Eng vol. 25, pp 469–478 . https://doi.org/10.1007/s13344-011-0038-1.

Statistics, I.S.(2010). Statistical Packages For Social Sciences (IBM SPSS) for windows, release 19.0.0.1 Chicago.

Shinsuke Aburatani, Takashi Koizuka, Hiroshi Sasayama, Katutoshi Tanimoto & Nobutaka Namerikawa (1996). Field Test on a Semi-Circular Caisson Breakwater, Coastal Engineering in Japan, vol. 39, pp 59-78. https://doi.org/10.1080/05785634.1996.11952821.

Sundar, V and Subbarao B V V (2002) Hydrodynamic Performance Characteristics of Quadrant Front-Face Pile-Supported Breakwater Journal of Waterway, Port, Coastal, and Ocean Engineering,

https://doi.org/10.1061/(ASCE)0733-950X(2003)129:1(22)

Sunder V, Raghu D (1997) Wave induced pressure on semi-circular breakwater. Proceeding of the 2nd Indian National Conference on Harbour and Ocean Engineering (INCHOE'97) Cochin University of Science and Technology, thiruvanthapuram, India pp278-39

Tanimoto, K. & Goda, Y. (1992). Historical development of breakwater structures in the world. Coastal structures and breakwaters. Institution of Civil Engineers. London, UK.

https://doi.org/10.1680/csab.16729.0013

Tanimoto, K., & Takahashi, S., (1994). Design and construction of caisson breakwaters-the Japanese experience. Coastal Engineering, vol.22, pp 57-77. https://doi.org/10.1016/0378-3839(94)90048-5.

Tseng, C.M., Jan, C.D., Wang, J.S. and Wang, C.M. (2007). Application of artificial neural networks in typhoon surge forecasting. Ocean Engineering, vol. 34, pp 1757–1768. https://doi.org/10.1016/j.oceaneng.2006.09.005

US Army Corps of Engineers (2002). Coastal engineering manual, US army corps of engineers. Washington, DC.

Van der Meer, Jentsje & Stam, Cor-Jan. (1992). Wave Runup on Smooth and Rock Slopes of Coastal Structures. Journal of Waterway Port Coastal and Ocean Engineering, vol 118, pp 534-543.

https://doi.org/10.1061/(ASCE)0733-950X(1992)118:5(534).

Wilamowski B. M., Iplikci S.,. Kaynak O and Efe, M. O. (2001) "An algorithm for fast convergence in training neural networks," IJCNN'01. International Joint Conference on Neural Networks. Proceedings (Cat. No.01CH37222), Washington, DC, USA, 2001, pp. 1778-1782 vol.3,

doi: 10.1109/IJCNN.2001.938431

Xie, S.L. (2001). Design of semi-circular breakwaters and estuary jetties, Proceedings of XXIX IAHR Congress, Beijing, pp. 90-95.

Yagci, O., Mercan, D.E., Cigizoglu, H.K., & Kabdasli, M.S. (2005). Artificial intelligence methods in breakwater damage ratio estimation. Ocean Engineering, vol.32, PP 2088–2106.

https://doi.org/10.1016/j.oceaneng.2005.03.004.

Yong Liu , Yucheng Li, Bin Teng , Junjie Jiang c, Baolian Ma (2008)Total horizontal and vertical forces of irregular waves on partially perforated caisson breakwaters. Coastal Engineering, Volume 55(6) pp 537-552

https://doi.org/10.1016/j.coastaleng.2008.02.005.

Yuan, D, and Tao, J. (2003). Wave forces on submerged, alternately submerged and emerged semicircular breakwaters. Coastal Engineering, vol.48, pp 75–93. https://doi.org/10.1016/S0378-3839(02)00169-2

ZamaniaAhmadreza, Dimitri Solomatine, Ahmadreza Azimiana, Arnold Heemi nk (2008) Learning from data for wind–wave forecasting, Ocean Engineering, Volume 35, Issue 10, July 2008, Pages 953-962. https://doi.org/10.1016/j.oceaneng.2008.03.007

Zanaganeh, M., Mousavi, S. J., Farshad, A., & Shahidi, E. (2009). A hybrid genetic algorithm – adaptive network based fuzzy inference system in prediction of wave parameters. Engineering Applications of Artificial Intelligence, vol.22, pp 1194–1202. https://doi.org/10.1016/j.engappai.2009.04.009.

Zanuttigh, B., & Van der Meer, J.W. (2008). Wave reflection from coastal structures in design conditions. Coastal Engineering, vol.55, pp 771–779. https://doi.org/10.1016/j.coastaleng.2008.02.009.

Zanuttigh, B., Mizar, S., & Briganti, R. (2013). A neural network for the prediction of wave reflection from coastal and harbor structures. Coastal Engineering, vol.80, pp 49–67https://doi.org/10.1016/j.coastaleng.2013.05.004.

PUBLICATIONS BASED ON PRESENT RESEARCH WORK

Publications in Journals (Indexed in SCI / Scopus /Web of Science)

1. N Ramesh, S Bhaskaran and Subba Rao (2022), “Prediction of wave reflection for quarter circle breakwaters using soft computing techniques”, Indian Journal of Geo-Marine Sciences, CSIR- NISCPR publication, Vol. 51 (06), pp. 511-516, June 2022.

2. N Ramesh, Hegde A.V., and Subba Rao, (2019) “Evaluation of Hydrodynamic Performance of Quarter Circular Breakwater Using Soft Computing Techniques” in the book titled “Lecture Notes in Civil Engineering” edited by Murali K., Sriram V., Samad A., Saha N. (eds.) Springer, Singapore/LNCE Vol.23/ pp71-88.

3. N Ramesh., Hegde A.V., and Subba Rao, (2019) “Prediction of the reflection coefficient of a perforated Quarter circle breakwater using artificial neural network (ANN)” in the book titled “Journal of Physics: conference series”, IOP Publishing, 2019 J. Phys.: Conf. Ser.

Journal Articles (Submitted for Publication)

1. N Ramesh., Subba Rao, and Hegde A.V., (2022), “Application of Decision Forest method to Predict Reflection Coefficient of a Quarter Circular Breakwater” Journal of soft computing in Civil Engineering (Submitted for review).

International Conferences / Symposium

1. N Ramesh., Hegde A V, Subba Rao and Vivekanandan N (2017), “Comparison of Hydrodynamic Performance of Quarter Circular Breakwater Using ANN and Auto Regression Methods”, Proceedings in (HYDRO-2017), organized by L. D. College of Engineering under the aegis of The Indian Society of Hydraulics, during December 21-23, 2017 held at L. D. College of Engineering, Ahmedabad, Gujarat, India.

2. N Ramesh., Hegde A V, Subba Rao and Vivekanandan N (2018) “Evaluation of Hydrodynamic performance of Quarter Circular Breakwater Using Soft Computing Techniques”, Proceedings of 4th International Conference in Ocean Engineering (ICOE 2018), during 18th – 21st February 2018 at IIT Madras, Chennai, India.

CURRICULUM VITAE

Name:	RAMESH N RAO
Permanent Address:	D 803, Venkatesh Serenity, Near DSK Vishwa Dhayari Pune.
Contact No.:	+91 8999571447
Email ID:	10ramesh64@gmail.com
Experience	Scientist 'E'
	Central Water and Power Research Station (CWPRS) Khadakwasla, Pune -411024
Education:	M.Tech. in Hydraulics and Water Resources Engineering, NITK (erstwhile KREC), Surathkal, Batch 1991
	B.E. in Civil Engineering) NITK (erstwhile KREC), Surathkal, Batch 1986
Memberships:	Life member Indian Society of Hydraulics
	Life member Indian Society for Technical Education, New Delhi.
	Life member Kannada Sahitya parisad, Bangalore.